



HAL
open science

The role of Notch signaling pathway during neural delamination in the vertebrate embryo

Chooyoung Baek

► **To cite this version:**

Chooyoung Baek. The role of Notch signaling pathway during neural delamination in the vertebrate embryo. Cellular Biology. Université Paris sciences et lettres, 2018. English. NNT : 2018PSLEE067 . tel-03284588

HAL Id: tel-03284588

<https://theses.hal.science/tel-03284588v1>

Submitted on 12 Jul 2021

HAL is a multi-disciplinary open access archive for the deposit and dissemination of scientific research documents, whether they are published or not. The documents may come from teaching and research institutions in France or abroad, or from public or private research centers.

L'archive ouverte pluridisciplinaire **HAL**, est destinée au dépôt et à la diffusion de documents scientifiques de niveau recherche, publiés ou non, émanant des établissements d'enseignement et de recherche français ou étrangers, des laboratoires publics ou privés.

THÈSE DE DOCTORAT

de l'Université de recherche Paris Sciences et Lettres
PSL Research University

Préparée à l'Ecole Normale Supérieure

Rôle de la voie de signalisation Notch au cours de la délamination neurale
chez l'embryon de vertébré

The role of Notch signaling pathway during neural delamination in the vertebrate embryo

Ecole doctorale n°515

Complexité du vivant

Spécialité Biologie cellulaire

Soutenue par **Chooyoung BAEK**
le **18 septembre 2018**

Dirigée par **Xavier MORIN**

COMPOSITION DU JURY :

Mme SCHNEIDER-MAUNOURY Sylvie
Sorbonne Université, Président du jury

Mme ALEXANDRE Paula
University College London, Rapporteur

Mme BEL-VIALAR Sophie
Université Paul Sabatier, Rapporteur

Mme DAVY Alice
Université Paul Sabatier, Examineur

M. BAFFET Alexandre
Institut Curie, Examineur

M. MORIN Xavier
Ecole Normale Supérieure,
Directeur de thèse

M. TOZER Samuel
Ecole Normale Supérieure,
Membre invité du jury



Acknowledgments

I would like to start by expressing my gratitude to the members of the jury: Drs Paula Alexandre and Sophie Bel-Vialar, for accepting to read and comment on the manuscript; Drs Sylvie Schneider-Maunoury, Alice Davy and Alexandre Baffet, for kindly accepting to evaluate my work.

I also thank my thesis committee members, Drs François Schweisguth, Julien Falk and Louis Gervais, for their insightful comments and suggestions during our two meetings.

Above all, I am extremely thankful to Xavier and Samuel who collectively supervised me during all these years. Xavier, thank you for welcoming me in your lab; you bet three years ago on a medical student who was not sure on pursuing a PhD after the M2 internship, but now I am happy to say that I cannot imagine a better lab for doing my PhD! It is a difficult task to thank you for everything you have done in a few words, but thank you for your guidance, for helping me to ask the right questions and for always proposing solutions. Knowing that your door was always open when needed has been a great comfort throughout my thesis. Samuel, words cannot fully express how grateful I am. Thank you for being an excellent supervisor in the daily lab life, for making me discover the little chick embryos, for teaching me all the techniques, for your availability whenever I encountered an issue and for all the trust you put on me. I would not have been able to complete this thesis without your support. Thank you for everything and I wish you all the best for your future career!

Similarly, I would like to acknowledge all the present and past members of the Morin lab: Evelyne, thank you for your kindness and for your sensible advices on both scientific and medical careers. Also, your enthusiasm and love for science are of great inspiration to me. Rosette, thank you for your daily availability whenever I needed help, for your assistance all along these years and for your sincere encouragements. Kamal, my daily tea-time partner, thank you for teaching me how to manipulate ESCs. I could never have done half of what I did without your precious help and I cannot be more thankful. Florencia, my elder sister in science, thank you for being such a good example, I have learned so many things from you during the first steps of my M2 and the beginning of my PhD. I have been incredibly lucky to work in this lab. Each of you has contributed to make my PhD such a wonderful experience and I thank you for that.

I also would like to thank all those who have directly or indirectly participated in this project, especially to the 7th floor people, for your technical help, scientific exchange and for making the everyday life so pleasant.

I warmly thank the teaching team of *'Médecine-Sciences'* of the University Paris Descartes, previously directed by Pr Jean-Claude Chottard, Pr Philippe Ascher and now by Pr Jean-Christophe Thalabard, for giving me the fabulous opportunity to live this adventure, for your energy, your perseverance and your unconditional support. I want to particularly thank Pr Philippe Ascher, whose neurosciences courses and advices were determinant for my bifurcation to research and my interest in neurobiology six years ago. Likewise, I acknowledge the *'Ecole de l'Inserm Liliane Bettencourt'* with their directors Dr Boris Barbour and Dr Eric Clauser as well as the *'Bettencourt Schueller foundation'* for their support in the promotion and development of dual curriculum in medicine and sciences.

Many thanks to all the people who helped me relax outside the lab. Specially, for those who went through the same steps of a PhD, thank you for sharing the good and not-too-good periods of my PhD, I am counting on you to do the same for the *'externat'* that is waiting for us! For those who stayed more 'medical', thank you for your support, for recalling me medical terms and reminding me where I must return.

Special thanks go to my family who has provided me through moral, emotional and spiritual support during my thesis. I thank my sister, for her endless encouragement and for all the fun we had and will continue to have. Lastly, I am deeply grateful to my parents, for trusting me and encouraging my decisions that sometimes were not easy to follow. Your prayer for me is what sustained me thus far. Thank you for your presence and for everything you have done, this thesis is dedicated to you.

Summary

The role of Notch signaling pathway during neural delamination in the vertebrate embryo

The embryonic neural tube is initially composed of elongated cycling neural progenitors whose apical attachments with their neighbors ensure a cohesive network surrounding the luminal surface. As neural progenitors commit to differentiation, prospective neurons translocate their nucleus to the basal side and eventually withdraw their apical endfoot from the ventricular surface. Nevertheless, the cellular and molecular events that accompany the delamination process and the mechanisms allowing the neural tube to preserve its epithelial integrity as increasing numbers of nascent neurons delaminate, have been little explored. At the level of gene regulation, the balance between proliferation and differentiation relies largely on the interplay between Notch target genes and proneural genes. Notably, neural differentiation is accompanied by increased levels of proneural genes and loss of Notch activity. However, the temporal coordination between these two events and importantly, how the loss of Notch signaling is integrated during the delamination process in order to preserve neuroepithelial integrity is still unknown.

To tackle these fundamental questions, I used the chick embryonic spinal cord as a model. By taking advantage of a Notch reporter transgenic chicken line, I have shown that Notch signaling, which is classically associated with an undifferentiated state, remains active in prospective neurons until they delaminate. During this transition period, prospective neurons rapidly reduce their apical surface and only later down-regulate N-cadherin levels. Disrupting this sequence through premature Notch blockade weakens the apical junctional network and eventually leads to breaches in the ventricular wall, suggesting that Notch activity needs to be maintained in prospective neurons prior to delamination in order to preserve tissue integrity. I then investigated the mechanisms regulating Notch signaling in prospective neurons. I provided evidence that the Notch ligand Delta-like 1 (Dll1) promotes differentiation by reducing Notch signaling through a cis-inhibition mechanism. However, the ubiquitin ligase Mindbomb1 (Mib1) transiently blocks the cis-inhibition process during the transition period that precedes delamination. This maintains Notch activity and defers differentiation, allowing prospective neurons to constrict their apical surface before they delaminate. Thus, the fine-tuned balance between Notch trans-activation and cis-inhibition is crucial to coordinate neuronal commitment with neuronal delamination and therefore preserve neuroepithelial integrity.

Keywords: neurogenesis, Notch, neural delamination, cis-inhibition, Mindbomb1

Résumé

Rôle de la voie de signalisation Notch au cours de la délamination neurale chez l'embryon de vertébré

Le tube neural embryonnaire est initialement composé de progéniteurs neuraux qui sont des cellules cyclantes et allongées, dont les attachements apicaux avec les cellules voisines assurent un réseau cohésif couvrant la surface luminale. Lorsque les progéniteurs neuraux s'engagent vers un processus de différenciation, ils transloquent leur noyau vers le côté basal et retirent leur pied apical de la surface ventriculaire. Néanmoins, les mécanismes cellulaires et moléculaires permettant un bon déroulement du processus de délamination tout en préservant l'intégrité du tissu neuroépithélial ont été peu explorés. En terme de régulation génique, l'équilibre entre la prolifération et la différenciation repose en grande partie sur l'interaction entre les gènes cibles de la voie Notch et les gènes proneuraux. Ainsi, la différenciation neuronale s'accompagne d'une augmentation des niveaux de gènes proneuraux et d'une perte de l'activité Notch. Cependant, la coordination temporelle entre ces deux événements et l'intégration de la perte de la signalisation Notch au cours du processus de délamination permettant de préserver l'intégrité neuroépithéliale, restent largement méconnues.

J'ai étudié ces questions fondamentales en utilisant la moelle épinière embryonnaire de poulet comme modèle. Grâce à une lignée de poulet transgénique rapportrice pour la voie Notch, j'ai montré que la signalisation Notch, classiquement associée à un état indifférencié, reste active dans les futurs neurones jusqu'à leur délamination. Au cours de cette période transitoire, les futurs neurones réduisent rapidement leur surface apicale mais ne régulent que plus tard les niveaux de N-cadhérine. La perturbation de cette séquence à travers un blocage de la voie Notch affaiblit le réseau de jonctions apicales et conduit finalement à des brèches dans la paroi ventriculaire, ce qui suggère que l'activité de la voie Notch doit être maintenue dans les futurs neurones avant la délamination afin de préserver l'intégrité tissulaire. J'ai ensuite étudié les mécanismes régulant la signalisation Notch dans les futurs neurones. Mes données suggèrent que le ligand Notch Delta-like 1 (Dll1) favorise la différenciation en réduisant la signalisation Notch grâce à un mécanisme de cis-inhibition. Cependant, l'ubiquitine ligase Mindbomb1 (Mib1) bloque cette cis-inhibition pendant la période transitoire qui précède la délamination. Ceci maintient l'activité Notch et diffère la différenciation, ce qui permet aux neurones naissants de réduire leur surface apicale avant de délaminer de la surface ventriculaire. Ainsi, un juste équilibre entre la trans-activation et la cis-inhibition de la voie Notch est crucial afin de coordonner la différenciation et la délamination neuronales et ainsi préserver l'intégrité neuroépithéliale.

Mots-clés : neurogenèse, Notch, délamination neurale, cis-inhibition, Mindbomb1

Table of contents

PREFACE	11
INTRODUCTION	
CHAPTER I. CELL BIOLOGY OF VERTEBRATE NEUROGENESIS	15
I.1. EARLY MORPHOGENESIS OF THE NERVOUS SYSTEM	15
I.2. PATTERNING ALONG ANTEROPOSTERIOR AND DORSOVENTRAL AXES	18
<i>I.2.1. Anteroposterior patterning in the spinal cord</i>	<i>18</i>
<i>I.2.2. Dorsal-ventral patterning in the spinal cord</i>	<i>19</i>
I.3. NEURAL PROGENITOR CELLS.....	21
<i>I.3.1. Stem and progenitor cell.....</i>	<i>21</i>
<i>I.3.2. Classification of neural progenitors.....</i>	<i>21</i>
<i>I.3.3. Cellular features of neural progenitors</i>	<i>22</i>
I.4. MECHANISMS REGULATING CELL FATE DETERMINATION	25
<i>I.4.1. Different modes of division</i>	<i>26</i>
<i>I.4.2. Extrinsic factors</i>	<i>27</i>
<i>I.4.3. Cell cycle consideration.....</i>	<i>29</i>
<i>I.4.4. Asymmetric division and neurogenesis.....</i>	<i>31</i>
CHAPTER II. NEURAL PROGENITOR MAINTENANCE: THE ROLE OF NOTCH SIGNALING	47
II.1. A BRIEF HISTORY OF NOTCH	47
II.2. THE CORE ELEMENTS OF THE NOTCH PATHWAY.....	48
<i>II.2.1. Notch pathway overview.....</i>	<i>48</i>
<i>II.2.2. Mechanistic features of the Notch pathway.....</i>	<i>49</i>
II.3. NOTCH LIGAND UBIQUITYLATION	52
<i>II.3.1. Role of E3 ubiquitin ligases in Notch signaling</i>	<i>52</i>
<i>II.3.2. Role of the ligand endocytosis for Notch signaling</i>	<i>54</i>
II.4. THE CIS SIDE OF NOTCH SIGNALING	58
<i>II.4.1. Ligands as inhibitors of Notch signaling</i>	<i>58</i>
<i>II.4.2. Molecular interactions underlying cis-inhibition</i>	<i>63</i>
<i>II.4.3. Dll3, an exception to the rule.....</i>	<i>64</i>
II.5. NOTCH SIGNALING AND CELL CONTACTS	64
II.6. THE INTERPLAY BETWEEN NOTCH AND PRONEURAL GENES.....	66
<i>II.6.1. Notch signaling counteracts neurogenesis.....</i>	<i>66</i>
<i>II.6.2. Proneural genes promote neurogenesis</i>	<i>67</i>
<i>II.6.3. Notch signaling oscillations: a revised view of lateral inhibition.....</i>	<i>68</i>
<i>II.6.4. Making a difference: role of Mib1 and Dll1 for asymmetric Notch activation.....</i>	<i>70</i>
CHAPTER III. THE BIRTH OF A NEURON: NEURAL DELAMINATION	75
III.1. AN EXAMPLE OF DELAMINATION: THE NEURAL CREST EMT PROGRAM.....	75
III.2. THE IMPORTANCE OF ADHERENS JUNCTIONS IN NEURAL TUBE ARCHITECTURE	77
<i>III.2.1. N-cadherin based adherens junctions structure.....</i>	<i>77</i>
<i>III.2.2. Gain- and loss-of-functions of junctional proteins.....</i>	<i>79</i>

III.3. MECHANISMS REGULATING NEURAL DELAMINATION	80
III.3.1. <i>Transcriptional regulation initiating delamination: down-regulation of AJ</i>	80
III.3.2. <i>Cellular remodeling: apical abscission and role of the centrosome</i>	83
SCIENTIFIC QUESTIONS AND OBJECTIVES OF THE PROJECT	87
CHAPTER IV. MATERIAL AND METHODS	91
IV.1. MIB1 PREVENTS <i>CIS</i> -INHIBITION TO DEFER DIFFERENTIATION AND PRESERVE NEUROEPITHELIAL INTEGRITY DURING NEURAL DELAMINATION	91
IV.2. PERSPECTIVES AND ON-GOING PROJECT	91
<i>Maintenance and differentiation of mouse ESCs</i>	91
<i>CRISPR-Cas9 and donor vector generation</i>	92
<i>Generation of Mib1-GFP knock-in ESC line</i>	93
<i>Immunohistochemistry</i>	93
<i>Image acquisition and processing</i>	94
CHAPTER V. RESULTS AND DISCUSSION	97
V.1. MIB1 PREVENTS NOTCH <i>CIS</i> -INHIBITION TO DEFER DIFFERENTIATION AND PRESERVE NEUROEPITHELIAL INTEGRITY DURING NEURAL DELAMINATION	97
V.2. DISCUSSION	135
V.2.1. <i>From cell cycle exit to neural delamination</i>	135
V.2.2. <i>Notch trans-activation and cis-inhibition balance during differentiation</i>	141
V.2.3. <i>Notch beyond neurogenesis in development and disease</i>	148
CHAPTER VI. PERSPECTIVES AND ON-GOING PROJECT	155
VI.1. INTRODUCTION AND AIMS OF THE PROJECT	155
VI.1.1. <i>Background</i>	155
VI.1.2. <i>Scientific objectives</i>	156
VI.2. PRELIMINARY RESULTS AND PERSPECTIVES	157
VI.2.1. <i>Experimental system: mESC-derived neural rosettes</i>	157
VI.2.2. <i>Mib1 dynamics over the course of differentiation</i>	162
VI.2.3. <i>Mib1 and Dll1 cooperation for Notch signaling regulation</i>	164
GENERAL CONCLUSION	165
ANNEX.....	167
BIBLIOGRAPHY.....	193

Table of figures

Figure 1. Neural tube formation in the chick embryo.....	16
Figure 2. Formation of brain vesicles.	17
Figure 3. Dorsoventral patterning of the spinal cord.	20
Figure 4. Neural progenitor architecture.....	22
Figure 5. Interkinetic nuclear migration (IKNM).	25
Figure 6. Spindle orientation and asymmetric division.	33
Figure 7. Centrosome asymmetry.	40
Figure 8. Notch signaling pathway.	49
Figure 9. Structural domains of Dll1 ligand and Notch1 receptor.....	51
Figure 10. Domain organization of Mib1.	53
Figure 11. Schematic of proposed two models for ubiquitin ligase-dependent ligand endocytosis.	56
Figure 12. Notch trans-activation and cis-inhibition.	58
Figure 13. Cis-interactions in cell culture assay.	60
Figure 14. Cis-inhibition in <i>Drosophila</i> ommatidia.	62
Figure 15. Oscillatory expression of Hes1.....	69
Figure 16. Structure of adherens junction in neural progenitors.	79
Figure 17. Proposed model of genetic pathway driving neural delamination.	83
Figure 18. Summary of cell morphological changes in the apical endfoot during neural delamination.....	85
Figure 19. Schematic representation of the differentiation protocol timeline.	92
Figure 20. Design of Mib1 targeting.....	93
Figure 21. Shroom3-mediated apical constriction.	138
Figure 22. Mib1 is expressed in the Golgi apparatus in neurons.....	144
Figure 23. P-p38 expression profile.....	146
Figure 24. Effects of gain- and loss- of p38 function on neurogenesis.	147
Figure 25. Proposed model of p38 MAPK activation pathway during neural differentiation.....	148
Figure 26. Temporal progression of neurogenesis in ESC-derived neural rosettes culture system.	159
Figure 27. ESC-derived neural rosettes display apical-basal polarity and undergo IKNM.....	161
Figure 28. Mib1 expression in ESCs and ESC-derived neural rosettes.....	163

Table of abbreviations

AJ	adherens junction
ANK	ankyrin repeats
aRG	apical radial glia
bHLH	basic helix-loop-helix
BMP	bone morphogenetic protein
bRG	basal radial glia
CDK	cyclin dependent kinase
ChIP	chromatin immunoprecipitation
CRD	cystein-rich domain
CSF	cerebrospinal fluid
CSL	CBF1-Suppressor of Hairless-LAG1; also known as RBP-Jk
Dll1	Delta-like 1
DOS	Delta and OSM-11-like proteins domain
DSL	Delta-Serrate-LAG2
E	embryonic day
ECD	extracellular domain
EGF	epidermal growth factor
EMT	epithelial-to-mesenchymal transition
ESC	embryonic stem cell
FGF	fibroblast growth factor
Foxp	forkhead transcription factors
GMC	ganglion mother cell
hae	hour after electroporation
HD	heterodimerization domain
Hes	homologs of <i>Drosophila</i> Hairy and Enhancer of split
HH	Hamburger-Hamilton stage
IKNM	interkinetic nuclear migration
IP	intermediate progenitor
ICD	intracellular domain
LNR	Lin12-Notch repeats
Maml	Mastermind-like
MAPK	mitogen-activated protein kinase
MCPH	primary recessive microcephaly in humans
MEF	mouse embryonic fibroblast
Mib1	Mindbomb1
MLC	myosin regulatory light chain
MN	motor neuron
mtROS	mitochondrial reactive oxygen species
MZ	mantle zone

NCC	neural crest cell
NECD	Notch extracellular domain
Neur	Neuralized
Neurog2	Neurogenin 2
NICD	Notch intracellular domain
NLS	nuclear localization signal
NRR	negative regulatory region
NT	neural tube
PDZ	PSD-95/Dlg/ZO1 motif
PEST	proline/glutamic acid/serine/threonine residues-rich motif
PKA	protein kinase A
pMLC	phosphorylated myosin regulatory light chain
pMN	motor neuron progenitor
RA	retinoic acid
RAM	RBP-Jk associated molecule
RG	radial glia
RMS	rhabdomyosarcoma
ROCK	Rho kinase
ROS	reactive oxygen species
Shh	Sonic hedgehog
SOP	sensory organ precursor
SSA	spindle size asymmetry
T-ALL	T-cell acute lymphoblastic leukemia
TAD	transactivation domain
TMD	transmembrane domain
Ub	ubiquitin
VE-cadherin	vascular endothelial cadherin
VZ	ventricular zone
ZO1	zonula occludens 1

Preface

Building the central nervous system implicates an initial phase of massive expansion of the progenitor pool followed by the production of a vast array of neuronal and glial cell types that must be generated in the correct numbers and at appropriate timings. Premature exit from the progenitor state would lead to precocious differentiation, leading to the appearance of neurodevelopmental disorders. Therefore, the initiation of differentiation must be held until the right time has come. Then, progenitors start their neuronal differentiation program, which coordinates cell cycle withdrawal, neural delamination and acquisition of terminal differentiation markers.

The first three chapters of this manuscript provide an introduction and overview of key concepts that are relevant for this thesis. The first chapter describes the mechanisms of cell fate acquisition during vertebrate neurogenesis; the second one is focused on the role and mechanisms of the Notch signaling pathway; and finally the third chapter introduces the current knowledge on a particular cellular remodeling undergone by the nascent neuron, the neural delamination process.

I

INTRODUCTION

CELL BIOLOGY OF VERTEBRATE NEUROGENESIS

Chapter I.

Cell Biology Of Vertebrate Neurogenesis

During development, nerve cells acquire specific neuronal identities and establish connections with one another under the influence of the extrinsic and intrinsic cues. The human brain is the assemblage of more than 10^{11} neurons and perhaps ten times that many glial cells and an almost uncountable number of synapses (Noctor et al., 2007). The balance between proliferation of neural progenitor cells and differentiation into neurons and glial cells must be regulated in a very precise spatiotemporal way in the embryo, to create the proper architecture of a fully functional nervous system in the adult. Various studies in invertebrate and vertebrate models have been performed to elucidate many common neurodevelopmental mechanisms. Dissecting those at the cellular and molecular level is at the basis of uncovering the etiology and proposing treatment for human neurodevelopmental disorders.

In this chapter, I will intend to provide an overview of the events regulating the generation of the vertebrate central nervous system, starting with the induction of the neuroectoderm and early neural morphogenesis. Then, I will briefly describe what qualifies a cell as a neural progenitor cell as well as some of their cell biological features. I will end by giving a special emphasis on the signals that instruct undifferentiated cycling neural progenitors to commit to fully differentiated neurons.

I.1. Early morphogenesis of the nervous system

The vertebrate central nervous system emerges from the neuroectoderm. During gastrulation, the most outer germ layer – the ectoderm – is under the influence of neuralizing signals secreted from a dorsal organizing center. This particular region of the gastrula, called the Spemann organizer in amphibian eggs, the Hensen's node in chick and the node in mammalian embryos, releases a cocktail of BMP (Bone Morphogenetic Protein) inhibitors, which promote neural fate rather than epidermal fate. This process of specifying neural tissue by inhibiting BMP signaling is referred to as the classical 'default model' (Stern, 2005). Nevertheless, it should be noted that neural induction is a more complex process than once thought and cannot be fully explained by the 'default model' on its own. As such, neural induction also requires FGF

(fibroblast growth factor) signaling and Wnt inhibition to induce neural fate (Stern, 2005). Finally, under the influence of neuralizing signals, the neural plate is formed.

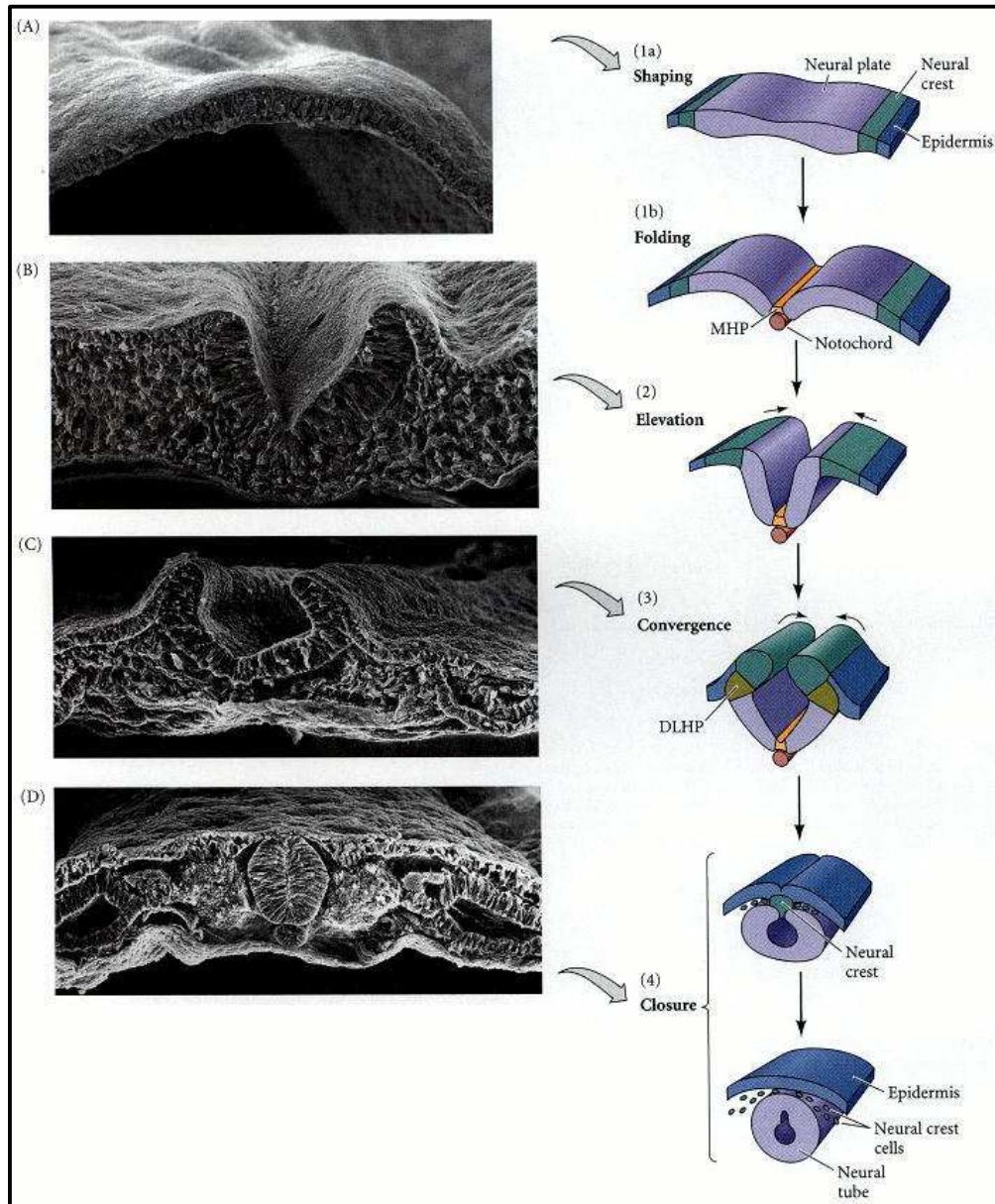


Figure 1. Neural tube formation in the chick embryo.

(A-D) Scanning electron micrographs of neural tube formation. (A, 1) Elongation and folding of the neural plate: folding begins as the medial hinge point (MHP) cells anchor to the notochord and change their shape. (B, 2) The neural folds are elevated. (C, 3) Convergence of the neural folds occurs as the cells at the dorsolateral hinge point (DLHP) become wedge-shaped and the epidermal cells push toward the center. (D, 4) Closure of the neural tube: the neural folds are brought together at the dorsal midline, while the neural crest cells disperse and migrate away. From *Developmental Biology*, 9e edition, Scott F. Gilbert (2010).

The neural plate is a sheet of elongated neuroectodermal cells from which the whole nervous system derives. The neural tube (NT) formation is a complex phenomenon that begins shortly after the neural plate has formed. The edges of the neural plate thicken and move upward to give rise to neural folds. Then the lateral sides of the neural plate migrate toward the midline of the embryo and finally fuse to generate the NT with a central lumen (Figure 1) (Gilbert, 2013).

The NT, precursor of the central nervous system, is composed of a monolayer of polarized and pseudostratified neuroepithelial cells, called the neuroepithelium. During development, the NT undergoes a series of morphogenetic events along both the anteroposterior and dorsoventral axes, to give rise to different structures building the central nervous system. The most anterior portion of the NT corresponds to the prospective brain. At the beginning, the NT balloons into three primary vesicles: the forebrain (prosencephalon), midbrain (mesencephalon), and hindbrain (rhombencephalon). Later, the forebrain becomes subdivided into the telencephalon and diencephalon, while the hindbrain becomes the metencephalon and myelencephalon, thus giving rise to a total of five secondary vesicles (Figure 2). On the other hand, the most posterior portion of the NT retains its straight structure and forms the spinal cord (Gilbert, 2013).

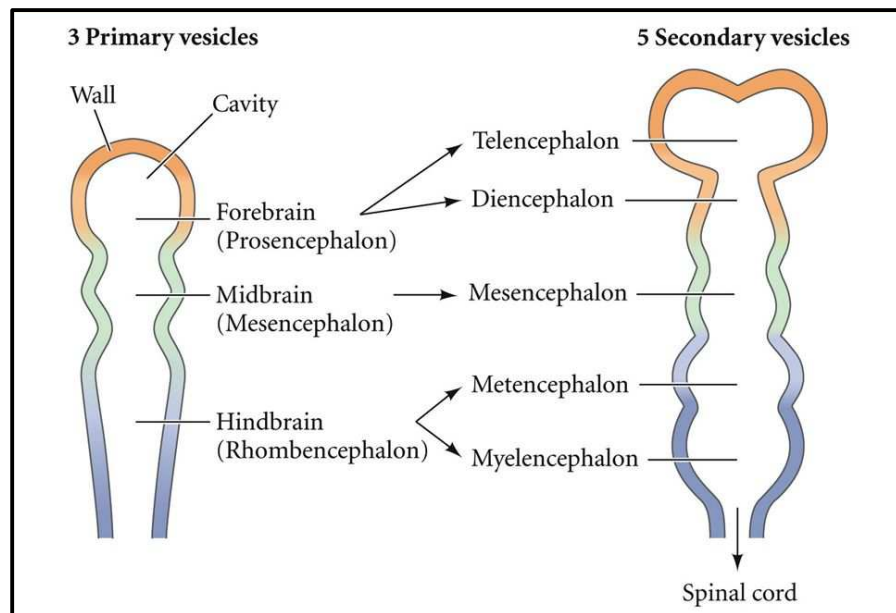


Figure 2. Formation of brain vesicles.

From *Developmental Biology*, 9e edition, Scott F. Gilbert (2010).

I.2. Patterning along anteroposterior and dorsoventral axes

The vertebrate nervous system is made of multiple structures that arise from the single NT. As development proceeds, neural progenitors located in the NT come under the influence of secreted factors that provide positional information, inducing the expression of specific transcription factors which combination defines neural subtype identity. Most of the pioneering work that has identified the mechanisms regulating NT patterning has been done in the spinal cord and is relatively well described. I will thus make a general introduction and expose very briefly these processes in this particular structure.

I.2.1. Anteroposterior patterning in the spinal cord

The developing spinal cord contains a multitude of neuronal subtypes that must differentiate at their correct positions with regard to the anteroposterior axis of the NT. This specific anteroposterior patterning is closely linked to the correct formation of neuronal circuits. As such, the cell bodies of motor neurons residing in the spinal cord form discrete columns at distinct positions along the anteroposterior axis, with particular axon projections and selective connections with target muscle cells (Dasen and Jessell, 2009).

The anteroposterior patterning of the spinal cord is regulated by a combination of morphogens among which the fibroblast growth factor (FGF) and the retinoic acid (RA) signaling. FGF is expressed in the presomitic mesoderm and maintains the undifferentiated state, while RA is expressed in the paraxial mesoderm and inhibits FGF signaling while inducing differentiation (reviewed in(Diez Del Corral and Morales, 2017; Diez del Corral and Storey, 2004)). Opposing gradients of FGF and RA establish a specific patterning of *Hox* genes along the anteroposterior axis. *Hox* genes (homeotic family genes) are transcription factors that were first characterized in *Drosophila* and were found highly conserved among animals. Cell transplantation, gene knockout or gene misexpression assays performed in zebrafish, chick and rodents indicate that *Hox* genes act as patterning master genes to create structures appropriate to particular anteroposterior positions (reviewed in(Philippidou and Dasen, 2013)). The patterned expression of *Hox* genes in response to FGF and RA signaling determines the fate of each segment of the spinal cord: cervical, thoracic, lumbar and sacral.

I.2.2. Dorsoventral patterning in the spinal cord

The NT is polarized not only along its anteroposterior axis, but also along the dorsoventral axis. In the spinal cord, the dorsal and intermediate regions receive inputs from sensory neurons located in the dorsal root ganglion, whereas the ventral region is where motor neurons reside. Anatomically, a longitudinal groove, called the *sulcus limitans*, separates the spinal cord into dorsal and ventral halves. This developmental anatomy generates the basis of spinal cord physiology (e.g. the reflex arch).

The ventral pattern is imposed in large part by a signaling protein called Sonic hedgehog (Shh). Shh is initially produced and secreted by the notocord lying just ventral to the NT. Within the NT, at the most ventral part, cells receiving higher levels of Shh become floor plate cells, which produce and secrete Shh on their own, therefore becoming a second signaling center. In consequence, a ventrodorsal gradient of Shh is established and induces ventral cell fates (motor neurons and ventral interneurons) while inhibiting dorsal cell fates (reviewed in(Dessaud et al., 2008; Jessell, 2000)). In parallel, the most dorsal cells of the NT (the roof plate cells) secrete BMP and Wnt family members. As a result, a dorsoventral gradient of BMP/Wnt is established and induces dorsal cell fates (neural crest and dorsal interneurons) while inhibiting ventral cell fates (reviewed in(Le Dreau and Marti, 2013)).

As a consequence of two opposing morphogenic gradients, the fate of a particular cell depends on its exposure to different concentration of the signaling molecule, which in turn depends on its distance to the signaling centers. In response to it, two classes of transcription factors are synthesized: (1) the expression of Class I (Pax6, Pax7, Irx3, Dbx1, Dbx2) genes is repressed by Shh and activated by BMP/Wnt; while (2) the expression of Class II (Nkx6.1, Nkx6.2, Olig2, Nkx2.2, Nkx2.9) is activated by Shh and repressed by BMP/Wnt. Cross repression of Class I and Class II genes generates specific boundaries between dorsoventral domains of the spinal cord, identified by a specific transcriptional code that instructs the final identity of their progeny (reviewed in(Le Dreau and Marti, 2013; Ulloa and Briscoe, 2007)). Thus, the developing spinal cord is divided into 11 discrete domains:

- five ventral domains of neural progenitors and the corresponding differentiated neurons (from ventral to dorsal, v3, MN, v2-0)
- six dorsal domains of neural progenitors and the corresponding differentiated neurons (from dorsal to ventral, dI1-6)

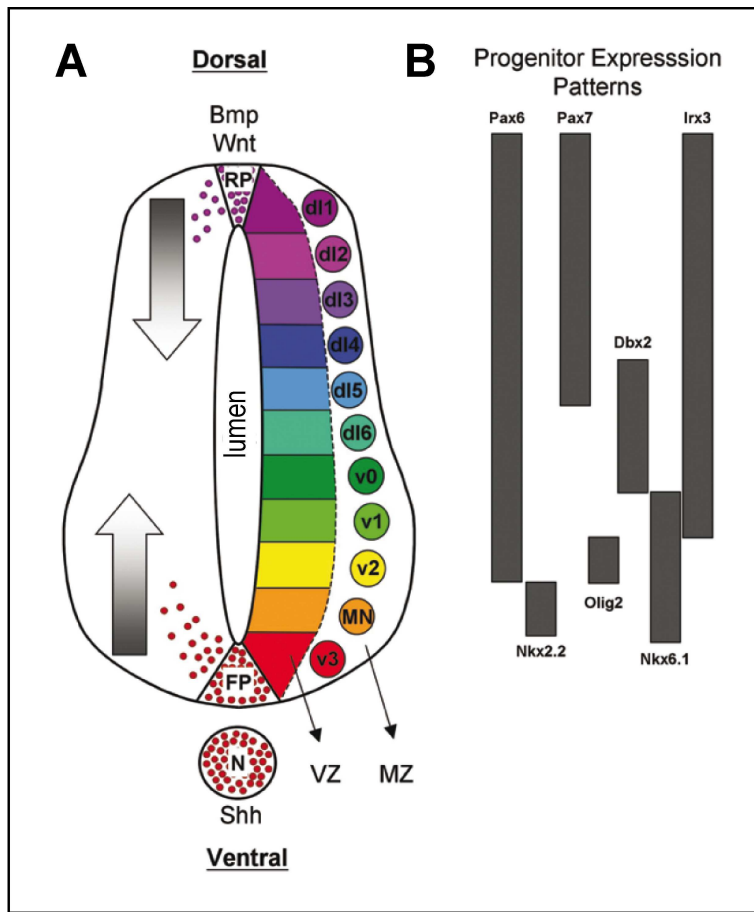


Figure 3. Dorsoventral patterning of the spinal cord.

(A) Schematic representation of a section of the spinal cord. Progenitors are located medially adjacent to the lumen in a region known as the ventricular zone (VZ). Post-mitotic differentiated neurons are located laterally in a region known as the mantle zone (MZ). Distinct neural subtypes are generated from different domains of progenitors along the dorsoventral axis, depending on the action of counteracting gradients of BMP/Wnt and Shh. RP, roof plate; FP, floor plate; N, notochord. (B) Along the dorsoventral axis, progenitors express different combinations of transcription factors (not all represented in this diagram). From Ulloa and Briscoe, 2007.

I.3. Neural progenitor cells

I.3.1. Stem and progenitor cell

Two criteria are generally used to define stem cells: (1) their unlimited self-renewal capacity and (2) their multipotency – potential to generate all cell types of a given lineage (Gotz and Huttner, 2005). The term ‘neural stem cell’ is often used to define cycling cells of the developing NT that divide several times but not necessarily for an unlimited number and that give rise to at least one type of cell (unipotent or multipotent). Those cells do not meet the two criteria of stem cell cited above, since they have a limited capacity of self-renewing and a limited differentiation potential. Thus, a more exact term to use would be a ‘neural progenitor cell’.

I.3.2. Classification of neural progenitors

The wall of the NT is initially composed of a single layer of dividing cells, called neuroepithelial cells, which are the neural progenitor cells that generate all of the neuronal and glial cell types of the adult central nervous system. How the size of an organ is determined is a fundamental question in biology. In the case of the mammalian brain, the evolution of cerebral cortex size expansion is considered to be a critical determinant for higher cognitive function. The size of the neocortex – the outer covering of the cerebral hemispheres – is predominantly due to differences in neuronal and glial cell number during development. One can think of several ways to increase the quantity of cells produced: (1) increase the length of the production period; (2) increase the number of cells produced per time unit through increased number of proliferative cell cycles; or (3) the appearance of “intermediate” transit-amplifying progenitor types. Indeed, number of studies has contributed to uncover additional types of cortical neural progenitors classified in many groups based on several criteria: the location of mitosis (apical versus basal), their morphology (monopolar versus bipolar) and their proliferative potential (one versus multiple rounds of division) (reviewed in(Florio and Huttner, 2014; Taverna et al., 2014)).

However, in the spinal cord, the existence of such diversity of neural progenitor cell morphology has not been reported. During development, the spinal cord is only composed of cycling cells called neuroepithelial cells forming a monolayered and pseudostratified neuroepithelium. Neuroepithelial cells are polarized along their apical-basal axis and occupy the entire length of the neuroepithelium, with thin processes extending both to the apical and basal

sides of the NT. Progenitors located in the spinal cord offer this advantage of being a relatively simple and homogenous population giving birth to only two different types of daughter cells: a progenitor or a neuron. This property makes this system a suitable model to study mechanisms regulating cell fate decision as well as their cellular behavior during neuronal differentiation. As my thesis work was performed for the most part in the chick spinal cord, I will simply use the term ‘neural progenitor’ or ‘neuroepithelial cell’.

I.3.3. Cellular features of neural progenitors

Neuroepithelial cells display a characteristic morphology: most of the cell volume is occupied by the nucleus while the cytoplasm is reduced to very thin apical and basal processes, exposed to the lumen at the ventricular surface and anchored to the basal lamina at the opposite side. During their cell cycle, their nuclei move between the apical and basal ends, a phenomenon called interkinetic nuclear migration (IKNM).

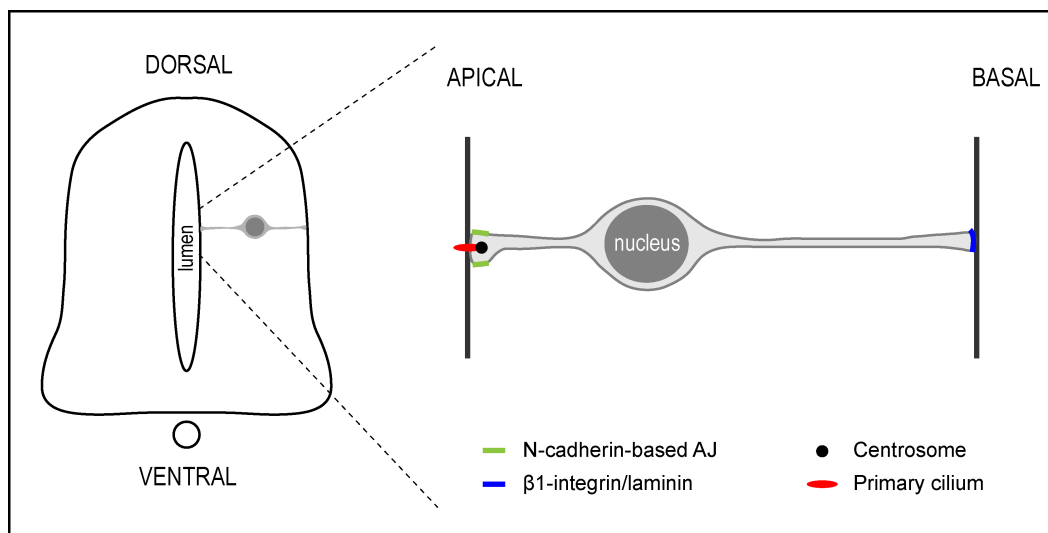


Figure 4. Neural progenitor architecture.

Left-Schematic transverse section of the spinal cord. Right-Neural progenitors have apical and basal attachments that link them to the lumen and to the basal lamina, respectively. At the apical side, they bear a primary cilium and the centrosome.

I.3.3.1. Apical domain

The apical domain of neuroepithelial cells is composed of apical plasma membrane and apical junctional complexes. The apical plasma membrane represents a very small portion (1-2%)

of total plasma membrane and bears the primary cilium (Figure 4). The apical endfoot of each neuroepithelial cell faces the ventricle of the NT so that the juxtaposition of all apical plasma membranes of all neuroepithelial cells forms together the apical/ventricular surface of the NT. The lumen of the NT is filled with the cerebrospinal fluid (CSF) and contains signaling molecules including FGF, Shh, RA, BMP and Wnt, therefore making the apical endfoot an important player in the course of neurodevelopment.

Adherens junctions (AJs) delimit the apical domain and ensure the cohesion between neuroepithelial cells at the ventricular surface. They are composed of N-cadherin protein associated with actin-myosin cables and the microtubule network. During early stages of neural development, the NT undergoes a dynamic remodeling of cellular junctions. Indeed, before the onset of neurogenesis, neuroepithelial cells are attached to each other through adherens and tight junctions. However, as neurogenesis proceeds, the expression of tight junction proteins decreases except that of ZO1 (zonula occludens 1), which associates with N-cadherin-based AJ (Aakusaraste et al., 1996). The apical domain of neuroepithelial cells also contains the apical polarity proteins Par3/aPKC/Par6 complex. More precisely, in the chick spinal cord, Par3 is present slightly more basally to aPKC/Par6 while N-cadherin-based AJ colocalizes with Par3 (Afonso and Henrique, 2006). Moreover, in the apical region is found the centrosome from which nucleates the primary cilium (Figure 4). Those apical junctional complexes play crucial roles in establishing and maintaining cell polarity as well as maintaining the progenitor identity (Miyamoto et al., 2015; Zhang et al., 2010) (and see chapter III).

I.3.3.2. Basal process

The basal process of neuroepithelial cells is the very thin basolateral plasma membrane that traverses the differentiated zone and reaches the basal lamina, where it is anchored with its basal endfoot, through $\alpha 2$ and $\alpha 4$ laminins as well as $\beta 1$ integrin (Figure 4). Historically, the basal process of radial glial cells was thought to serve only as a scaffold for neuron migration (Misson et al., 1991; Rakic, 1971), but nowadays it is regarded as an active subcellular compartment important for signaling and fate determination. This particular property will be further discussed in section I.4.

I.3.3.3 Cell cycle dynamics

A hallmark of neuroepithelial cells is the migration of the nucleus in concert with the cell cycle – a process termed interkinetic nuclear migration (IKNM) (Sauer, 1935). In the spinal cord, contrary to the cerebral cortex, mitosis occurs exclusively at the ventricular surface. Cell nuclei move back and forth along the apical-basal axis, undergoing mitosis at the apical side, and returning back to the basal side during G1 phase. There, cells enter S-phase and move towards the apical side during G2 phase (Figure 5). This particular rhythmic movement of cell nuclei confers the apparent pseudostratified structure of the neuroepithelium, with cell nuclei occupying different positions all along the width of the neural tube. Although IKNM is not a recently discovered process, the origin of the molecular forces driving the migration during G1 and G2 phases remains controversial (reviewed in(Spear and Erickson, 2012)). Microtubule and actin-myosin networks are believed to be at the basis of the molecular machinery of the basal-to-apical movement of nuclei in G2 phase. In particular, according to many studies, it is now well accepted that the microtubule-based dynein motor system is the major driving force of the nuclei during G2 phase (Tsai et al., 2010). Disrupting the activity of the dyneins regulator Lis1, NudC or dynactin, interferes with the IKNM progression (Cappello et al., 2011; Del Bene et al., 2008; Tsai et al., 2005). In addition, some centrosomal proteins such as Cep120, TACC, Hook3 and PCM1 (Ge et al., 2010; Xie et al., 2007) have also been suggested to be necessary for the basal-to-apical nuclear migration. On the other hand, the mechanisms underlying apical-to-basal movement in G1 phase are more controversial and several models have been proposed. Some studies propose that nuclei are driven along microtubules via kinesin3 (Tsai et al., 2010) or along the actin-myosin cytoskeleton (Schenk et al., 2009), while others suggest that this movement is passive. Indeed, magnetic beads implemented in neural progenitor nuclei were observed to migrate basally, whereas when the apical nuclear migration of neighboring cells is blocked in S-phase, beads fail to move towards the basal side, suggesting that the basal movement is passively driven by active apical nuclear migration of surrounding cells (Kosodo et al., 2011).

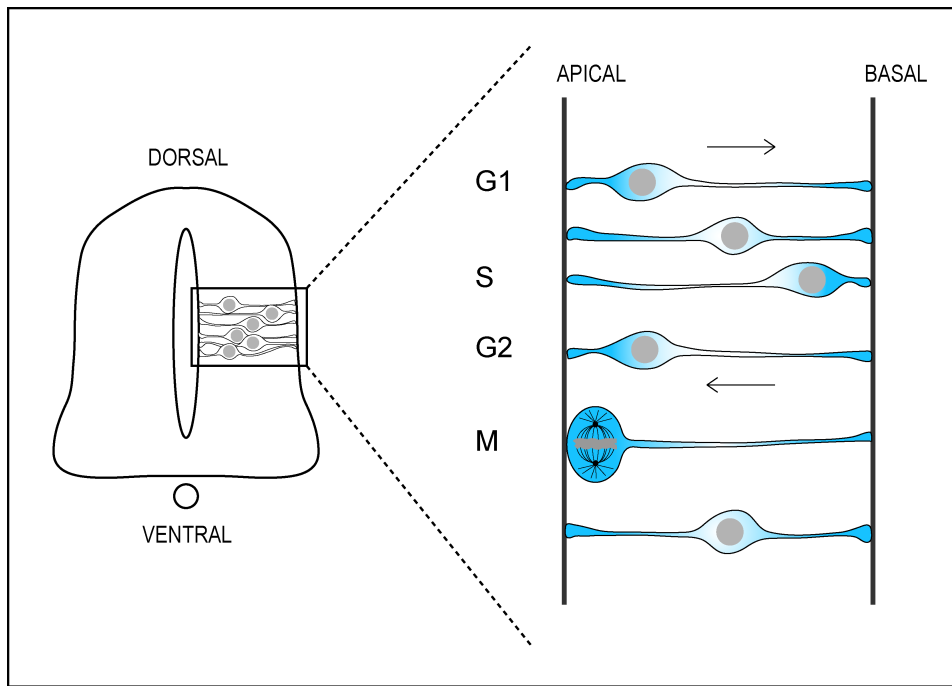


Figure 5. Interkinetic nuclear migration (IKNM).

Nuclei of neural progenitors transit along the apical-basal axis during their cell cycle, with S-phase occurring at the basal side and M-phase occurring at the apical side.

A major question is to determine the role of this particular IKNM. Several reasons have been proposed: one would be to allow more cells to be packed in the limited space of the NT while restricting mitoses to the ventricular surface (Taverna and Huttner, 2010). Another hypothesis would be to differentially expose cell nuclei to signals present all along an apical-basal gradient, therefore linking the IKNM to cell fate determination (see section I.4.3.2.).

I.4. Mechanisms regulating cell fate determination

Neural progenitors undergo several cell cycles to expand their initial pool before starting to produce neurons through asymmetric neurogenic divisions, and eventually symmetric terminal divisions. Cellular features of neural progenitors, including apical and basal components, cell cycle kinetics, but also other extrinsic and intrinsic events contribute to the cell fate decision and control the balance between proliferation and differentiation.

I.4.1. Different modes of division

Different analyses showed the existence of symmetric and asymmetric modes of division, first in lineage-tracing experiments using retroviruses (Gray et al., 1988; Luskin et al., 1988; Price and Thurlow, 1988), then in live-imaging observations of brain slices cultures (Miyata et al., 2004; Miyata et al., 2002; Noctor et al., 2001) and isolated cells *in vitro* (Qian et al., 2000; Shen et al., 2002).

In the spinal cord, progenitors sequentially go through three different modes of divisions (Morin et al., 2007; Wilcock et al., 2007):

- symmetric proliferative divisions: one neural progenitor cell (P) divides into two new neural progenitor cells (P-P divisions). These divisions are the first to appear in the developing NT, and allow progenitor cells to increase their number exponentially.
- asymmetric neurogenic divisions: one neural progenitor cell (P) divides into two distinct cell types, one neural progenitor cell (P) and one differentiated post-mitotic neuron (N) (P-N divisions).
- symmetric terminal divisions: one neural progenitor cell (P) divides into two neurons (N) (N-N divisions). These divisions generally start at later stages. Still, in the chick NT, the first N-N divisions appear at relatively early stages (Wilcock et al., 2007).

It is important to note that those different modes of division are largely overlapping over the course of the neural tube development (Le Dreau et al., 2014; Saade et al., 2013).

When to switch the mode of division and accordingly the balance between proliferation and differentiation must be specifically determined in order to avoid precocious neuronal differentiation and loss of late-born neurons, or conversely an abnormal growth and impaired differentiation, both situations leading to various neurodevelopmental disorders (reviewed in (Lui et al., 2011; Peyre and Morin, 2012; Thornton and Woods, 2009)). What are the molecular mechanisms determining the mode of division of neural progenitor cells?

We can consider two main sources of information to produce either symmetric or asymmetric outcomes:

- extrinsic factors influencing either the identity of the mother cell before division or the fate decision of the daughter cells after division. These signals are coming from the extracellular environment.
- intrinsic factors established in the mother cell before division such as cell cycle parameters, a/symmetric segregation of fate determinant molecules or cellular components. In the context of

asymmetric cell division, fate determinants can be defined as molecules present in the mother cell before division, distributed asymmetrically during mitosis and inherited unequally by the two daughter cells where they regulate fate choices.

Those different mechanisms are not mutually exclusive and none is sufficient on its own. Instead, cell fate decision derives from a combination of different factors that act in parallel or within a same signaling pathway. Furthermore, those processes differ depending on which species, developmental stage or region of the nervous system is considered.

I.4.2. Extrinsic factors

During spinal cord development, the so-called morphogens influence the patterning of neural progenitors along the anterior-posterior and dorsal-ventral axis: FGF/RA gradient establishes the anteroposterior patterning while the dorsoventral patterning is controlled by Wnt and BMP diffusing from dorsal sources and Shh emanating from ventral sources. These molecules induce specification of different neural subtypes depending on their concentration and/or duration of exposure (see section I.2). Nevertheless, they were also shown to have an impact on the mode of division, by their ability to (1) promote growth and cell survival and to (2) influence the switch of the mode of division. However, as mentioned earlier, in the spinal cord, neural progenitors are elongated cells polarized along the apical-basal axis with apical and basal processes reaching the ventricular surface and the basal lamina, respectively. Thus, it is difficult to imagine that morphogens present homogeneously in the extracellular space could be involved in a binary decision process between two daughter cells. Rather, they are likely to play a role at the level of the mother cell by giving a temporal instruction and to be correlated with the general progression of neurogenesis to help the immature neural tissue acquiring the competence to differentiate.

I.4.2.1. Factors promoting cell survival and proliferation

First, several lines of evidences show that those molecules control proliferation. Early during nervous system development, the presumptive spinal cord grows along an anterior-posterior sequence in parallel to the body axis extension. The caudal growth of the NT relies on the activity of a caudally moving stem zone, which is under the influence of FGF signals emanating from the presomitic mesoderm and the primitive streak. FGF signaling promotes proliferation while inhibiting the expression of several factors that are later induced in neural

progenitors (Diez del Corral and Storey, 2004). With the growth of the tissue, neural precursors are relatively more distant from the signal source, thus escaping FGF signals and falling under the influence of RA provided anteriorly by the somites. Under the cross-repression of FGF and RA signals, cells leaving the caudal stem zone start to enter a transition zone and switch from a proliferative undifferentiated state to a more mature neural progenitor state, by expressing the transcription factor Pax6 or the bHLH protein Olig2 and proneural genes. Thus, FGF signaling is initially important to establish the population of neural progenitor cells possessing the competence to differentiate into neurons (Diez del Corral et al., 2003; Ribes et al., 2009).

Wnt signaling has also been shown to promote proliferation by positively regulating cell cycle progression. In the spinal cord, Wnt1 and Wnt3a were shown to promote proliferation by up-regulating cyclin D1 and cyclin D2 transcription thereby promoting G1/S transition (Megason and McMahon, 2002). Moreover, disruption of Wnt activity by overexpressing a dominant-negative Tcf4 in chick spinal cord or analysis of β -catenin deficient mouse embryos show reduction of proliferation and increase of differentiation (Megason and McMahon, 2002; Zechner et al., 2003). On the other hand, Shh signaling controls proliferation by regulating cyclin D1 expression, therefore G1 progression, but also G2 phase progression by controlling late cyclin expression including cyclin A and cyclin B and the G2/M transition regulator CDC25B (Alvarez-Medina et al., 2009). In the developing NT, Wnt is secreted dorsally by the roof plate cells while Shh is secreted ventrally by the floor plate cells. Thus, the way they control the actual growth of the NT in respect to the dorsoventral axis still needs to be clarified.

I.4.2.2. Factors influencing the switch of the division mode

Recently, taking advantage of a combination of reporters to identify P-P, P-N and N-N divisions, the group of Elisa Marti has shown that Shh and BMP affect the progression of the division mode in the chick spinal cord (Le Dreau et al., 2014; Saade et al., 2013). To determine the three modes of division, they used a combination of Sox2 and Tis21 enhancers driving the expression GFP and RFP, respectively. Sox2-GFP⁺/Tis21-RFP⁻, Sox2-GFP⁺/Tis21-RFP⁺, and Sox2-GFP⁻/Tis21-RFP⁺ mitotic cells undergo P-P, P-N, and N-N modes of division, respectively. Electroporation of these reporters in the chick NT show that Shh and BMP signaling pathways promote proliferative P-P divisions at the expense of terminal N-N divisions (Le Dreau et al., 2014; Saade et al., 2013). More precisely, maintaining Shh activity high by electroporating a dominant active form of Smoothed receptor promotes P-P divisions and prevents neurogenic

divisions (P-N and N-N), while reducing Shh activity with a dominant negative form of Patched1 receptor increases N-N divisions at the expense of P-P divisions (Saade et al., 2013). Along the same line, in the dorsal spinal cord, they were able to show that different levels of the BMP effectors SMAD1/5 activity are correlated with different modes of division: high, intermediate and low SMAD activity is linked with P-P, P-N and N-N divisions, respectively (Le Dreau et al., 2014).

Taken together, these signaling molecules not only control the patterning of the developing the spinal cord, but also play important roles in maintaining cells in a proliferative state while controlling the switch of the division mode. However, as previously mentioned, those morphogens coming from the extracellular space are not likely to directly instruct fate decision between two sister cells during asymmetric divisions. Rather, the combination of morphogens present in the NT may provide a basal level of mitogenic signals promoting cell survival and proliferation at the initial phase of NT development, while their progressive decrease could instruct the temporal progression of PP-PN-NN modes of division.

I.4.3. Cell cycle consideration

I.4.3.1. Cell cycle length

Changes to the cell cycle length have been proposed to control cell fate decisions (reviewed in(Agius et al., 2015; Dehay and Kennedy, 2007)). First proposed in the mouse developing brain, where authors described a lengthening of the cell cycle, particularly of the G1 phase, concomitantly with the switch from proliferative to neurogenic divisions (Takahashi et al., 1995), many studies further suggested a link between the length of the cell cycle and the progression of neurogenesis. Taking advantage of a Tis21-GFP knock-in mouse embryos to discriminate between proliferative and neurogenic divisions, Calegari and colleagues showed that at the onset of neurogenesis, neural progenitors of the developing cortex have a longer cell cycle, mainly due to a lengthening of the G1 phase (Calegari et al., 2005; Calegari and Huttner, 2003). This lengthening seems to be a cause rather than a consequence of the progression toward neurogenic fates. Indeed, in the developing mouse cortex, the forced reduction of G1 length via cyclinD1, cyclinE or CDK4/cyclinD1 heterodimer *in utero* electroporation, promotes expansion of the progenitor pool while inhibiting neuronal differentiation. Conversely, lengthening the G1

phase by interfering with the CDK4/cyclinD1 function leads to the opposite effect (Calegari and Huttner, 2003; Lange et al., 2009; Pilaz et al., 2009). Another study also performed in mouse developing cortex compared apical radial glia (aRG) and a more committed progenitor population, basal intermediate progenitors (bIPs) and noticed that bIPs have a longer G1 phase than aRG, consistent with the more committed state of bIPs (Arai et al., 2011).

Despite the overall shortening of cell cycle length, proliferative progenitors were found to have a longer S phase than neurogenic progenitors, suggesting that careful DNA replication takes place during the proliferative phase. One may speculate that a higher fidelity of DNA replication is needed in proliferative phase to avoid replication errors to be passed on the progeny, while the lack of DNA correction and therefore the occurrence of somatic mutations may be a means of increasing neuronal diversity (Arai et al., 2011).

However, neural progenitors of the chick developing spinal cord display a different cell cycle length profile: progenitor cells in the neurogenic phase (HH24, (Hamburger and Hamilton, 1992)) have a shorter total cell cycle length than those in the proliferative stage (HH14) and this is due to a shortening of the S and G2 phases (Saade et al., 2013). No changes in the G1 length were found, though the time spent in the G1 phase was proportionally longer in neurogenic phase (HH24) than in proliferative one (HH14), which would be consistent with a lengthening of the G1 phase with the progression toward neurogenesis observed during mouse corticogenesis (Lange et al., 2009; Pilaz et al., 2009; Saade et al., 2013). Moreover, lengthening G2 phase following down-regulation of the G2/M regulator CDC25B phosphatase is correlated with an increase in the number of proliferative cells at the expense of differentiated neurons, suggesting that the control of the G2 phase length is important for cell fate decision (Peco et al., 2012).

Altogether, cell cycle length and cell fate decisions seem to be highly correlated. Nevertheless, despite important efforts on studying and measuring cell cycle kinetics over the years, there is no consensus and the precise molecular mechanisms involved are not yet understood. It will be thus important to directly address how changes of cell cycle kinetics in the mother cell before division can affect fate choices in the daughter cells after division.

I.4.3.2. Interkinetic nuclear migration

As previously mentioned, cell nuclei of progenitors move along the apical-basal axis within the spinal cord. Given that apical and basal environments are different, it has been proposed that exposing cell nuclei to different signals and during different durations can

influence daughter cell fate (Baye and Link, 2007; Del Bene et al., 2008; Murciano et al., 2002). For instance, Del Bene and colleagues proposed that nuclei movement along the apical-basal axis during IKNM of zebrafish retina controls cell fate decision in a Notch-dependent manner (Del Bene et al., 2008). Briefly, the Notch pathway is regulated by cell-to-cell interactions, in which transmembrane Notch ligands (Delta, Serrate/Jagged) in the signal-sending cell, activate Notch receptors at the surface of the signal-receiving cell. Upon activation of Notch, the Notch Intracellular Domain (NICD) is released from the cytoplasmic portion and translocated to the nucleus where it activates transcription of target genes, allowing the inhibition of neuronal differentiation and maintenance of neural progenitor identity (reviewed in (Bray, 2006; Pierfelice et al., 2011)). In the zebrafish retina, the Notch ligand Delta transcripts were found to be highly enriched at the basal half of the developing retina while Notch transcripts and NICD were preferentially located at the apical side, therefore creating a gradient of Notch activity. Thus, inhibiting basal-to-apical IKNM alters the duration and level of exposure of nuclei to Notch signaling, which leads to premature cell cycle exit and differentiation (Del Bene et al., 2008). However, analysis of Delta ligand mRNA expression in the chick and mouse embryo shows that Delta-like 1 (Dll1) is expressed in all phases of the cell cycle without any specific enrichment in either apical or basal sides (Hammerle and Tejedor, 2007). Thus, elucidating the role of Notch signaling, IKNM and cell fate acquisition will require further investigation.

I.4.4. Asymmetric division and neurogenesis

I.4.4.1. *Drosophila* neuroblasts: a historical view of orientation and cell fate determination

In the last two decades, number of studies has proposed that the orientation axis of the division correlates with the decision between symmetric and asymmetric modes of division, by unequally segregating intrinsic fate determinants. This hypothesis assumes a biased distribution of intrinsic cell fate determinants prior to mitosis, and their unequal distribution between daughter cells after mitosis (reviewed in (di Pietro et al., 2016; Knoblich, 2008; Morin and Bellaiche, 2011)). The plane of cell division is mainly controlled by the orientation of the mitotic spindle in anaphase. Thus, differential orientation of the mitotic spindle was proposed to instruct the choice between symmetric and asymmetric cell divisions (Figure 6A).

The notion that mitotic spindle orientation controls binary fate choices largely derives from early studies carried in *C. elegans* and *Drosophila* embryos. Among these, one of the best-documented examples is the *Drosophila* neuroblast division. In *Drosophila*, neuroblasts delaminate from the neuroectoderm and divide asymmetrically giving rise to a self-renewed neuroblast and a ganglion mother cell (GMC) that will further divide once to produce two neurons. Neuroblasts are polarized along their apical-basal axis with apical (Bazooka (*Drosophila* Par3 homolog), Par6, aPKC) and basal (Brat, Prospero and Numb) determinants. Numb is a regulator of the membrane trafficking that promotes endocytosis of Notch and negatively regulates Notch activation (Couturier et al., 2012), thereby promoting neural differentiation while inhibiting proliferation. During mitosis, Numb is asymmetrically segregated in the basal pole and further inherited in the GMC (Spana et al., 1995). Prospero is a transcription factor that is also accumulated basally and inherited in the GMC where it activates transcription of GMC genes and inhibits neuroblast-specific genes (Knoblich et al., 1995; Spana and Doe, 1995). Finally, Brat is also distributed and inherited asymmetrically in the GMC where it is thought to inhibit proliferation (Betschinger et al., 2006). In such system, the angle of mitotic division is crucial to ensure the correct partitioning of fate determinants. Indeed, during mitosis, the spindle is oriented along the apical-basal axis, which allows the apical and basal partitioning of apical and basal determinants, respectively, therefore resulting in an asymmetric cell fate acquisition. Thus, in the *Drosophila* neuroblast division, it is well established that mitotic spindle orientation is crucial for asymmetric fate choice determination (Figure 6B).

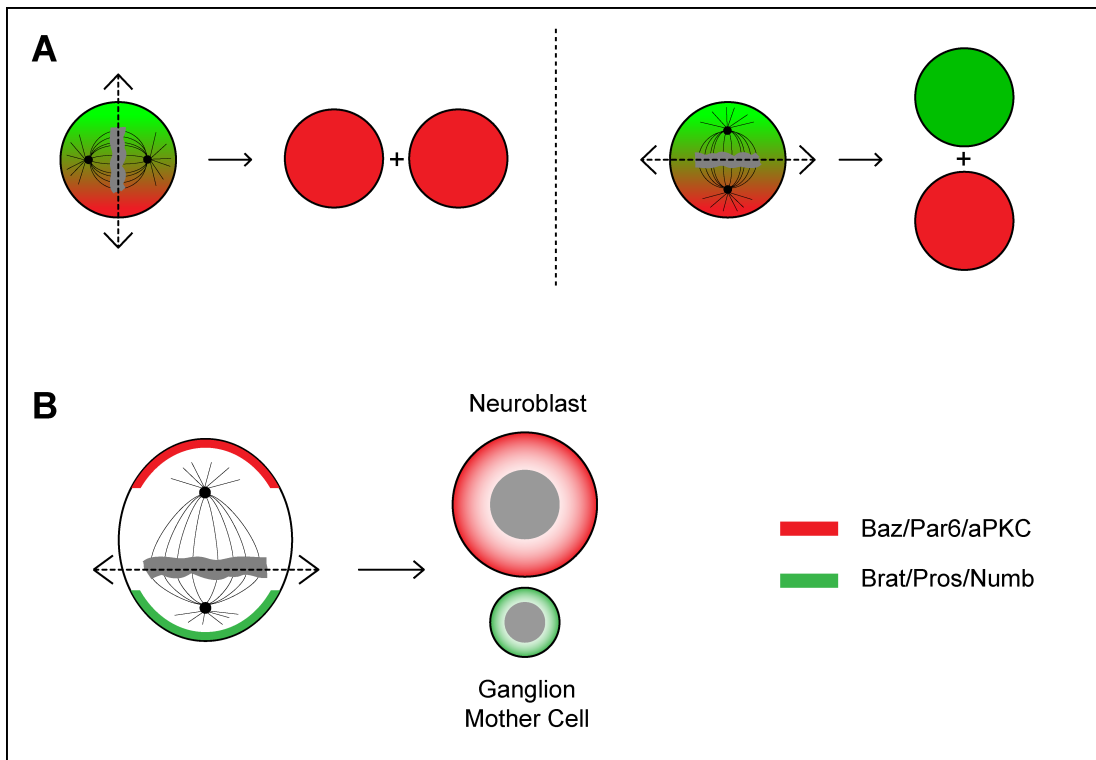


Figure 6. Spindle orientation and asymmetric division.

(A) Unequal distribution of fate determinant (red and green) in respect to the cleavage plane. Left-Vertical cleavage plane allows an equal distribution of fate determinants in the two daughter cells leading to a symmetric division. Right-Horizontal cleavage plane allows an unequal distribution of fate determinants leading to differential fate choices. (B) Asymmetric division of *Drosophila* neuroblast: spindle orientation allows the asymmetric segregation of intrinsic cell fate determinants leading to an asymmetric fate decision.

I.4.4.2. Cell fate determinants in vertebrate neurogenesis

By analogy with the *Drosophila* neuroblast, many studies have tried to identify cell fate determinant molecules during vertebrate asymmetric neurogenic divisions. Cell fate determinants can be defined as molecules present in the mother cell before division, distributed asymmetrically during mitosis and inherited unequally by the two daughter cells where they regulate fate choices. In the following sections, I will present a number of candidates that have emerged as potential fate determinants.

Notch signaling

Notch signaling is an evolutionarily conserved pathway involved in binary fate decisions and well known to be a key regulator of neural progenitor maintenance and differentiation in animals (reviewed in(Louvi and Artavanis-Tsakonas, 2006; Pierfelice et al., 2011)). By analogy

with the *Drosophila* neuroblast division where the Notch regulator Numb is a cell fate determinant asymmetrically segregated in the basal daughter cell, unequally segregated molecules regulating either directly or indirectly Notch signaling appeared to be potential fate determinants during neurogenic divisions in the vertebrate embryo.

Initial observations based on live-imaging of dividing neural progenitors in ferret neocortex slices proposed that the Notch1 receptor is accumulated asymmetrically and inherited unequally between daughter cells (Chenn and McConnell, 1995). These data were reinforced by the description of the asymmetric inheritance of Numb in the *Drosophila* neuroblast that appeared at a similar time (Spana et al., 1995). However, this asymmetric accumulation of Notch1 transcripts observed in the ferret cortex has not been described in any other system.

As Numb has been identified as an intrinsic fate determinant in the fly neuroblast, its vertebrate homologs, Numb and Numb-like were also proposed to perform similar roles during vertebrate neurogenesis. Strongly inspired by the asymmetric distribution of Numb in *Drosophila*, initial studies described an apical and basal crescent of Numb in mouse and chick neural progenitors, respectively (Wakamatsu et al., 1999; Zhong et al., 1996). More recently, in mouse developing cortex, the Golgi component ACBD3 has been proposed to be involved in Numb asymmetry: in dividing RG cells, ACBD3 would be released from the Golgi complex and distributed into the cytoplasm where it functions together with Numb to repress Notch signaling (Zhou et al., 2007).

In addition, the mammalian Par3 protein complex has been implicated in various vertebrate species to regulate neural progenitor maintenance and asymmetric divisions. First of all, in the mouse cerebral cortex, knockdown of Par3 promotes cell cycle exit and premature neuronal differentiation, while overexpression of both Par3 and Par6 enhances progenitor proliferation (Costa et al., 2008). Moreover, Par3 in the mouse cortex and Par1 in *Xenopus* embryo were suggested to have positive and negative impacts on Notch signaling, respectively (Bultje et al., 2009; Ossipova et al., 2009). However, given that Par3 is an important molecular organizer of the apical domain together with N-cadherin-based AJ, and as neuroepithelial integrity and neural differentiation are closely linked, it was difficult to discriminate the actual role of Par3 during neural cell fate decision. This difficulty has been partially overcome when Par3 has been observed to be detached from the apical domain. Indeed, in the mouse cortex, it was observed that Par3 was not constantly restricted to the apical membrane domain as previously suggested, but released in the cytoplasm during mitosis and in some cases inherited

asymmetrically by one of the two daughter cells (Bultje et al., 2009). This dynamic distribution of Par3 was proposed to lead to an asymmetric Numb activity and result in a differential Notch signaling activation in daughter cells. According to this model, the daughter cell that inherits a greater amount of Par3 has less Numb activity, develops a higher Notch signaling activity and remains a RG cell; whereas the daughter cell receiving less Par3 has high Numb activity, retains low Notch signaling activity and adopts a differentiated fate. Nevertheless, cell tracking analyses showing the direct link between Par3 inheritance and daughter cell fate were not carried out in this study. Interestingly, the cell fate related to Par3 inheritance in the zebrafish and chick embryos seems to be opposite to mouse developing brain. In the zebrafish brain and chick spinal cord, time-lapse imaging analyses show that the daughter cell inheriting Par3 is likely to differentiate into a neuron (Alexandre et al., 2010; Das and Storey, 2012; Dong et al., 2012). The other cell born without the apical domain rapidly re-establishes its apical contact and retains its progenitor fate (Alexandre et al., 2010).

Mindbomb1 (Mib1), another regulator of the Notch pathway was also proposed to be involved in asymmetric division of vertebrate neural progenitors. In the zebrafish developing central nervous system, an asymmetric activation of Notch signaling between sister cells was observed and proposed to rely on an asymmetric localization of Mib1 (Dong et al., 2012) or DeltaD (Kressman et al., 2015). Mib1 is an E3 ubiquitin ligase that ubiquitylates the Notch ligand Delta, and this is required for Notch signaling activation (Itoh et al., 2003; Weinmaster and Fischer, 2011). In the zebrafish forebrain, Mib1 is asymmetrically inherited in the apical daughter, which activates Notch signaling in its sister basal daughter, thereby maintaining progenitor fate while the apical daughter differentiates. This intra-lineage Notch signaling mediated by an asymmetric segregation of Mib1 was proposed to require Par3 asymmetric segregation, as *par3*-morphant embryos have disrupted Mib1 asymmetry (Dong et al., 2012). Additionally, in the zebrafish spinal cord, differential activation of Notch between sister cells during asymmetric division was proposed to rely on an unequal segregation of Mib1 and DeltaD both internalized in Sara endosomes (Kressman et al., 2015). However, the molecular basis of these asymmetries was not explored *in vivo*.

More recently, the neuronal polarity protein Shootin1 was suggested to play a similar role to Par3 in the mouse neuroepithelium. In this case, Shootin1 is preferentially localized in apical domain of dividing progenitors. Once inherited asymmetrically by one of the two daughter cells, it increases polyubiquitylation of Numb and reduces polyubiquitylation of NICD (Notch

intracellular domain), both enhancing Notch signaling (Sapir et al., 2017). However, no clear time-lapse imaging data linking Shootin1 inheritance with daughter cell fates are provided.

Overall, Notch signaling is indeed an essential player for the maintenance of self-renewal potential. It can act through different ways to control the balance between proliferation and differentiation. This specific aspect will be further developed in chapter II.

Other intrinsic fate determinants

Another proposed fate determinant relies on the functional conservation of Brat. Brat is one of the fate determinants asymmetrically segregated and governing binary fate choice during *Drosophila* neuroblast division (Betschinger et al., 2006). In mammalian neocortex, the Brat homolog Trim32 was shown to be localized asymmetrically during mitosis, preferentially concentrated in one of the two daughter cells and induced neuronal cell fate in cultured neural progenitor cells (Schwamborn et al., 2009). However, whether Trim32 triggers neuron differentiation *in vivo* was not proven.

Similarly, an EGF receptor was also proposed to segregate asymmetrically during mouse cortical neurogenesis (Sun et al., 2005). *In vitro* cultures show that the daughter cell inheriting EGF receptor responds differentially to EGF, thus contributing to the asymmetric fate choice between sister cells. However, asymmetric segregation of the EGF receptor occurs in a small fraction of progenitors (20%) even at the peak of neurogenesis and cannot account for all the asymmetric neurogenic divisions observed. Moreover, whether this asymmetry correlates with the fate choices of the daughter cells *in vivo* has not been addressed.

In conclusion, in the last years, an increasing amount of investigations have proposed candidates for intrinsic cell fate determinants. However, regardless of the nature of these determinants, one necessary condition for its a/symmetric distribution between sister cells after division is the asymmetric segregation of fate determinants during mitosis. What are the mechanisms involved in the asymmetric partitioning of fate determinants?

I.4.4.3. Mitotic spindle orientation and cell fate determination in vertebrate neurogenesis

Inspired by the *Drosophila* neuroblast division, it was first proposed that the orientation of cell division, controlled by the orientation of the mitotic spindle, might dictate fate choices also in

vertebrate neural progenitors. It has been suggested that cells dividing with a spindle oriented parallel to the apical-basal axis (“apical-basal division”) undergo asymmetric divisions, whereas cells dividing with a spindle oriented parallel to the plane of the ventricular surface (“planar division”) undergo symmetric divisions (Chenn and McConnell, 1995). In support to this model, defects in spindle orientation correlated with an increase of apical-basal divisions and accelerated neurogenesis in mouse cortex and chick spinal cord (Das and Storey, 2012; Godin et al., 2010). Furthermore, dissection of the etiology of human microcephaly gave some credit to this hypothesis. Early exhaustion of the progenitor pool and a loss of late-born neurons by the premature occurrence of asymmetric division are thought to be a cause of human microcephaly. In this context, some authors have proposed that defective spindle orientation might generate microcephaly. Indeed, many genes associated with primary recessive microcephaly in humans (MCPH) are involved in the regulation of spindle orientation. However, the analyses are hampered by the fact that those genes are also involved in other cellular functions and almost all of them encode for centrosomal proteins. Therefore it is difficult to discriminate the role of spindle orientation only in MCPH.

For instance, it has been shown that in mouse line overexpressing Plk4, extra centrosomes are detected, and this leads to microcephaly (Marthiens et al., 2013). Centrosome amplification resulted in aneuploidy, defects in cell division and increased apoptosis, which cause depletion of the progenitor pool and generate microcephaly; but no defect in spindle orientation was found (Marthiens et al., 2013). Thus, the abnormal neurogenesis phenotype may result from defects in multiple cellular processes and it is difficult to assign a role to spindle orientation in microcephaly. On the other hand, genetic ablation of centrosomes in mouse *Sas4* mutant brain resulted in the appearance of microcephaly accompanied by p53-dependent apoptosis (Insolera et al., 2014). Interestingly, *Sas4*^{-/-};*p53*^{-/-} double knock-out rescued cell death and microcephaly, even though mitotic spindle orientation was randomized. These data support the notion that the orientation defects arising from the absence of centrosome cannot explain microcephalic phenotype on its own.

Another way to test this model is to directly alter mitotic spindle orientation and evaluate its effect on fate determination and neurogenesis. Knocking-down spindle orientation effectors (Gai, LGN, NuMA) in the mouse cortex and chick spinal cord led to randomized cleavage planes, but contrary to the models prediction, it does not significantly affect the fate of daughter cells. Instead, this resulted in the production of ectopic cycling progenitors in the mantle zone and

mostly disrupts neuroepithelial organization (Konno et al., 2008; Morin et al., 2007; Peyre et al., 2011).

Taken together, all these data strongly suggest that the causal link between mitotic spindle orientation and cell fate acquisition in the *Drosophila* neuroblast cannot strictly apply to vertebrates. So far, the exact role of spindle orientation in controlling the mode of division during vertebrate neurogenesis remains controversial. It is therefore essential to identify other mechanisms allowing asymmetric segregation of fate determinants during division and regulating fate choices of daughter cells.

I.4.4.4. Other mechanisms of cell fate acquisition

If not spindle orientation, then what can regulate cell fate decisions during vertebrate asymmetric divisions?

Epithelial substructures

As previously discussed, the role of mitotic spindle orientation in regulating asymmetric partitioning of intrinsic fate determinants during vertebrate neurogenesis is still a matter of debate (reviewed in (Peyre and Morin, 2012)). Moreover, in the mouse cortex and in the chick spinal cord, most divisions are planar, even at the peak of neurogenesis (Noctor et al., 2008; Wilcock et al., 2007). To reconcile this observation with the proposed causal relationship between spindle orientation and cell fate, one emerged idea was that subtle changes in spindle orientation might regulate symmetric and asymmetric division, by causing a slight deviation in the angle of the cleavage plane to either bisect or bypass the apical domain, respectively. Indeed, unlike *Drosophila* neuroblasts where intrinsic fate determinants are accumulated as large crescents, vertebrate neural progenitor cells are elongated and possess very thin apical and basal processes. Thus, classical models based on the analogy with asymmetric divisions in flies predict that in asymmetric division, a minor shift in the cleavage furrow is enough to bypass the apical domain, leading to its asymmetric inheritance between daughter cells, which would instruct asymmetric fate choices (Huttner and Kosodo, 2005; Kosodo et al., 2004; Marthiens and French-Constant, 2009). However, live-imaging of mouse cortical slices has revealed equal division of the apical domain even in asymmetric divisions (Konno et al., 2008; Shitamukai et al., 2011; Wilcock et al., 2007).

By contrast, the basal fiber has also been proposed to contribute to cell fate determination. During neural progenitor divisions, the basal fiber was shown to be either bisected between the two daughter cells or asymmetrically partitioned and inherited by only one daughter cell (Alexandre et al., 2010; Kosodo et al., 2008). In mouse cortex and zebrafish hindbrain, lineage analyses have shown that upon oblique cleavage planes, the daughter cell that inherits the basal process often maintains self-renewal capacity, while the apical cell that does not inherit a basal attachment differentiates (Alexandre et al., 2010; Konno et al., 2008; Shitamukai et al., 2011). What is the link between the basal fiber inheritance and the acquisition of cell fate? One possibility is that signals coming from the extracellular matrix components in the basal lamina promote proliferation. In this sense, integrin signaling was proposed to be essential for the maintenance of proliferative capacity (Loulier et al., 2009; Stenzel et al., 2014). In addition, proliferation signals can also be confined in the basal endfoot by local protein synthesis, as shown for the pool of cyclin D2 mRNA, responsible for G1 progression (Tsunekawa et al., 2012). In this case, only the daughter cell inheriting the basal endfoot would continue its cell cycle therefore maintaining its proliferative potential. Importantly, other signaling molecules yet to be discovered and asymmetrically distributed in the basal fiber during division may also contribute to cell fate decision.

More recently, tissue packing and physical strains have been connected to the regulation of differentiation rate in the zebrafish NT (Hiscock et al., 2018). When neural progenitor nuclei are displaced far from the apical surface due to apical crowding via experimentally blocking apical mitosis, progenitors tend to differentiate in a Notch-dependent manner. This study proposes an interesting link between cell geometrical properties and fate determination. Further analyses will be required to precisely dissect how Notch signaling transduces differences in tissue packing to control neurogenesis.

Centrosome asymmetry

The centrosome has been recently introduced as a new potential player driving the asymmetric inheritance of fate determinants in vertebrates (reviewed in (Reina and Gonzalez, 2014; Roubinet and Cabernard, 2014)). The centrosome, the main mitotic spindle-organizing center, consists of a pair of mother and daughter centrioles surrounded by an amorphous pericentriolar material. During each cell cycle, the centrosome replicates in a semi-conservative manner during interphase, resulting in the formation of two centrosomes: the “old” and “young”

centrosomes contain the original mother (now grandmother) and daughter (now mother) centrioles, respectively, each having been used as a scaffold to synthesize the new daughter centrioles. The older grandmother centriole, which is at least two cell cycles old, carries more pericentriolar material and satellites that bear specific “maturation marks” and support ciliogenesis (Figure 7). Thus, the two centrosomes are intrinsically asymmetric. Remarkably, a link between centrosome asymmetry and cell fate acquisition was reported first in *Drosophila* male germline then in neuroblasts (Januschke et al., 2011; Yamashita et al., 2007). Increasing evidence supports that this model could also apply in vertebrates. During mouse RG divisions, self-renewing daughter cells preferentially inherit the “old” centrosome while the other daughter cell committing to differentiation inherits the “young” centrosome. Knocking-down the mature centriole-specific protein ninein interfered with centrosome maturation and this led to premature neuronal differentiation, suggesting that asymmetric centrosome inheritance is strongly correlated with differential fate choices (Wang et al., 2009).

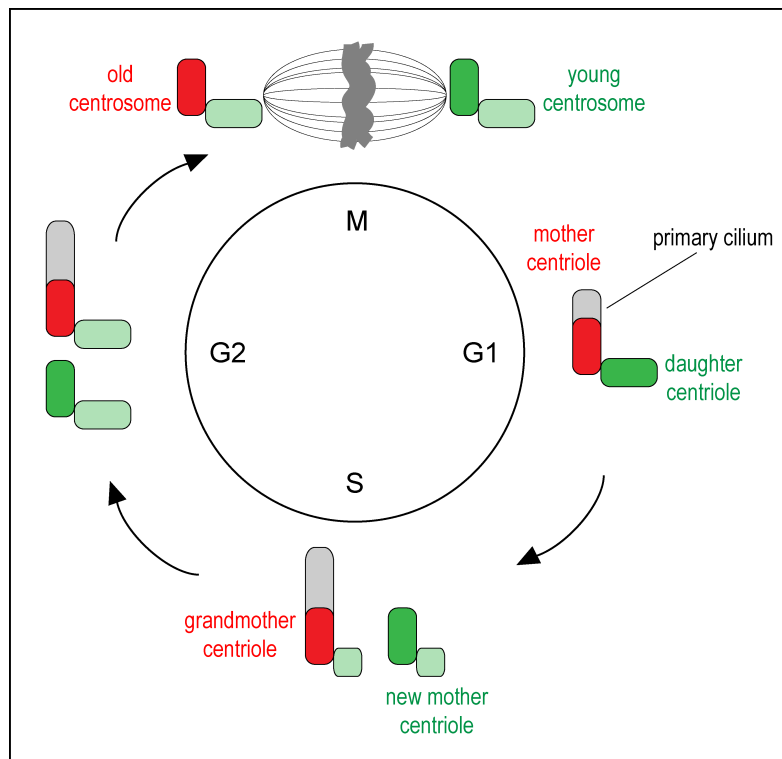


Figure 7. Centrosome asymmetry.

The centrosome is composed of two centrioles: the mother (red) and daughter (green) centriole. During S-phase, each centriole replicates to produce new daughter centrioles (light green) resulting in the formation of intrinsically asymmetric centrosomes: the “old” and “young” centrosomes contain the original mother (now grandmother, red) and daughter (now mother, green) centrioles, respectively. Following mitosis, each cell then inherits either the original mother centriole or its daughter.

Hence, a molecule associated with a unique centrosome is likely to alter binary fate choices during asymmetric divisions, independently of mitotic spindle orientation. Recent findings in chick spinal cord have now begun to reveal a link between centrosome asymmetry and signaling pathways involved in fate acquisition (Saade et al., 2017; Tozer et al., 2017).

Saade and colleagues recently proposed a link between Shh/Gli pathway and centrosome asymmetry via a differential PKA centrosome docking in symmetric versus asymmetric divisions (Saade et al., 2017). Shh signaling promotes proliferative P-P divisions in motor neuron progenitors of the chick spinal cord (Saade et al., 2013). Briefly, upon Shh binding to its receptor Patched1, the cilium-localized transcription factors Gli2/3 are released and maintained in their activator forms so that they can activate target gene expression when translocated into the nucleus (Louvi and Grove, 2011). Protein kinase A (PKA) negatively regulates Gli proteins, rendering them inactive. Segregation of PKA to the centrosome is thought to block PKA activity, shifting the balance towards more active Gli, thereby more Shh target gene expression (Saade et al., 2017). In the early chick spinal cord when most divisions are proliferative (P-P), activation of the Shh/Gli pathway was correlated with a symmetric localization of PKA in both mitotic centrosomes. At later stage, when proliferative symmetric (P-P) and neurogenic asymmetric (P-N) divisions coexist, two different situations could take place: (1) symmetric PKA centrosome docking, which in turns activates Shh signaling in dividing progenitors undergoing P-P divisions or (2) asymmetric localization of PKA into one centrosome in dividing progenitors undergoing P-N divisions, where the latter are identified by the expression of the neurogenic marker Tis21 (Saade et al., 2013). Over-activation of Shh signaling resulted in symmetric centrosomal localization of PKA and symmetric P-P outcome of the daughter cells (Saade et al., 2017). These findings propose a model in which Shh provides an instructive signal in the mother cell for P-P dividing cells to overcome intrinsic centrosomal asymmetry and to result in symmetric and asymmetric Shh signaling in daughter cells.

On the other hand, a study carried out in the lab and to which I contributed proposes a link between centrosome asymmetry and the regulation of Notch signaling via an asymmetric segregation of the ubiquitin ligase Mib1 (Tozer et al., 2017). As previously mentioned, Mib1 is crucial to activate Notch signaling in neighboring cells (Itoh et al., 2003; Weinmaster and Fischer, 2011). Using live-imaging of chick NT to follow cell division and subsequent cell fate decisions, we have found that Mib1 is asymmetrically associated with the “young” centrosome through its direct interaction with the centriolar satellite protein AZI1, and is preferentially

inherited by the prospective neuron during asymmetric division. Interfering with Mib1 centrosomal localization results in a loss of asymmetry, altered Notch activity and reduced neurogenesis. Asymmetric inheritance of Mib1 in the prospective neuron is thus important to bias Notch activation towards its sister cell to maintain it undifferentiated (Tozer et al., 2017). In contrast, in symmetric divisions, a pool of Mib1 associated with the Golgi apparatus in interphase is released in the cytoplasm during mitosis, accumulates on the “old” centrosome initially devoid of Mib1, resulting in a symmetric inheritance of Mib1 between sister cells (Tozer et al., 2017). We thus propose that Mib1 is a fate determinant whose differential localization to the “young” centrosome regulates fate choices during asymmetric divisions of neural progenitors. A full version of the article can be found at p. 167 of this thesis manuscript.

Spindle size asymmetry

A physical asymmetry in size of the two spindle poles during mitosis has been proposed to occur in asymmetric divisions of the mouse cerebral cortex (Delaunay et al., 2014). Measuring the size and the shape of the mitotic spindle *per se* by labeling microtubules and centrosomes revealed that spindle size asymmetry (SSA) does not exist before the onset of neurogenesis but parallels the peak of asymmetric cell divisions. Based on live-imaging assays, the larger spindle is correlated with neuron generation while the smaller spindle correlates with progenitor maintenance. Disruption of SSA via down-regulation of Vangl2 reduced the number of progenitors and resulted in a loss of late-born neurons (Delaunay et al., 2014). This form of SSA was further shown to take place during division of macaque cortical precursors, pointing an evolutionarily conserved mechanism in mammals (Delaunay et al., 2015).

Primary cilia

Neural progenitors harbor a primary cilium on the apical domain. This microtubule-based organelle protrudes from the apical plasma membrane into the lumen of the ventricle and is nucleated at its base by the so-called basal body, which consists of the oldest centriole in the cell – the mother centriole. The primary cilium is an antenna-like structure sensing a number of extracellular signals such as Shh, FGF or Wnt (reviewed in(Louvi and Grove, 2011; Taverna et al., 2014)).

Although the common belief is that primary cilia are disassembled prior to mitosis, Paridaen and colleagues have shown that the primary cilium is not completely dismantled but

cilia remnants stay attached to the mother centriole over the course of mitosis in mouse developing cortex (Paridaen et al., 2013). Because of the intrinsic centrosome asymmetry, after division, one of the two daughter cells that inherits both the mother centriole (now grandmother) and the cilia remnant can proceed to cilium re-growth faster and transduce extracellular signals before its sister cell. This contributes to generate distinct cell fates: the daughter cell inheriting the mother centriole and the cilia remnant retains its progenitor identity, while the other one acquires a neurogenic fate (Paridaen et al., 2013). The daughter cell that differentiates after cell division identified by a *Tbr2* positive signal, is more likely to dock a primary cilium at its basolateral membrane rather than on the apical membrane and delaminates from the ventricular zone (Wilsch-Brauninger et al., 2012). On the other hand, following mitotic exit, in the developing spinal cord, the prospective neuron (identified by the early neuronal marker *Tuj1*) will eventually lose its apical attachment through a process termed ‘apical abscission’ whereby the primary cilium is dismantled as the cell delaminates from the ventricular surface (Das and Storey, 2014). One can speculate that this apical abscission may be a means to rapidly shut down mitogenic signals received through the primary cilium and help to achieve final differentiation.

Mitochondria

Mitochondria are energy-generating organelles that participate in various metabolic pathways. They are also highly dynamic organelles that continuously modify their morphological state through fission and fusion events (Khacho and Slack, 2018). Mitochondria are crucial in post-mitotic cells to provide energy particularly given the high-energy demanding nature of neurons. Recent studies have started to uncover the importance of mitochondria dynamics not only in the adult brain but also during embryonic neurogenesis. First of all, in the chick spinal cord, mitochondrial morphology is different between motor neuron progenitors (pMN) and motor neurons (MN) (Mils et al., 2015). In pMNs, mitochondria appeared as short and thick well-delineated elements while in MNs they appeared thinner and more elongated (Mils et al., 2015). Similarly, in the mouse developing brain, mitochondrial morphology has been reported to differ as the cell progresses toward differentiation: mitochondria display an elongated shape in aRG and neurons while it has a fragmented appearance in IP (Khacho et al., 2016). Alteration in mitochondrial function in aRG causes defects in proliferation, in cell cycle exit and in its ability to differentiate into neurons (Khacho et al., 2017). In line with this study, the level of mitochondrial reactive oxygen species (mtROS) was shown to be significantly decreased in

differentiating cells as compared to neural progenitors that display higher ROS levels (Inoue et al., 2017; Le Belle et al., 2011). Overexpression or knockdown of Prdm16, a transcription factor regulating mtROS levels, provoked aberrant morphologies of differentiating cells and their abnormal migration in the cortical layers (Inoue et al., 2017). All of these data point out that mitochondria and changes in ROS levels could be another level of differential fate choices regulation during vertebrate neurogenesis. Notably, in human mammary epithelial cell culture, mammary stem-like cells unequally distribute its “old” and “young” mitochondria, as the daughter cell containing the “young” mitochondria retains stem cell properties (Katajisto et al., 2015). During interphase, mammary stem-like cells accumulate aged, potentially damaged mitochondria. Thus, this unequal retention of “young” mitochondria by the stem cell could be a way to segregate the potentially damaged “old” mitochondria away from the stem cell pool. It is tempting to speculate that an asymmetric distribution of mitochondria (old/young, shape, number) between daughter cells could also govern fate choices in the case of neural progenitors.

Concluding remarks

During development, a single cell, the fertilized oocyte, gives rise to a wide variety of cell types and tissues. One of these tissues, the central nervous system, is the seat of various glial and neural cell types, generated from a limited number of neural progenitors by symmetric and asymmetric divisions. The fundamental issue of the switch of neural progenitor cells from proliferation to differentiation has been investigated from various angles, including their the apical-basal polarity, cell-cycle parameters, epithelial characteristics and intracellular organelles. As a result of intense studies, our understanding of the mechanisms governing fate choices has improved, but the mechanisms involved differ between central nervous system regions (cortex/spinal cord) and vertebrate species, thus rendering difficult the integration of information into a single complete picture. Regarding the specific question of one fate determinant, deeper investigation of the molecular basis driving its a/symmetric localization will be needed to complete the fragmented scheme.

Notably, a variety of signaling pathways are known to act over the course of neurogenesis. Among them, the Notch signaling pathway is prominent to regulate neural progenitor maintenance and differentiation in animals; this was at the heart of my thesis work and is the subject of the next chapter.

II

INTRODUCTION

NEURAL PROGENITOR MAINTENANCE: THE ROLE OF NOTCH SIGNALING

Chapter II.

Neural Progenitor Maintenance: The Role Of Notch Signaling

*“If one was asked to choose the single, most important genetic variation concerned with the expression of the genome during embryogenesis in *Drosophila melanogaster*, the answer would have to be the Notch locus.” (Wright, 1970)*

II.1. A brief history of Notch

A century ago, John S. Dexter and T.H. Morgan’s group first described a mutant in *Drosophila* named *Notch* because of its ‘notched’ wing phenotype associated with the haploinsufficiency of the Notch locus (Dexter, 1914; Mohr, 1919; Morgan, 1917). Since then, seminal works performed by Poulson (Poulson, 1936) and Welshons (Welshons, 1956; Welshons, 1965) led to the cloning of the *Notch* locus in *Drosophila*, which consists of a 300kDa transmembrane receptor (Artavanis-Tsakonas et al., 1983; Kidd et al., 1983). From a functional point of view, as already recognized early on by Poulson, the deletion of *Notch* results in defects of cell fate choices between epidermal versus neural cell lineages, leading to a hypertrophy of the neural tissue, giving rise to a ‘neurogenic’ phenotype. Over the years, the Notch signaling pathway has been shown to play critical roles in neural progenitor maintenance and neurogenesis in both invertebrates and vertebrates species (Chenn and McConnell, 1995; Chitnis, 1995; Dornseifer et al., 1997; Henrique et al., 1995). However, the developmental role of Notch is certainly not limited to the nervous system. It is involved in the formation of numerous organs including heart, kidney, pancreas, muscle, limb and affecting various cellular processes such as stem cell maintenance, differentiation and apoptosis, both in the embryo and in the adult. In addition to this highly pleiotropic action in normal development, Notch is also involved in pathological context, such as in cancer (reviewed in(Aster et al., 2017; Louvi and Artavanis-Tsakonas, 2012; Zhang et al., 2017)).

Many different ways have been proposed to activate Notch signaling, but the classical DSL (Delta-Serrate-LAG2) ligand-dependent activation is the best described and known as the “canonical” Notch pathway.

The aim of this chapter is to provide an insight into the canonical Notch pathway in the context of vertebrate embryonic neurogenesis. During neural development, progenitors proliferate massively at early stages before they start differentiating into neurons and glia. It is crucial to maintain the pool of progenitors undifferentiated until the right moment has come. In this context, the Notch pathway is well known to regulate the balance between neural progenitor maintenance and differentiation. Notch signaling activation leads to the inhibition of neurogenesis, thus maintaining neural progenitor character (reviewed in(Louvi and Artavanis-Tsakonas, 2006)). In order to introduce in more details the role of the Notch pathway, I will start by describing the ligand-receptor interaction that leads to Notch signaling activation. Then, I will present the current knowledge of a more debated ligand-receptor interaction termed ‘*cis*-inhibition’, as well as some aspects of Notch signaling regulation in the context of cellular and tissue morphology. Finally, I will focus on the primordial role of Notch signaling in regards to neurogenesis. While *Drosophila* studies have contributed hugely to our current understanding of Notch signaling (Artavanis-Tsakonas et al., 1999), this thesis chapter will primarily focus on the work performed in vertebrate neural development.

II.2. The core elements of the Notch pathway

II.2.1. Notch pathway overview

Notch signaling relies on cell-to-cell interactions, as both ligands and receptors are transmembrane proteins. Notch ligands (Delta and Serrate/Jagged) present on the surface of one cell bind to Notch receptors present on the surface of a neighboring cell. Upon activation of Notch, two series of cleavages occur: S2 cleavage by the metalloprotease ADAM (a disintegrin and metalloprotease) and S3 cleavage by the γ -secretase complex, which releases the Notch intracellular domain (NICD) from the plasma membrane. Once released, the NICD enters the nucleus, and together with the DNA-binding protein CSL (named after CBF1-Suppressor of Hairless-LAG1; also known as RBP-Jk) and the co-activator Mastermind-like (Maml), forms a tri-partite complex that activates transcription of target genes. In the absence of NICD, CSL forms complexes with a variety of co-repressors to inhibit the transcription of target genes

(Figure 8) (reviewed in(Bray, 2006; Kopan and Ilagan, 2009)). In addition to this well-characterized role for Notch signaling activation through cell-to-cell interactions (*trans*-activation), ligands and receptors can also interact within the same cell leading to Notch signaling inhibition (*cis*-inhibition). The nature and mechanisms underlying *cis*-inhibition of Notch signaling will be further discussed in section II.4.

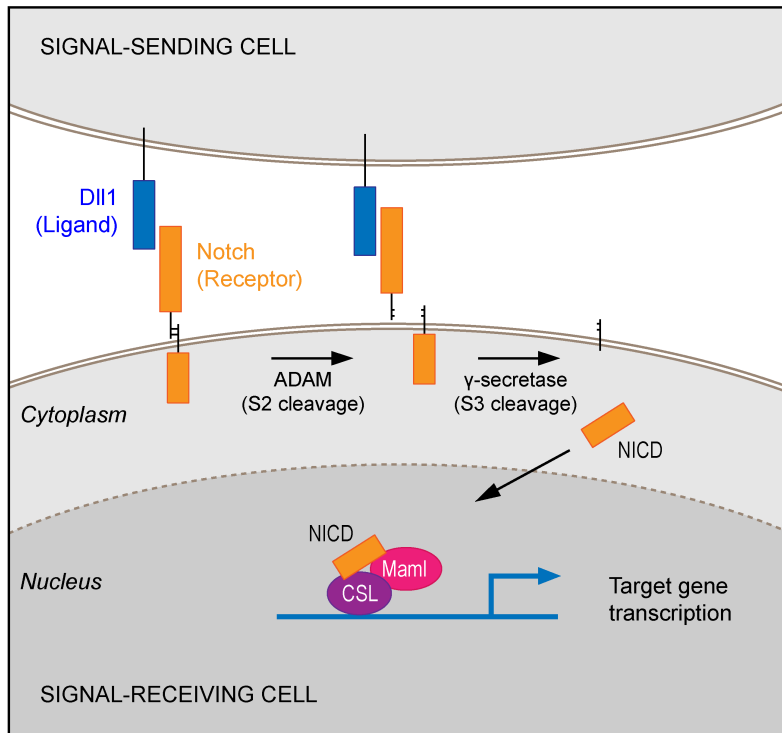


Figure 8. Notch signaling pathway.

Dll1 ligand present in the signal-sending cell activates Notch receptor present in the signal-receiving cell. Upon activation of Notch, the receptor undergoes a series of cleavages that finally releases the intracellular domain (NICD). The latter is translocated to the nucleus, where it forms a complex with the DNA-binding protein CSL and the co-activator Maml to induce transcription of Notch target genes.

II.2.2. Mechanistic features of the Notch pathway

Core elements of the Notch pathway are highly conserved across species, though the number of paralogues of each element differs (reviewed in(Bray, 2016; Kopan and Ilagan, 2009)). On the basis of structural homology to the two *Drosophila* ligands Delta and Serrate, five ligands were identified in mammals, designated as either Delta-like (Dll1, Dll3 and Dll4) or Serrate-like (also named Jagged1 and Jagged2). In terms of receptor, *Drosophila* has only one

Notch receptor while in mammals four Notch receptors exist (Notch1–4). In humans, additional Notch2-like receptors were recently found (Fiddes et al., 2018; Suzuki et al., 2018).

II.2.2.1. Ligands

The canonical Notch ligands are single-pass transmembrane proteins that share four main structural motifs in their extracellular region: an N-terminal (NT) domain, the DSL (Delta-Serrate-LAG2) domain, a specialized tandem of EGF (epidermal growth factor) repeats called the DOS (Delta and OSM-11-like proteins) motif, and multiple tandem EGF-like repeats. Additionally, Serrate (or its homologs in vertebrates Jagged1 and Jagged2) ligands have a cysteine-rich domain (CRD) not found in Delta family ligands, and harbor almost twice the number of EGF repeats as Delta ligands (reviewed in(D’Souza et al., 2010; Kopan and Ilagan, 2009)). NT, DSL and DOS domains are together involved in receptor binding. Surprisingly, it has been reported that Dll3, Dll4 and all *C.elegans* DSL ligands lack a DOS motif; in this case, optimal activation of Notch signaling would require a cooperative Notch binding with other DOS motif-containing non-canonical ligands. For instance, Dlk1 and Dlk2 DOS-containing co-ligands can cooperate with DSL-only ligand DSL1, to activate Notch signaling during *C.elegans* vulval development (Komatsu et al., 2008).

The intracellular regions of DSL ligands exhibit very low sequence homology except two conserved features (Pintar et al., 2007). Firstly, all DSL ligands with the exception of Dll3, contain multiple lysine residues that are required for modification by E3 ubiquitin ligases (the role for ubiquitylation will be further detailed in section II.3). Secondly, most DSL ligands contain a C-terminal PDZ (PSD-95/Dlg/ZO-1) motif, which is required for interactions with the actin cytoskeleton independently from Notch signaling. Indeed, the intracellular tail of Notch ligands interacts with proteins containing PDZ-binding domains. Those proteins are involved in the organization of cell-cell junctions, such as Dll1 with Dlg1 in cell culture assays (Six et al., 2004) or DeltaD with MAG1 family members in the zebrafish embryo (Wright et al., 2004).

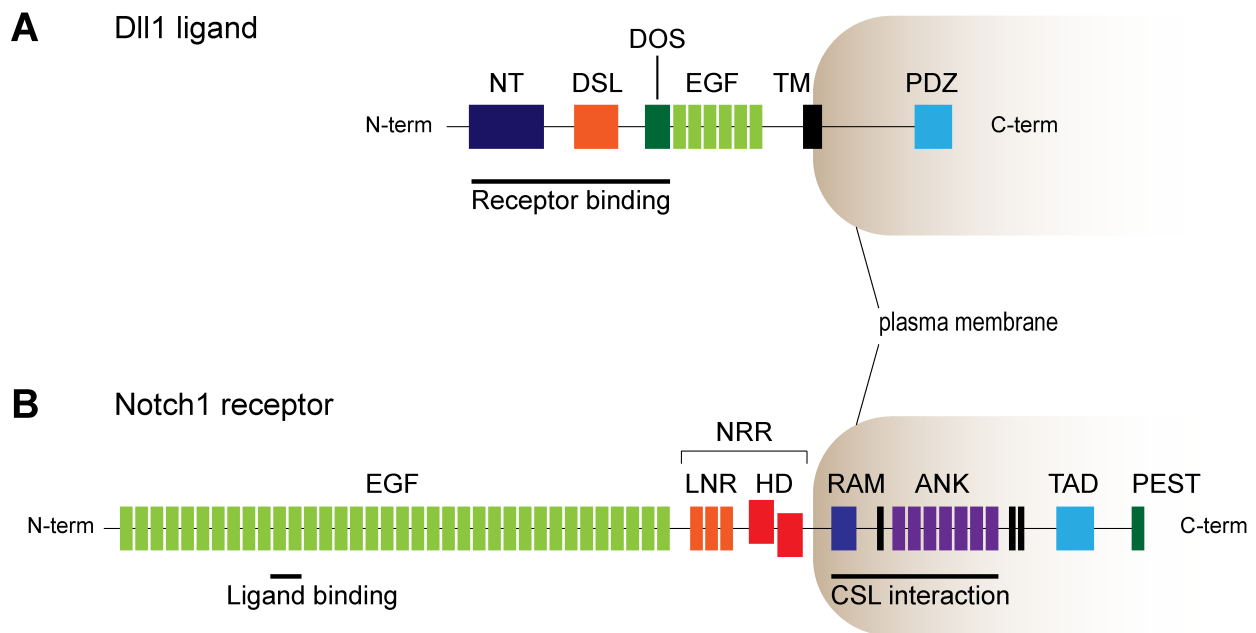


Figure 9. Structural domains of Dll1 ligand and Notch1 receptor.

(A) Domain organization of Dll1 ligand. The extracellular domain is composed of an NT domain (blue), followed by a DSL domain (orange) and multiple EGF-like repeats (green), among which the DOS domain. NT, DSL and DOS are all required for interaction with the Notch receptor. (B) Domain organization of Notch1 receptor. EGF repeats 11-12 in the extracellular domain of Notch is involved in binding with the ligand. Notch receptors are heterodimers: the two HD domains (red) interact with LNR (orange), together forming the NRR, which blocks the cleavage site for proteases. The NICD contains RAM (blue) and ANK domains (purple), both of which required for interactions with the DNA-binding protein CSL. The ANK domain is flanked by several nuclear localization signals (dark).

II.2.2.2. Receptors

Similarly to ligands, Notch receptors are single-pass transmembrane proteins. From a structural point of view, Notch receptors are divided into three regions: Notch extracellular domain (NECD), transmembrane domain (TMD) and Notch intracellular domain (NICD) (Kopan and Ilagan, 2009).

The NECD of all Notch receptors contains 29-36 EGF-like repeats, involved in interactions with the Notch ligand, and a unique negative regulatory region (NRR), composed of three cysteine-rich Lin12-Notch repeats (LNR) and a heterodimerization domain (HD). During its maturation in the Golgi apparatus, Notch undergoes a Furin-dependent cleavage at the S1 site within the HD domain, which produces a heterodimeric receptor comprised of NECD and NTMIC (Notch transmembrane and intracellular domain) held together by noncovalent interactions (Fiuza and Arias, 2007; Kopan and Ilagan, 2009). As for the NRR, it prevents activation of Notch in the absence of ligand (Bray, 2006; Kopan and Ilagan, 2009).

On the other hand, NICD is composed of a RAM (RBP-Jk association molecule) domain, a nuclear localization signal (NLS), seven ankyrin repeats (ANK) followed by two additional NLS, a transactivation domain (TAD) and finally a C-terminal very conserved PEST (rich in proline/glutamic acid/serine/threonine residues) motif that contains degradation signals important to regulate the stability of NICD (Lubman et al., 2007). In the nucleus, the NICD associates with the DNA-binding protein CSL through its RAM and ANK domains. The latter also interacts with the coactivator Maml to induce expression of Notch target genes (Bray, 2016; Kopan and Ilagan, 2009).

In conclusion, the Notch signaling pathway is relatively simple in its mode of operation: receptor-ligand binding directly releases the biologically active NICD that activates transcription of target genes (Figure 8). This highly conserved pathway functions in many different developmental processes to produce different functional outputs. How is this pathway regulated to generate such diverse outcomes? Many different mechanisms acting at various levels are deployed to tune the activity of the Notch pathway, ranging from the control of receptor-ligand availability and affinity at the cell membrane by Fringes and other modifying enzymes, to the regulation of transcription factor binding and epigenetic mechanisms in the nucleus. In the following sections, I will highlight three particular aspects of this deployment that are relevant for this thesis: endocytosis of receptors and ligands by ubiquitin ligases (II.3), the contribution from cis-inhibition (II.4) and the effects of cell-cell contacts and tissue morphology on Notch signaling (II.5).

II.3. Notch ligand ubiquitylation

II.3.1. Role of E3 ubiquitin ligases in Notch signaling

Work from many groups have now clearly demonstrated that ubiquitylation of Notch ligands in the signal-sending cell is a fundamental prerequisite for effective Notch signaling activation in the signal-receiving cell (reviewed in(D'Souza et al., 2010; Fortini and Bilder, 2009; Weinmaster and Fischer, 2011)). Two types of E3 ubiquitin ligases, Mindbomb (Mib) and Neuralized (Neur) are able to ubiquitylate Notch ligands. While both Mib and Neur are required for the Notch pathway activation in *Drosophila* (Le Borgne and Schweisguth, 2003), studies in various mutant mice have shown that this is not the case in vertebrates. Mammals have two Mib

homologs (Mib1 and Mib2) and two Neur homologs (Neur1 and Neur2). *Neur1/Neur2* double knockout mice do not exhibit the characteristic Notch phenotypes displayed in *Drosophila Neur* mutant (Koo et al., 2007). Moreover, mice defective for *Neur1/Neur2/Mib2* gene also lack obvious Notch signaling defects (Koo et al., 2007), while the *Mib1*^{-/-} knockout mice exhibit clear Notch mutant phenotype, such as defects in somitogenesis, vascular remodeling and premature neurogenesis. Furthermore, analysis of Notch effectors gene expression pattern shows that *Mib1*^{-/-} embryos have defects in Notch activation, therefore identifying Mib1 as the only E3 ubiquitin ligase absolutely required for Notch activation in vertebrates (Koo et al., 2005). But what is the functional link between ligand ubiquitylation and signaling activation?

As previously mentioned, the intracellular domain of most DSL ligands except Dll3 contains multiple lysine residues that are potential sites for the addition of ubiquitin (Ub) by E3 ubiquitin ligases. Mib and Neur have RING domains at the C-terminus that allow direct transfer of ubiquitin (Ub) to substrates (Haddon et al., 1998; Itoh et al., 2003; Lai and Rubin, 2001). In terms of substrate binding, recent analysis indicates that human Mib1 (MIB1) binds to two motifs in the ICD of mammalian Jagged1 named the N- and C-Box, through two domains present in the Mib1 N-terminus, named MZM and REP (Figure 10) (McMillan et al., 2015).

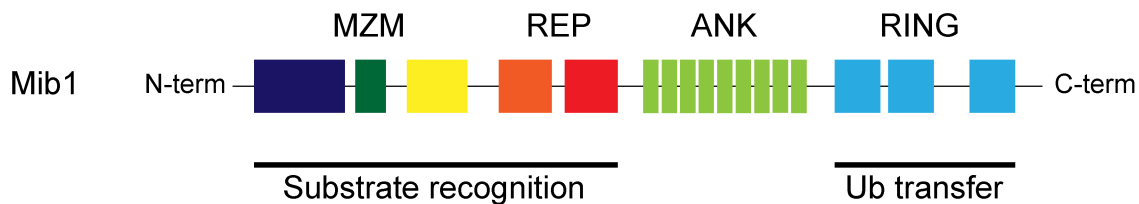


Figure 10. Domain organization of Mib1.

The MZM domain contains two Mib1-Herc2 domains (blue and yellow) flanking a ZZ Zinc finger (green). The REP domain contains two tandem Mib1 repeats elements (orange and red). The ANK domain is composed of nine ankyrin-type repeats (light green). The RING domain is composed of three RING elements (light blue). MZM and REP domains ensure the substrate recognition while the RING domain catalyzes Ub transfer to substrate proteins. The most C-terminal RING domain is critical for Mib1 function (Itoh et al., 2003).

While poly-ubiquitylation is associated with proteasome degradation, the addition of one Ub to lysine residues on their target DSL ligands stimulates their removal from the cell membrane and targets them for endocytosis (Daskalaki et al., 2011). Then, why would Notch signaling activation require ligand endocytosis?

II.3.2. Role of the ligand endocytosis for Notch signaling

Ubiquitylation of Notch ligands by Mib and Neur leads to endocytosis of ligands from the membrane. At first glance, it seems counterintuitive that ligands need to be removed from the cell surface to trigger Notch activation in neighboring cells. Two distinct major models have been proposed to explain this apparent conundrum: (1) ligand recycling and maturation and (2) endocytosis-mediated pulling-force (Figure 11). While evidence exists to support both these two scenarios, we will further see in the following sections whether the first, second or both events are necessary to activate Notch signaling (reviewed in(Weinmaster and Fischer, 2011)).

II.3.2.1. Ligand recycling model

In the first scenario, the newly synthesized ligand at the cell surface is not an “active” form but needs to be internalized into endosomes, processed and recycled back to the cell membrane with modifications that enable the ligand to be “active” (Figure 11A).

Two studies performed in *Drosophila* sensory organ precursor (SOP) cells first showed ligand endocytosis. These papers proposed that the recycling proteins Rab11 and Sec15 are required for Delta recycling, but without mentioning the requirement for ubiquitylation (Emery et al., 2005; Jafar-Nejad et al., 2005). However, in neither paper it was shown that Rab11 and Sec15 are required to obtain the “active” form of Delta ligand. Instead, ligand recycling might be an effective manner for a precise spatial positioning to ensure specific cellular responses. Along that line, it was shown in *Drosophila* SOP and cultured MDCK cells that Delta is translocated from the basolateral membrane to the apical membrane in a Neur-dependent manner. As Notch receptors are also found at the apical membrane in these two systems (SOP and MDCK), this relocalization of Delta would facilitate its interaction with Notch apically (in neighboring cells) and thus enable it to signal (Benhra et al., 2010). Nevertheless, recent data challenge this hypothesis. Using photo-bleaching of GFP-tagged Notch and photo-convertible version of Notch, Trylinski and colleagues were able to characterize *in vivo* the pool of Notch contributing to signaling in *Drosophila* SOP cells. This study indicates that ligand-receptor interaction and activation of Notch signaling occur in the basolateral membrane rather than the apical plasma membrane in SOP cells (Trylinski et al., 2017).

By contrast, experiments performed in cell culture suggest that ubiquitylation is not necessary for ligand endocytosis or recycling (Heuss et al., 2008). Given that ubiquitylation is achieved on multiple lysine residues present at the intracellular domain of ligands, mutation of all

17 intracellular lysine residues in mouse Dll1 resulted in a ubiquitin-defective mutant form of mouse Dll1 (Heuss et al., 2008). Nevertheless, this lysine-less mutant form of Dll1 could still be endocytosed, but was unable to recycle back to the cell surface or to bind and activate Notch receptor in cell culture assays. In contrast, a Dll1/Dll3 chimeric ligand containing the ECD (extracellular domain) of Dll1 and the transmembrane and ICD (intracellular domain) of Dll3 (endogenously without lysine residues) was endocytosed, recycled and exhibited high-affinity binding to Notch receptor, but unable to activate it *in vitro*. This surprising result suggests that ubiquitylation is required for neither endocytosis nor recycling (Heuss et al., 2008). Nevertheless, whether these results can be applied for *in vivo* situations further needs to be tested.

Taken together, these observations argue that ligand recycling is neither a core feature of Notch activation nor an absolute requirement for ligand activation, especially as in some cases, recycling seems to occur in a ubiquitin-independent manner (Heuss et al., 2008). Rather, ligand recycling could serve as an additional layer of regulation, to modulate receptor levels at the cell surface, to help the ligand acquire high-affinity towards the receptor or to differentially arrange ligand localization.

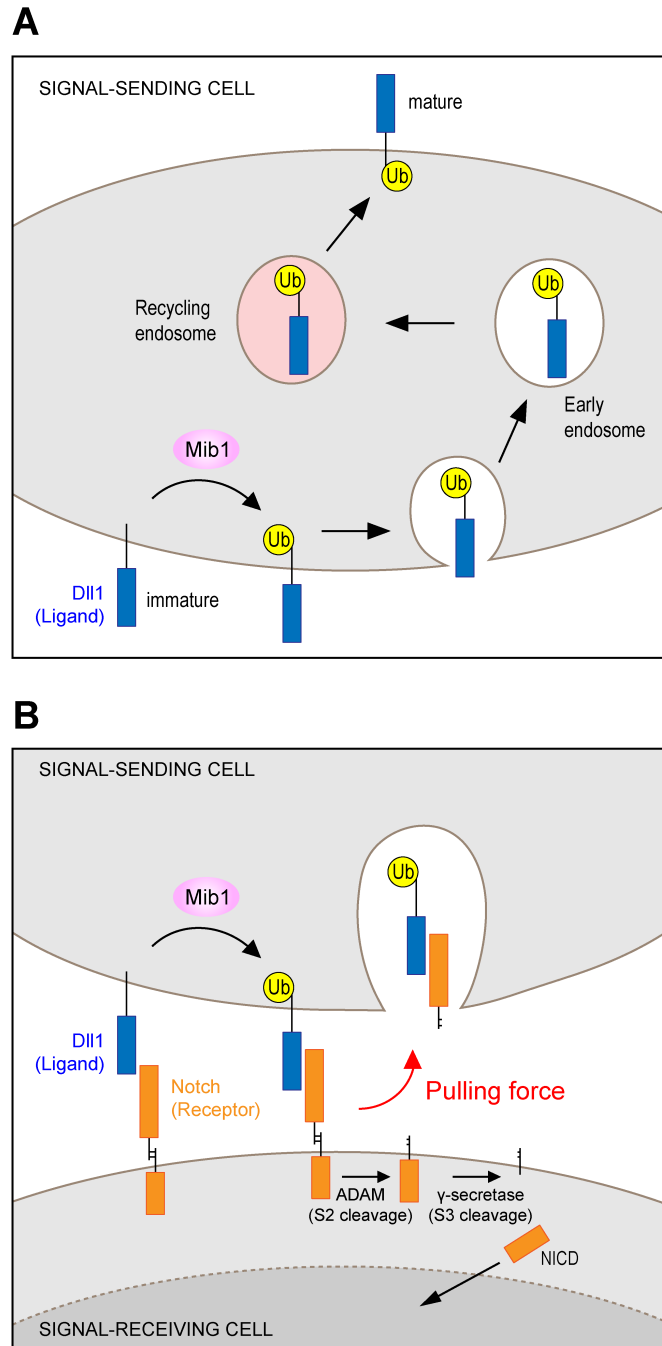


Figure 11. Schematic of proposed two models for ubiquitin ligase-dependent ligand endocytosis.

(A) Ligand recycling model: immature ligand delivered to the cell surface is ubiquitylated, which promotes ligand endocytosis. Following internalization, the ligand is delivered to the early endosome then to the recycling endosome from which it is returned to the plasma membrane in its mature form. (B) Pulling-force model: ligand endocytosis in the signal-sending cell exerts a pulling-force on the Notch receptor in signal-receiving cell. Internalization of ligand-bound NECD exposes the remaining membrane-associated Notch to activating proteolysis, which finally releases the NICD that moves to the nucleus to activate transcription of Notch target genes. Adapted from Weinmaster and Fischer, 2011.

II.3.2.2. Pulling-force model

Ligand endocytosis has been suggested to be a key process to induce the important conformational changes of Notch receptor required for active signaling. Whereas in the ligand-recycling model endocytosis occurs before ligand binding with receptors, in the pulling-force model, endocytosis takes place when the ligand is already bound to the Notch receptor. Structural studies suggest that in the absence of ligand interaction, Notch receptors are locked in a compact conformation preventing protease-driven cleavages. Thus, major structural changes are required to expose Notch to activating proteolysis (Kovall and Blacklow, 2010). Mono-ubiquitylation by ubiquitin ligases triggers the signal for endocytosis of transmembrane proteins (reviewed in(Hicke, 2001)). As such, the endocytosis of the ligand-receptor complex by ubiquitin ligases would exert a mechanical force on the Notch receptor present in the adjacent cell and help to dissociate the NECD from the remaining membrane-bound Notch. Internalization of the ligand-NECD complex induces conformational changes that unmask cleavage sites of the remaining membrane-bound Notch: first for the metalloprotease ADAM at S2 site then for the γ -secretase complex at S3 site, together leading to the generation of NICD and effective intracellular signaling (Figure 11B).

This model is compatible with an early study performed in *Drosophila* imaginal discs that observed NECD colocalizing with Delta in the endosomes of cells known to activate Notch signaling (Parks et al., 2000). In further support of this model, *in vitro* studies indicate that NECD is localized in vesicles in cells expressing Delta following co-culture with Notch-expressing cells (Nichols et al., 2007).

Recent biophysical studies employing molecular force measurements have given the possibility to directly confirm this hypothesis and measure the forces required for activating ligand-receptor complexes. Using different force measurement methods, experiments performed in independent groups collectively agree that forces between 4 and 9 pN are sufficient to trigger Notch activation (Chowdhury et al., 2016; Gordon et al., 2015; Seo et al., 2016; Wang and Ha, 2013).

To conclude, both models argue that ligand endocytosis is absolutely required for active Notch signaling. In contrast to the lack of firm correlation between ligand recycling and signaling activation, it seems clear that ubiquitin-dependent ligand endocytosis exerts a pulling-force that is necessary to activate signaling.

II.4. The cis side of Notch signaling

II.4.1. Ligands as inhibitors of Notch signaling

As discussed in the previous sections, Notch ligands present in a sender cell activate Notch receptors present in neighboring cells, which leads to the activation of the Notch signaling pathway in the receptor cell – a process termed trans-activation (Figure 12A). However, studies have indicated that receptors and ligands interactions can also take place in the same cell: Notch ligands can inhibit the signaling activity of Notch receptors present within the same cell. This process is known as cis-inhibition of the receptor by the ligand (Figure 12B).

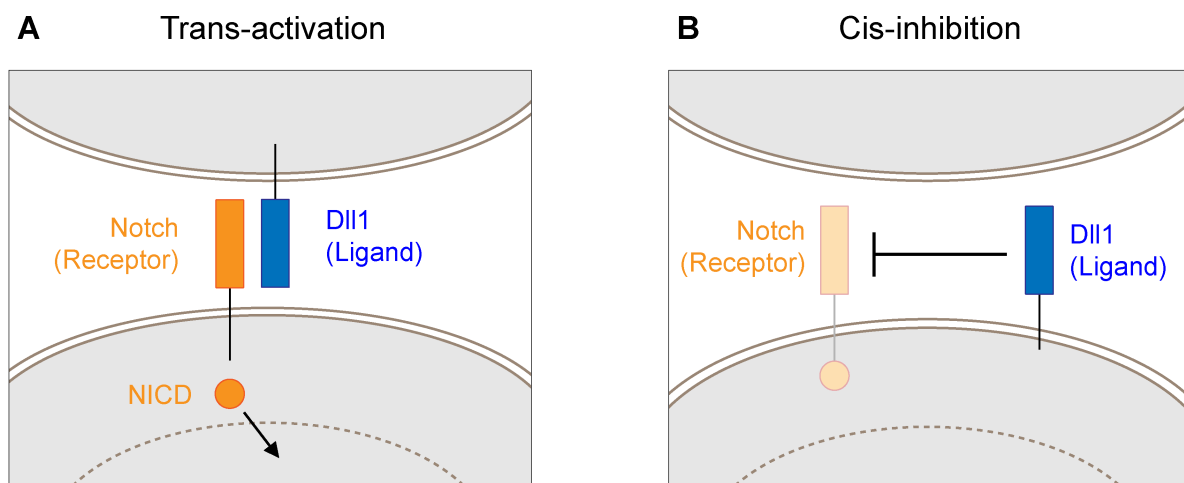


Figure 12. Notch trans-activation and cis-inhibition.

(A) The ligand (blue) at the surface of the signal-sending cell activates the receptor (orange) at the surface of the signal-receiving cell. Upon receptor activation, Notch is cleaved and NICD is released then translocated into the nucleus to activate the transcription of target genes. (B) The presence of ligand and receptor in the same cell leads to the inhibition of the receptor by the ligand (light orange).

First identified through genetic experiments in *Drosophila* (de Celis and Bray, 1997; Klein et al., 1997; Micchelli et al., 1997), cis-inhibition has been suggested to take place in various organisms ranging from *C. elegans* through mammals (reviewed in (D'Souza et al., 2010; del Alamo et al., 2011)).

II.4.1.1. *in vitro* studies

To begin, *in vitro* cell culture experiments using Notch activity reporter have given clues to support the existence of cis-inhibition in vertebrates. Sakamoto and colleagues have shown that when cells expressing both mouse Notch receptor and Hes5(Notch target gene)-luciferase reporter were co-cultured with cells expressing chick Dll1 or chick Jagged1, the Notch activity, as monitored by Hes5-luciferase reporter, was increased, indicative of Notch trans-activation. However, when the ligands Dll1 or Jagged1 were co-expressed with the receptor in the same cell, Notch activity was significantly decreased (Sakamoto et al., 2002). Similarly, transfection of a Notch activity reporter cell line with both Notch receptor and *Xenopus* Delta1 within the same cell showed that *Xenopus* Delta1 inhibits Notch signaling cell autonomously (Itoh et al., 2003).

In addition, an elegant study using a mammalian cell line and mathematical modeling has provided insight into the mechanism of cis-inhibition in vertebrates (Sprinzak et al., 2010). In this study, authors precisely measured Notch activity using a stable cell line for Notch activity reporter, in response to various concentrations of Dll1 in trans and in cis. Trans-Dll1 is presented by the substrate (plate-bound Dll1) while cis-Dll1 is regulated by a doxycycline-inducible promoter (Figure 13A). This led to three key observations (Figure 13B):

- a graded response to trans-Dll1: as trans-Dll1 concentration increases, Notch response increases gradually,
- a sharp response to cis-Dll1: as cis-Dll1 increases, Notch response decreases sharply,
- a fixed threshold for cis-inhibition independently of trans-Dll1 concentration: at varying concentrations of trans-Dll1, a similar sharp response to cis-Dll1 is observed.

These three observations can fit in only one mathematical model that assumes the existence of cis-inhibition. Of note, in this model, cis-regulation accounts not only for the inhibition of the receptor by the ligand but also of the ligand by the receptor. The latter needs to be further explored (Sprinzak et al., 2010).

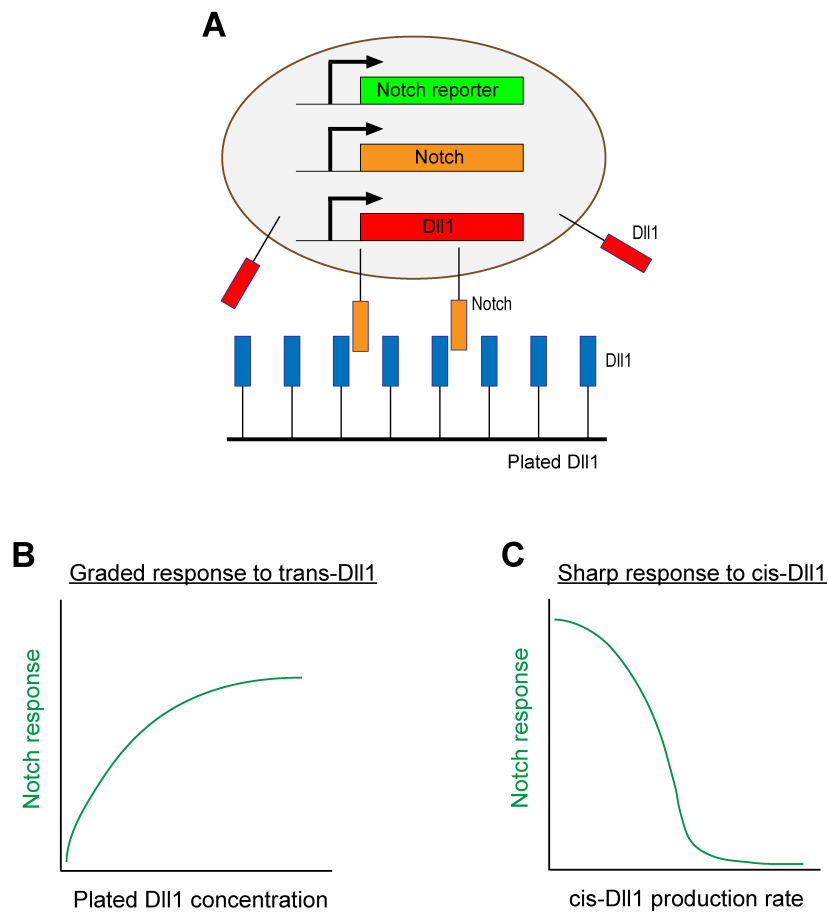


Figure 13. Cis-interactions in cell culture assay.

(A) Experimental assay used in Sprinzak et al., 2010. The stable cell line expressing a reporter for Notch activity (green), Notch1 receptor (orange) and a doxycycline-inducible Dll1 (red) proteins is cultured on Dll1-bound plate. Notch activity is measured as a function of trans-Dll1 and cis-Dll1. (B) Graph representing Notch activity as a function of trans-Dll1 (plated Dll1). As plated Dll1 concentration increases, Notch response increases gradually. (C) Graph representing Notch activity as a function of cis-Dll1 (Dll1 production rate). Adapted from del Alamo et al., 2011.

II.4.1.2. *in vivo* studies

Although several *in vitro* studies have strongly suggested a potential cis-inhibitory activity of Notch ligands, whether endogenous cis-inhibition exist in vertebrates *in vivo* has not been demonstrated. Nevertheless, addressing the question of cis-inhibition *in vivo* is complicated, as any Notch ligand gain- or loss-of-function will affect both trans- and cis- activities. There is, however, one example where the role of cis-inhibition has been clearly demonstrated by loss-of-function experiments, in the *Drosophila* eye (Miller et al., 2009).

The *Drosophila* developing eye is formed by about 800 units called ‘ommatidia’, each of which being composed of a group of 8 photoreceptors (R1-R8). During ommatidial development,

photoreceptor precursors R1-R8 have a very precise sequential pattern of differentiation (Miller et al., 2009). Lateral inhibition between R1/R6/R7 precursors determines their specific fate with cells differentiating either into R1/R6 fate or R7 fate in a Notch-dependent manner: cells with high Notch activity adopt a R7 fate while cells with low Notch activity remain R1/R6 cells. During ommatidial development, R1/R6 cells have physiologically higher levels of Dll1 than R7 cell and activate Notch signaling to the neighboring R7 cell, in order to inhibit the R1/R6 fate in this cell. In principle, two alternative models could explain the fate specification of R1/R6/R7 precursors (Figure 14):

- lateral inhibition with a feedback-loop: the signal-receiving cell (R7) down-regulates the expression of ligands. In this way, the signal-receiving cell (R7) is less likely to activate Notch in return, thus leading to Notch signaling reduction in the signal-sending cell (R1/R6).
- cis-inhibition mechanism: ligands present in the signal-sending cell (R1/R6) inhibit receptors, thus leading to Notch signaling reduction cell autonomously.

To discriminate between the two models, Miller and colleagues performed clonal analysis of *Drosophila* mutant for *Delta* and showed that only the cis-inhibition model could account for the differentiation pattern observed when Delta was removed from R1 cells, thus demonstrating that endogenous ligands can exert inhibitory effects *in vivo* in *Drosophila* (Miller et al., 2009) (see Figure 14).

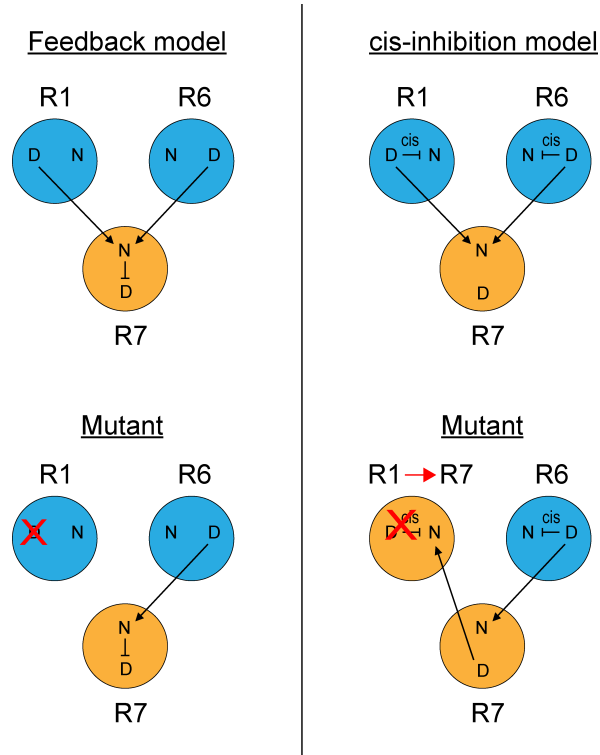


Figure 14. Cis-inhibition in *Drosophila* ommatidia.

During ommatidium differentiation, a group of three cells differentiate either in R1/R6 cells (blue, Notch^{low}) or R7 cell (orange, Notch^{high}). Top-Two models can account for the differentiation pattern observed in the wild-type situation. Bottom-The two models can be discriminated by a D(Delta) mutant in R1, which would be expected to produce different patterns. Left-According to the feedback model, signaling from R6 activates N(Notch) in R7, which in turn down-regulates Delta in R7, preventing it from signaling to R1. Right-By contrast, in the cis-inhibition model, Delta in R7 would not be down-regulated, and therefore could signal to R1, which then adopts the R7 fate. Experimentally, the cis-inhibition model is the one that has been observed *in vivo* (Miller et al., 2009). Adapted from del Alamo et al., 2011.

However, in vertebrates, evidence of cis-inhibition *in vivo* remains scarce and is so far based only on overexpression experiments. Overexpression of the Dll1 ligand in chick and mouse neural progenitor cells increased neurogenesis in isolated cells (Henrique et al., 1997; Kawaguchi et al., 2008). Although both papers at that time explained this phenotype through the classic paradigm of lateral inhibition with a feedback loop, these observations also match with the cis-inhibition model. On the other hand, overexpression of truncated forms of Delta ligands lacking most of the intracellular domain functions cell autonomously as a dominant negative to block Notch signaling and promote neurogenesis in *Xenopus* and chick embryos, a phenotype that cannot be solely explained by the classical lateral inhibition with feedback model (Chitnis, 1995; Cordes et al., 2004; Henrique et al., 1997). Instead, it suggests that the truncated version of Delta can perform a cis-inhibitory activity, even though none of these papers claimed for it at that time.

Overall, overexpression *in vitro* and *in vivo* studies have shown that the ability of ligands to cis-inhibit receptors is conserved in vertebrates. However, as previously mentioned, proving the existence of cis-inhibition *in vivo* in vertebrates is difficult because Notch ligand loss-of-function will impact both trans- and cis- mechanisms. Therefore, it is important to find a way to discriminate between these two phenomena and fill the gap in the literature by clearly demonstrating whether endogenous cis-inhibition takes place *in vivo* in vertebrates.

II.4.2. Molecular interactions underlying cis-inhibition

The molecular mechanisms of ligand inhibitory activity remain poorly defined but several lines of evidence indicate that it involves the direct ligand-receptor interaction through their extracellular domains. More precisely, structural analyses have proposed that both parallel (cis-interaction) and antiparallel (trans-interaction) binding orientations between ligand and receptor can take place and that the DSL domain of Jagged1 interacts with the EGF repeats 11-12 of the Notch receptor for both trans- and cis-interactions (Becam et al., 2010; Cordle et al., 2008; Fiuza and Arias, 2007). As ligand-receptor binding sites for trans- and cis-interactions overlap, a competition between trans- and cis-ligand binding is likely to underlie the ability of ligands to trans-activate or cis-inhibit Notch signaling. Analyses of synthetic Notch receptors (synNotch) responses were consistent with these data. A synNotch receptor is an engineered receptor that contains the core Notch cleavage domain but has the ligand binding part of NECD and the NICD replaced by artificial molecules (Morsut et al., 2016). In this study, the authors observed that the synNotch receptor only activates the signal when the ligand is presented in trans by an opposing neighboring cell, but fails to activate signaling when the ligand is present on the same cell surface in cis. By this way, synNotch recapitulates native cis-inhibition, which strengthens the argument that the binding sites for trans-activation and cis-inhibition are likely to be the same (Morsut et al., 2016).

Still, several questions remain. How can ligand-receptor interaction involving the same binding sites produce opposite effects in cis and in trans? How is cis-inhibition regulated and what are the roles of cis-inhibition in the nervous system? These different questions will be further addressed in chapter V.

II.4.3. Dll3, an exception to the rule

Intriguingly, the mammalian ligand Dll3 represents an exception to the rule as it operates only in a cis-inhibitory mode. From a structural point of view, Dll3 is the most divergent DSL ligand, displaying a highly divergent DSL domain and lacking both the DOS motif and intracellular lysin residues (reviewed in(D'Souza et al., 2010)). Overexpressed Dll3 was unable to bind Notch in trans and activate Notch signaling in mammalian cell culture assays, and in *Xenopus* embryos it mimicked a Notch loss-of-function phenotype (Ladi et al., 2005). Importantly, gene replacement studies in mice demonstrated that Dll3 is unable to rescue Dll1 mutant phenotype in developing mouse embryos, indicating that Dll1 and Dll3 ligands are not functionally equivalent (Geffers et al., 2007). Nevertheless, loss of Dll3 function led to contradictory results. On the one hand, analyses of *Dll3* mouse mutant showed no increase but rather a decrease of Notch targets (Dunwoodie et al., 2002) and NICD (Geffers et al., 2007), suggesting that Dll3 is an activator of the Notch pathway. On the other hand, loss of Dll3 led to an increase of Notch activity during T-cell development (Hoyne et al., 2011) and to broadened expression of Notch signaling in the presomitic mesoderm (Chapman et al., 2011), consistent with the inhibitory activity. Altogether, whether and in which context Dll3 performs cis-inhibition endogenously *in vivo*, how it acts as an antagonist of the Notch pathway and how its function is regulated during development, are currently not known.

II.5. Notch signaling and cell contacts

Another layer of Notch signaling regulation relies on the cellular and tissue context. Given that Notch signaling functions between two juxtaposed cells, the cell-cell contacts and tissue morphology is likely to influence the strength and/or the duration of Notch signaling.

Neuroepithelial cells residing in the neural tube are highly polarized cells connected to neighboring cells at the ventricular surface through apical junctional complexes. Adherens junctions (AJs), with cadherins as their core component, were shown to be important for mediating Notch signaling. In the chick and mouse spinal cords, it was observed that numerous nascent neurons retain apical contacts transiently and form AJ with the neighboring progenitor cells. Disrupting AJ in nascent neurons by specifically overexpressing a dominant-negative form of N-cadherin under the control of the Dll1 promoter, down-regulated Notch signaling in neighboring cells and caused precocious neurogenesis (Hatakeyama et al., 2014). However, given

the broad expression of Dll1, it is difficult to assume the specificity of Dll1 promoter for nascent neurons only. Furthermore, the actual level of Notch signaling in those cells was not reported. On the other hand, it was shown in zebrafish retina that the apical domain size could affect Notch signaling. Expansion of the apical domain size, through manipulation of Llg1 (Llg1-morpholino) or Shroom3 (dominant-negative Shroom3), increased Notch signaling activity cell autonomously as measured by two different Notch activity reporters and significantly reduced neurogenesis (Clark et al., 2012).

In the last years, an increasing amount of investigations suggest that Notch signaling might also be mediated by thin and dynamic actin-based protrusions such as filopodia. Studies performed in the *Drosophila notum* by the group of Buzz Baum revealed the importance of dynamic basal filopodia in the patterning of SOP cells (Cohen et al., 2010; Hunter et al., 2016). Live-imaging analysis suggests that cells are able to send Notch signaling over a long-range distance through dynamic filopodia and interfering with these protrusions perturbs the normal spacing of SOP cells (Cohen et al., 2010). Moreover, differences in the level of signaling between SOP and its primary (direct apical contact) and secondary (contact through filopodia) neighbors correlate with the progression of SOP patterning (Hunter et al., 2016). In vertebrates, two recent studies on the development of pigmented stripes in zebrafish indicated that Notch signaling could also be mediated through long cellular protrusions (Eom et al., 2015; Hamada et al., 2014). However, to date, there is still no direct experimental proof of Notch signaling through filopodia, and no potential mechanism to explain Notch signaling activation by ligand-containing filopodia, since endocytosis does not occur in filopodia ((Kovall et al., 2017), and see section II.3 for the role of ligand endocytosis). Notably, there is evidence against the filopodia model of SOP, showing that Notch signaling is restricted in range to one cell diameter (Troost et al., 2015). Moreover, it is currently unknown whether a similar mechanism exists during vertebrate neurogenesis. This kind of long-range Notch signaling communication beyond their immediate neighbors would provide a possibility of neuronal spacing pattern formation without the need of diffusible factors. It will thus be interesting in the future to investigate whether such long-range Notch signaling takes place in vertebrate central nervous system by providing robust experimental data on the localization of ligands and receptors in those filopodia and investigating the functional role of this type of signaling.

Finally, recent modeling experiments have addressed the question of how cell-cell contact geometry (measured as contact areas) and dynamics of membrane distribution of Notch ligands

(measured as the diffusion coefficient of the Dll1 ligand) could affect the levels and patterns of Notch signaling (Khait et al., 2016; Shaya et al., 2017). Models based on mammalian cell culture predict two possible scenarios: for large contact areas and slow diffusion of the ligand Dll1, signal is proportional to the contact area between cells. By contrast, for small contact areas and fast diffusion of Dll1, signal is independent of contact area but only depends on the diffusion coefficient of Dll1 in the effective contact area (Khait et al., 2016). To experimentally test the dependence of Notch signaling on contact area *in vitro* and to understand the functional outcomes of such dependence *in vivo*, Shaya and colleagues measured Notch signaling between two cells cultured on micro-pattern. Consistent with the model prediction, Notch signaling is proportional with the contact area between two adjacent cells. In addition, simulations predicted that the smallest cells tend to be the signal-sending differentiating cells, while the largest cells tend to be the signal-receiving progenitor cells. In agreement with this model, differentiating presumptive hair cells in the chick inner ear have smaller apical size than their neighbors (Shaya et al., 2017). These results suggest that the dependence of Notch signaling on contact geometry can have implications on cell fate determination. However, further evidence providing a causal link between cell size geometry and Notch signaling is needed to confirm this idea. In addition, Shaya and colleagues do not take into account the situation of filopodia-mediated signaling and this still needs to be elucidated.

II.6. The interplay between Notch and proneural genes

During development, neural progenitors initially proliferate to increase their pool of progenitors and then, in a second time, start to give rise to neurons and glia. The Notch signaling pathway plays a pivotal role in the regulation of progenitor maintenance and neural differentiation, by controlling the expression of multiple bHLH (basic helix-loop-helix) genes: the Notch target genes and the proneural genes.

II.6.1. Notch signaling counteracts neurogenesis

Upon Notch signaling activation, the NICD translocates into the nucleus and associate with CSL (also known as RBP-Jk) and Maml proteins to activate the expression of target genes. Indeed, in knock-out mouse for the Notch intracellular effector RBP-Jk, almost all neural

progenitor cells prematurely differentiated into neurons, revealing the crucial role of Notch signaling in the maintenance of neural progenitors pool (Imayoshi et al., 2010).

In the nervous system, Notch target genes are bHLH (basic helix-loop-helix) transcriptional repressors including the *Hes* family genes. There are seven members in the *Hes* family (homologs of *Drosophila* Hairy and Enhancer of split), among which *Hes1*, *Hes3* and *Hes5* are the ones expressed by neural progenitors. In *Hes1;Hes3;Hes5* triple knock-out mice, the expression of proneural genes is up-regulated, leading to premature neurogenesis, rapid depletion of neural progenitor pool and disruption of structural integrity in the developing spinal cord (Hatakeyama et al., 2004). Mechanistically, these bHLH *Hes* family genes form homodimers and bind to specific DNA elements to inhibit the transcription of target genes (Imayoshi and Kageyama, 2014), which are, in the context of neural development, the proneural genes. As a result, neuronal differentiation is inhibited and neural progenitor state maintained (Kageyama et al., 2005).

II.6.2. Proneural genes promote neurogenesis

By contrast, proneural genes such as *Mash1*, *Math* and *Neurogenins* promote neural differentiation (Bertrand et al., 2002). These genes were first discovered in *Drosophila* and belong to the *Achaete-Scute* complex and *Atonal* genes family. They are bHLH transcriptional activators that form complexes with bHLH E proteins, and bind to E-box consensus sequences in target DNA via their basic domains. Gain- and loss-of-function studies have shown that proneural genes are both necessary and sufficient to activate pan-neuronal differentiation programs and also to specify neuronal subtype identity (Bertrand et al., 2002; Kageyama et al., 2005; Wilkinson et al., 2013). They control a large panel of genes regulating different steps of neurogenesis including: the Notch signaling pathway by up-regulating the expression of the Notch ligand Dll1 (Castro et al., 2006; Lacomme et al., 2012), cell cycle exit (Lacomme et al., 2012), neuronal migration (Heng et al., 2008; Pacary et al., 2013) and acquisition of neuronal subtype identity (Imayoshi and Kageyama, 2014).

The proneural gene Neurogenin2 (*Neurog2*) is a good example of these various implications. For instance, in the developing chick spinal cord, *Neurog2* represses genes expressed in neural progenitors such as *Sox1/2/3* while up-regulating the expression of the Notch ligand Dll1 (Lacomme et al., 2012). *Neurog2* controls a subset of cell cycle regulators, thus triggering cell cycle exit (Lacomme et al., 2012). On the other hand, *Neurog2* activates the

expression of a cascade of neural differentiation genes such as NeuroD family genes while inhibiting gliogenesis (Bertrand et al., 2002; Sun et al., 2001). Furthermore, it contributes to the specification of the motor neuron fate in the ventral spinal cord by activating the expression of the spinal motor neuron marker HB9 (Lee and Pfaff, 2003; Ma et al., 2008). Neurog2 also enhances neuronal migration of cortical pyramidal neurons by inhibiting RhoA expression in mouse developing cortex (Heng et al., 2008). Finally, Neurog2 was shown to play a central role in the cellular remodeling events accompanying neuronal birth, including neural delamination, as we will see in more details in chapter III.

II.6.3. Notch signaling oscillations: a revised view of lateral inhibition

The initial view of Notch-mediated lateral inhibition largely comes from studies of *Drosophila* neurogenesis and *C. elegans* gonadogenesis (Artavanis-Tsakonas et al., 1999; Chitnis, 1995). Among apparently equivalent progenitors expressing similar levels of proneural genes and Notch ligands, a random increase of Notch ligands in one single cell relative to others could lead to a higher activation of Notch signaling in neighboring cells. The latter down-regulate Notch ligand expression and are therefore less likely to activate Notch in return, which forces the former cell to eventually differentiate. Thus, lateral inhibition relies on a small and stochastic difference, which is amplified by a feedback loop until one cell expresses levels of proneural genes and Notch ligands above the threshold required to adopt a differentiated cell fate. These selected cells then activate Notch signaling in neighboring cells and maintain them in an undifferentiated state.

Along this line, initial studies have stated that only committed cells express proneural genes and Notch ligands and are able to activate Notch signaling in neighboring cells, thereby preventing these from differentiating (Artavanis-Tsakonas et al., 1999; Chitnis, 1995; Henrique et al., 1995; Myat et al., 1996). Nevertheless, several studies including those performed in the developing mouse telencephalon, chick spinal cord and chick retina show that proneural genes and Notch ligands are also expressed in neural progenitors at early stages of development, at various levels, forming a ‘salt-and-pepper’ pattern, even when these cells are not yet giving rise to neurons, indicating that the expression of proneural genes and Notch ligands are not restricted to committed cells that will soon become post-mitotic neurons, as previously thought (Hammerle and Tejedor, 2007; Hatakeyama et al., 2004; Nelson and Reh, 2008).

Importantly, the classical view of ‘salt-and-pepper’ pattern has been challenged in vertebrates, because the expression of proneural genes and Notch ligands is found to be

oscillatory in neural progenitors (Imayoshi et al., 2013; Kageyama et al., 2008; Shimojo et al., 2015; Shimojo et al., 2008; Shimojo et al., 2011). Real-time imaging analysis of a luciferase reporter under the control of the *Hes1* promoter in slice culture of mouse telencephalon has revealed that *Hes1* oscillates with a period of about 2-3h in neural progenitors, due to an autonomous negative feedback mechanism. Indeed, *Hes1* represses its own expression by a direct binding to its promoter, which in turn results in the disappearance of *Hes1* mRNA and proteins. Subsequently, the degradation of *Hes1* protein allows the next round of its expression. By this way, *Hes1* protein expression is oscillating in neural progenitors of the mouse cortex (Figure 15). Notably, proneural gene *Neurog2* and Notch ligand *Dll1* expression were also found to oscillate in these cells but with an opposite phase to *Hes1* oscillation. It is likely that the oscillating expression of *Hes1* periodically represses *Neurog2* expression, leading to oscillating *Neurog2* expression, which in turn induces an oscillating *Dll1* expression and to the mutual activation of Notch signaling between neural progenitors (Shimojo et al., 2008). The same oscillatory expression was observed for the proneural gene *Ascl1* in the mouse telencephalon using different approaches (Imayoshi et al., 2013).

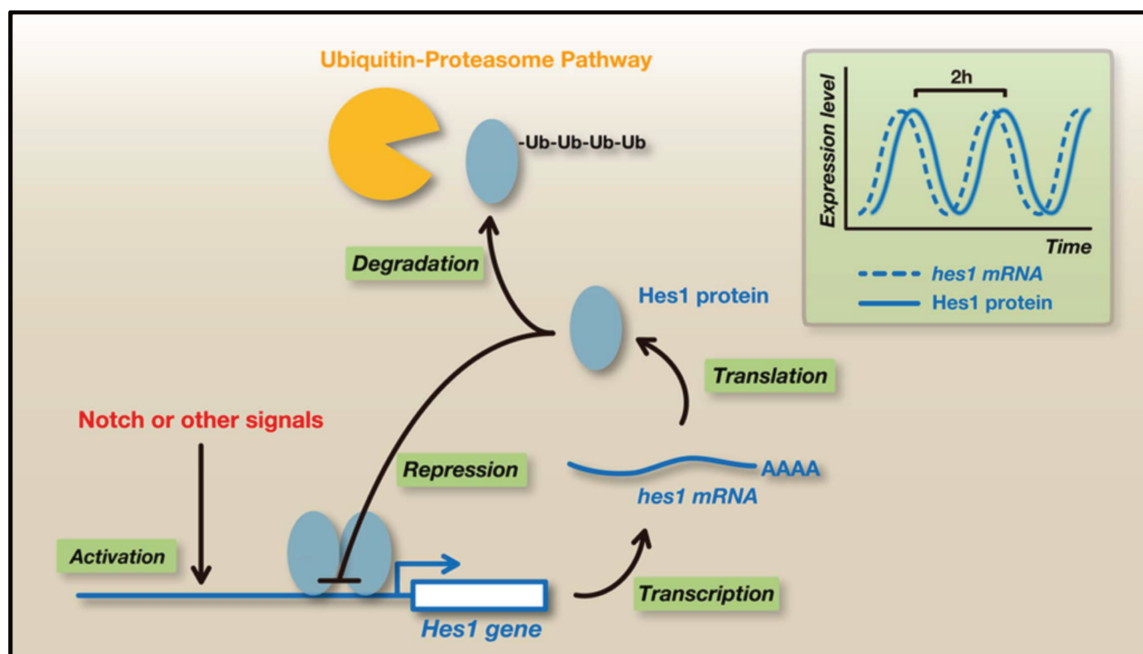


Figure 15. Oscillatory expression of *Hes1*.

Hes1 represses its own expression by directly binding to its promoter. This negative feedback leads to the disappearance of *Hes1* mRNA and protein, because they are extremely unstable, allowing the next round of its expression. In this way, *Hes1* autonomously starts an oscillatory expression pattern. From Shimojo et al., 2011.

In light of these findings, the salt-and-pepper pattern previously observed may not be the result of amplified stochastic differences but only a snapshot of the dynamics of gene expression at a given time point. Contrary to the classic vision of lateral inhibition, the salt-and-pepper pattern is no more stable but dynamically changing and reversible in neural progenitors, thereby making us re-evaluate the classical view of lateral inhibition (Kageyama et al., 2008). Moreover, it is expected that when Neurog2 expression oscillates, it cannot induce neuronal differentiation, probably because downstream effectors are not sufficiently expressed, but rather induces the maintenance of neural progenitor state. At the contrary, it seems that when Neurog2 expression becomes sustained at high levels (and Hes1 stabilized at low levels), it induces neuronal differentiation. Nevertheless, the precise mechanism by which Hes1 oscillations stop and stabilize at low levels is not known. In addition, it is worth to note that this dynamic oscillating activity of Notch signaling was demonstrated in the mouse cortex; how this phenomenon is conserved in other regions of the central nervous system and in other species is currently unknown.

Overall, the classic paradigm of lateral inhibition, assuming an initial uniformly distributed ligand and receptor patterning that is biased through stochastic differences in ligands levels, is reconsidered with the observations of Notch signaling oscillations. With regard to asymmetric division, if not stochastic differences in ligands, then what biases the binary fate outcome between two cells? What are the mechanisms that introduce bias for Notch asymmetric activation?

II.6.4. Making a difference: role of Mib1 and Dll1 for asymmetric Notch activation

Increasing data from the literature now point out that the spatial and temporal regulation of the expression profiles of Notch signaling regulators modulate the asymmetric activation of Notch signaling during asymmetric divisions.

As mentioned in section II.3., ubiquitylation of Notch ligands is a key event that drives ligand endocytosis and effective signaling. In vertebrates, the E3 ubiquitin ligase Mib1 plays an essential role for activating Notch signaling. During mammalian development, Mib1 regulates the endocytosis of all canonical Notch ligands and its disruption leads to pan-Notch defects (Koo et al., 2005; Koo et al., 2007). With regards to neural development, a conditional inactivation of

Mib1 in the mouse telencephalon results in a complete loss of Notch activation, depletion of RG progenitor cells and precocious neuronal differentiation of RG cells into either post-mitotic neurons or into IPs that eventually differentiate into post-mitotic neurons (Yoon et al., 2008). Importantly, based on *in situ* hybridization, the authors suggest that Mib1 is only expressed in IP or newborn neurons but not in RG cells. The formers send Notch signal to neighboring RG cells and maintain them in an undifferentiated state. Thus, these results identify Mib1 as a key player of the Notch signaling pathway to maintain the pool of RG progenitors during mammalian neurogenesis. In addition, as already mentioned in the previous chapter, our own recent work has demonstrated that Mib1 is expressed in neural progenitors of the chick spinal cord, and is preferentially inherited by the prospective neuron following asymmetric division by a centrosome-dependent mechanism. As a result, the Mib1-containing prospective neuron would send Notch signal to its sister cell, thereby maintaining it as a progenitor (Tozer et al., 2017).

Remarkably, the Notch ligand Dll1 was also shown to be asymmetrically distributed during mitosis in the mouse embryonic cortex (Kawaguchi et al., 2013). Together, it is tempting to speculate that Mib1 and Notch ligand Dll1 are both asymmetrically inherited following asymmetric neurogenic divisions but through independent routes, therefore increasing the robustness of Notch asymmetric activation. However, it is not known so far whether Dll1 asymmetric inheritance is conserved in other species and regions of the nervous system and which mechanisms regulate this distribution.

Concluding remarks

Notch signaling is an evolutionarily conserved pathway involved in binary fate decisions during embryonic development and well known to control the switch between neural progenitor maintenance and differentiation. Despite the apparent simplicity of its core pathway, Notch signaling is able to carry out a myriad of tasks and is regulated at different scales to adapt the pathway to each context. Significant studies have provided detailed mechanistic understanding of the signaling activation and ligand-receptor interaction mechanism. A major gap yet to be filled is related to the issue of cis-inhibition mechanism and significance in vertebrate neural development.

In the journey toward differentiation, neural progenitors switch their balance of Notch and proneural genes expression, exit the cell cycle and acquire their characteristic morphology of

differentiated neurons. Related to this issue, the coordination between the dynamics of Notch reduction and the acquisition of neuronal properties, as well as the cellular behavior changes accompanying the birth of a neuron are still poorly characterized.

III

INTRODUCTION

THE BIRTH OF A NEURON: NEURAL DELAMINATION

Chapter III.

The Birth Of A Neuron: Neural Delamination

As previously described in chapter I, neural progenitors are elongated cells displaying strong apical-basal polarity. After neuronal fate commitment, prospective neurons undergo dramatic morphological changes: they translocate their nucleus to the basal side and migrate away to occupy their final position. A prerequisite for this migration is the detachment of the prospective neuron from the ventricular surface, a process called neural delamination. Though delamination of nascent neurons is important for the correct formation of the nervous system, little is known as to the precise intracellular and molecular mechanisms operated to release the newborn neuron from its proliferating neighbors. Insight could be obtained from classical models of epithelial-to-mesenchymal transition (EMT), as cells lose their apical-basal polarity and exit from the proliferative ventricular zone (VZ). The EMT occurs in various tissues and organs during development and is very diverse in terms of genes involved but also concerning the behavior and number of delaminating cells. While in some tissues, all cells are delaminating, in other cases only a few delaminate, posing the problem of the remaining cells. How does the remaining tissue compensate for the departure of the delaminating cell?

To introduce the current knowledge of neural delamination process, after briefly presenting one classical example of the EMT, the delamination of neural crest cells (NCCs), I will describe the structure and the importance of N-cadherin-based AJ (adherens junction) in the developing nervous system. Then I will discuss what can be extrapolated from the typical model of EMT employed by NCCs. This section will end with a description of a recently characterized cellular remodeling process that accompanies neural delamination of prospective neurons.

III.1. An example of delamination: the neural crest EMT program

Sometimes referred to as the ‘fourth germ layer’, the neural crest is a transient population of progenitor cells that generates a wide variety of derivatives, including glial cells, most neurons of the peripheral nervous system, cartilage and bone of the face and melanocytes (reviewed in(Dupin and Le Douarin, 2014)). Initially positioned at the dorsal border of the neural plate, neural crest precursors are induced by the expression of neural crest specifier genes, such as

FoxD3 and Sox10 to become bona fide NCCs (reviewed in(Simoes-Costa and Bronner, 2015)). Then NCCs delaminate from the NT via an EMT (reviewed in(Nieto et al., 2016; Thiery et al., 2009)). After delamination, they collectively migrate, often along long distances throughout the body, and eventually colonize different territories, where they cooperate with other cell populations to form a large collection of cell types. Although our understanding of the EMT program of NCC has increased over the last years (Sauka-Spengler and Bronner-Fraser, 2008), the gene regulatory network operating during EMT is not completely established and importantly, varies across regions (cranial/vagal/trunk) and species.

EMT is a complicated process involving several signaling pathways as well as a precise control of hundreds of effector genes with many regulatory loops, but the major driver of EMT is the direct repression of cell-cell junction genes induced by the neural crest specifier genes (reviewed in(Simoes-Costa and Bronner, 2015)). This process involves the down-regulation of type I cadherins (E-cadherin and N-cadherin) and up-regulation of type II cadherins (Cadherin 7 and Cadherin 11). Since type II cadherins are less adhesive, this switch allows NCC to migrate away from the NT. In the chick embryo, Sox9, Sox10, FoxD3 and Snail family genes orchestrate the switch from type I cadherins to type II cadherins. Indeed, Sox9 and Sox10 repress N-cadherin in cephalic and trunk NCC (Cheung et al., 2005; McKeown et al., 2005). FoxD3 gene is also involved in the transcriptional regulation of cadherins: overexpression of FoxD3 leads to down-regulation of N-cadherin and up-regulation of Cadherin 7 in chick embryos (Cheung et al., 2005; Dottori et al., 2001). However, whether this induction is direct has not been proven. In addition, Snail transcription factors (Snail1 and Snail2) are transcriptional repressors playing important roles in cadherin dissolution: in the chick NT, in the presence of Sox9, forced expression of Snail is sufficient to induce down-regulation of N-cadherin and ectopic delamination of cells (Cheung et al., 2005). Cadherin 6B, which is a type II cadherin that also needs to be down-regulated for the EMT to proceed (Coles et al., 2007), is also down-regulated by Snail2 through direct DNA-binding in the Cadherin 6B regulatory region (Taneyhill et al., 2007). Apart from this transcriptional repression via neural crest specifier genes, cadherins can also be down-regulated via post-translational modifications: for instance at trunk NCCs, BMP4 coming from the adjacent roof plate induces N-cadherin cleavage by ADAM10 then by γ -secretase and promotes neural crest migration (Shoval et al., 2007).

Subsequently to the transcriptional switch from type I to type II cadherins, NCCs undergo important cytoskeletal reorganization to separate from the NT and commence their migration. *In*

in vivo live-imaging of chick trunk and zebrafish hindbrain allowed visualizing the morphological changes exhibited by NCC during EMT (Ahlstrom and Erickson, 2009; Berndt et al., 2008). In both species, premigratory NCCs first lose their AJ. Then, chick NCCs retract the apical cell tail from the lumen of the NT and translocate out of the neuroepithelium and apical-basal polarity is lost (Ahlstrom and Erickson, 2009). In the zebrafish hindbrain, after breaking down AJ, NCCs round up at the basal edge of the NT and extend membrane bleb protrusions. The cell body then translocates to the basal side and retracts from the apical side to migrate out of the NT (Berndt et al., 2008). During this process, the RhoGTPase and its effector Rho kinase (ROCK) play a critical role in regulating those cell morphological changes. Pharmacological inhibition of ROCK or myosin II activity disrupted membrane blebbing and reduced the number of delaminating NCC (Berndt et al., 2008). More precisely, Rho/ROCK activity and F-actin were shown to be enriched in the apical region of the delaminating NCC in an Arhgap1-dependent manner. Arhgap1 is a RhoGTPase activating protein that inactivates RhoGTPase and by this way restricts Rho activation in the apical region during apical detachment. Knocking down Arhgap1 resulted in a broadened activation area of Rho, which prevented delamination. Thus, in zebrafish NCC, Arhgap1 is crucial to concentrate Rho activity in the apical-most region to trigger ROCK-driven actin-myosin contraction apically thereby promoting apical detachment and delamination (Clay and Halloran, 2013). Additional studies are needed to further dissect the regulatory machinery involved in cytoskeletal remodeling in chick NCCs.

In summary, although the complex gene regulatory network underlying the NCC development has not been completely uncovered yet, NCCs stand as an excellent model to study EMT and delamination in vertebrates. Similarly, newborn neurons within the NT must dissociate their cell-cell junctions at the apical surface and undergo massive cell morphological changes to initiate neural delamination and move out from the VZ.

III.2. The importance of adherens junctions in neural tube architecture

III.2.1. N-cadherin based adherens junctions structure

The NT is a pseudostratified epithelium composed of neural progenitor cells. In the spinal cord, progenitor cells adopt a characteristic bipolar morphology with membrane contacting both the apical and basal side of the NT. At the basal end, neural progenitors are attached to the sub-pial extracellular matrix through integrin-laminin interactions, while at the apical side, each

progenitor establishes cadherin-based AJ with its neighbors, maintaining the tissue architecture. AJ, despite involving many actors, is based at its core on N-cadherin protein. The latter starts to be expressed in the nervous system concomitantly with neurulation, where E-cadherin initially expressed by ectodermal cells is replaced by N-cadherin in the developing chick embryo (Dady et al., 2012).

The classical cadherin family comprises 20 members that share a common domain organization. Their extracellular domain is composed of five repetitive subdomains, called cadherin repeats (Meng and Takeichi, 2009). Localized at the apical region of neural progenitors, N-cadherin is a type I classical cadherin that binds to other N-cadherin on neighboring cells through trans-homophilic binding of its extracellular domain. The intracellular domain is highly conserved among the classical cadherin members and binds common catenins. The juxtamembrane portion of N-cadherin is connected to p120-catenin while the C-terminal half of the intracellular domain binds to β -catenin. N-cadherin-based AJ is also associated with the actin cytoskeleton and microtubules. On the one hand, β -catenin binds α -catenin, which in turn, binds actin filaments (F-actin). The interaction between α -catenin and F-actin is rarely direct; rather it involves one or several actin-binding proteins, such as formin (Kobielak et al., 2004), vinculin (Watabe-Uchida et al., 1998) or EPLIN (Abe and Takeichi, 2008). On the other hand, as compared with the actin cytoskeleton, N-cadherin-based AJ associates with the microtubules via p120-catenin. A link between microtubules and p120-catenin is thought to be Plekha7, which binds to microtubules minus-ends and to p120-catenin, thereby associating microtubules and AJ (Meng et al., 2008). Additionally, Plekha7 was also shown to interact with Afadin, which links the transmembrane protein nectin to the actin cytoskeleton (Shah et al., 2016). In this way, the microtubule network and the actin cytoskeleton can interact, via Plekha7 and Afadin (Figure 16).

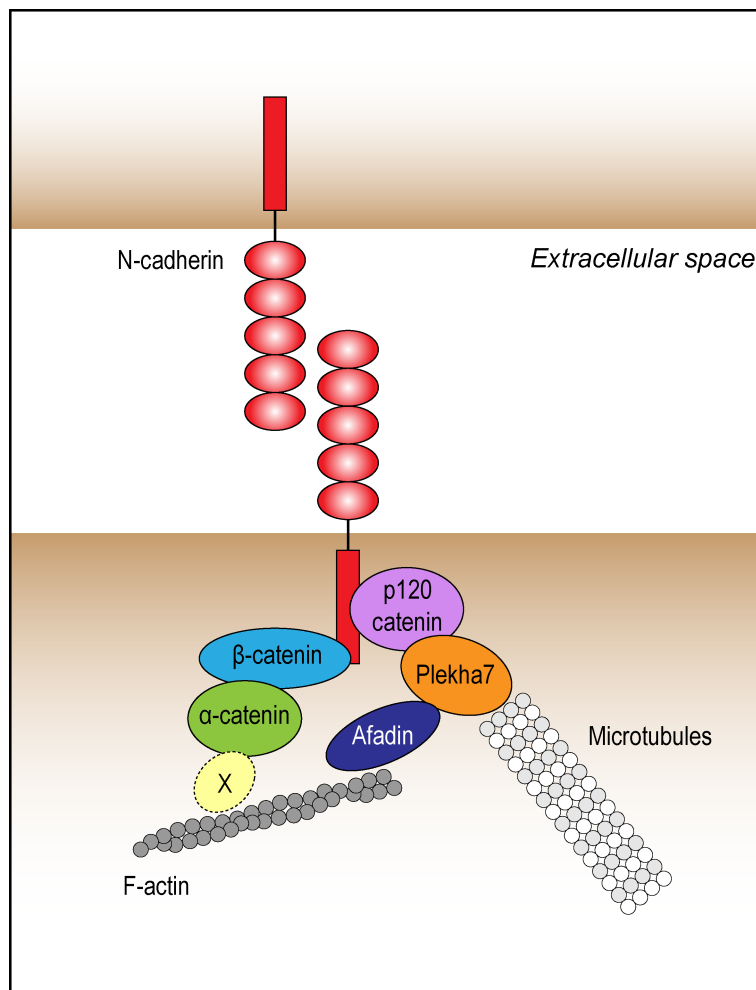


Figure 16. Structure of adherens junction in neural progenitors.

Extracellular domains of N-cadherin on the adjacent cells bind to each other through homophilic interactions, while the intracellular domain of N-cadherin is connected directly or indirectly to β -catenin, α -catenin, F-actin, p120 catenin, Plekha7, microtubules. Actin-binding protein (X) mediates the connection between α -catenin and F-actin. Afadin associated with the transmembrane protein nectin (not represented in this figure) is connected to Plekha7 and F-actin.

III.2.2. Gain- and loss-of-functions of junctional proteins

To further understand the role of N-cadherin-based AJs in the nervous system, insights can be obtained from various mutant mice for junctional protein as well as gain- and loss-of-function experiments for AJ proteins.

First, mutant mice for AJ proteins exhibit many defects in delamination and the integrity of the tissue. Indeed, *N-cadherin* conditional knock-out mice exhibit loss of AJs in the developing cortex, disorganization of cortical layers and mitotic cells localized ectopically throughout the cortex (Kadowaki et al., 2007). Similarly, conditional genetic ablation of the AJ

protein Afadin in mouse dorsal telencephalon results in ‘double-cortex’ formation with disruption of AJs, dispersion of progenitors throughout the cortical wall and neuronal migration defects (Gil-Sanz et al., 2014; Yamamoto et al., 2015). Thus, N-cadherin-based AJs are important for the physical adhesion of neural progenitors and maintain them connected tightly to each other, to preserve the integrity of the neuroepithelium.

In addition, maintenance of AJs seems to be crucial for a well-balanced proliferation and differentiation rates. Loss of N-cadherin function using *in utero* electroporation of shRNA constructs leads to increased cell detachment of neural progenitor cells from the ventricular zone and precocious neuronal differentiation (Zhang et al., 2010). Furthermore, overexpression of a dominant negative form of N-cadherin construct lacking its extracellular domain results in disintegration of AJs, increased neurogenesis, abnormal delamination and ectopic positioning of neurons in the zebrafish retina (Wong et al., 2012) and chick spinal cord (Rousso et al., 2012). Conversely, forced expression of N-cadherin in the chick spinal cord inhibits differentiation and cell detachment from the apical surface (Das and Storey, 2014; Rousso et al., 2012).

All these experiments suggest that N-cadherin-based AJs are key elements to safeguard the proper architecture of the neuroepithelium and to regulate the progression of neurogenesis. Furthermore, they play important roles in the process of delamination. Dismantling of N-cadherin-based AJs is a prerequisite for the onset of delamination of prospective neurons. Then what is the molecular machinery that down-regulates N-cadherin to initiate neural delamination?

III.3. Mechanisms regulating neural delamination

As development proceeds, differentiating cells must detach from neighboring progenitor cells at the apical side and migrate out of the VZ to occupy their final positions. The apical detachment process, known as neural delamination, involves two principal steps: first, the dismantling of AJ and second, the remodeling of the cytoskeleton and the withdrawal of the apical endfoot from the apical surface to initiate movement out of the VZ.

III.3.1. Transcriptional regulation initiating delamination: down-regulation of AJ

To detach from the apical surface, prospective neurons first need to lose their N-cadherin-based AJs. In the chick spinal cord, N-cadherin is positively regulated by the transcription factor Sox2 expressed in neural progenitors (Matsumata et al., 2005) and negatively by the forkhead

transcription factors Foxp2/4 (Roussio et al., 2012). Indeed, during motor neuron development, Roussio and colleagues have shown that overexpression of Foxp2 or Foxp4 results in a rapid loss of N-cadherin and other apical junction proteins, premature detachment of neural progenitors and accumulation of differentiated cells retained closed to the ventricular surface. Consistently, knockdown of Foxp2/4 leads to the opposite phenotype: increase of N-cadherin expression, inhibition of neural delamination and reduction of differentiation. Generation of *Foxp4* knock-out mice gave a similar phenotype in the cerebral cortex and spinal cord, suggesting that the role of Foxp transcription factors is conserved between species and regions of the central nervous system. Moreover, chromatin immunoprecipitation (ChIP) assay shows that Foxp4 binds to a regulatory element in the N-cadherin gene, therefore indicating that Foxp2/4 directly down-regulate N-cadherin to induce delamination. Importantly, the authors propose that upon neural differentiation, the proneural gene *Neurog2* is responsible of inducing Foxp2/4 expression, thus providing a link between neuronal fate commitment and the onset of delamination (Roussio et al., 2012).

Another study has shown that Snail superfamily members *Scratch1/2* regulate delamination in the developing mouse cortex (Itoh et al., 2013). *Scratch1/2* are expressed downstream of proneural genes *Neurog2* and *Ascl1* in committed cells. Knockdown of *Scratch1/2* by *in utero* electroporation of shRNA maintained cells attached to the ventricular surface and prevented their migration, while overexpression of *Scratch1/2* increased the number of cells detached from the apical surface. Together, these data indicate that *Scratch1/2* are important to trigger apical detachment of neural progenitors. Furthermore, by combining overexpression and knockdown of *Scratch1/2* and/or E-cadherin, authors suggest that *Scratch1/2* promote delamination by down-regulating E-cadherin expression. As Snail superfamily transcription factors are known to directly bind to the promoter of E-cadherin to repress its expression in neural crest cells (Thiery et al., 2009), *Scratch*-induced delamination is likely to be mediated by a direct transcriptional repression of E-cadherin (Itoh et al., 2013), as for Foxp2/4 induced N-cadherin down-regulation (Roussio et al., 2012). However, it is worth noting that *Scratch1/2* overexpression had no effect on neurogenesis, unlike Foxp2/4 (Roussio et al., 2012). Rather, it led to ectopic progenitors accumulating out of the ventricular zone (Itoh et al., 2013). Of note, overexpression of *Scratch1/2* down-regulated E-cadherin but not N-cadherin in the mouse developing cortex (Itoh et al., 2013) suggesting that cadherins could have different expression pattern between species (mouse/chick) and/or between regions of the central nervous

system (cortex/spinal cord). Indeed, while the temporal switch from E- to N-cadherin during neurulation has been precisely dissected in the chick embryo (Dady et al., 2012), it is not clear so far whether this timing can strictly be applied to the mouse nervous system. In contrast, E-cadherin expression is detected in the mouse developing cortex later after neurulation (Itoh et al., 2013; Rasin et al., 2007), suggesting that in this system, E-cadherin and N-cadherin both contribute to the maintenance of neuroepithelial integrity and the onset of delamination.

On the other hand, N-cadherin can also be regulated by mechanisms other than transcriptional regulation. For instance, Slit-Robo signaling promotes apical detachment probably by inhibiting N-cadherin-based cell adhesion in the zebrafish retina (Wong et al., 2012) and the developing mouse cortex (Borrell et al., 2012). In these studies, down-regulation of Slit-Robo signaling through morpholino injection in zebrafish or mutant mouse for *Robo*, resulted in an up-regulation of N-cadherin while forced expression of a dominant negative form of N-cadherin was able to rescue the Slit-Robo morphant phenotype (Borrell et al., 2012; Wong et al., 2012). These results suggest that Slit-Robo signaling is capable of inhibiting N-cadherin. Nevertheless, the exact molecular pathway linking Slit-Robo signaling with N-cadherin down-regulation has not been investigated.

In addition, N-cadherin can also be regulated post-transcriptionally via miRNAs. During mouse cortex development, overexpression of the miR379-410 cluster in neural progenitors repressed N-cadherin expression and other AJ proteins and disrupted cortical organization. Furthermore, it increased neurogenesis and neuronal migration, while knockdown of miR379-410 led to the opposite phenotype, suggesting a role for miRNA in regulating neural differentiation and migration (Rago et al., 2014).

Altogether, prospective neurons have increased levels of proneural genes, which in turn activate the transcription program (Foxp2/4 or Scratch1/2) to initiate down-regulation of cadherins (N-cadherin or E-cadherin) and detachment from the apical surface, allowing delamination to take place. These findings, together with the well-documented role of forkhead and Snail transcription factors in regulating cadherins in other systems during EMT (Cheung et al., 2005; Rousso et al., 2012; Thiery et al., 2009), reinforce the close resemblance of the mechanisms underlying down-regulation of AJ between neural delamination of nascent neurons and the EMT program of NCCs.

More recently, a study from the group of Huttner has provided a complementary mechanism to explain the process of basal progenitor delamination in the developing mouse

cortex (Tavano et al., 2018). This study shows how the transcription factor Insm1 (Insulinoma-associated 1), previously known to promote the generation of basal progenitors (Farkas and Huttner, 2008), induces neural progenitor delamination by identifying a transcriptionally repressed target, the apical AJ protein Plekha7. Indeed, forced expression of Insm1 by *in utero* electroporation increased aRG delamination and converted them into bRG. The use of CRISPR/Cas9-mediated disruption of Plekha7 phenocopied the forced expression of Insm1, while forced expression of Plekha7 rescued Insm1-induced delamination phenotype. Interestingly, Insm1 is a downstream target of the proneural gene Neurog2 (Farkas and Huttner, 2008) and transcriptomic analysis upon Insm1 overexpression revealed that Insm1 induced Foxp4 and Scratch2 expression (Tavano et al., 2018), two transcription factors that have also been found to regulate neural delamination as discussed above (Itoh et al., 2013; Rousso et al., 2012), suggesting that different pathways are not mutually exclusive but various genes contribute together to the loss of AJ components and neural delamination process (Figure 17).

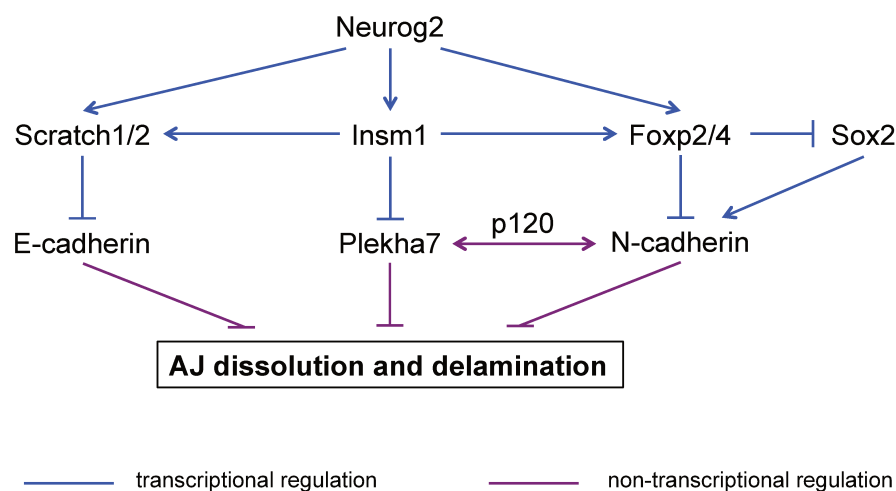


Figure 17. Proposed model of genetic pathway driving neural delamination.

In the mouse developing cortex, the proneural gene Neurog2 induces the expression of Scratch1/2 and Insm1, which in turn repress E-cadherin and Plekha7 expression, respectively. In the chick spinal cord, Foxp2/4 induced by Neurog2 inhibit N-cadherin expression either directly or indirectly by repressing Sox2 expression. As a result, both in the cortex (E-cadherin and Plekha7) and in the spinal cord (N-cadherin), AJ are disassembled and nascent neurons delaminate.

III.3.2. Cellular remodeling: apical abscission and role of the centrosome

Apart from dismantling their AJ, prospective neurons undergo dramatic changes in polarity and cellular architecture, recently addressed in two elegant studies by the group of Kate

Storey. The authors investigated in great detail the cellular remodeling that accompanies neuronal birth using live-imaging assays in the chick spinal cord (Das and Storey, 2014; Kasioulis et al., 2017). Apical detachment of differentiating cells involves a novel cell biological process called ‘apical abscission’ (Das and Storey, 2014). Prior to neural delamination and following down-regulation of N-cadherin, the prospective neuron cuts off its apical-most cell membrane (Figure 18). This apical abscission event is driven by the contraction of actin-myosin cables, as blocking the activity of myosin inhibited apical abscission. Further imaging revealed that the abscission involves shedding of the primary cilium, while the centrosome moves basally from the abscission site and is retained by the delaminating neuron. This dismantling of the primary cilium might be a way for the future neuron to curtail mitogenic signals coming from the intraluminal space, such as Shh signaling, thereby promoting cell cycle exit (Das and Storey, 2014).

Recent work has further addressed the role of cytoskeletal dynamics and the centrosome during neural delamination (Kasioulis et al., 2017). Live-imaging of chick spinal cord slices revealed that the neural delamination process not only requires actin-myosin (Das and Storey, 2014) but also the dynamic microtubule network, as depolymerization or stabilization of microtubules inhibited neural delamination (Kasioulis et al., 2017). More precisely, the retention of the centrosome by the delaminating prospective neuron depends on actin-myosin and microtubule dynamics. Remarkably, actin-myosin and microtubule network changes dramatically their conformation and form a tunnel-like structure at the future abscission site, with the centrosome at the center of the “tunnel”. Then the centrosome translocates basally through the tunnel-like actin-myosin-microtubule ring (Figure 18). During this process, the centrosome plays a critical role by nucleating microtubules at the presumptive abscission site. Indeed, destroying the centrosome in cells poised to delaminate reduced its microtubule nucleating potential and accordingly reduced the number of delaminating cells (Kasioulis et al., 2017).

In terms of the molecules regulating these dynamics during neural delamination, the authors further suggest that the actin binding protein Drebrin may link actin-myosin cable and microtubule network in prospective neurons. In line with this, knockdown of Drebrin by shRNA in Neurog2-induced prospective neurons reduces the number of delaminating cells (Kasioulis et al., 2017). Interestingly, Drebrin has been previously identified as a direct transcriptional target of the proneural gene Neurog2 (Gohlke et al., 2008), linking again transcriptional regulation upon fate commitment and cellular remodeling following neuronal birth.

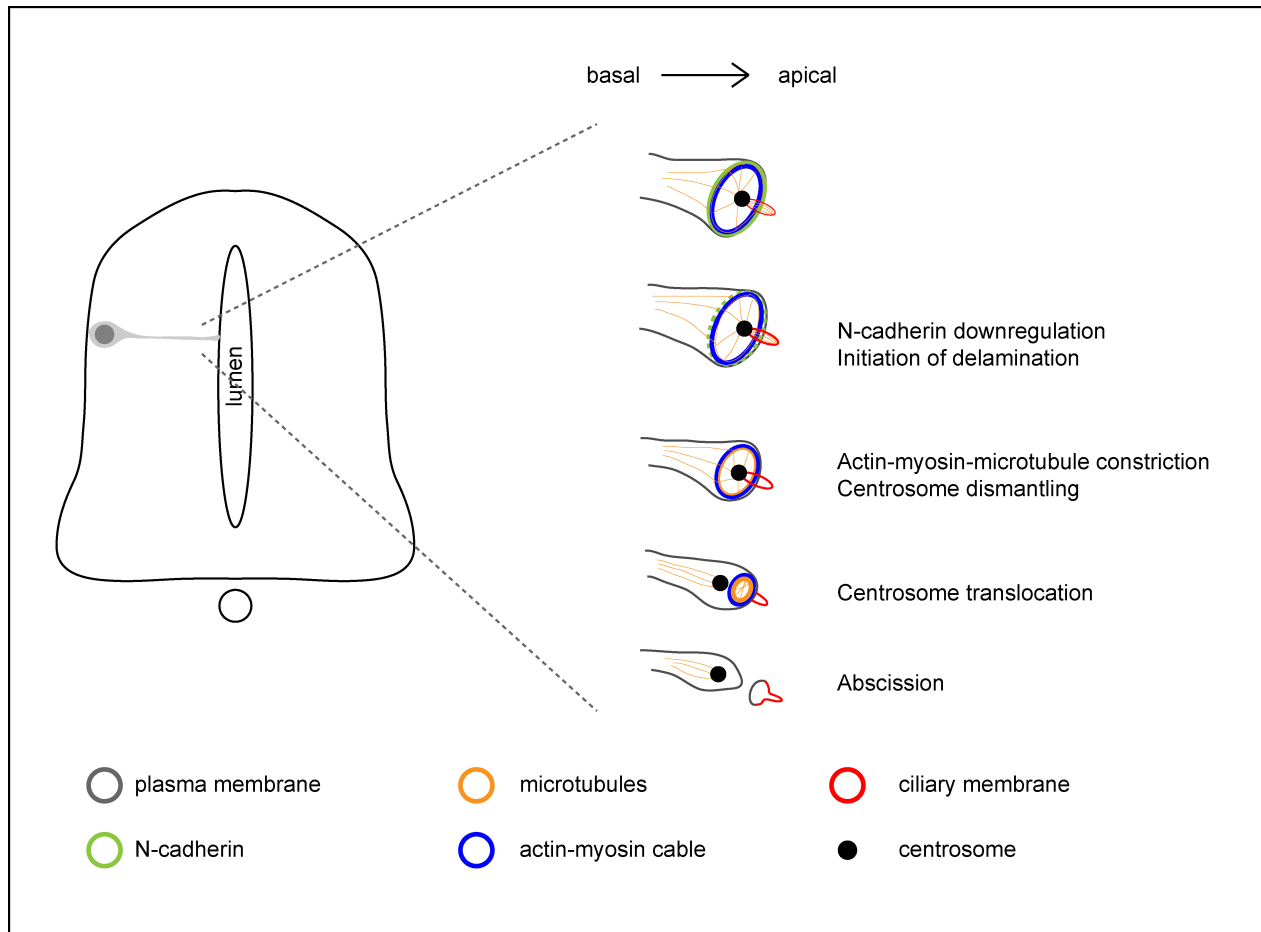


Figure 18. Summary of cell morphological changes in the apical endfoot during neural delamination.

The apical endfoot of prospective neurons contains N-cadherin-based AJ connected to actin-myosin cable and microtubule network. Apical abscission commences with the down-regulation of N-cadherin-based AJ and the constriction of actin-myosin ring. The actin-myosin and microtubule networks acquire a tunnel-like conformation through with the centrosome translocates basally and dismantles from the ciliary membrane. Finally, abscission takes place leaving behind a particle that contains the ciliary and apical-most membranes.

Altogether, these new findings indicate that from a cellular point of view, neural delamination involves a new form of cell sub-division called apical abscission, and that this is driven by actin-myosin constriction and a tunnel-like microtubule configuration generated by the centrosome of the delaminating cell. It will be important to test whether this particular cellular remodeling is conserved across species and regions of the central nervous system, and how this is integrated with the complex gene regulatory network controlling delamination.

Concluding remarks

From the studies discussed here, it seems that while the EMT program engaged by NCC is quite well established, the molecular mechanism driving delamination of newborn neurons in the central nervous system are now starting to be enlighten. Part of these mechanisms resembles some of the classical EMT features of NCC, such as transcriptional repression leading to down-regulation of AJ components and loss of apical-basal polarity. Importantly, as development proceeds, the number of differentiating neurons increases. How does the developing NT preserve its epithelial integrity as increasing numbers of nascent neurons delaminate? How does the tissue compensate for the departure of delaminating neurons? Finally, how are the transcriptional regulation of fate commitment and cellular remodeling coordinated during the birth of a neuron? This thesis aims at providing some elements of answer, which are presented in the next chapter.

Scientific questions and objectives of the project

The development of the central nervous system relies upon the ability of neural progenitor cells to generate neurons and glial cells that further complete specific function in a complex neural network. Throughout development, balancing the rate of proliferation and differentiation is a fundamental issue to generate an organ of robust size and organization, essential to achieve correct function.

My thesis work revolves around two main questions:

- How does the developing neuroepithelium cope with the increasing number of cells delaminating from the ventricular surface?
- What is the temporal progression of Notch down-regulation in the differentiating neuron and what is the contribution of Notch cis-inhibition?

Taking advantage of the chick spinal cord, I have shown that prospective neurons transiently maintain Notch activity and this is required to couple the cellular remodeling during delamination and acquisition of neuronal traits, thereby enabling maintenance of neuroepithelial tissue integrity. Moreover, I have found that Dll1 promotes differentiation by cis-inhibiting Notch activity while Mib1 is able to block this effect to maintain Notch signaling in prospective neurons. These results are presented in the form of published paper.

IV

MATERIAL AND METHODS

Chapter IV. Material and Methods

IV.1. Mib1 prevents *Cis*-inhibition to defer differentiation and preserve neuroepithelial integrity during neural delamination

For materials and methods details, see the appropriate section in the published manuscript presented at p. 99.

IV.2. Perspectives and on-going project

Maintenance and differentiation of mouse ESCs

The ESC lines used were E14Tg2a (a gift from S.L. Ang) and *Tis21*-GFP knock-in line (a gift from W.B. Huttner, (Haubensak et al., 2004)). ESC were maintained at 37°C in a 5% (v/v) CO₂ incubator in ES medium on 0.1% gelatin-coated dishes with mitotically inactivated MEF (mouse embryonic fibroblast) feeder cells. ES medium consists of knockout DMEM medium (Invitrogen) supplemented with 15% FCS (ES-qualified, Millipore), 1% penicilline/streptomycine, L-glutamine, nonessential amino acids, 0.1mM 2-mercaptoethanol and 1000u/ml LIF (Millipore). Cells were passaged every other day and medium was changed every day.

To start a differentiation protocol, ESCs were dissociated and plated at high density (1.5×10^5 cells/cm²) on 0.1% gelatin-coated dishes the day prior to initiation of differentiation and maintained in ES medium. After 24 h (Day 0), ESCs were dissociated using 0.5% trypsin (Invitrogen) and plated at 2×10^4 cells/cm² on 0.1% gelatin-coated dishes in N2B27 medium supplemented with SB431542 (20µM, Stemgent) and LDN193189 (20µM, Stemgent). N2B27 medium consists of a 1:1 mixture of Advanced DMEM/F12 (Invitrogen) and Neurobasal medium (Invitrogen) supplemented with N2 (Gibco) and B27 (Gibco), 1% penicilline/streptomycine, L-glutamine, 0.1mM 2-mercaptoethanol. At Day 2, medium was changed into N2B27 medium supplemented with SB431542 (20µM, Stemgent), LDN193189 (20µM, Stemgent), SAG (500nM, Calbiochem), RA (100nM, Sigma). At Day 3, cells were dissociated with 0.5% trypsin (Invitrogen) and plated at 4×10^4 cells/cm² on poly-L-ornithin (20 µg/ml, Sigma-Aldrich) and

laminin (5 $\mu\text{g/ml}$, Invitrogen) coated dishes in N2B27 medium supplemented with SB431542 (20 μM , Stemgent), LDN193189 (20 μM , Stemgent), SAG (500nM, Calbiochem), RA (100nM, Sigma). For immunohistochemistry and time-lapse experiments, cells were plated on coverslips and glass bottom plates (MatTek), respectively, coated with poly-l-ornithin and laminin. At Day 5, medium was changed into non-supplemented N2B27 medium. Rosettes formation starts at Day 5.

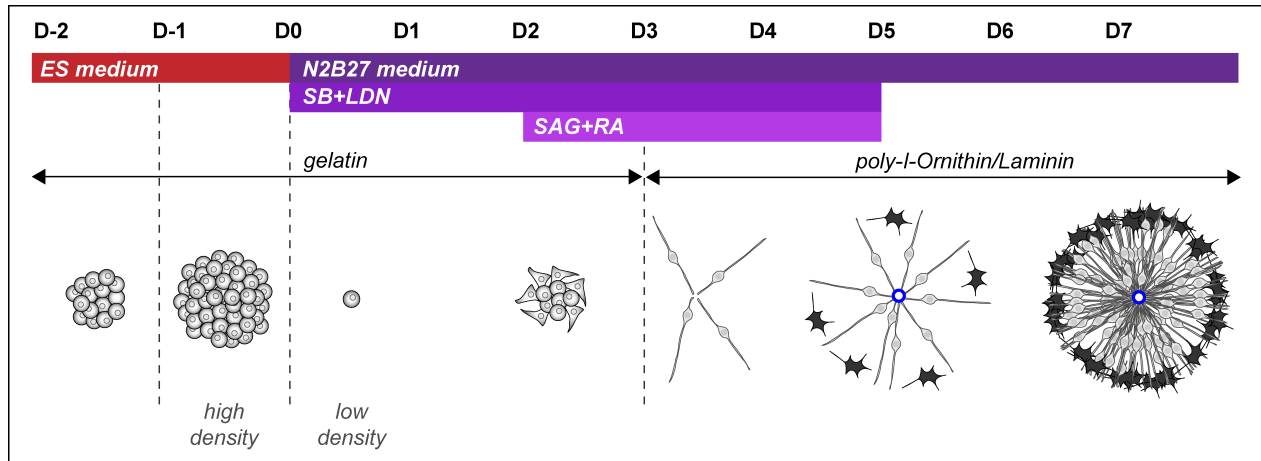


Figure 19. Schematic representation of the differentiation protocol timeline.

CRISPR-Cas9 and donor vector generation

Guide RNAs were designed using the CRISPR design tool (<http://crispor.tefor.net>). A pair of complementary oligonucleotides for each gRNA sequence were hybridized and ligated into Cas9 coding vector (pX330-U6-Chimeric_BB-CBh-hSpCas9, a gift from Feng Zhang (Addgene plasmid #42230) (Cong et al., 2013)). Five gRNA sequences were transfected into MEFs to test their ability to target the 3' end of the Mib1 locus. gRNA cutting efficiency was validated by using the TIDE (Tracking Indels by Decomposition) tool (<https://tide.nki.nl/>) and the following gRNA was selected: 5'-GTCGCAAGGCAATTGAACGA.

For donor vector, we designed a construct to fuse a monomeric GFP at the 3' end of Mib1 locus. Fragments of ~500bp of genomic sequences containing the 3' end (left) and the 3'UTR (right) of mouse Mib1 were synthesized by GenScript in pUC57-mini vector to obtain left and right homology arms. GFP followed by Puromycin cassette sequence was PCR amplified and inserted between the left and right homology arms to obtain the final donor vector (Figure 20).

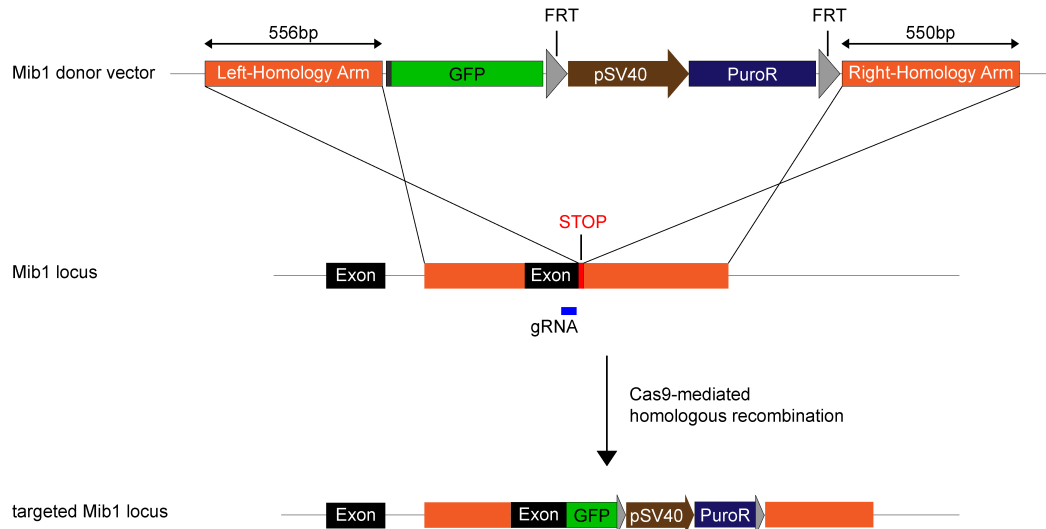


Figure 20. Design of Mib1 targeting.

Generation of Mib1-GFP knock-in ESC line

For the generation of the Mib1-GFP knock-in stable line, E14Tg2a ESCs were electroporated using Amaxa Nucleofector (Lonza) and mouse ESC kit (Lonza) following manufacturer's instructions. Briefly, ESCs (4×10^6 cells) were resuspended in 100 μ l of nucleofection solution, mixed with 3 μ g of donor vector and 1 μ g of Cas9/gRNA vector and electroporated. Immediately after electroporation, cells were replated on 0.1% gelatin-coated dishes with mitotically inactivated MEF feeder cells. Puromycin (Invivogen) selection started 48 h later at 1.5 μ g/ml. Concentration was increased up to 2 μ g/ml 2 d later. After 8 d of selection, resistant ESC clones were picked and cultured in a 96-well plate until most wells were ~80% confluent with cells. Cells were then dissociated with 0.5% trypsin and split into three 96-well plates. Two 96-well plates were frozen at -80°C and the other one was used to prepare genomic DNA for PCR screening of positive clones. To screen knock-in positive ESC clones, genomic PCR was performed using specific primers flanking the left and right homology arms.

Immunohistochemistry

Cells were fixed for 4 min in ice-cold 4% formaldehyde/PBS, rinsed 3 times in PBS, and permeabilized with 0.25% Triton/PBS for 5 min. Cells were blocked for 1 h in PBS-

0.1%Triton/10% Fetal Calf Serum (FCS) and stained with the primary antibodies diluted in the blocking solution at 4°C overnight. The following day, cells were washed 3 times 5 min in PBS-0.1%Triton, incubated 1 h with the adequate secondary antibodies at room temperature, washed again 3 times, and mounted with DAPI containing Vectashield (Vector Labs).

Primary antibodies used are: mouse anti- γ -Tubulin (clones GTU-88, Sigma, 1:500); rabbit anti-Mib1 (Biorbyt, 1:50); mouse anti-Giantin (clones G1/133, Enzo Life Sciences, 1:500); rabbit anti-FOP (FGFR1 Oncogene Partner, 1:500, a gift from Olivier Rosnet, (Acquaviva et al., 2009)); mouse anti-Arl13b (Abcam, 1:500); rabbit anti-Olig2 (Millipore, 1:500); mouse anti-Isl1/2 (clone 39.4D5, DSHB, 1:20); chicken anti-GFP (Aves Lab, 1:800); mouse anti-HuCD (clone 16A11, Life Technologies, 1:50); rabbit anti-phospho-Histone H3 (Millipore, 1:250); mouse anti-N-Cadherin (clone GC-4, Sigma Aldrich, 1:100) (BD Biosciences, 1:250); mouse anti- β III-tubulin (clone Tuj1; Covance, 1:500); rabbit anti-Par3 (Millipore, 1:1000); mouse anti-ZO1 (clone 1A12, ThermoFischer, 1:100); goat anti-Sox2 (clone Y-17, Santa Cruz, 1:100) (R&D systems, 1:1000).

For Mib1 antibody, cells were fixed for 1 min in ice-cold 4% formaldehyde/PBS. For Mib1 and γ -Tubulin antibody, cells were incubated for 10 sec in 100% acetone pre-equilibrated at -20°C, and rinsed twice in PBS at room temperature before the blocking step.

Secondary antibodies coupled to Alexa Fluor 488, Cy3 or Alexa Fluor 649 were obtained from Jackson laboratories.

Image acquisition and processing

Optical sections of fixed samples after immunofluorescence were obtained on a confocal microscope (model SP5; Leica) using 20 \times , 40 \times and 63 \times (Plan Neofluar NA 1.3 oil immersion) objectives and Leica LAS software. For time-lapse experiments, images were acquired in an inverted microscope (Nikon Ti Eclipse) equipped with a spinning disk confocal head (Yokogawa CSU-W1), an sCMOS Camera (OrcaFlash4LT, Hamamatsu) and a 40 \times or a 100 \times oil immersion objective (APO VC, NA 1.4, Nikon), using MicroManager software (Edelstein et al., 2010). Cells were incubated in a microscope chamber at 37°C, under 5% CO₂ in a humidified atmosphere. For image processing and data analysis, we used the ImageJ and FIJI softwares (Schindelin et al., 2012; Schneider et al., 2012). Images were finally subjected to brightness and contrast adjustments to equilibrate channel intensities and background using ImageJ and FIJI software.

V

RESULTS AND DISCUSSION

Chapter V. Results and Discussion

V.1. Mib1 prevents Notch *Cis*-inhibition to defer differentiation and preserve neuroepithelial integrity during neural delamination

During development, the vertebrate neuroepithelium is composed of elongated and polarized dividing progenitor cells. Neural progenitors initially actively proliferate through symmetric divisions, before starting to generate post-mitotic neurons through asymmetric and eventually symmetric neurogenic divisions. In the spinal cord, neural progenitors display a characteristic morphology of bipolar cells that are attached at the apical side to their neighbors through apical junctional complexes and to the basal lamina at the opposite side. As they commit to differentiation, prospective neurons translocate their nucleus to the basal side and eventually withdraw their apical attachment from the ventricular surface.

In the present study, using a Notch reporter transgenic chicken line, we show that the Notch signaling pathway remains transiently active in prospective neurons. This transition period is essential for prospective neurons to allow actin-dependent apical domain constriction to take place before the down-regulation of apical junction proteins and neural delamination. Upon Notch blockade, newborn neurons disassemble their apical junctions but fail to reduce their apical surface and this results in breaches in the ventricular wall, suggesting that Notch activity needs to be transiently maintained in prospective neurons prior to delamination in order to preserve tissue integrity. Secondly, we provide evidence that the Notch ligand Delta-like 1 (Dll1) represses Notch signaling through a *cis*-inhibition mechanism and therefore promotes differentiation. However, the ubiquitin ligase Mindomb1 (Mib1) blocks *cis*-inhibition during the transition period that precedes delamination. This allows Notch activity to be transiently maintained in prospective neurons, which defers differentiation and permits the disassembly of apical junctional complexes to take place only after apical constriction has been completed. Taken together, our results reveal that the temporal control of Notch down-regulation is crucial to coordinate neuronal commitment with neural delamination and therefore preserve neuroepithelial integrity.

A manuscript presenting these data has been published in PLoS Biology (2018).

**Mib1 prevents Notch *Cis*-inhibition to defer differentiation
and preserve neuroepithelial integrity during neural
delamination**

Chooyoung Baek, Lucy Freem, Rosette Goïame, Helen Sang, Xavier Morin
and Samuel Tozer

PLoS Biology, April 30, 2018
<https://doi.org/10.1371/journal.pbio.2004162>

RESEARCH ARTICLE

Mib1 prevents Notch *Cis*-inhibition to defer differentiation and preserve neuroepithelial integrity during neural delamination

Chooyoung Baek^{1,2}, Lucy Freem³, Rosette Goïame¹, Helen Sang³, Xavier Morin^{1*}, Samuel Tozer^{1,4*}

1 Cell Division and Neurogenesis, Institut de Biologie de l'Ecole Normale Supérieure (IBENS), Ecole Normale Supérieure, CNRS, Inserm, PSL Université Paris, Paris, France, **2** Sorbonne Universités, UPMC Univ Paris 06, IFD, Paris, France, **3** The Roslin Institute and Royal (Dick) School of Veterinary Studies, The University of Edinburgh, Easter Bush, Midlothian, United Kingdom, **4** Sorbonne Universités, UPMC Univ Paris 06, UMRS 968, UMR 7210, Institut de la Vision, Paris, France

* samuel.tozer@ens.fr (ST); xavier.morin@ens.fr (XM)



OPEN ACCESS

Citation: Baek C, Freem L, Goïame R, Sang H, Morin X, Tozer S (2018) Mib1 prevents Notch *Cis*-inhibition to defer differentiation and preserve neuroepithelial integrity during neural delamination. *PLoS Biol* 16(4): e2004162. <https://doi.org/10.1371/journal.pbio.2004162>

Academic Editor: Marianne Bronner, California Institute of Technology, United States of America

Received: September 6, 2017

Accepted: March 29, 2018

Published: April 30, 2018

Copyright: © 2018 Baek et al. This is an open access article distributed under the terms of the [Creative Commons Attribution License](https://creativecommons.org/licenses/by/4.0/), which permits unrestricted use, distribution, and reproduction in any medium, provided the original author and source are credited.

Data Availability Statement: All relevant data are within the paper and its Supporting information files.

Funding: INSERM Avenir (grant number R08221JS) to X. Morin's lab. The funder had no role in study design, data collection and analysis, decision to publish, or preparation of the manuscript. Fondation pour la Recherche Médicale (FRM) (grant number DEQ20150331735) "équipe labellisée" grant to X. Morin's lab. The funder had no role in study design, data collection and

Abstract

The vertebrate neuroepithelium is composed of elongated progenitors whose reciprocal attachments ensure the continuity of the ventricular wall. As progenitors commit to differentiation, they translocate their nucleus basally and eventually withdraw their apical endfoot from the ventricular surface. However, the mechanisms allowing this delamination process to take place while preserving the integrity of the neuroepithelial tissue are still unclear. Here, we show that Notch signaling, which is classically associated with an undifferentiated state, remains active in prospective neurons until they delaminate. During this transition period, prospective neurons rapidly reduce their apical surface and only later down-regulate N-Cadherin levels. Upon Notch blockade, nascent neurons disassemble their junctions but fail to reduce their apical surface. This disrupted sequence weakens the junctional network and eventually leads to breaches in the ventricular wall. We also provide evidence that the Notch ligand Delta-like 1 (Dll1) promotes differentiation by reducing Notch signaling through a *Cis*-inhibition mechanism. However, during the delamination process, the ubiquitin ligase Mindbomb1 (Mib1) transiently blocks this *Cis*-inhibition and sustains Notch activity to defer differentiation. We propose that the fine-tuned balance between Notch *Trans*-activation and *Cis*-inhibition allows neuroepithelial cells to seamlessly delaminate from the ventricular wall as they commit to differentiation.

Author summary

The process of neural delamination, whereby nascent neurons detach from the ventricular surface of the neural tube after differentiation, is still poorly characterized. The vertebrate neural tube is initially exclusively composed of neuroepithelial progenitors whose apical attachments ensure the integrity of the ventricular wall. However, as differentiation takes place, increasing numbers of progenitors exit the cell cycle and delaminate, therefore challenging the integrity of the apical surface. Here, we have analyzed the mechanisms

analysis, decision to publish, or preparation of the manuscript. Fondation ARC (grant number RAC12013) to X. Morin's lab. The funder had no role in study design, data collection and analysis, decision to publish, or preparation of the manuscript. Agence Nationale pour la Recherche (ANR) (grant number ANR-12-BSV2-0014-01) to X. Morin's lab. The funder had no role in study design, data collection and analysis, decision to publish, or preparation of the manuscript. AFM Théléthon (grant number R16078JJ) "trampoline grant" to X. Morin's lab. The funder had no role in study design, data collection and analysis, decision to publish, or preparation of the manuscript. Cancéropôle Ile-de-France (grant number 2013-2-INV-05) "moyen équipement," microscopy equipment for X. Morin's lab. The funder had no role in study design, data collection and analysis, decision to publish, or preparation of the manuscript. Fédération pour la recherche sur le Cerveau (FRC) (grant number AOE-9 2014) "Espoir en tête-Rotary," microscopy equipment for X. Morin's lab. The funder had no role in study design, data collection and analysis, decision to publish, or preparation of the manuscript. ANR (grant number ANR-10-LABX-54 MEMO LIFE) labex MemoLife, IBENS. The funder had no role in study design, data collection and analysis, decision to publish, or preparation of the manuscript. ANR (grant number ANR-11-IDEX-0001-02 PSL) IDEX PSL*, IBENS. The funder had no role in study design, data collection and analysis, decision to publish, or preparation of the manuscript. Neuropôle de Recherche Francilien to the imaging platform at IBENS. The funder had no role in study design, data collection and analysis, decision to publish, or preparation of the manuscript. Institut National du Cancer (INCa) (grant number R10074JJ) postdoctoral fellowship to S. Tozer. The funder had no role in study design, data collection and analysis, decision to publish, or preparation of the manuscript. Ministère de l'Enseignement supérieur et de la Recherche (MESR) doctoral fellowship to C. Baek. The funder had no role in study design, data collection and analysis, decision to publish, or preparation of the manuscript. Wellcome Trust (grant number WT094182AIA) to H. Sang's lab. The funder had no role in study design, data collection and analysis, decision to publish, or preparation of the manuscript. BBSRC Strategic Support to H. Sang's lab. The funder had no role in study design, data collection and analysis, decision to publish, or preparation of the manuscript.

Competing interests: The authors have declared that no competing interests exist.

underlying the delamination process in the neuroepithelial tissue. We show that the Notch signaling pathway is active in all progenitors and that its repression is critical for prospective neurons to commit to differentiation. Moreover, we find that the Notch ligand Delta-like 1 (Dll1) represses Notch activity through *Cis*-inhibition of the Notch receptor and induces differentiation. Strikingly, we show that the ubiquitin ligase Mind-bomb1 blocks the *Cis*-inhibition process and allows Notch activity to be transiently sustained, which defers differentiation. This transition period is essential for prospective neurons to constrict their apical domain before delamination, as the alteration of this sequence results in breaches in the ventricular wall, followed by massive tissue disorganization. Taken together, our results reveal that the temporal control of Notch down-regulation needs to be tightly coordinated with the delamination process to preserve the integrity of the ventricular wall while allowing neuroepithelial cells to differentiate.

Introduction

The vertebrate neuroepithelium is initially composed of elongated progenitors polarized along the apical–basal axis that actively proliferate. After a phase of expansion, these progenitors start producing neurons through asymmetric and eventually symmetric neurogenic divisions. Following mitosis, daughter cells committed to differentiation translocate their nucleus to the basal side of the neural tube (NT) before they delaminate from the ventricular surface. Neuroepithelial cells are attached to their neighbors through apical junctional complexes. As they enter differentiation, they down-regulate N-Cadherin levels, a prerequisite for the retraction of the apical endfoot and expression of neuronal markers [1, 2]. Nevertheless, the cellular events that accompany the delamination process and make it compatible with the maintenance of tissue integrity are still unclear.

The balance between proliferation and differentiation in the NT, although involving a long list of regulators, relies at its core on the antagonistic action of Notch downstream targets and proneural genes [3]. Notch signaling plays a well-documented role in binary fate decisions in many systems and specifically promotes the maintenance of the undifferentiated state in the nervous system [4–7]. On the other hand, proneural genes are basic helix-loop-helix (bHLH) transcription factors that promote cell cycle exit and neural commitment [8]. Thus, neural differentiation is accompanied by increased levels of proneural gene expression and loss of Notch activity. However, the functional connection between these two processes during the transition from progenitor to neuron remains to be clarified. Although proneural genes induce differentiation, they cannot directly inhibit Notch signaling. Instead, they control the expression of Notch ligands [9–12], which were shown to promote differentiation in individual cells [13, 14]. However, their mode of action during that process has proven difficult to characterize. According to the "lateral inhibition with feedback" model, the increased expression of Notch ligands in the signal-sending future neuron would strongly *Trans*-activate Notch signaling and therefore down-regulate Notch ligand expression in the neighboring progenitors. These would, in return, poorly *Trans*-activate Notch in the signal-sending cell, and shutdown of the signaling pathway would allow this cell to differentiate [15]. While there is good evidence suggesting that increased Notch ligand expression inhibits differentiation non-cell autonomously (i.e., through lateral inhibition) [16, 17], whether a feedback mechanism down-regulates Notch activity in the signal-sending cell has not been proven in vertebrates. On the other hand, studies in *Drosophila* have shown that Notch ligands are able to inhibit the signaling activity of Notch receptors present in the same cell, a process termed "*Cis*"-inhibition [18–20].

Abbreviations: Δ Maml1, dominant-negative Mastermind-like 1; Δ Mib1, dominant-negative Mib1; bHLH, basic helix-loop-helix; cHes5.1, chicken Hairy and Enhancer of Split 5.1; CFSE, carboxyfluorescein succinimidyl ester; DAPT, N-(3,5-difluorophenylacetyl-L-alanyl)-S-phenylglycine t-ButylEster; dl6, dorsal interneuron domain 6; Dll1, Delta-like 1; Dll3, Delta-like 3; E, embryonic day; EdU, 5-ethynyl-2'-deoxyuridine; EP, electroporation; Epb4115, Erythrocyte membrane protein band 4.1-like 5; FCS, fetal calf serum; FERM, band 4.1 protein/Ezrin/Radixin/Moesin domain; FoxP2/4, Forkhead transcription factors FoxP2 and FoxP4; FT, FlashTag; GFP, green fluorescent protein; hae, hour after electroporation; Hes5, Hairy and Enhancer of Split 5; HuCD, neuron-specific RNA-binding proteins HuC and HuD; H2B, Histone 2B; H2B-Cherry, Histone 2B fused to Cherry; H2B-GFP, Histone 2B fused to GFP; iRFP, infrared fluorescent protein; Mib1, Mindbomb1; mbMib1, Mib1 constitutively tethered to the plasma membrane; Neurog2, Neurogenin 2; NICD, Notch intracellular domain; NT, neural tube; Par3, Partition defective protein 3; Pax6, Paired box gene 6; p120-catenin, Adherens junction protein p120; ROCK, Rho kinase; RII-C1, Shroom3 binding site on ROCK2; shDll1, shRNA against Dll1; shRNA, short hairpin RNA; Shroom3, Shroom family member 3; Sox2, SRY (sex determining region Y) box 2; V1, intermediate ventral interneuron domain 1; VNP, Venus-NLS-PEST; VZ, ventricular zone; ZO1, Zonula Occludens 1.

This would in theory allow the direct inhibition of Notch receptors by their ligands in the differentiating cell. In vitro experiments and overexpression studies in vivo have shown that the ability of Delta ligands to *Cis*-inhibit Notch receptors is conserved in vertebrates [21, 22]. However, proving the existence of *Cis*-inhibition in vivo is hampered by the fact that Notch ligand loss-of-function will affect both *Trans*- and *Cis*- activities. In this regard, Delta-like 3 (Dll3) represents an interesting exception to the rule, as it can *Cis*-inhibit Notch receptors but is unable to *Trans*-activate, possibly due to a divergent structure in its extracellular domain [23–26]. However, whether *Cis*-inhibition by other Notch ligands takes place endogenously and how it integrates with *Trans*-activation during development still need to be addressed.

Here, we show that Notch signaling is maintained in prospective neurons, i.e., cells that have completed mitosis but are not yet expressing neuronal differentiation markers. This sustained activity is crucial to allow them to constrict their apical endfoot before they reduce apical junction markers, thus preserving the integrity of the tissue. Moreover, we provide evidence that differentiation is achieved through *Cis*-inhibition of Notch by its ligand Delta-like 1 (Dll1). Finally, we show that the ubiquitin ligase Mindbomb1 (Mib1), by transiently favoring *Trans*-activation at the expense of *Cis*-inhibition in prospective neurons, defers differentiation and allows the tissue to reconcile neuronal commitment with epithelial maintenance.

Results

Notch signaling is maintained in prospective neurons

Following the completion of mitosis, prospective neurons remain attached to the ventricular surface for a transition period of up to 20 h before they eventually retract their apical endfoot as they start expressing the early differentiation marker class III β -tubulin (Tuj1) [1, 27]. While it is accepted that Notch activity is switched off in differentiated cells, the state of signaling during the transition period that precedes has never been explored. We decided to address this point in a chicken transgenic line carrying a fluorescent reporter of Notch activity. A transgene containing the promoter of the Hairy and Enhancer of Split 5 (Hes5) gene (a target of the Notch pathway) upstream of a destabilized nuclear Venus coding sequence (Venus-NLS-PEST [VNP]) [28] was inserted into the chicken genome (Fig 1A, and see Materials and methods). We first investigated the intensity of the VNP signal through immunostaining (the native VNP signal does not allow direct visualization) in normal conditions. Hes5-VNP distribution was consistent with the endogenous chicken Hairy and Enhancer of Split 5.1 (cHes5.1) expression at embryonic day (E) 4 (S1A Fig, [29]), while nuclear localization of the VNP signal provided a better cellular resolution. Transverse sections of the spinal cord were analyzed during early neurogenesis (E3 and E4), and VNP signal intensity was compared between progenitors and neurons (Fig 1B, the red line delimits the boundary of the differentiated zone in the color code panel). While progenitors displayed a wide spectrum of VNP intensities, all neurons (identified by the expression of the neuron-specific RNA-binding proteins HuC and HuD [HuCD]) showed low VNP levels. This is consistent with data obtained in the mouse cortex using a Hes1 reporter suggesting that Notch target gene expression oscillates in progenitors and is switched off during differentiation [3].

We next assessed whether VNP intensities would reliably reflect perturbations of Notch signaling activity. Notch gain-of-function through overexpression of the Notch intracellular domain (NICD) resulted in a 6-fold increase in VNP intensities as well as a blockade of differentiation (S1B Fig). Conversely, incubation of NT explants with the Notch signaling inhibitor N-(3,5-difluorophenylacetyl-L-alanyl)-S-phenylglycine t-ButylEster (DAPT) led to a rapid reduction of the VNP signal, suggesting a half-life of the reporter of less than 4 h, reaching down to the background level measured in neurons within 6 h of incubation (S1C Fig). Thus,

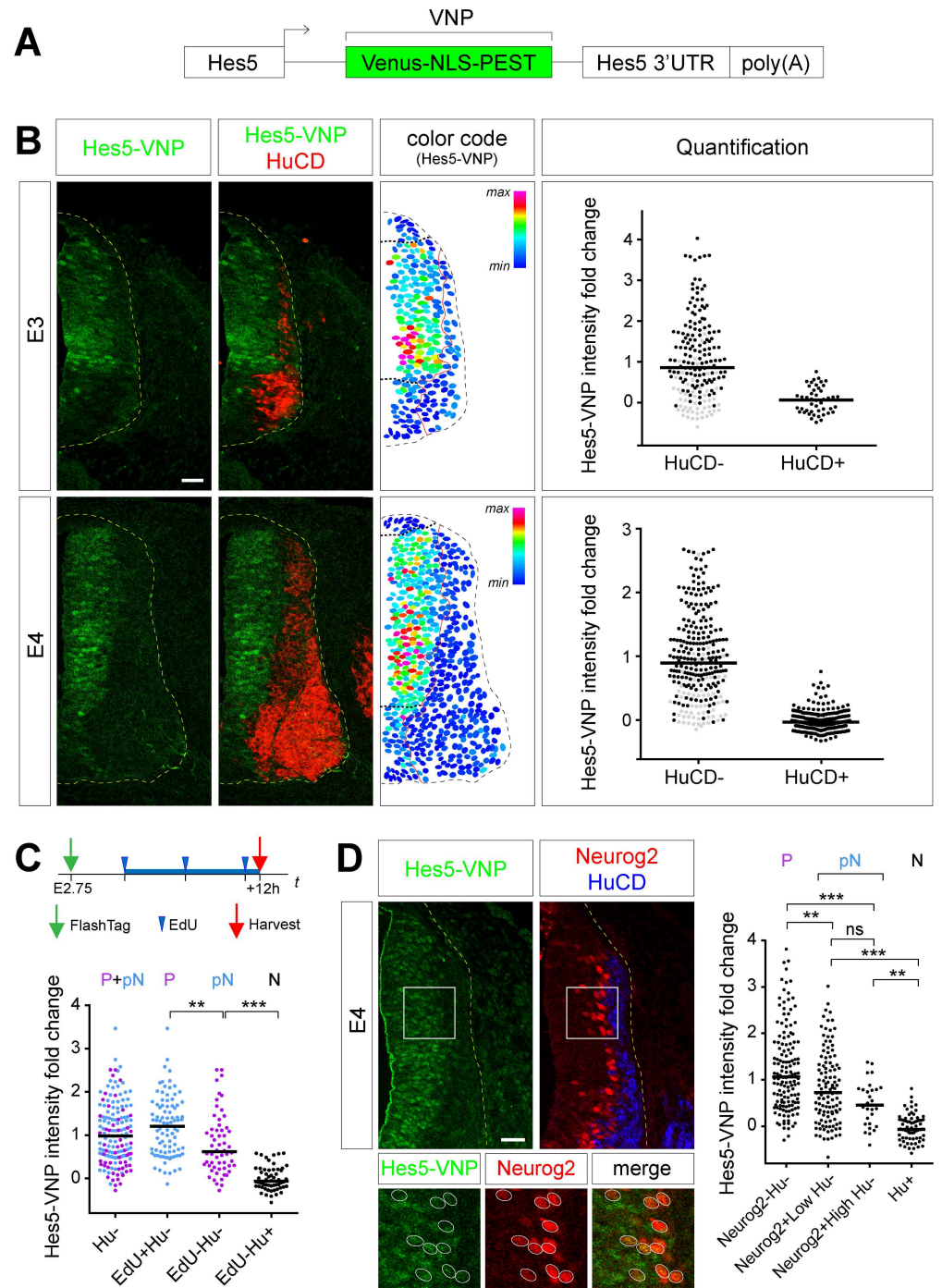


Fig 1. Notch signaling is maintained in prospective neurons. (A) Schematic representation of the Hes5-VNP sequence that was inserted in the Notch reporter transgenic chick line. (B) Left: Transverse sections of the NT of the Hes5-VNP transgenic line at E3 and E4 immunostained for Venus (green) and HuCD (red) to label neurons. Middle: Color coded map of Hes5-VNP intensity. The red line separates HuCD⁻ from HuCD⁺ cells. The black dotted lines delineate the ventral limit of the roof plate and dorsal limit of the motor neuron domain. Right: Distribution of the Hes5-VNP signal intensity in HuCD⁻ and HuCD⁺ cells. Note that cells within the limits of the black dotted lines of the color code panel were labeled in black in the HuCD⁻ population. (C) Top: Time course of the protocol. Bottom: Distribution of the Hes5-VNP signal intensity in FT⁺/HuCD⁻ cells. This population is then divided into EdU⁺ (blue) and EdU⁻ (magenta) cells. A minimum of 58 cells collected from four embryos were analyzed for each group. (D) Left: Transverse sections of the dorsal NT in the Hes5-VNP transgenic line at E4 immunostained for Venus (green), Neurog2 (red), and HuCD (blue). Bottom: Enlarged view of the boxed area showing representative examples of

Neurog2⁺ cells. Right: Distribution of the Hes5-VNP signal intensity in Neurog2⁻ and Neurog2⁺ cells. The latter population was divided based on Neurog2⁺ signal intensity. A minimum of 75 cells collected from six embryos were analyzed for each group. Horizontal bars correspond to medians. ns, $p > 0.05$; ** $p < 0.01$, *** $p < 0.001$ (Kruskal-Wallis test). Underlying data are provided in [S1 Data](#). Scale bar represents 25 μm . See also [S1](#) and [S2](#) Figs. E, embryonic day; EdU, 5-ethynyl-2'-deoxyuridine; FT, FlashTag; Hes5, Hairy and Enhancer of Split 5; HuCD, neuron-specific RNA-binding proteins HuC and HuD; Neurog2, Neurogenin 2; ns, nonsignificant; NT, neural tube; VNP, Venus-NLS-PEST.

<https://doi.org/10.1371/journal.pbio.2004162.g001>

the Hes5-VNP chicken line appears as an excellent tool to monitor the dynamics of Notch signaling in the embryonic spinal cord. Progenitors located in the roof plate region, and ventrally up to the dorsal limit of the motor neuron progenitor domain (delimited by the black dotted lines in [Fig 1B](#), Middle) displayed a lower Notch activity compared to the rest of the ventricular zone (VZ) ([Fig 1B](#), Right; cells in those regions are represented by gray dots). This pattern is consistent with previous reports that floor and roof plates are signaling centers displaying low Notch activity, while the reduced Notch levels measured in the motor neuron progenitor domain may be associated with the early and massive motor neuron differentiation process [30].

Then, we sought to characterize the level of Notch activity in prospective neurons. To this end, we first took advantage of the FlashTag (FT) technique, based on the ability of the cell-permeant dye carboxyfluorescein succinimidyl ester (CFSE) to fluorescently label intracellular proteins. Previous experiments in the mouse developing cortex have shown that upon injection in the ventricles, FT dyes preferentially enter progenitor cells undergoing mitosis, offering a convenient means to synchronously label a cohort of dividing cells and track their progeny over different time periods [31]. To validate the technique and calibrate its dynamics in the chick spinal cord, FT was injected in the NT at E2.75 and fluorescence was monitored at different time points. Fifteen minutes after injection, FT⁺ cells' nuclei were exclusively located near the ventricular surface, and many were positive for phospho-Histone H3, consistent with the preferential labeling of cells undergoing mitosis ([S2A Fig](#)). Increasing incubation times (1 h, 4 h) correlated with FT⁺ nuclei being located at progressively more basal positions and no longer in mitotic cells. This indicates that incorporation into mitotic cells was restricted to a short time period after FT injection, allowing the labeling of a cohort of cells that collectively undergo mitosis in a very narrow time window. We then asked whether the progeny of mitotic cells labeled with FT entered S phase or exited the cell cycle and differentiated. Embryos were injected with the FT dye at E2 or E2.75 (respectively before and after the onset of neurogenic divisions). EdU (5-ethynyl-2'-deoxyuridine) was injected 3 h after FT injection and then every 4 h in order to cumulatively label the whole population of cycling cells ([S2B Fig](#)). Embryos were harvested at different time points after FT injection and labeled for EdU incorporation and HuCD expression ([S2C and S2D Fig](#)). In both conditions, the number of FT⁺/EdU⁺ cells reached a plateau by 12 h after FT injection, indicating a saturating labeling of cycling progenitors with EdU ([S2C and S2D Fig](#)). Consistent with the fact that virtually all progenitors undergo symmetric proliferative divisions at E2 (excluding the motor neuron domain, which differentiates earlier than the rest of the NT and was excluded from the analysis), the plateau of FT⁺/EdU⁺ was close to 100% in embryos injected at E2 ([S2D Fig](#)), and no FT⁺/HuCD⁺ cells were found. By contrast, in embryos injected at E2.75, the plateau of FT⁺/EdU⁺ cells remained below 65% ([S2D Fig](#)). Thus, about one third of FT⁺ cells remained EdU⁻. Within this population, the proportion of HuCD⁺ neurons increased between 12 h and 16 h ([S2C and S2D Fig](#)). Therefore, three populations could be discriminated based on EdU incorporation and HuCD expression: cycling progenitors (EdU⁺/HuCD⁻), prospective neurons (EdU⁻/HuCD⁻), and neurons (EdU⁻/HuCD⁺). We then investigated the level of Notch signaling in these three

populations using FT injection in the Hes5-VNP chicken line. Strikingly, levels of Notch activity in EdU⁻/HuCD⁻ prospective neurons remained elevated 12 h after mitosis (with a median of 0.62 and a mean of 0.80 ± 0.09 , the average VNP intensities measured in HuCD⁻ and HuCD⁺ cells being normalized to 1 and 0, respectively [Fig 1C]). This sustained activity is not due to inertia of the Venus reporter fluorescence, because DAPT treatment of NT explants results in complete loss of Venus fluorescence within 6 h (S1C Fig). Hence, prospective neurons maintain high Notch signaling activity up to 12 h after they exit the cell cycle and until they enter differentiation.

To strengthen these results, we sought to identify the population of prospective neurons by another means. As proneural genes promote cell cycle exit and neural commitment [8], they are likely to be expressed at high levels in prospective neurons. We focused on the proneural gene Neurogenin 2 (Neurog2), which is widely expressed in the chick spinal cord [32]. Neurog2 was strongly expressed at the basal limit of the VZ but also in scattered cells within the VZ, albeit at lower levels (Fig 1D). Cumulative EdU incorporation and HuCD staining indicated that these two populations, referred to as Neurog2^{Low} and Neurog2^{High}, had mostly exited the cell cycle (S2E Fig), while only a fraction had differentiated (S2F Fig). Thus, the vast majority of Neurog2⁺/HuCD⁻ cells correspond to prospective neurons, amongst which, Neurog2^{High} cells are likely to be closer to differentiation (as twice more Neurog2^{High} than Neurog2^{Low} have started to express the differentiation marker HuCD [S2F Fig]). We compared the level of Notch activity in Neurog2⁻/HuCD⁻ cells (which closely match the progenitor population), Neurog2^{Low}/HuCD⁻ and Neurog2^{High}/HuCD⁻ cells (prospective neurons), and HuCD⁺ neurons. Remarkably, Neurog2 negative, Low, and High populations of HuCD⁻ cells exhibited progressively lower Notch activity but remained above the level measured in the HuCD⁺ neuronal population (Fig 1D).

Taken together, these results indicate that Notch signaling is maintained in prospective neurons until they eventually differentiate. This raises the question of the importance of maintaining Notch activity during the events preceding differentiation.

Maintenance of Notch signaling is required for proper neuronal delamination

A hallmark of neuronal differentiation is the withdrawal of the apical attachment from the ventricular surface [1, 2, 27, 33]. To gain insight into the cellular events that accompany this delamination process, we investigated three parameters in parallel: the size of the apical area, the level of N-Cadherin at apical junctions, and the expression of the early differentiation marker Tuj1 at the apical surface (i.e., in nascent neurons that are still attached). These parameters were analyzed at 6, 12, 18, and 24 hours after electroporation (hae), focusing on single electroporated cells surrounded by non-transfected neighbors (the latter were used as a reference for measurements; see Materials and methods). Electroporation targets a mix of cycling progenitors and apically attached prospective neurons. While early time points (6 h, 12 h) will still retain many progenitors, these will eventually divide and appear as pairs that will be discarded from the analysis, such that at later time points (18 h, 24 h), the selected population will be enriched in prospective neurons. In cells transfected with a ZO1-GFP control vector alone, a decrease in the apical area was apparent at 18 hae and was further enhanced at 24 hae (Fig 2A, top panel). We also observed a modest decrease of N-Cadherin levels at 24 hae, which was not significant when considering the whole population (Fig 2A, top panel). However, when “small” (below the median) and “large” (above the median) areas were discriminated at 24 hae, we observed a significantly lower level of N-Cadherin in cells with a small apical area (Fig 2B). Moreover, the differentiation marker Tuj1 was almost exclusively expressed in this population

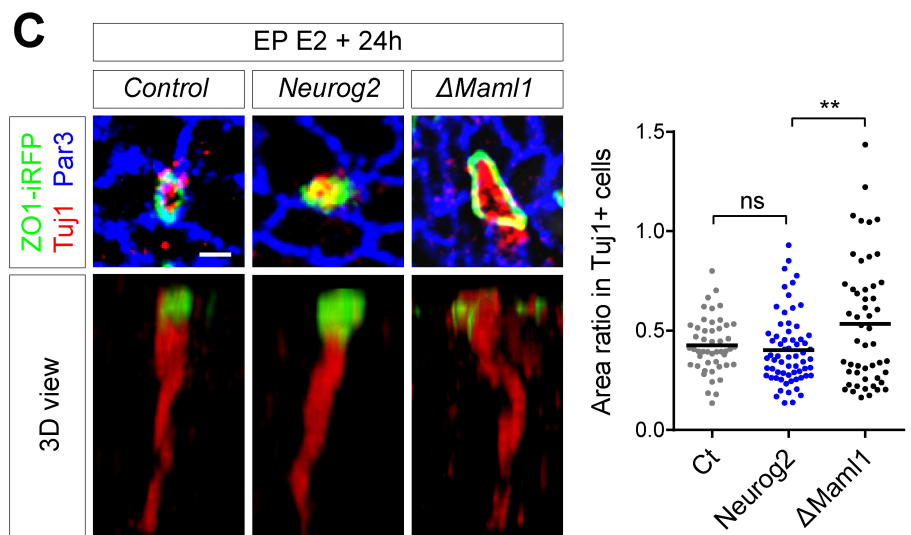
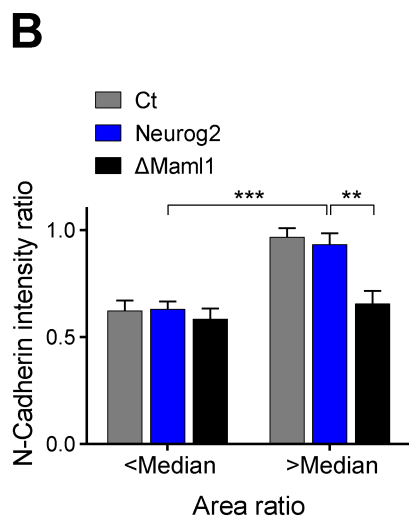
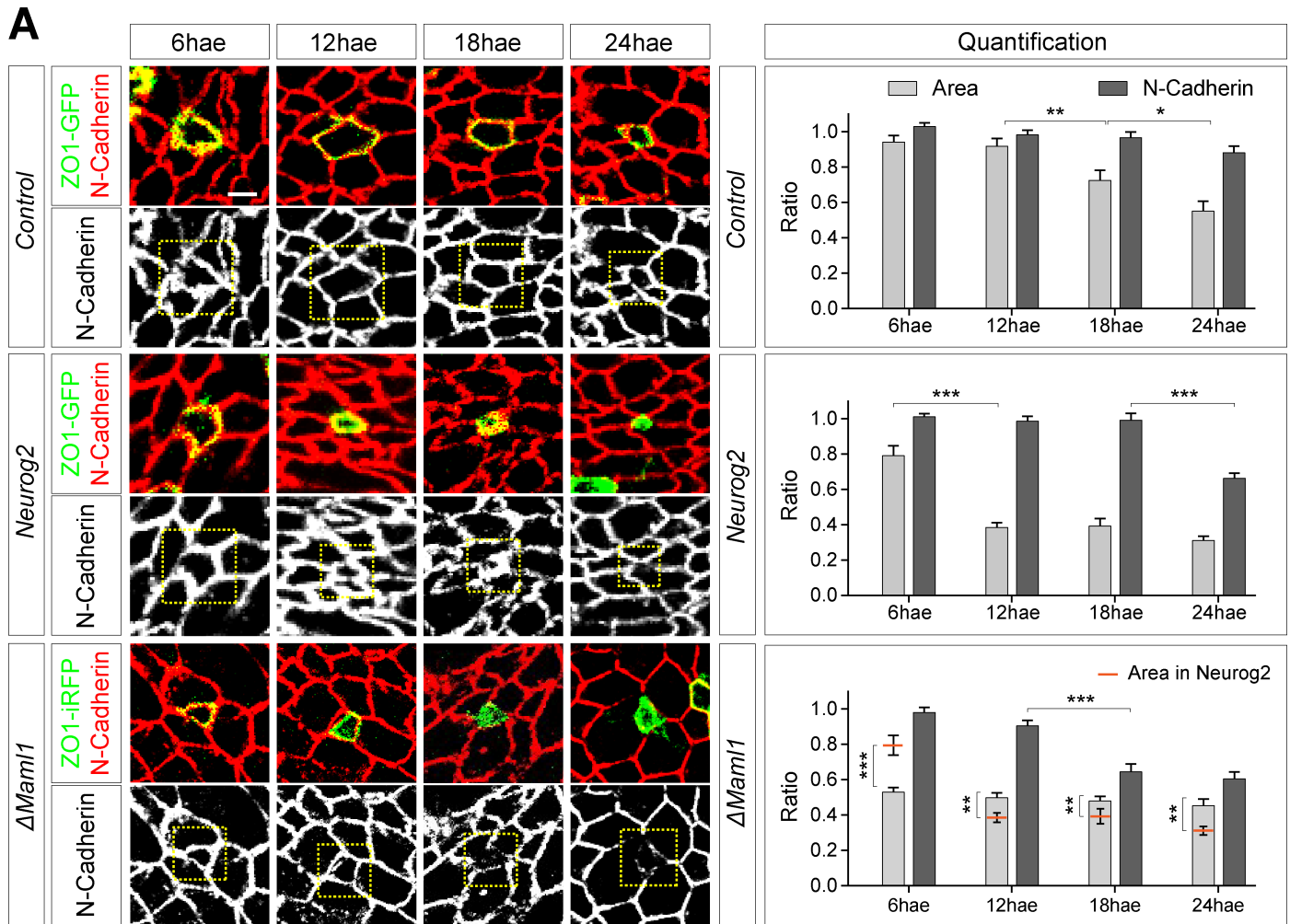


Fig 2. Sequence of events leading to neuron delamination. (A) Left: Apical view of the NT electroporated at E2 with ZO1-GFP/iRFP (green), along with the constructs indicated on the left, and harvested at different hae, followed by an immunostaining for N-Cadherin. The boxed area indicates the cell of interest. Right: Quantification of the apical area ratio (ratio of the area of one transfected cell versus the mean area of four of its close non-transfected neighbors) and N-Cadherin

level ratio (ratio of the average pixel intensity within the apical circumference of one transfected cell corrected by the background versus the mean of average pixel intensity of four of its close non-transfected neighbors) at different hae. Data represent mean + SEM. (B) N-Cadherin intensity ratio as a function of apical area ratio at 24 hae. Data were taken from (A). The “median” used as a threshold to discriminate between small and large apical areas corresponds to the median of the control (0.62). ** $p < 0.01$; *** $p < 0.001$ (one-way ANOVA). (C) Top: Apical view of the NT transfected with ZO1-iRFP (green) along with the indicated constructs and immunostained for Tuj1 (red) and Par3 (blue). Bottom: Three-dimensional view of the cell represented above but showing only the ZO1-iRFP and Tuj1 stainings. Right: Scatterplot of the mean apical area ratio for Tuj1⁺ cells. Each point represents one apical area ratio calculated as in (A). $n = 49, 66, 51$ cells collected from five embryos were analyzed for control, Neurog2, and Δ Maml1, respectively. ns, $p > 0.05$; *** $p < 0.001$ (Kruskal-Wallis test). Horizontal bars correspond to means. Underlying data are provided in [S1 Data](#). Scale bar represents 2 μ m. See also [S3 Fig](#). Δ Maml1, dominant-negative Mastermind-like 1; E, embryonic day; EP, electroporation; GFP, green fluorescent protein; hae, hour after electroporation; iRFP, infrared fluorescent protein; Neurog2, Neurogenin 2; ns, nonsignificant; NT, neural tube; Par3, Partition defective protein 3; ZO1, Zonula Occludens 1.

<https://doi.org/10.1371/journal.pbio.2004162.g002>

([Fig 2C](#)). These results are consistent with a differentiation process, as apical constriction and N-Cadherin reduction are features associated with neuronal delamination [[1](#), [2](#), [27](#), [33](#)].

To characterize the evolution of these parameters over time more specifically in cells committing to differentiation, we sought to synchronize the differentiation process. To this end, cells were transfected with the proneural gene Neurog2. As previously reported [[34–36](#)], Neurog2 repressed the expression of the progenitor marker Paired box gene 6 (Pax6) ([S3A Fig](#)), induced cell cycle exit after 24 h ([S3B Fig](#)), and strongly increased the differentiation rate at 48 hae ([S3D Fig](#)). In this case, we observed a strong reduction of the apical area from 12 hae, while reduction of N-Cadherin was detected only at 24 hae ([Fig 2A](#), middle panel). In addition, reduction of N-Cadherin levels and expression of Tuj1 were observed almost exclusively in cells with a “small” area 24 hae ([Fig 2B](#) and [2C](#)). Thus, control and Neurog2-induced differentiating cells appear to follow a similar sequence of events: constriction of the apical area precedes the reduction of N-Cadherin levels at apical junctions and the expression of Tuj1. Importantly, 24 h after Neurog2 electroporation, when most electroporated cells have exited the cell cycle ([S3B Fig](#)), the majority of Neurog2⁺/HuCD⁻ cells correspond to prospective neurons, and accordingly, these cells retained high levels of Notch reporter expression ([S3C Fig](#)).

We next wanted to assess the role of Notch signaling in this context. To this end, we measured these same parameters in cells transfected with a dominant negative version of the Notch pathway transcriptional coactivator Mastermind-like 1 (Δ Maml1) [[37](#), [38](#)]. In contrast to Neurog2, Δ Maml1 directly inhibits Notch transcriptional targets. Consistent with this, transfection of Δ Maml1 induced a massive decrease of Notch activity at 24 hae in the HuCD⁻ population and pushed cells to differentiate faster than Neurog2 ([S3E](#) and [S3F Fig](#)). These cells reduced their apical area ratio and their N-Cadherin level earlier than in the Neurog2 situation ([Fig 2A](#), bottom panels). However, while the constriction of the apical surface appeared earlier (6 hae), at later time points the average apical surface remained significantly larger than in the Neurog2 case ([Fig 2A](#), 12, 18, and 24 hae, apical surface values for Neurog2 were inserted in the Δ Maml1 graph for comparison). Moreover, unlike in the control and Neurog2 situations, low N-Cadherin levels were no longer restricted to cells with a small apical surface ([Fig 2B](#)) and Tuj1-positive nascent neurons with abnormally large apical domains were observed ([Fig 2C](#)). Taken together, these data suggest that upon precocious blockade of Notch signaling, N-Cadherin reduction and neuronal differentiation occur before apical constriction is complete.

We then investigated whether the effects observed at the single cell level would have a global impact on the integrity of the NT. Very strikingly, in contrast to control and Neurog2 situations, Δ Maml1 overexpression led to a noticeable decrease of all apical markers analyzed on transverse views at 24 hae ([Fig 3A](#) and [S4B Fig](#)). This resulted one day later in a severe disruption of the ventricular wall associated with the presence of ectopic neuronal masses protruding into the spinal cord lumen ([Fig 3B](#)). Remarkably, only a fraction of these ectopic neurons corresponded to transfected cells ([Fig 3B](#), see arrowheads), suggesting that the down-regulation of

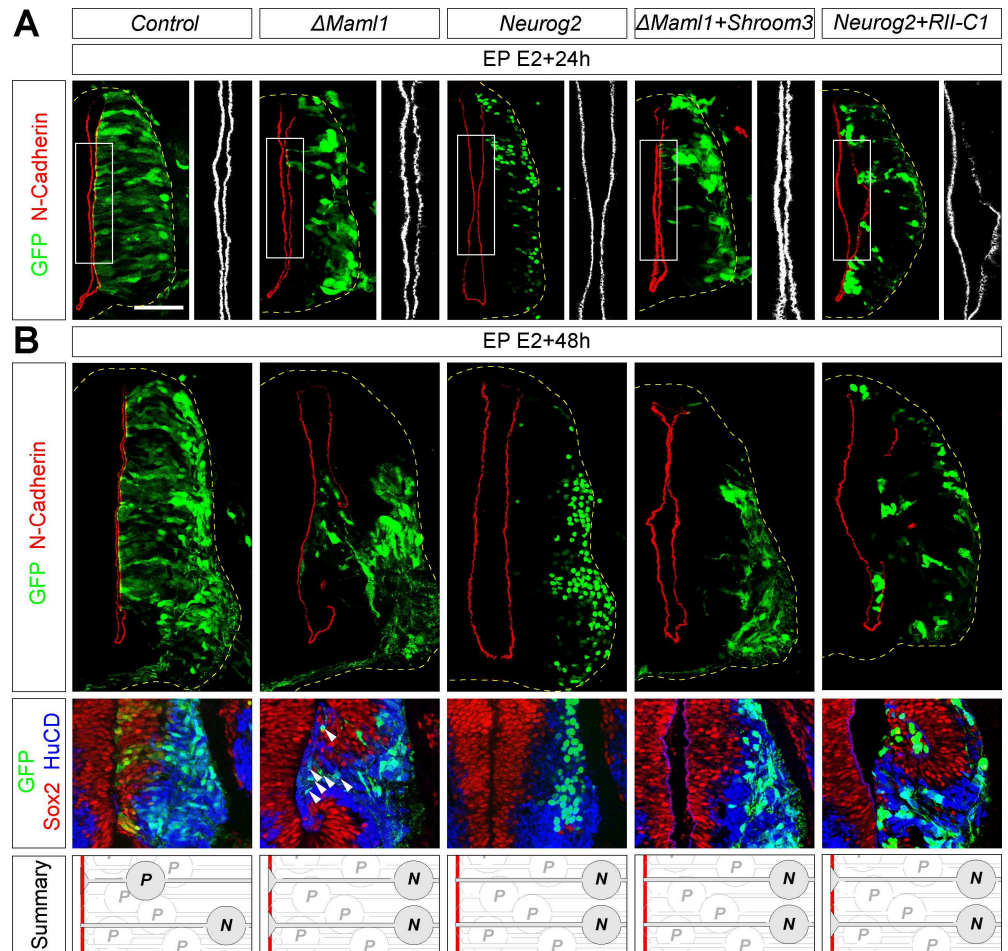


Fig 3. Effects of Notch signaling and apical constriction modulators on apical markers and tissue integrity. (A) Transverse sections of the NT transfected at E2 with the indicated constructs, harvested at E3 and immunostained for N-Cadherin (red). (B) Transverse sections of the NT transfected at E2 with the indicated constructs, harvested at E4 and immunostained for N-Cadherin (red); and for Sox2 (red) and HuCD (blue) to label progenitors and neurons, respectively. Transfection is reported by GFP expression. Summary: Schematic of the effects observed on tissue integrity. Gray cells correspond to electroporated cells. Scale bar represents 50 μ m. See also S4 Fig. Δ Maml1, dominant-negative Mastermind-like 1; E, embryonic day; EP, electroporation; GFP, green fluorescent protein; HuCD, neuron-specific RNA-binding proteins HuC and HuD; N, neuron; *Neurog2*, *Neurogenin 2*; NT, neural tube; P, progenitor; *Rii-C1*, *Shroom3* binding site on *ROCK2*; *Shroom3*, *Shroom family member 3*; Sox2, SRY (sex determining region Y) box 2.

<https://doi.org/10.1371/journal.pbio.2004162.g003>

apical markers in the transfected population was sufficient to induce a massive disorganization at the tissue scale. While blocking Notch activity results in a decrease of apical markers all along the dorsal–ventral axis at 24 hae (Fig 3A and S4B Fig), breaches in the ventricular wall were observed one day later almost exclusively in the ventral region of the NT. Motor neurons are the first neurons to be detected in the spinal cord (at E2) and are already extensively differentiated at E3 in the ventral NT. This suggests that a large population of nascent motor neurons has collectively delaminated between E2 and E3, which may render the ventral NT more sensitive to a weakening of the apical network.

The down-regulation of apical markers following Notch blockade is correlated with the presence of differentiating cells displaying large apical domains (Fig 2C). This suggests that in the control situation (or in *Neurog2* expressing cells), apical constriction may help to confine low N-Cadherin levels to only small fractions of the apical junction network and contribute to

preserving epithelial integrity when neurons delaminate. To functionally test this hypothesis, we sought to alter the size of the apical area in differentiating cells. Apical constriction was shown to rely on actomyosin contraction and is regulated by Rho-GTPases family members [39]. A typical example of apical constriction is observed in the neurulation process, during which the actin-binding protein Shroom family member 3 (Shroom3) induces apical constriction by recruiting Rho kinases (ROCKs) to adherens junctions [40]. We found that overexpression of Shroom3 forced apical constriction. Conversely, a fragment of ROCK2 designated as RII-C1 (Shroom3 binding site on ROCK2) shown to dominantly interfere with the interaction between endogenous full-length ROCK2 and Shroom3 led to an increase in apical areas, suggesting that Shroom family members are active at neurogenic stages and regulate the size of the apical footprint of neuroepithelial cells (S4C and S4D Fig). Co-transfection of Shroom3 with Δ Maml1 strongly reduced the apical area, bringing it down to the value measured in the Neurog2 situation, and increased N-Cadherin apical level (S4C and S4E Fig). Strikingly, this rescued the Δ Maml1 phenotypes: apical markers distribution was restored at 24 hae (Fig 3A, S4B Fig) and tissue integrity was no longer affected at 48 hae (Fig 3B). By contrast, inhibiting Shroom-ROCK2 interaction in Neurog2 transfected cells through overexpression of the RII-C1 fragment led to an increase of the apical area (S4C and S4D Fig), which correlated with a decrease of apical markers on transverse (S4B Fig) and apical views (S4C and S4E Fig), mimicking the Δ Maml1 overexpression phenotype. Consistently, this was followed by a disruption of the ventricular wall at 48 hae (Fig 3B), while Shroom3 and RII-C1 alone had no effect on apical marker localization (S4B Fig).

Taken together, these results suggest that sustained Notch activity is necessary in prospective neurons to allow reduction of the apical size to take place before apical junction markers are down-regulated and neurons delaminate, therefore preserving the integrity of the ventricular wall.

Dll1 levels control differentiation through the regulation of Notch activity

Having shown that maintenance of Notch signaling is critical during the last steps leading to differentiation, we next investigated the mechanisms regulating the level of Notch activity during this transition. Increase in proneural gene expression is known to be required for differentiation and is correlated with a reduction of Notch activity. However, the connection between these two events remains to be clarified. In the chick spinal cord, the Notch ligand Dll1 is an early target of Neurog2 [35], and functional approaches in the mouse cortex suggested that Dll1 expression was necessary and sufficient for neural differentiation [14]. We first investigated the role of Dll1 on neurogenesis in the chick spinal cord. Consistent with published results, we observed a strong increase in the differentiation rate of Dll1 transfected cells 48 hae (S5A Fig). By contrast, down-regulation of Dll1 following mosaic electroporation of a short hairpin RNA (shRNA) against chick Dll1 [41] reduced differentiation (S5B Fig). We then used the Hes5-VNP transgenic line to investigate the level of Notch activity following gain and loss of Dll1 function, focusing on HuCD⁻ undifferentiated cells. Consistent with their impact on differentiation, gain and loss of Dll1 function led to a decrease and an increase of Notch activity, respectively (S5C and S5D Fig). It should be noted that Dll1 is widely expressed in the spinal cord except for the dorsal dI6 and intermediate V1 interneuron domains. As Notch activity and differentiation rate following Dll1 misexpression were analyzed in the dorsal and intermediate regions of the NT irrespective of the endogenous expression of Dll1, our results may be slightly underestimated.

Mib1 blocks the ability of Dll1 to Cis-inhibit Notch signaling

Dll1 expression in a differentiating cell could lead to reduced Notch activity either indirectly by *Trans*-activation of Notch signaling in the neighbors that would therefore not *Trans*-

activate in return (according to the lateral inhibition with feedback model) or directly through *Cis*-inhibition of Notch receptors in the same cell [20]. However, answering this question *in vivo* cannot be obtained solely by Dll1 misexpression, which would impact both *Trans* and *Cis* phenomena. Thus, we decided to take advantage of the ability of the ubiquitin ligase Mind-bomb1 (Mib1) to promote Notch *Trans*-activation. We first tested the ability of Dll1 alone or with Mib1 to induce *Trans*-activation of Notch signaling in undifferentiated cells (HuCD-negative) 24 h after transfection. To this end, the intensity of the Hes5-VNP reporter was measured in non-transfected “neighbor cells” contacted by a minimum of four transfected cells. Dll1 alone was unable to *Trans*-activate signaling in neighbors (Fig 4B). In contrast, our measures upon Mib1 co-transfection indicated a trend towards increased Notch activity, although it failed to reach statistical significance (Fig 4B). We recently reported that in normal conditions, Mib1 is strongly enriched at the centrosome and barely detectable at the membrane in the NT, suggesting that only a fraction of it interacts with Dll1 [27]. To potentiate this interaction, we engineered a version of Mib1 constitutively tethered to the plasma membrane (mbMib1) by addition of an N-terminal myristoylation sequence. Remarkably, co-transfection of Dll1 with mbMib1 resulted in a significant increase of Notch activity in neighbor cells (Fig 4B). We reasoned that this higher Notch activity in neighbors should hinder their ability to differentiate. Indeed, while Dll1 alone had no impact on the differentiation rate of neighboring cells, the latter was consistently reduced following co-transfection of Mib1 and mbMib1 (Fig 4A and 4C). These data suggest that endogenous Mib1 is limiting and that Dll1 can *Trans*-activate the Notch pathway only when co-transfected with Mib1.

We then analyzed the same parameters in transfected cells. Dll1 alone led to a noticeable decrease of Notch activity 24 hae in HuCD⁻ cells (Fig 4D), accompanied by an increased differentiation rate 48 hae (Fig 4A and 4E). If this effect was relying on a feedback-based lateral inhibition mechanism, as it was previously proposed, one would expect Mib1 to enhance the phenotype observed with Dll1 by promoting *Trans*-activation in neighbors. On the contrary, we observed that Mib1 and mbMib1 induced an increase of Notch signaling (Fig 4D) and a reduction of the differentiation rate compared to Dll1 alone (Fig 4A and 4E).

Taken together, these results indicate that Dll1 overexpression promotes differentiation of neural progenitors cell autonomously through *Cis*-inhibition of Notch signaling and that Mib1 is able to block this effect by converting Dll1 from a *Cis*-inhibiting to a *Trans*-activating ligand.

Mib1 blocks Notch *Cis*-inhibition to defer differentiation and preserve neuroepithelial integrity

We then sought to address whether *Cis*-inhibition of the Notch pathway by endogenous ligands occurs in the neuroepithelium. The above results suggest that Mib1 may promote Notch response not only in signal-receiving neighbors through *Trans*-activation but also in the signal-sending cell by blocking the *Cis*-inhibition process. To test this, we interfered with Mib1 function using a dominant negative version lacking its ring finger domain (Δ Mib1) [42], which retains the interaction with Delta ligands but is unable to promote their maturation and endocytosis. Blocking Mib1 activity should therefore enhance *Cis*-inhibition and reduce Notch signaling cell autonomously. Indeed, overexpression of Δ Mib1 reduced Notch activity (Fig 5A) and increased differentiation (Fig 5B), thus mimicking the effects of Dll1 alone, while co-electroporation of Dll1 and Δ Mib1 did not significantly enhance the effect of either construct. However, blocking Mib1 function in a massive manner is also likely to alter Notch *Trans*-activation among contacting neighbor and sister cells. Thus, to restrict our analysis to isolated cells, embryos were electroporated under clonal conditions at E3 in order to target

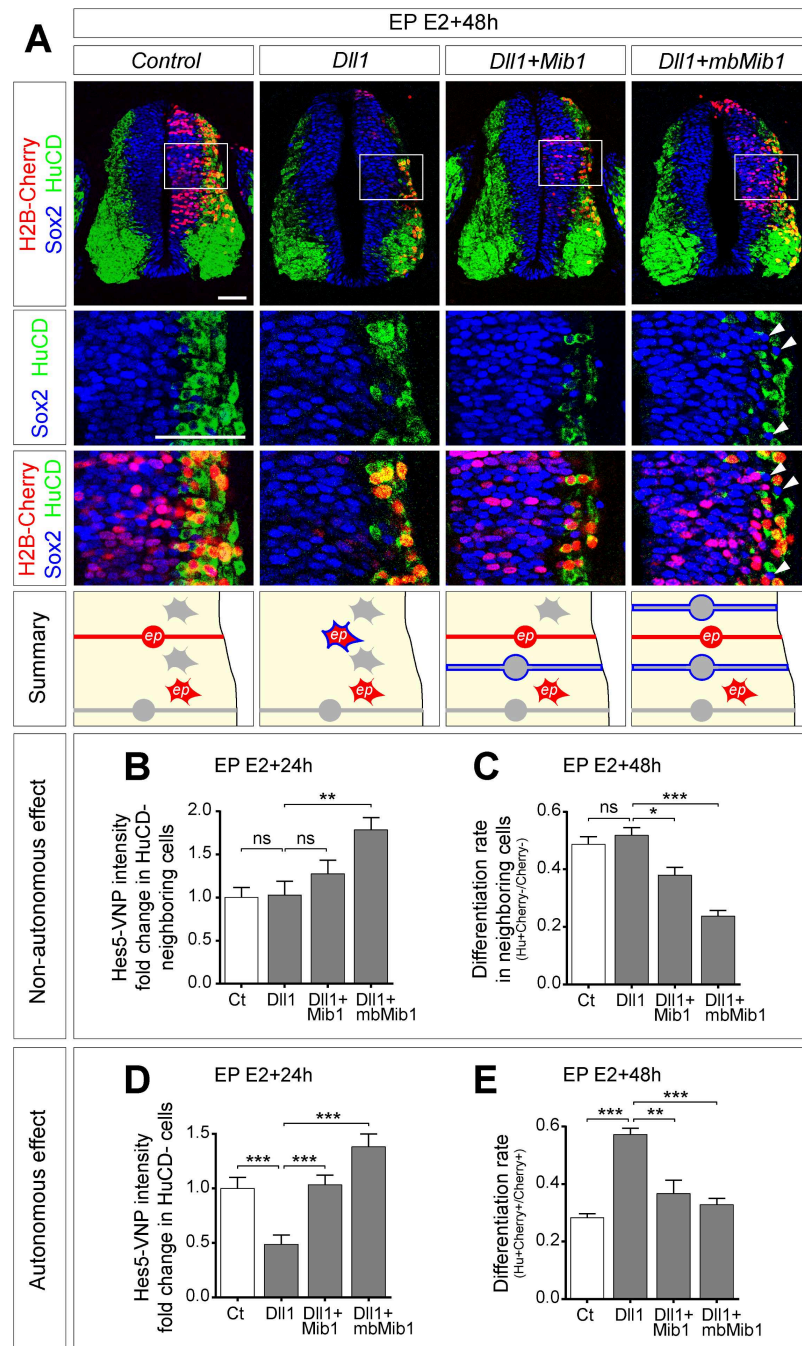


Fig 4. Mib1 blocks the ability of Dll1 to Cis-inhibit Notch signaling. (A) Top: Transverse sections of the NT transfected at E2, with the indicated constructs and harvested at E4. Immunostaining for Sox2 (blue) and HuCD (green) labels progenitors and neurons, respectively. Transfection is reported by H2B-Cherry expression. Arrowheads indicate ectopic Sox2⁺ progenitors adjacent to HuCD⁺ transfected neurons. Bottom: Summaries of the effects of Dll1 and Mib1 on neurogenesis. Red and gray cells correspond to electroporated (ep) and non-electroporated cells, respectively. Round and star-shaped cells correspond to progenitors and neurons, respectively. Blue outlines indicate cells changing fate, autonomously or non-autonomously, in each condition. (B, D) Quantification of the Hes5-VNP signal intensity in HuCD⁻ cells either (B) non-transfected (surrounded by at least four transfected cells) or (D) transfected 24 hae with the indicated constructs. Data represent fold change compared to control. (B) $n = 54, 35, 35, 54$ cells were analyzed for control, Dll1, Dll1+Mib1, and Dll1+mbMib1, respectively. (D) $n = 58, 59, 59, 66$ cells were analyzed for control, Dll1, Dll1+Mib1, and Dll1+mbMib1, respectively. Data were collected from four to six embryos for each experimental group. ns, $p > 0.05$; ** $p < 0.01$; *** $p < 0.001$ (Kruskal-Wallis test). (C, E) Quantification of the differentiation rate in (C) non-transfected neighbors (number of non-transfected HuCD⁺ cells adjacent to a HuCD⁺

transfected cell on the total number of adjacent cells) or (E) transfected cells (number of HuCD⁺ cells on total transfected cells) 48 hae with the indicated constructs. Data represent mean + SEM. $n = 14$ (6 embryos), 10 (8 embryos), 14 (6 embryos), 18 (6 embryos) sections were analyzed for control, Dll1, Dll1+Mib1, and Dll1+mbMib1, respectively. ns, $p > 0.05$; * $p < 0.05$; ** $p < 0.01$; *** $p < 0.001$ (one-way ANOVA). Analyses were performed on the same sections for (B) and (D), and for (C) and (E). Underlying data are provided in [S1 Data](#). Scale bar represents 50 μm . See also [S5 Fig](#). Ct, control; Dll1, Delta-like 1; E, embryonic day; ep, electroporated; hae, hour after electroporation; Hes5, Hairy and Enhancer of Split 5; HuCD, neuron-specific RNA-binding proteins HuC and HuD; H2B-Cherry, Histone 2B fused to Cherry; mbMib1, Mib1 constitutively tethered to the plasma membrane; Mib1, Mindbomb1; ns, nonsignificant; NT, neural tube; Sox2, SRY (sex determining region Y) box 2; VNP, Venus-NLS-PEST.

<https://doi.org/10.1371/journal.pbio.2004162.g004>

cells during the neurogenic peak and harvested shortly after (8 h) to minimize the probability of cell division. Clonal inhibition of Mib1 resulted in a significant decrease of Notch activity in electroporated cells as early as 8 hae ([Fig 5C](#)), providing strong evidence that *Cis*-inhibition takes place endogenously in the vertebrate nervous system.

While Mib1 blockade reduces Notch activity ([Fig 5A and 5C](#)), unlike Neurog2 it is not sufficient to rapidly force cells to exit the cell cycle and differentiate. However, it is essential for the process of asymmetric division and Mib1 loss-of-function will increase neurogenesis on a longer term [27]. Consistent with this, differentiation was only mildly increased at 24 hae compared to Neurog2 overexpression ([Fig 5D](#)), with no effect on N-Cadherin levels ([Fig 5E](#)). However, longer incubation times resulted in more neurons induced ([Fig 5B](#)) and large breaches in the ventricle ([Fig 5E](#)), suggesting that Mib1 regulates both the differentiation rate and the delamination process. Importantly, Shroom3 co-expression rescued NT morphology at 48 and 72 hae ([Fig 5E](#)). These results suggest that Mib1-dependent Notch maintenance is required to regulate the pace of differentiation and to allow proper neuronal delamination.

To bypass the effects of Mib1 in binary fate decisions and further characterize its function in the delamination and differentiation of prospective neurons, we performed similar experiments in cells also expressing Neurog2. Δ Mib1 and Neurog2 co-expression led to a sharp decrease of Notch activity in prospective neurons at 8 hae ([Fig 5C](#)) and to a dramatic increase in differentiated HuCD⁺ cells at 24 hae compared to Δ Mib1, Neurog2, or even Δ Maml1 alone (compare [Fig 5D](#) with [S3F Fig](#)). We then assessed the localization of apical markers at different times following transfection of Neurog2 and/or Δ Mib1 ([Fig 5E and 5F](#)). Whereas neither Δ Mib1 nor Neurog2 alone had any effect, N-Cadherin level was reduced upon co-expression at 24 hae, and breaches along the ventricular wall could be observed one day later and occasionally as early as 24 hae ([Fig 5F](#)). Moreover, co-transfection of Shroom3 rescued the morphology of the NT at 48 hae ([Fig 5F](#)).

Mib1 was previously shown to control the rate of neurogenesis in vertebrates by promoting Notch *Trans*-activation [43]. Our results suggest that Mib1 promotes Notch activity not only through *Trans*-activation in signal-receiving neighbors but also in the signal-sending cell by blocking the *Cis*-inhibition process. Overall, our data indicate that Mib1 actively sustains Notch signaling in prospective neurons to regulate the pace of differentiation and to allow proper neuronal delamination.

Discussion

Taken together, our results suggest a model in which the regulation of Notch *Cis*-inhibition through the interplay between Dll1 and Mib1 allows prospective neurons to delaminate from the ventricle while preserving the integrity of the NT ([Fig 6](#)). Following mitotic exit, prospective neurons maintain a high level of Notch activity until they start expressing neuronal markers. During that transition period, they first contract their apical domain and later reduce their level of N-Cadherin. Hence, apical adhesion is reduced only in restricted areas of the

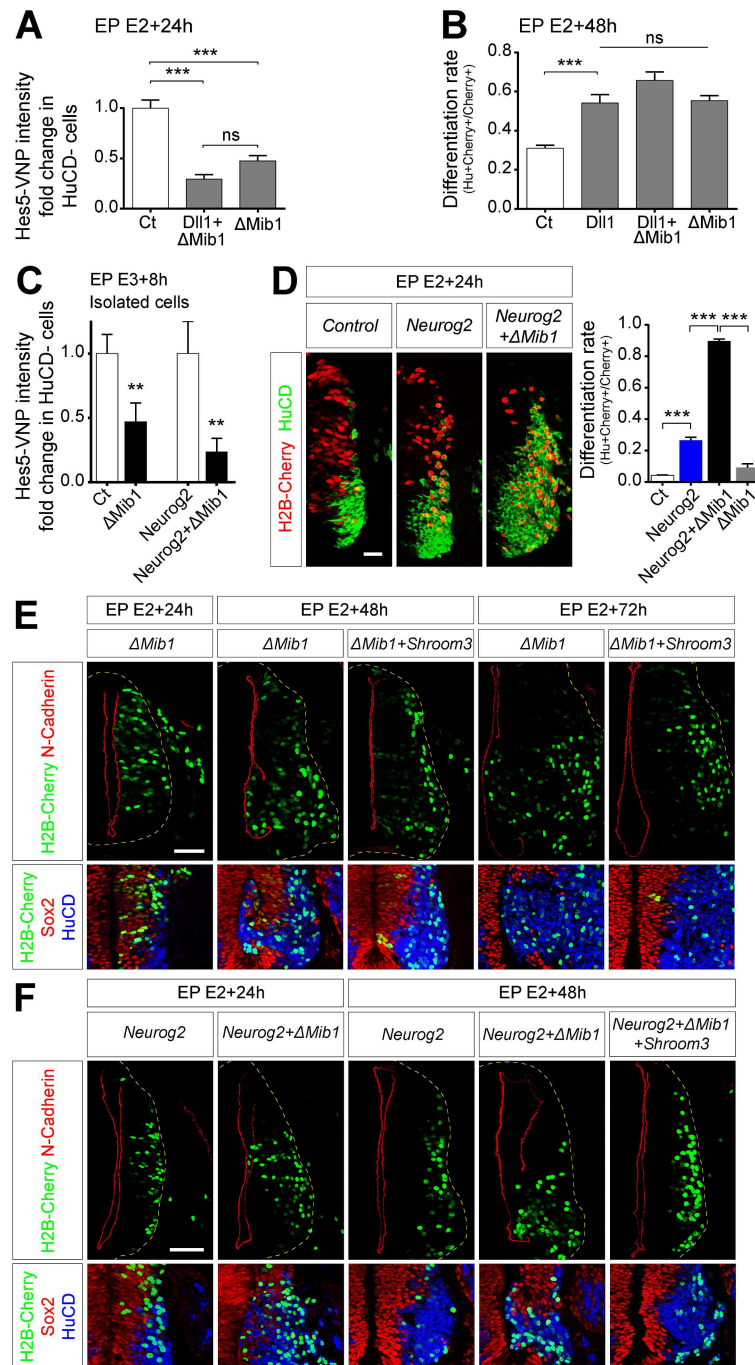


Fig 5. Mib1 blocks Notch *Cis*-inhibition to defer differentiation and preserve neuroepithelial integrity. (A) Quantification of Hes5-VNP intensity in HuCD⁻ cells transfected with the indicated constructs at E2 and harvested 24 hae. Data represent fold change compared to control. A minimum of 108 cells were analyzed for each group. ns, $p > 0.05$; *** $p < 0.001$ (Kruskal-Wallis test). (B) Quantification of the differentiation rate (number of HuCD⁺ cells on total transfected cells). Data represent mean + SEM. $n = 12$ (3 embryos), 13 (6 embryos), 15 (6 embryos), 12 (4 embryos) sections were analyzed for control, Dll1, Dll1+ΔMib1, and ΔMib1, respectively. ns, $p > 0.05$; *** $p < 0.001$ (one-way ANOVA). (C) Quantification of the Hes5-VNP signal intensity in HuCD⁻ and isolated cells transfected at E3 with the indicated constructs at low voltage (15 V) and harvested 8 h later. Data represent fold change compared to control. $n = 37$ (3 embryos), 31 (7 embryos), 15 (3 embryos), and 25 (4 embryos) cells were analyzed for control, ΔMib1, Neurog2, and Neurog2+ΔMib1, respectively. ** $p < 0.01$ (Mann-Whitney *U* test). (D) Left: Transverse sections of the NT transfected at E2 with the indicated constructs, harvested at E3 and immunostained for HuCD (green) to label neurons. Transfection is reported by H2B-Cherry expression. Right: Quantification of the differentiation rate

(number of HuCD⁺ cells on total transfected cells). Data represent mean + SEM. For 24 hae, $n = 14, 12, 19, 7$ sections collected from six embryos for each experimental group were analyzed for control, Neurog2, Neurog2+ Δ Mib1, and Δ Mib1, respectively. $***p < 0.001$ (one-way ANOVA). Underlying data are provided in [S1 Data](#). (E, F) Transverse sections of the NT transfected at E2 with the indicated constructs and immunostained for N-Cadherin (red); and for Sox2 (red) and HuCD (blue) to label progenitors and neurons, respectively. Transfection is reported by H2B-Cherry expression (green). Scale bar represents 50 μ m. Δ Mib1, dominant-negative Mib1; Ct, control; DLL1, Delta-like 1; E, embryonic day; EP, electroporation; hae, hour after electroporation; Hes5, Hairy and Enhancer of Split 5; HuCD, neuron-specific RNA-binding proteins HuC and HuD; H2B-Cherry, Histone 2B fused to Cherry; Mib1, Mindbomb1; Neurog2, Neurogenin 2; ns, nonsignificant; NT, neural tube; *Shroom3*, shroom family member 3; Sox2, Sox2, SRY (sex determining region Y) box 2; VNP, Venus-NLS-PEST.

<https://doi.org/10.1371/journal.pbio.2004162.g005>

ventricular surface, making final delamination compatible with the preservation of the apical junctional network. Moreover, we show that the maintenance of Notch activity in prospective neurons relies on the ability of Mib1 to block the *Cis*-inhibitory activity of DLL1.

The transition period that separates the mitotic exit of prospective neurons from the appearance of the earliest differentiation markers is at the moment poorly defined. It was suggested that the proneural gene Neurog2 induces an early cell cycle arrest later followed by an irreversible cell cycle exit associated with differentiation [35]. Using a Notch reporter chick line, we provide evidence that Notch signaling remains elevated until prospective neurons have differentiated, suggesting that sustained Notch activity is compatible with cell cycle arrest. Although Notch signaling is classically associated with a proliferative and undifferentiated status, several lines of evidence challenge this view. Remarkably, we found that Notch gain-of-function strictly kept Neurog2 from inducing differentiation but did not prevent Neurog2-induced cell cycle arrest (S6A and S6B Fig). Consistent with this, Neurog2 was documented to

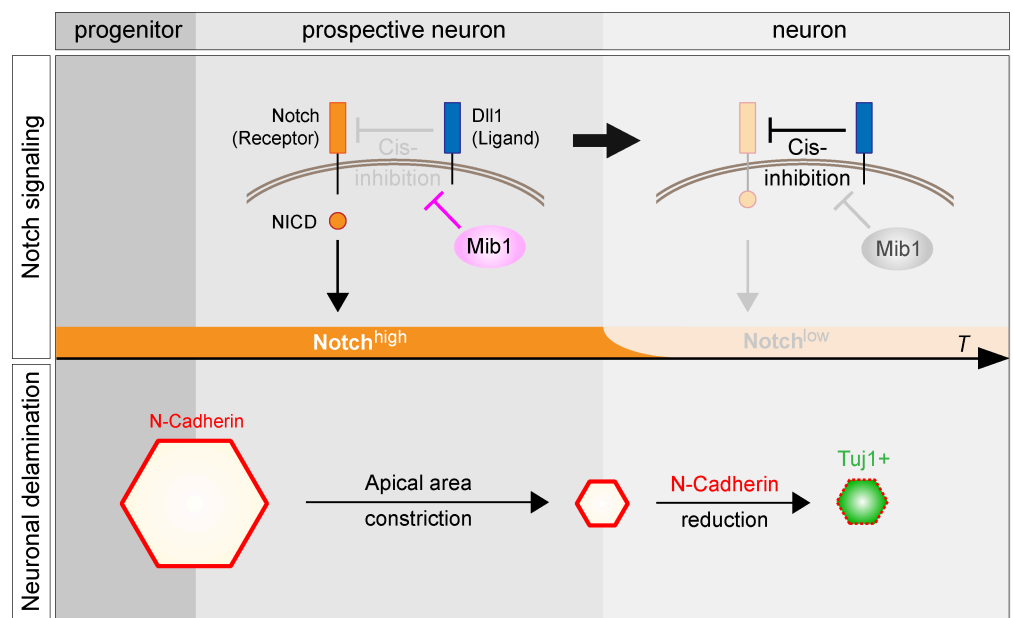


Fig 6. Model for the role of Mib1-dependent Notch activity in the regulation of neuronal delamination. Top: Prospective neurons maintain a high level of Notch activity until they fully differentiate. Mib1 is required during this transition phase to keep Dll1 from *Cis*-inhibiting the Notch receptor. This allows Notch to be *Trans*-activated by Dll1 present on neighboring cells (not represented here), resulting in the release of the NICD. When the Dll1/Mib1 ratio is sufficiently high, *Cis*-inhibition takes place and Notch activity is rapidly turned off. Bottom: Sustained Notch activity allows prospective neurons to shrink their apical area and keeps them from differentiating. As Notch activity is decreased, N-Cadherin levels are down-regulated and neuronal differentiation markers start being expressed. Dll1, Delta-like 1; Mib1, Mindbomb1; NICD, Notch intracellular domain; *T*, time.

<https://doi.org/10.1371/journal.pbio.2004162.g006>

drive cell cycle exit and differentiation independently [35]. Moreover, in the adult mouse Notch is required to maintain neural stem cells in a quiescent and undifferentiated state and keep them from proliferating [44]. Taken together, these results suggest that Notch signaling is a powerful guardian of the undifferentiated state but is not necessarily associated with a proliferative behavior.

Furthermore, we show that maintaining Notch activity in prospective neurons is necessary for neuronal delamination to take place properly. The principles that underlie neuronal delamination have only started to be investigated. While N-Cadherin reduction is a mandatory event of the delamination process in the spinal cord [2], we show that this down-regulation needs to be preceded by a reduction of the apical area. Apical constriction is blocked by a dominant negative construct (RII-C1) that was shown to hinder the interaction between Shroom3 and ROCK2 (S4 Fig, [40]). The RII-C1 construct may affect the activity of other Shroom family members that are also expressed in the NT and can drive apical constriction under certain conditions [45, 46]. While Shroom3 is a key regulator of apical constriction previously involved in various morphogenetic events [40, 47, 48], we implicate here for the first time a Shroom-like activity in a delamination process. Interestingly, Shroom blockade results in increased apical areas in all transfected cells (S4C and S4D Fig), suggesting it plays a role in cycling progenitors to control the stability of the apical surface and becomes more active as cells commit to differentiation. This profile makes Shroom family members good candidates to be direct targets of Neurog2. Consistent with this possibility, the levels of Shroom1 and 3 transcripts were up-regulated within 6 h by Neurog2 overexpression in the chick NT (personal communication, S. Bel-Vialar). By contrast, down-regulation of N-Cadherin in the spinal cord involves a transcriptional relay through expression of the Forkhead transcription factors FoxP2 and FoxP4 (FoxP2/4) transcription factors acting downstream of Neurog2 [2]. Thus, Neurog2 up-regulation may orchestrate a two-step mechanism, reducing first the apical area and later down-regulating N-Cadherin expression. A recent study carried out in zebrafish suggested that increased Notch ligand expression during differentiation may recruit Mib1 away from the band 4.1 protein/Ezrin/Radixin/Moesin domain (FERM) protein Erythrocyte membrane protein band 4.1-like 5 (Epb41l5), allowing the latter to accumulate and reduce Cadherin apical levels [49]. This may provide prospective neurons at the verge of differentiation with an additional layer of regulation to dismantle adherens junctions. Whether a similar mechanism also takes place in higher vertebrates will need to be further investigated. We propose that the constriction of the apical domain is necessary to restrict low N-Cadherin levels to small fractions of the junctional network, failure to do so resulting in breaches in the ventricular wall. The actual delamination process was shown in the NT to involve the abscission of the apical cell membrane, leaving an apical remnant at the surface [1]. This event could act as a final stitching step, ensuring the continuity of the ventricular network.

While Notch activity needs to be maintained in prospective neurons, its role during this transition period will need to be clarified. Following Notch blockade, the sequence of events leading to delamination is no longer respected, leading to the appearance of differentiation markers in cells displaying large apical domains. Remarkably, forcing apical constriction through Shroom3 overexpression is sufficient to allow proper delamination. The Notch pathway itself is unlikely to regulate a Shroom-like activity, as forced expression of Neurog2 led to apical constriction from 12 hae onwards (Fig 2A), while Notch levels remained unaffected up to 24 hae (S3C Fig). However, it may play a permissive role in prospective neurons by maintaining epithelial features. Shroom3 was shown to be recruited to adherens junctions by the p120-catenin protein (Adherens junction protein p120) [50]. Thus, Shroom activity may only be compatible with the presence of the apical junctional complex and be lost as neuronal differentiation takes place.

We have investigated the mechanisms that regulate the level of Notch activity during these steps. We confirm previous results showing that Dll1 is required for differentiation [14]. However, in contrast to what had been proposed based on in vitro assays [14], we provide here strong evidence that Dll1 reduces Notch activity cell autonomously through a *Cis*-inhibition mechanism. The ability of Notch ligands to *Cis*-inhibit the receptors has been previously documented in *Drosophila* (for review see [20]). However, in vivo evidence for *Cis*-inhibition in vertebrates is still scarce. Dll3 acts exclusively as a *Cis*-inhibitor [23] and was shown to play a role in T-cell development [26]. But all other Notch ligands can carry out both *Trans*- and *Cis*-activities, making loss-of-function experiments extremely difficult to interpret. In this study, we have taken advantage of the ubiquitin ligase Mib1's ability to promote *Trans*-activation, to distinguish between *Trans*- and *Cis*- phenomena. Mib1 promotes *Trans*-activation and blocks the ability of Dll1 to induce differentiation. Conversely, blocking Mib1 activity strongly reduces Notch activity cell autonomously and accelerates differentiation, providing a strong demonstration that *Cis*-inhibition takes place in the vertebrate nervous system.

In addition, our study reveals that Mib1 controls a dynamic switch between an initial, transient *Trans*-activating role and a subsequent *Cis*-inhibitory activity of Dll1 during the neural differentiation process (Fig 6). The timing of this switch is not only important for the differentiating cell but also non-cell autonomously, to maintain tissue architecture during the delamination process. The mechanisms underlying both Dll1 *Cis*-inhibition and its blockade by Mib1 will need to be carefully investigated in the future. *Cis*-inhibition was proposed to rely either on the degradation of the Notch receptor or on its titration [20, 51]. Mib1, as it promotes *Trans*-activation, induces the endocytosis of Dll1 and may therefore reduce the amount of Dll1 available for *Cis*-inhibition. It is also possible that Mib1 enhances the affinity of Dll1 for Notch receptors located in *Trans*. Finally, the mechanisms that allow *Cis*-inhibition to take place and the cell to eventually differentiate will need to be addressed. This is likely to result from an increase in the Dll1/Mib1 ratio at the cell membrane. Dll1 is an early target of Neurog2 [35] and was described to increase progressively during differentiation [3]. Dll1 may therefore be progressively induced by Neurog2 and eventually reach a threshold sufficient to carry out *Cis*-inhibition. Consistent with this, co-expression of Dll1 with Neurog2 increases the effect of either construct on differentiation and induces breaches in the ventricular surface (S6D and S6E Fig), whereas shRNA against Dll1 (shDll1) reduces the effect of Neurog2 expression (S6F Fig). On the other hand, Mib1 levels can be decreased through microRNA targeting of its messenger or protein degradation [52, 53].

The developing NT displays the fascinating capacity to transit from a tightly packed epithelium to a meshwork of differentiated neurons and glia while maintaining a cohesive luminal surface. By studying early steps of neurogenesis, we show that prospective neurons maintain epithelial features until their apical endfoot has sufficiently shrunk and can extract itself harmlessly from the ventricular surface. It will be interesting in the future to investigate whether more complex mechanisms are involved as the progenitor pool is used up and ependymal cells are faced with the difficult task of tiling the ventricular system and spinal cord central canal.

Materials and methods

Ethics statement

All animal experiments, breeding, and care was compliant with the UK Animals (Scientific Procedures) Act 1986 and was authorized under a project license approved by the Roslin Institute Animal Welfare and Ethical Review Body and the UK Home Office.

Experiments performed with non-hatched avian embryos in the first two thirds of embryonic development time are not considered animal experiments according to the Directive 2010/63/EU.

Embryos

JA57 chicken fertilized eggs were provided by EARL Morizeau (8 rue du Moulin, 28190 Dangers, France). They were incubated at 38 °C in a Sanyo MIR-253 incubator for the appropriate time.

Production of the Hes5-VNP transgenic chicken line

The Hes5-VNP-NLS-PEST (Hes5-VNP) reporter transgene [28] was cloned into a lentiviral vector in reverse orientation to prevent the polyA sequence of the transgene from negatively affecting lentiviral packaging efficiency. Transgenic chicken production was carried out by injection of packaged pseudovirus generated from the Hes5-VNP lentiviral vector into blastoderm-stage chicken embryos in new laid eggs. Injected embryos were cultured to hatch and of six chicks, one male was shown to have the transgene present in blood DNA and, at sexual maturity, in semen DNA. The chimeric male (NOR4-21) was bred with stock hens and two transgenic G₁ male offspring were identified at hatch (NOR4-21:92 and:108). The position of the transgene insert sites in the chicken genome was determined by nested primer amplification of the insert site followed by sequencing, for both G₁ cockerels. Both carried a single transgene insert site in noncoding regions of the genome. A homozygous transgenic line was established from NOR4-21:92 to provide embryos homozygous for the Hes5-VNP transgene.

In ovo electroporation and plasmids

Electroporation in the chick NT was performed at E2 or E3 by applying 5 pulses of 50 ms at 25 V with 100 ms in between. For mosaic transfection analysis (Fig 5C, S5B and S5D Fig), lower voltage (3 pulses of 50 ms at 15 V with 950 ms in between) were applied to obtain isolated cells.

The following constructs have been previously described: pCX-EGFP-ZO1 [54], a gift from F. Matsuzaki; pCIG [55]; pCAGGS- Δ Maml1-EGFP [41], a gift from C. Marcelle; pRFP-RNAiC-cDil1-A and pRFP-RNAi-cDil1-B [41], a gift from C. Marcelle, were electroporated together and pRFP-RNAiC [56] was used as a control; pCA-Flag-Shroom3-Full and pCA-EGFP-HA-RII-C1 [40], a gift from M. Takeichi; pCAGGS-cMib1 [27]; pCAGGS-NICD was purchased from Addgene [57].

The following constructs were generated for this study: pCAGGS-Ngn2 was obtained by removing the IRES-GFP fragment from pCIG-Ngn2 [58], a gift from K. Storey. The chick version of Dil1 (cDil1) was cloned and inserted into pCAGGS and pCAGGS-IRES-H2B-Cherry. To generate a membrane-tethered version of Mib1 (pCAGGS-mbMib1), a myristoylation membrane localization sequence (MGCIKSKEDKGPAM from c-Yes kinase [59]) was inserted N-terminally upstream of Mib1, to not interfere with the C-terminal ring finger enzymatic domain of Mib1. For the dominant negative Mib1 (Δ Mib1) [60], a version lacking the ring finger domain (aa 1–767) was amplified from the cMib1 and inserted into pCAGGS and pCAGGS-IRES-H2B-Cherry [27]. Other plasmids used are: pCX-EGFP (0.5 μ g/ μ L), pCX-H2B-EGFP (0.5 μ g/ μ L), pCX-iRFP-ZO1 (0.2 μ g/ μ L), and pCAGGS-TetOn-IRES-H2B-iRFP (0.2 μ g/ μ L). All plasmids were used at 1 μ g/ μ L except where otherwise mentioned.

FlashTagging

FlashTagging procedures were adapted from [31]. CellTrace CFSE (Life Technologies, #C34554) was injected at 0.5 mM concentration into E2(HH12) or E2.75 chick NT. Embryos

were incubated at 38 °C for the appropriate time until dissection. EdU was deposited at 4 h intervals as described below and schematized in [Fig 1C](#) and [S2B Fig](#).

EdU labeling

Proliferating cells in the NT were labeled by in ovo incorporation of 5-ethynyl-2'-deoxyuridine (EdU). One hundred microliters of a 100 μM solution of EdU diluted in PBS was deposited on the embryo. Embryos were incubated for 1 h ([S3B Fig](#)) or more for cumulative EdU labeling ([Fig 1C](#), [S2C–S2E Fig](#)), then dissected and fixed as described above. Immunodetection of EdU incorporated cells was carried out on cryostat sections using the Click-iT EdU imaging kit (Invitrogen).

Immunohistochemistry

Chick embryos were fixed for 1 h in ice-cold 4% formaldehyde/PBS and rinsed 3 times in PBS. For cryosections, they were equilibrated at 4 °C in PB/15% sucrose and embedded in PB/15% sucrose/7.5% gelatin before sectioning. Before immunostaining, cryosections were equilibrated at room temperature, degelatinized in PBS at 37 °C 3 times 5 min, before a 30-min blocking step in PBS-0.1% Triton/10% fetal calf serum (FCS). Slides were then incubated with the primary antibodies diluted in the blocking solution at 4 °C overnight. The following day, slides were washed 3 times 5 min in PBS-0.1% Triton, incubated 2 h with the adequate secondary antibodies at room temperature, washed again 3 times, and mounted with DAPI containing Vectashield (Vector Labs).

For en face views, fixed embryos were cut along their midline and bathed 1 h in blocking solution (PBS-0.3% Triton/10% FCS), followed by overnight incubation at 4 °C with the primary antibodies diluted in the blocking solution. The next day, embryos were washed 4–5 times with PBS-0.3% Triton, incubated overnight at 4 °C with the secondary antibodies, washed again 3 times 10 min in PBS-0.3% Triton and flat-mounted (apical side facing the coverslip) with DAPI containing Vectashield.

Primary antibodies used are: chicken anti-GFP (Aves Lab, 1:800); mouse anti-HuCD (clone 16A11, Life Technologies, 1:50); guinea-pig anti-Neurog2 (a gift from B. Novitsch [[61](#)] 1:32,000); rabbit anti-phospho-Histone H3 (Millipore, 1:250); rabbit anti-Pax6 (Millipore, 1:500); mouse anti-N-Cadherin (clone GC-4, Sigma Aldrich, 1:100) (BD Biosciences, 1:250); mouse anti-βIII-tubulin (clone Tuj1; Covance, 1:500); rabbit anti-Par3 (Millipore, 1:1,000); mouse anti-ZO1 (clone 1A12, ThermoFischer, 1:100); goat anti-Sox2 (clone Y-17, Santa Cruz, 1:100). Secondary antibodies coupled to Alexa Fluor 488, Cy3, or Alexa Fluor 649 were obtained from Jackson laboratories.

In situ hybridization

In situ hybridization on gelatin mounted cryosections was performed as previously described [[62](#)]. All of the probes were synthesized using a DIG RNA labeling kit (Roche) as specified by the manufacturer. Antisense probes were prepared from the following linearized plasmids: cHes5.1 (a gift from D. Henrique), cHes1 (a gift from S. Bel-Vialar), and cDll1 (a gift from Olivier Pourquié). To generate hΔMaml1, cMib1, mShroom3, and mRii-C1 antisense probes, primers containing T3 and T7 overhangs were used to PCR amplify a region from the corresponding expression plasmids. The purified amplicon was then used as the template for antisense probe synthesis using T3 or T7 RNA polymerase.

Gelatin-mounted cryosections from overnight-fixed tissue were equilibrated at room temperature and degelatinized in PBS at 37 °C 3 times 5 min. Slides were treated 20 min in RIPA buffer (150 mM NaCl, 1% NP-40, 0.5% Na deoxycholate, 0.1% SDS, 1 mM EDTA, 50 mM Tris

pH 8.0), postfixed in 4% paraformaldehyde/PBS for 10 min, and washed 3 times 5 min with PBS. The slides were then transferred in Triethanolamine buffer (100 mM triethanolamine, acetic acid 0.25% pH 8.0) for 15 min and washed 3 times 5 min in PBS. Slides were prehybridized during 1 h with 500 μ L of hybridization solution (50% formamide, 5X SSC, 5X Denhardt's, 500 μ g/mL herring sperm DNA, 250 μ g/mL yeast RNA) and hybridized overnight at 70 °C with the same solution in the presence of the heat-denatured DIG-labeled RNA probes. The following day, slides were placed in post-hybridization solution (50% Formamid; 2X SSC; 0.1% Tween20) at 70 °C, then washed in 0.2X SSC for 30 min at 70 °C and finally in 0.2X SSC at RT for 5 min. Slides were washed with buffer 1 (100 mM maleic acid, pH 7.5, 150 mM NaCl, 0.05% Tween 20) during 20 min at room temperature, blocked for 30 min in buffer 2 (buffer 1/10% FCS), followed by overnight incubation at 4 °C with the anti-DIG antibody (Roche) diluted 1:2,000 in buffer 2. The following day, slides were washed 3 times 5 min with buffer 1 and equilibrated for 30 min in buffer 3 (100 mM Tris pH 9.5, 100 mM NaCl, 50 mM MgCl₂). The signal was visualized by a color reaction using 500 μ L of BM-Purple (Roche). The color reaction was allowed to develop in the dark at room temperature during 30 min–4 h and was stopped with PBS-0.1% Tween20.

Image acquisition and processing

Optical sections of fixed samples (en face views from half embryos or transverse views from cryosections) after immunofluorescence were obtained on a confocal microscope (model SP5; Leica) using 20 \times and 63 \times (Plan Neofluar NA 1.3 oil immersion) objectives and Leica LAS software. For image processing and data analysis, we used the ImageJ and FIJI software [63, 64]. Images were finally subjected to brightness and contrast adjustments to equilibrate channel intensities and background using ImageJ and FIJI software.

Image quantifications

Hes5-VNP signal intensity measurement and color code. Hes5-VNP signal intensity was obtained by measuring the VNP fluorescence average pixel intensity of a nuclei area defined using the DAPI channel. As Notch blockade with DAPT treatment reduced the Hes5-VNP signal intensity down to the level measured in neurons (S1C Fig), we considered the latter as background. Therefore, for each experiment, the VNP intensity measured in neurons was averaged and subtracted from all values, which were then all normalized to the average value measured in progenitors. Importantly, for each experimental condition and its control, all pictures were taken at the confocal microscope using identical parameters and during a unique session, except for clonal analyses (Fig 5C and S5D Fig). In this last case, pictures taken during different confocal sessions were normalized between them using the mean of VNP fluorescence average pixel intensity (minus background) of HuCD⁺ nuclei of the non-electroporated side as reference. Quantifications in Fig 4D (two first columns) and S5C Fig; S3B and S6A Figs (two first columns) come from the same data sets. The color coded map of Hes5-VNP signaling (Fig 1B) was obtained using two consecutive macros in FIJI software. Briefly, the VNP fluorescence average pixel intensity (minus background) of a nucleus area manually defined using the DAPI channel and its x–y position and shape descriptors were recorded in a FIJI Results Table using a first macro. A second macro was then used to generate the color coded map, in which each nucleus was redrawn as an ellipse using the recorded x, y, and shape descriptor values and assigned a given color based on its VNP fluorescence intensity.

Apical area and N-Cadherin intensity ratio. The apical area ratio was obtained by dividing the apical area of a transfected cell by the mean apical area of four of its non-transfected

close neighbors (spaced by one cell row from the transfected cell). The N-Cadherin intensity ratio was obtained by dividing the average pixel intensity (minus background) measured within the apical circumference of a transfected cell by that of four of its close non-transfected neighbors.

Differentiation and proliferation rate. The proliferation and differentiation rates were obtained by dividing the number of transfected EdU⁺ and HuCD⁺ cells by the total number of transfected cells. As progenitors differentiate much earlier in the ventrally located motor neuron domain, we concentrated our analysis on the dorsal two thirds of the NT in order to reason on a more homogenous progenitor population. The differentiation rate in neighboring cells (Fig 4C) was obtained by dividing the number of non-transfected HuCD⁺ cells adjacent to a transfected HuCD⁺ cell by the total number of non-transfected cells adjacent to the transfected HuCD⁺ cell.

Statistical analyses

The number of embryos and analyzed cells or sections are indicated in the figure legends. All data processing and statistical analyses were performed using Excel and GraphPad Prism softwares. For data following a normal distribution, significance was assessed using either a Student *t* test (S1B-Right, S2E, S2F, S3A, S3B, S3D, S3E, S5A, S5B and S6C Figs) to compare the mean of two groups or one-way ANOVA (Figs 2A–2C, 4C, 4E, 5B and 5D, S2D, S4D, S4E, S6A, S6B, S6D and S6F Figs) with Tukey correction to compare the mean of three or more groups. Data represent mean + SEM, ns, $p > 0.05$; * $p < 0.05$; ** $p < 0.01$, *** $p < 0.001$. For the analysis of Hes5-VNP intensity distributions, significance was assessed using a Mann-Whitney *U* test (Fig 5C, S1B-Left, S3C, S3E, S5C and S5D Figs) to compare the median of two groups or a Kruskal-Wallis test (Figs 1C, 1D, 4B, 4D and 5A, S1C Fig) with Dunn's correction to compare the median of three or more groups. ns, $p > 0.05$; * $p < 0.05$; ** $p < 0.01$, *** $p < 0.001$.

DAPT NT culture

A trunk explant spanning the brachial to lumbar region was dissected from E3 Hes5-VNP embryos and grown in culture medium (F12/Penicillin Streptomycin/Sodium pyruvate 1 mM) for 8 h at 38.5 °C. We added to the culture medium either DAPT (N-(3,5-difluorophenylacetyl-L-alanyl)-S-phenylglycine t-ButylEster [InSolution γ -Secretase Inhibitor IX; Calbiochem] at a final concentration of 10 μ M dissolved in DMSO) or DMSO alone at the indicated time (see schematic in S1C Fig). At the end of the culture period, embryos were fixed as described above and processed for immunohistochemistry.

Supporting information

S1 Fig. Hes5-VNP Notch reporter chicken line. (A) Transverse sections of the NT of the Hes5-VNP transgenic line at E4. Adjacent sections were used to visualize the Hes5-VNP signal revealed by anti-Venus immunostaining (green), with *cHes5.1* and *cHes1* expression detected by in situ hybridization. (B) Left: Transverse section of the NT of the Hes5-VNP transgenic line transfected at E2 with NICD, harvested at E3 and immunostained for Venus (green) and HuCD (blue) to label neurons. Transfection is reported by H2B-iRFP expression (red). Middle: Quantification of the Hes5-VNP intensity measured in HuCD⁻ cells transfected at E2 in control (non-electroporated side) and NICD conditions and harvested 24 hae. Data represent fold change compared to control, calculated from 105 cells collected from five embryos for each group. *** $p < 0.001$ (Mann-Whitney *U* test). Right: Quantification of the differentiation rate (number of HuCD⁺ cells on total transfected cells) in control and NICD conditions 24 and 48 hae. Data represent mean + SEM. For 24 hae, $n = 14$ (4 embryos), 13 (4 embryos) for

control and NICD, respectively. For 48 hae, $n = 14$ (3 embryos), 15 (4 embryos) sections for control and NICD, respectively. $***p < 0.001$ (Student *t* test). (C) Left: Transverse sections of the NT of the Hes5-VNP transgenic line at E3 treated with DMSO or DAPT during the indicated times. The time course of the protocol is schematized below. All embryos were cultured for 8 h; DAPT (10 μM) was added to the culture medium at the indicated time. Right: Quantification of the Hes5-VNP signal intensity fold change in HuCD^- cells, in DMSO and DAPT treated embryos. At least 100 cells were measured from two embryos for each experimental group. $***p < 0.001$ (Kruskal-Wallis test). Underlying data are provided in [S1 Data](#). Scale bar represents 50 μm . DAPT, N-(3,5-difluorophenylacetyl-L-alanyl)-S-phenylglycine t-ButylEster; E, embryonic day; H2B, Histone 2B; hae, hour after electroporation; Hes5, Hairy and Enhancer of Split 5; HuCD neuron-specific RNA-binding proteins HuC and HuD; iRFP, infrared fluorescent protein; NICD, Notch intracellular domain; NT, neural tube; VNP, Venus-NLS-PEST. (TIF)

S2 Fig. Characterization of prospective neurons. (A) Transverse sections of the NT injected with FT at E2.75, harvested at the indicated time points, and immunostained with phospho-Histone H3. (B) Schematic outline of the experimental protocol represented in (C). All embryos were injected with FT at the same time; EdU was administrated 3 h after FT, then every 4 h, and harvested at the indicated time. (C) Transverse sections of the NT injected with FT at E2.75, incubated with continuous EdU, and harvested at the indicated time points. FT is shown in green; red stainings reveal EdU (middle row) or the neuronal marker HuCD (bottom row). Arrowheads indicate double $\text{FT}^+/\text{HuCD}^+$ cells. (D) Quantification of the proliferation rate (number of EdU^+ cells on total FT^+ cells) and differentiation rate (number of HuCD^+ cells on total FT^+ cells) in embryos injected with FT at E2(HH12) or at E2.75 and analyzed at the indicated time points. ns, $p > 0.05$ (one-way ANOVA). (E) Left: Transverse sections of the dorsal NT incubated with continuous EdU (red) and stained with Neurog2 (green). Right: Quantification of the proliferation rate (proportion of EdU^+ cells in Neurog2^- and Neurog2^+ populations). Data represent mean + SEM. $n = 10$ collected from five embryos were analyzed. $***p < 0.001$ (Student *t* test). (F) Left: Transverse sections of the dorsal NT at E4 immunostained for Neurog2 (green) and HuCD (red). Right: Quantification of the differentiation rate (number of HuCD^+ cells on $\text{Neurog2}^{\text{Low}}$ and $\text{Neurog2}^{\text{High}}$ cells). Data represent mean + SEM. $n = 9$ sections collected from six embryos were analyzed. $*p < 0.05$ (Student *t* test). Underlying data are provided in [S1 Data](#). Scale bar represents 25 μm . E, embryonic day; EdU, 5-ethynyl-2'-deoxyuridine; FT, FlashTag; HH12, Hamburger-Hamilton stage 12; HuCD, neuron-specific RNA-binding proteins HuC and HuD; Neurog2, Neurogenin 2; ns, nonsignificant; NT, neural tube. (TIF)

S3 Fig. Effects of Neurog2 and ΔMaml1 overexpression on Notch signaling and neurogenesis. (A) Left: Transverse sections of the NT transfected at E2 with Neurog2, harvested at E3 and immunostained for Pax6 (red). Transfection is reported by GFP expression. Right: Quantification of the number of Pax6^+ cells on total transfected cells. Note that the quantification was performed on the Pax6 positive domain (inside the white dotted lines). Electroporation with Neurog2 results in efficient knockdown of Pax6. Data represent mean + SEM. $n = 8$ and 6 sections collected from three embryos were analyzed for control and Neurog2, respectively. $***p < 0.001$ (Student *t* test). (B) Left: Transverse sections of the NT transfected at E2 with the indicated constructs and harvested at E3. Transfection is reported by GFP expression. S-phase proliferating cells were labeled by EdU after a 1 h pulse (red). Right: Quantification of the proliferation rate (number of EdU^+ cells on total transfected cells) 24 hae. Data represent mean +

SEM. $n = 10$ (4 embryos) and 12 (4 embryos) sections were analyzed for control and Neurog2, respectively. $***p < 0.001$ (Student t test). (C, E) Left: Transverse sections of the dorsal NT in the Hes5-VNP transgenic line transfected at E2 with the indicated constructs harvested at E3 and immunostained for Venus (green). Transfection is reported by H2B-iRFP expression (red). Right: Quantification of the Hes5-VNP signal intensity in $HuCD^-$ cells in control (non-electroporated side), (C) Neurog2, and (E) $\Delta Maml1$ conditions. A minimum of $n = 84$ cells (C) or $n = 51$ cells (E) collected from four embryos were analyzed for each group. ns, $p > 0.05$; $***p < 0.001$ (Mann-Whitney U test). (D, F) Left: Transverse sections of the NT transfected at E2 with the indicated constructs, harvested 24 hae or 48 hae and immunostained for $HuCD$ (red) to label neurons. Transfection is reported by GFP expression. Right: Quantification of the differentiation rate (number of $HuCD^+$ cells on total transfected cells) 24 hae and 48 hae. Data represent mean + SEM. (D) For 24 hae, $n = 13$ (9 embryos) and 13 (6 embryos) were analyzed for control and Neurog2, respectively. For 48 hae, $n = 13$ (6 embryos) and 15 (6 embryos) sections were analyzed for control and Neurog2, respectively. (F) For 24 hae, $n = 14$ (9 embryos) and 15 (9 embryos) sections were analyzed for control and $\Delta Maml1$, respectively. For 48 hae, $n = 10$ (6 embryos) and 17 (6 embryos) sections were analyzed for control and $\Delta Maml1$, respectively. $***p < 0.001$ (Student t test). Underlying data are provided in [S1 Data](#). (G) Transverse sections of the NT transfected at E2 with $\Delta Maml1$ and harvested at E3. Adjacent sections were used to visualize electroporation efficiency with GFP expression and to reveal $h\Delta Maml1$ expression by in situ hybridization. + indicates the electroporated side of the NT. Scale bar represents 50 μm (A–B, D, F–G) or 25 μm (C, E). $\Delta Maml1$, dominant-negative Mastermind-like 1; E, embryonic day; EdU, 5-ethynyl-2'-deoxyuridine; GFP, green fluorescent protein; H2B-iRFP, Histone 2B fused to infrared fluorescent protein; hae, hour after electroporation; Hes5, Hairy and Enhancer of Split 5; $HuCD$, neuron-specific RNA-binding proteins HuC and HuD ; iRFP, infrared fluorescent protein; Neurog2, Neurogenin 2; ns, nonsignificant; NT, neural tube; Pax6, Paired box gene 6; VNP, Venus-NLS-PEST. (TIF)

S4 Fig. Effects of Shroom3 and RII-C1 overexpression on neuron delamination. (A) Transverse sections of the NT transfected at E2 with the indicated constructs and harvested at E3. Adjacent sections were used to visualize electroporation efficiency with GFP expression and to reveal $mShroom3$ or $mRII-C1$ expression by in situ hybridization. Scale bar represents 50 μm . (B) Transverse views of the NT transfected at E2 with the indicated constructs, harvested at E3 and immunostained for the apical markers Par3 and ZO1. + indicates the transfected side of the NT. Scale bar represents 25 μm . (C) Apical views of the NT at E2 transfected with ZO1-iRFP (green) along with the indicated constructs, harvested 18 hae and immunostained for N-Cadherin. The boxed areas indicate the cell of interest. Scale bar represents 2 μm . (D, E) Quantification of the apical area ratio (ratio of the area of a transfected cell on the mean area of four of its close non-transfected neighbors) and N-Cadherin level ratio (ratio of the average pixel intensity within the apical circumference of one transfected cell corrected by the background versus the mean of average pixel intensity of four of its close non-transfected neighbors). Data represent mean + SEM. ns, $p > 0.05$; * $p < 0.05$; ** $p < 0.01$; *** $p < 0.001$ (one-way ANOVA). Underlying data are provided in [S1 Data](#). E, embryonic day; GFP, green fluorescent protein; hae, hour after electroporation; iRFP, infrared fluorescent protein; ns, nonsignificant; NT, neural tube; Par3, Partition defective protein 3; RII-C1, Shroom3 binding site on ROCK2; Shroom3, shroom family member 3; ZO1, zonula occludens 1. (TIF)

S5 Fig. Dll1 levels control neurogenesis through the regulation of Notch activity. (A, B) Left: Transverse sections of the NT transfected at E2 (A) or E3 (B) with the indicated

constructs, harvested at E4 (A) or E5 (B) and immunostained for HuCD (green) to label neurons. Transfection is reported by H2B-Cherry or RFP expression. In (B), electroporation was performed at low voltage (15 V) to obtain mosaic transfections. Right: Quantification of the differentiation rate (number of HuCD⁺ cells on total transfected cells). Data represent mean + SEM. (A) $n = 12$ and 15 sections collected from six embryos for each experimental group were analyzed for control and Dll1, respectively. (B) $n = 36$ sections (6 embryos) and 40 sections (8 embryos) were analyzed for control and shDll1, respectively. $***p < 0.001$ (Student t test). (C, D) Left: Transverse section of the NT of the Hes5-VNP transgenic line transfected at E2 with Dll1 (C) or at E3 with shDll1 (D) constructs and their respective controls, harvested 24 hae and immunostained for Venus (green) and HuCD (blue) to label neurons. Transfection is reported by H2B-iRFP (C) or RFP (D) expression (red). Right: Quantification of Hes5-VNP intensity in HuCD⁻ cells transfected with the indicated constructs at E2 (C) or E3 (D) with a normal (C) or low voltage (D) condition and harvested 24 hae. Data represent fold change compared to control. (C) $n = 58$ and 59 cells collected from six embryos for each experimental group were analyzed for control and Dll1, respectively. (D) $n = 35$ and 42 cells collected from 11 embryos for each experimental group were analyzed for control and shDll1, respectively. $**p < 0.01$; $***p < 0.001$ (Mann-Whitney U test). Underlying data are provided in [S1 Data](#). (E) Transverse sections of the NT transfected at E2 with the indicated constructs and harvested at E3. Adjacent sections were used to visualize electroporation efficiency with H2B-GFP or H2B-Cherry expression and to reveal *cDll1* or *cMib1* expression by in situ hybridization. + indicates the electroporated side of the NT. Scale bar represents 50 μm . Dll1, Delta-like 1; E, embryonic day; hae, hour after electroporation; H2B-Cherry, Histone 2B fused to Cherry; H2B-GFP, Histone 2B fused to GFP; Hes5, Hairy and Enhancer of Split 5; HuCD, neuron-specific RNA-binding proteins HuC and HuD; iRFP, infrared fluorescent protein; NT, neural tube; RFP, red fluorescent protein; shDll1, shRNA against Dll1; VNP, Venus-NLS-PEST. (TIF)

S6 Fig. Synergistic effects of Neurog2 and Dll1 forced expression on differentiation and neuroepithelial integrity. (A) Quantification of the proliferation rate (number of EdU⁺ cells on total transfected cells) 24 hae. Data represent mean + SEM. $n = 10, 12, 23,$ and 20 sections collected from four embryos for each experimental group were analyzed for control, Neurog2, Neurog2+NICD, and NICD, respectively. (B) Quantification of the differentiation rate (number of HuCD⁺ cells on total transfected cells) 48 hae. Data represent mean + SEM. $n = 9, 9, 9,$ and 7 sections collected from three embryos for each experimental group were analyzed for control, Neurog2, Neurog2+NICD, and NICD, respectively. ns, $p > 0.05$; $**p < 0.01$; $***p < 0.001$ (one-way ANOVA). (C, D) Left: Transverse sections of the NT transfected at E2 with the indicated constructs, harvested at E3 and immunostained for HuCD (green) to label neurons. Transfection is reported by H2B-Cherry expression (red). Right: Quantification of the differentiation rate (number of HuCD⁺ cells on total transfected cells). Data represent mean + SEM. (C) $n = 10$ and 12 sections collected from four embryos for each experimental group were analyzed for control and Dll1, respectively. (D) $n = 8, 9,$ and 15 sections collected from six embryos for each experimental group were analyzed for control, Neurog2, and Neurog2+Dll1, respectively. $**p < 0.01$; $***p < 0.001$ (one-way ANOVA). (E) Transverse sections of the NT transfected at E2 with the indicated constructs, harvested at E3, and immunostained for N-Cadherin (red). Transfection is reported by H2B-Cherry expression (green). N-cadherin is down-regulated on the electroporated side upon double Neurog2+Dll1 expression; asterisk indicates breach to the ventricular wall. (F) Left: Transverse sections of the NT transfected at E2 with the indicated constructs, harvested at E4 and immunostained for HuCD (green) to label neurons. Transfection is reported by RFP expression (red). Right: Quantification of the

differentiation rate (number of HuCD⁺ cells on total transfected cells). Data represent mean + SEM. ** $p < 0.01$ (one-way ANOVA). $n = 14, 11,$ and 16 sections collected from five embryos for each experimental group were analyzed for control, Neurog2, and Neurog2+shDll1, respectively. Underlying data are provided in [S1 Data](#). Scale bar represents 50 μm . Dll1, Delta-like 1; E, embryonic day; H2B-Cherry, Histone 2B fused to Cherry; hae, hour after electroporation; HuCD, neuron-specific RNA-binding proteins HuC and HuD; Neurog2, Neurogenin 2; NICD, Notch intracellular domain; ns, nonsignificant; NT, neural tube; RFP, red fluorescent protein; shDll1, shRNA against Dll1.
(TIF)

S1 Data.
(XLSX)

Acknowledgments

We are very grateful to F. di Pietro, E. Fischer, F. Schweisguth and J. Livet for helpful discussions on the manuscript and we thank F. Matsuzaki, C. Marcelle, S. Bel-Vialar, B. Novitch, M. Takeichi, and K. Storey for the kind gift of reagents. We thank K. Storey and D. Henrique for discussions of the Notch reporter, F. Vilas-Boas and D. Henrique for providing the reporter construct, H. Gilhooley for technical support, and A. Sherman and the staff of the Transgenic Chicken Facility at the Roslin Institute for technical support and breeding and maintenance of the chickens. We acknowledge B. Mathieu and the IBENS imaging platform for excellent assistance.

Author Contributions

Conceptualization: Xavier Morin, Samuel Tozer.

Formal analysis: Chooyoung Baek, Samuel Tozer.

Funding acquisition: Helen Sang, Xavier Morin.

Investigation: Chooyoung Baek, Rosette Goïame, Samuel Tozer.

Resources: Lucy Freem, Helen Sang.

Software: Xavier Morin.

Supervision: Xavier Morin, Samuel Tozer.

Writing – original draft: Xavier Morin, Samuel Tozer.

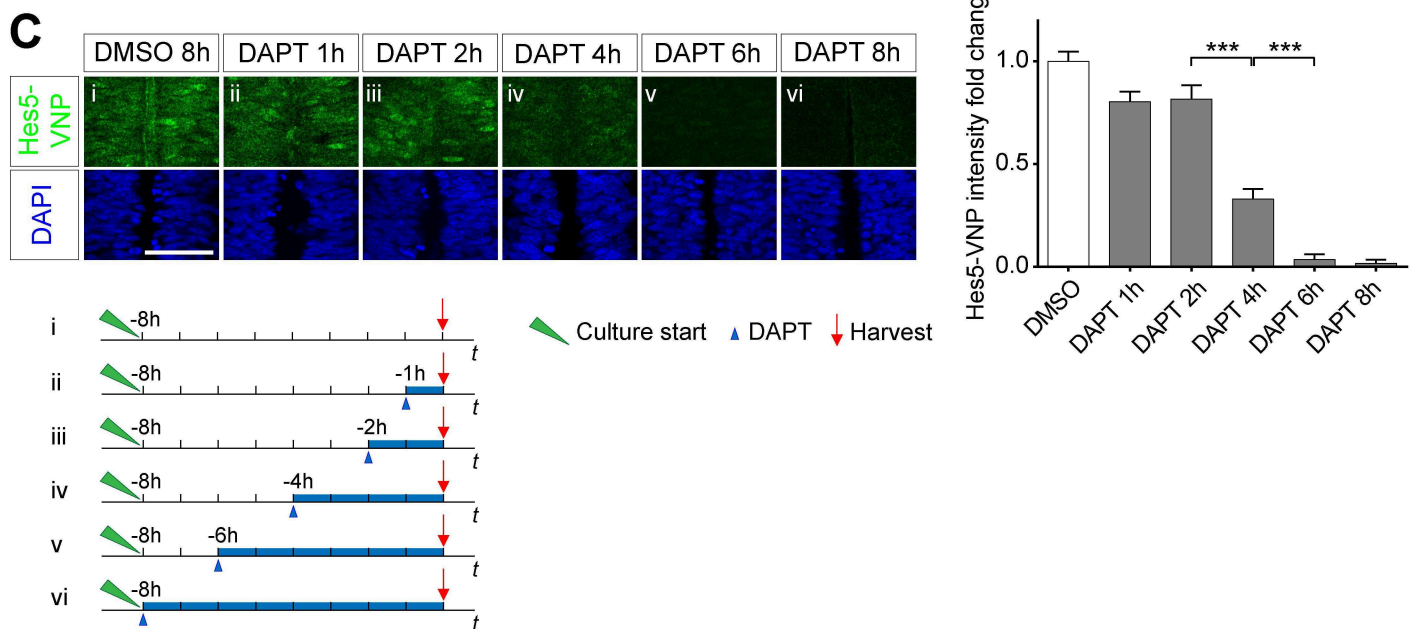
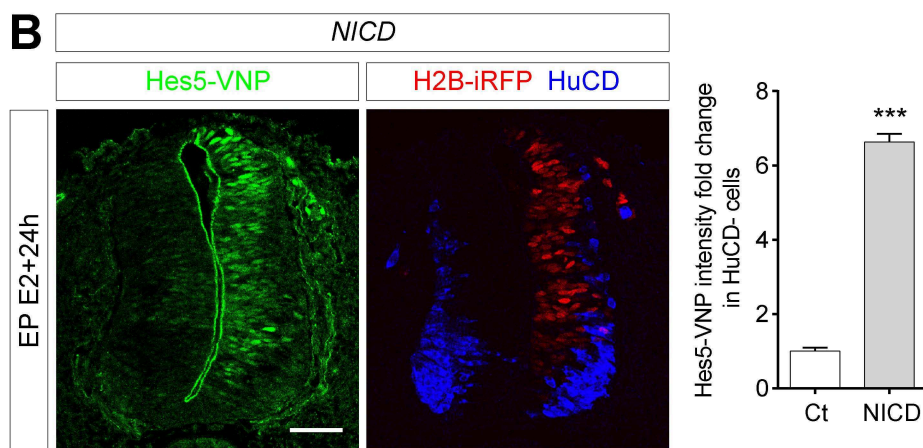
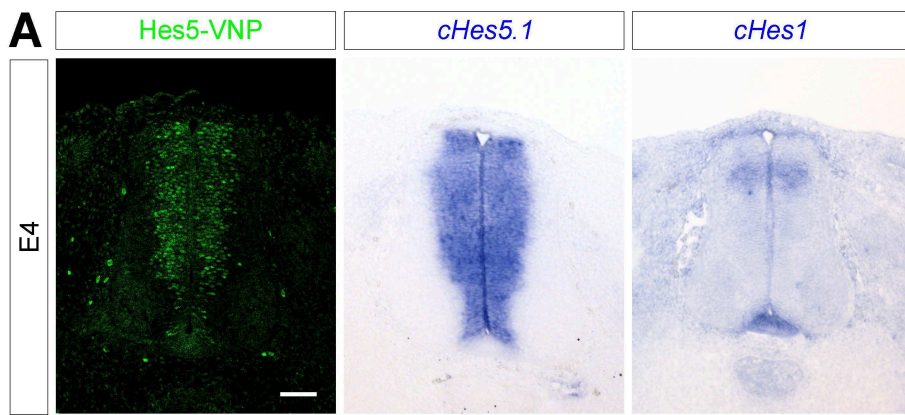
References

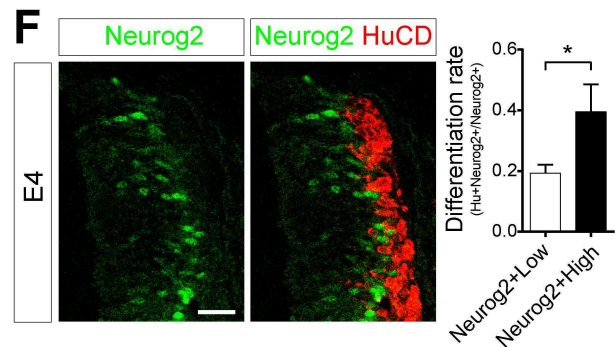
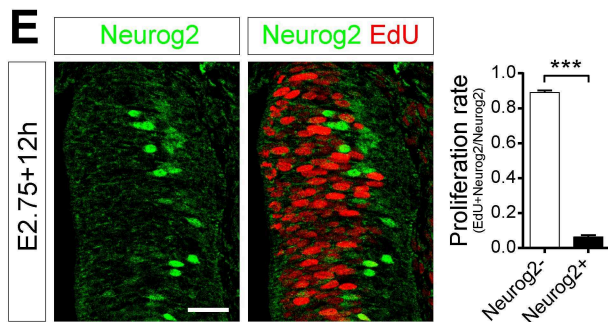
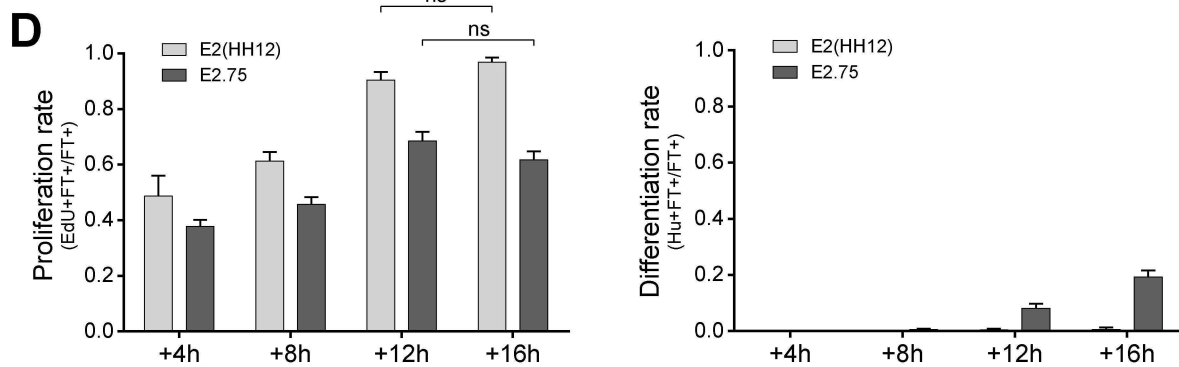
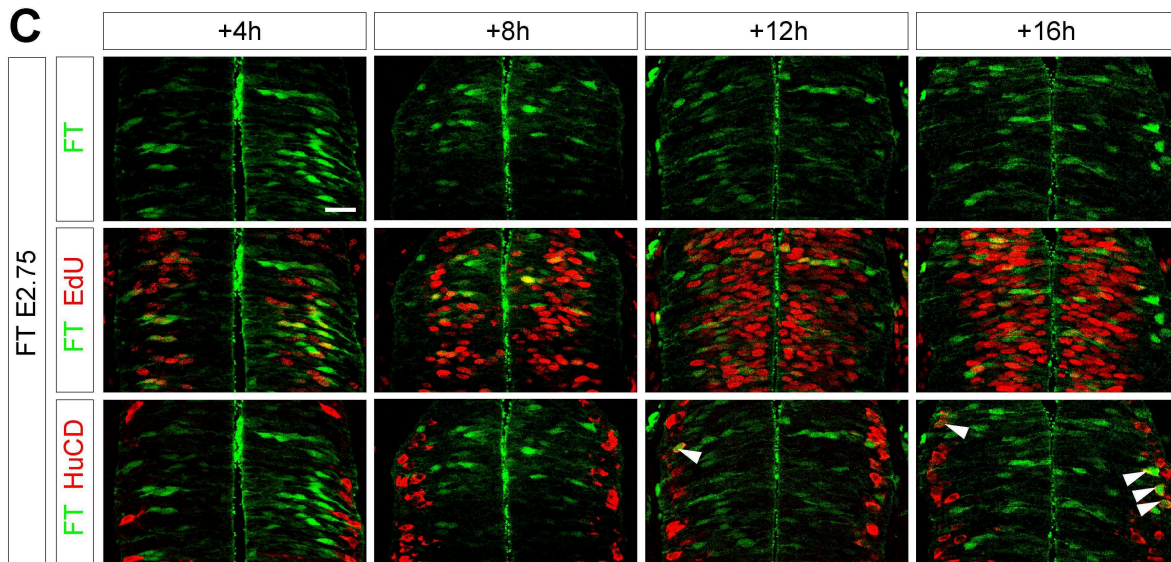
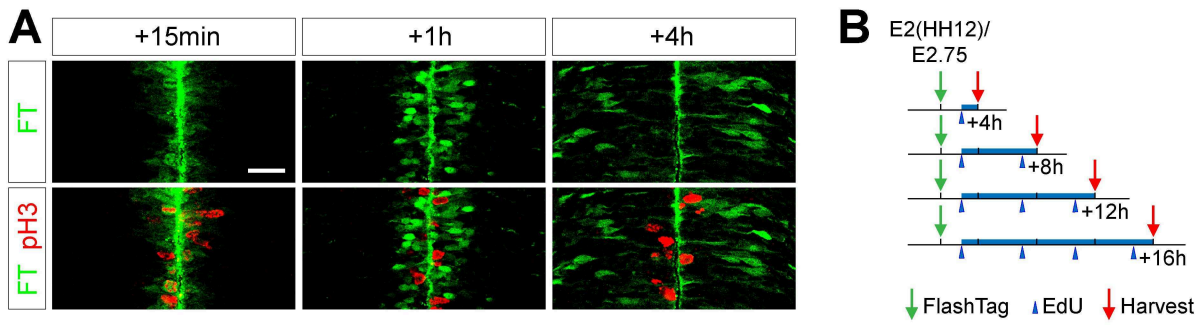
1. Das RM, Storey KG. Apical abscission alters cell polarity and dismantles the primary cilium during neurogenesis. *Science*. 2014; 343(6167):200–4. <https://doi.org/10.1126/science.1247521> PMID: [24408437](https://pubmed.ncbi.nlm.nih.gov/24408437/); PubMed Central PMCID: PMC4066580.
2. Rouso DL, Pearson CA, Gaber ZB, Miquelajauregui A, Li S, Portera-Cailliau C, et al. Foxp-mediated suppression of N-cadherin regulates neuroepithelial character and progenitor maintenance in the CNS. *Neuron*. 2012; 74(2):314–30. <https://doi.org/10.1016/j.neuron.2012.02.024> PMID: [22542185](https://pubmed.ncbi.nlm.nih.gov/22542185/); PubMed Central PMCID: PMC3444171.
3. Shimojo H, Ohtsuka T, Kageyama R. Oscillations in notch signaling regulate maintenance of neural progenitors. *Neuron*. 2008; 58(1):52–64. <https://doi.org/10.1016/j.neuron.2008.02.014> PMID: [18400163](https://pubmed.ncbi.nlm.nih.gov/18400163/).
4. Hatakeyama J, Bessho Y, Katoh K, Ookawara S, Fujioka M, Guillemot F, et al. Hes genes regulate size, shape and histogenesis of the nervous system by control of the timing of neural stem cell differentiation. *Development*. 2004; 131(22):5539–50. <https://doi.org/10.1242/dev.01436> PMID: [15496443](https://pubmed.ncbi.nlm.nih.gov/15496443/).
5. Pierfelice T, Alberi L, Gaiano N. Notch in the vertebrate nervous system: an old dog with new tricks. *Neuron*. 2011; 69(5):840–55. <https://doi.org/10.1016/j.neuron.2011.02.031> PMID: [21382546](https://pubmed.ncbi.nlm.nih.gov/21382546/).

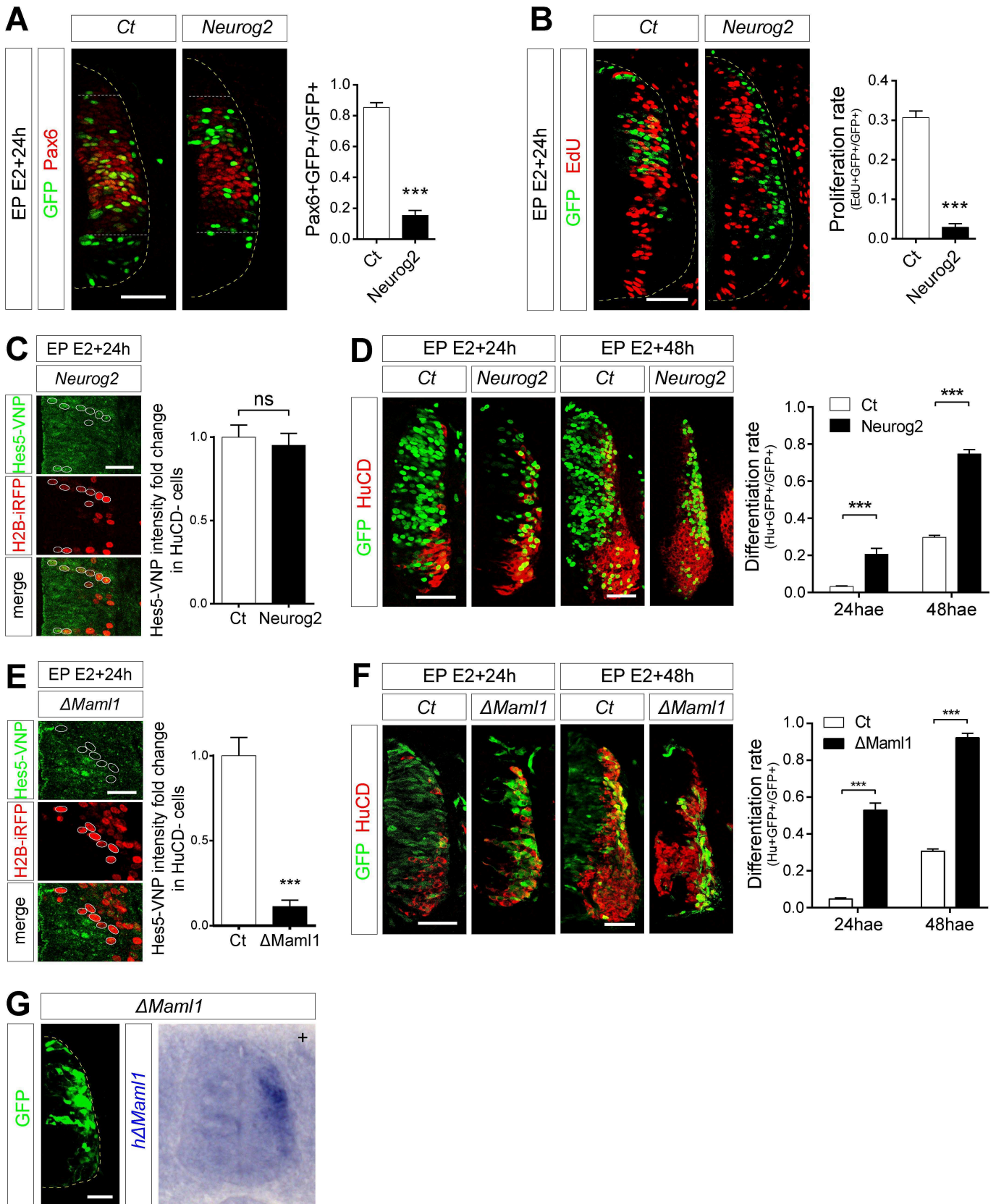
6. Rocha SF, Lopes SS, Gossler A, Henrique D. Dll1 and Dll4 function sequentially in the retina and pV2 domain of the spinal cord to regulate neurogenesis and create cell diversity. *Dev Biol.* 2009; 328(1):54–65. <https://doi.org/10.1016/j.ydbio.2009.01.011> PMID: [19389377](https://pubmed.ncbi.nlm.nih.gov/19389377/).
7. de la Pompa JL, Wakeham A, Correia KM, Samper E, Brown S, Aguilera RJ, et al. Conservation of the Notch signalling pathway in mammalian neurogenesis. *Development.* 1997; 124(6):1139–48. Epub 1997/03/01. PMID: [9102301](https://pubmed.ncbi.nlm.nih.gov/9102301/).
8. Guillemot F. Spatial and temporal specification of neural fates by transcription factor codes. *Development.* 2007; 134(21):3771–80. Epub 2007/09/28. <https://doi.org/10.1242/dev.006379> PMID: [17898002](https://pubmed.ncbi.nlm.nih.gov/17898002/).
9. Casarosa S, Fode C, Guillemot F. Mash1 regulates neurogenesis in the ventral telencephalon. *Development.* 1999; 126(3):525–34. Epub 1999/01/07. PMID: [9876181](https://pubmed.ncbi.nlm.nih.gov/9876181/).
10. Agius E, Bel-Vialar S, Bonnet F, Pituello F. Cell cycle and cell fate in the developing nervous system: the role of CDC25B phosphatase. *Cell Tissue Res.* 2015; 359(1):201–13. <https://doi.org/10.1007/s00441-014-1998-2> PMID: [25260908](https://pubmed.ncbi.nlm.nih.gov/25260908/).
11. Fode C, Gradwohl G, Morin X, Dierich A, LeMeur M, Goridis C, et al. The bHLH protein NEUROGENIN 2 is a determination factor for epibranchial placode-derived sensory neurons. *Neuron.* 1998; 20(3):483–94. Epub 1998/04/16. PMID: [9539123](https://pubmed.ncbi.nlm.nih.gov/9539123/).
12. Ma Q, Kintner C, Anderson DJ. Identification of neurogenin, a vertebrate neuronal determination gene. *Cell.* 1996; 87(1):43–52. Epub 1996/10/04. PMID: [8858147](https://pubmed.ncbi.nlm.nih.gov/8858147/).
13. Henrique D, Hirsinger E, Adam J, Le Roux I, Pourquie O, Ish-Horowicz D, et al. Maintenance of neuroepithelial progenitor cells by Delta-Notch signalling in the embryonic chick retina. *Curr Biol.* 1997; 7(9):661–70. Epub 1997/09/01. doi: [S0960-9822\(06\)00293-4](https://doi.org/10.1016/S0960-9822(06)00293-4) [pii]. PMID: [9285721](https://pubmed.ncbi.nlm.nih.gov/9285721/).
14. Kawaguchi D, Yoshimatsu T, Hozumi K, Gotoh Y. Selection of differentiating cells by different levels of delta-like 1 among neural precursor cells in the developing mouse telencephalon. *Development.* 2008; 135(23):3849–58. <https://doi.org/10.1242/dev.024570> PMID: [18997111](https://pubmed.ncbi.nlm.nih.gov/18997111/).
15. Lewis J. Neurogenic genes and vertebrate neurogenesis. *Current opinion in neurobiology.* 1996; 6(1):3–10. Epub 1996/02/01. PMID: [8794055](https://pubmed.ncbi.nlm.nih.gov/8794055/).
16. Chitnis A, Henrique D, Lewis J, Ish-Horowicz D, Kintner C. Primary neurogenesis in *Xenopus* embryos regulated by a homologue of the *Drosophila* neurogenic gene Delta. *Nature.* 1995; 375(6534):761–6. Epub 1995/06/29. <https://doi.org/10.1038/375761a0> PMID: [7596407](https://pubmed.ncbi.nlm.nih.gov/7596407/).
17. Henrique D, Hirsinger E, Adam J, Le Roux I, O. P, Ish-Horowicz D, et al. Maintenance of neuroepithelial progenitor cells by Delta-Notch signalling in the embryonic chick retina. *Curr Biol.* 1997; 7:661–70. PMID: [9285721](https://pubmed.ncbi.nlm.nih.gov/9285721/)
18. Miller AC, Lyons EL, Herman TG. cis-Inhibition of Notch by endogenous Delta biases the outcome of lateral inhibition. *Curr Biol.* 2009; 19(16):1378–83. <https://doi.org/10.1016/j.cub.2009.06.042> PMID: [19631544](https://pubmed.ncbi.nlm.nih.gov/19631544/); PubMed Central PMCID: [PMC2761761](https://pubmed.ncbi.nlm.nih.gov/PMC2761761/).
19. Fiuza UM, Klein T, Martinez Arias A, Hayward P. Mechanisms of ligand-mediated inhibition in Notch signaling activity in *Drosophila*. *Dev Dyn.* 2010; 239(3):798–805. Epub 2010/01/12. <https://doi.org/10.1002/dvdy.22207> PMID: [20063416](https://pubmed.ncbi.nlm.nih.gov/20063416/).
20. del Alamo D, Rouault H, Schweisguth F. Mechanism and significance of cis-inhibition in Notch signaling. *Curr Biol.* 2011; 21(1):R40–7. <https://doi.org/10.1016/j.cub.2010.10.034> PMID: [21215938](https://pubmed.ncbi.nlm.nih.gov/21215938/).
21. Itoh M, Kim CH, Palardy G, Oda T, Jiang YJ, Maust D, et al. Mind bomb is a ubiquitin ligase that is essential for efficient activation of Notch signaling by Delta. *Dev Cell.* 2003; 4(1):67–82. Epub 2003/01/18. PMID: [12530964](https://pubmed.ncbi.nlm.nih.gov/12530964/).
22. Sakamoto K, Ohara O, Takagi M, Takeda S, Katsube K. Intracellular cell-autonomous association of Notch and its ligands: a novel mechanism of Notch signal modification. *Dev Biol.* 2002; 241(2):313–26. <https://doi.org/10.1006/dbio.2001.0517> PMID: [11784114](https://pubmed.ncbi.nlm.nih.gov/11784114/).
23. Ladi E, Nichols JT, Ge W, Miyamoto A, Yao C, Yang LT, et al. The divergent DSL ligand Dll3 does not activate Notch signaling but cell autonomously attenuates signaling induced by other DSL ligands. *J Cell Biol.* 2005; 170(6):983–92. <https://doi.org/10.1083/jcb.200503113> PMID: [16144902](https://pubmed.ncbi.nlm.nih.gov/16144902/); PubMed Central PMCID: [PMC2171428](https://pubmed.ncbi.nlm.nih.gov/PMC2171428/).
24. Dunwoodie SL, Clements M, Sparrow DB, Sa X, Conlon RA, Beddington RSP. Axial skeletal defects caused by mutation in the spondylocostal dysplasia/pudgy gene Dll3 are associated with disruption of the segmentation clock within the presomitic mesoderm. *Development.* 2002; 129:1795–806. PMID: [11923214](https://pubmed.ncbi.nlm.nih.gov/11923214/)
25. Geffers I, Serth K, Chapman G, Jaekel R, Schuster-Gossler K, Cordes R, et al. Divergent functions and distinct localization of the Notch ligands DLL1 and DLL3 in vivo. *J Cell Biol.* 2007; 178(3):465–76. <https://doi.org/10.1083/jcb.200702009> PMID: [17664336](https://pubmed.ncbi.nlm.nih.gov/17664336/); PubMed Central PMCID: [PMC2064846](https://pubmed.ncbi.nlm.nih.gov/PMC2064846/).
26. Hoyne GF, Chapman G, Sontani Y, Pursglove SE, Dunwoodie SL. A cell autonomous role for the Notch ligand Delta-like 3 in $\alpha\beta$ T-cell development. *Immunology and Cell Biology.* 2010; 89(6):696–705. <https://doi.org/10.1038/icb.2010.154> PMID: [21151194](https://pubmed.ncbi.nlm.nih.gov/21151194/)

27. Tozer S, Baek C, Fischer E, Gojame R, Morin X. Differential Routing of Mindbomb1 via Centriolar Satellites Regulates Asymmetric Divisions of Neural Progenitors. *Neuron*. 2017; 93(3):542–51 e4. <https://doi.org/10.1016/j.neuron.2016.12.042> PMID: 28132826.
28. Vilas-Boas F, Fior R, Swedlow JR, Storey KG, Henrique D. A novel reporter of notch signalling indicates regulated and random Notch activation during vertebrate neurogenesis. *BMC Biol*. 2011; 9:58. <https://doi.org/10.1186/1741-7007-9-58> PMID: 21880129; PubMed Central PMCID: PMC3201213.
29. Rabadan MA, Cayuso J, Le Dreau G, Cruz C, Barzi M, Pons S, et al. Jagged2 controls the generation of motor neuron and oligodendrocyte progenitors in the ventral spinal cord. *Cell Death Differ*. 2012; 19:209–19. <https://doi.org/10.1038/cdd.2011.84> PMID: 21720386
30. Stasiulewicz M, Gray SD, Mastromina I, Silva JC, Bjorklund M, Seymour PA, et al. A conserved role for Notch signaling in priming the cellular response to Shh through ciliary localisation of the key Shh transducer Smo. *Development*. 2015; 142(13):2291–303. <https://doi.org/10.1242/dev.125237> PMID: 25995356; PubMed Central PMCID: PMC4510595.
31. Telley L, Govindan S, Prados J, Stevant I, Nef S, Dermitzakis E, et al. Sequential transcriptional waves direct the differentiation of newborn neurons in the mouse neocortex. *Science*. 2016; 351(6280):1443–6. <https://doi.org/10.1126/science.aad8361> PMID: 26940868
32. Lee SK, Pfaff SL. Synchronization of Neurogenesis and Motor Neuron Specification by Direct Coupling of bHLH and Homeodomain Transcription Factors. *Neuron*. 2003; 38:731–45. PMID: 12797958
33. Kasioulis I, Das RM, Storey KG. Inter-dependent apical microtubule and actin dynamics orchestrate centrosome retention and neuronal delamination. *Elife*. 2017; 6. <https://doi.org/10.7554/eLife.26215> PMID: 29058679; PubMed Central PMCID: PMC5653239.
34. Mizuguchi R, Sugimori M, Takebayashi H, Kosako H, Nagao M, Yoshida S, et al. Combinatorial roles of olig2 and neurogenin2 in the coordinated induction of pan-neuronal and subtype-specific properties of motoneurons. *Neuron*. 2001; 31(5):757–71. Epub 2001/09/25. PMID: 11567615.
35. Lacomme M, Liaubet L, Pituello F, Bel-Vialar S. NEUROG2 drives cell cycle exit of neuronal precursors by specifically repressing a subset of cyclins acting at the G1 and S phases of the cell cycle. *Mol Cell Biol*. 2012; 32(13):2596–607. <https://doi.org/10.1128/MCB.06745-11> PMID: 22547683; PubMed Central PMCID: PMC3434497.
36. Bel-Vialar S, Medevielle F, Pituello F. The on/off of Pax6 controls the tempo of neuronal differentiation in the developing spinal cord. *Dev Biol*. 2007; 305(2):659–73. <https://doi.org/10.1016/j.ydbio.2007.02.012> PMID: 17399698.
37. Wu L, Aster JC, Blacklow SC, Lake R, Artavanis-Tsakonas S, Griffin JD. MAML1, a human homologue of *Drosophila* Mastermind, is a transcriptional co-activator for NOTCH receptors. *Nat Genet*. 2000; 26:484–9. <https://doi.org/10.1038/82644> PMID: 11101851
38. Weng AP, Nam Y, Wolfe MS, Pear WS, Griffin JD, Blacklow SC, et al. Growth Suppression of Pre-T Acute Lymphoblastic Leukemia Cells by Inhibition of Notch Signaling. *Molecular and Cellular Biology*. 2003; 23(2):655–64. <https://doi.org/10.1128/MCB.23.2.655-664.2003> PMID: 12509463
39. Sawyer JM, Harrell JR, Shemer G, Sullivan-Brown J, Roh-Johnson M, Goldstein B. Apical constriction: a cell shape change that can drive morphogenesis. *Developmental Biology*. 2010; 341(1):5–19. Epub 2009/09/16. <https://doi.org/10.1016/j.ydbio.2009.09.009> PMID: 19751720; PubMed Central PMCID: PMC2875788.
40. Nishimura T, Takeichi M. Shroom3-mediated recruitment of Rho kinases to the apical cell junctions regulates epithelial and neuroepithelial planar remodeling. *Development*. 2008; 135(8):1493–502. <https://doi.org/10.1242/dev.019646> PMID: 18339671.
41. Rios AC, Serralbo O, Salgado D, Marcelle C. Neural crest regulates myogenesis through the transient activation of NOTCH. *Nature*. 2011; 473(7348):532–5. <https://doi.org/10.1038/nature09970> PMID: 21572437.
42. Zhang C, Li Q, Jiang YJ. Zebrafish Mib and Mib2 are mutual E3 ubiquitin ligases with common and specific delta substrates. *J Mol Biol*. 2007; 366(4):1115–28. <https://doi.org/10.1016/j.jmb.2006.11.096> PMID: 17196985.
43. Yoon KJ, Koo BK, Im SK, Jeong HW, Ghim J, Kwon MC, et al. Mind bomb 1-expressing intermediate progenitors generate notch signaling to maintain radial glial cells. *Neuron*. 2008; 58(4):519–31. <https://doi.org/10.1016/j.neuron.2008.03.018> PMID: 18498734.
44. Kawaguchi D, Furutachi S, Kawai H, Hozumi K, Gotoh Y. Dll1 maintains quiescence of adult neural stem cells and segregates asymmetrically during mitosis. *Nat Commun*. 2013; 4:1880. <https://doi.org/10.1038/ncomms2895> PMID: 23695674; PubMed Central PMCID: PMC3675328.
45. Dietz ML, Bernaciak TM, Vendetti F, Kielec JM, Hildebrand JD. Differential actin-dependent localization modulates the evolutionarily conserved activity of Shroom family proteins. *J Biol Chem*. 2006; 281(29):20542–54. <https://doi.org/10.1074/jbc.M512463200> PMID: 16684770.

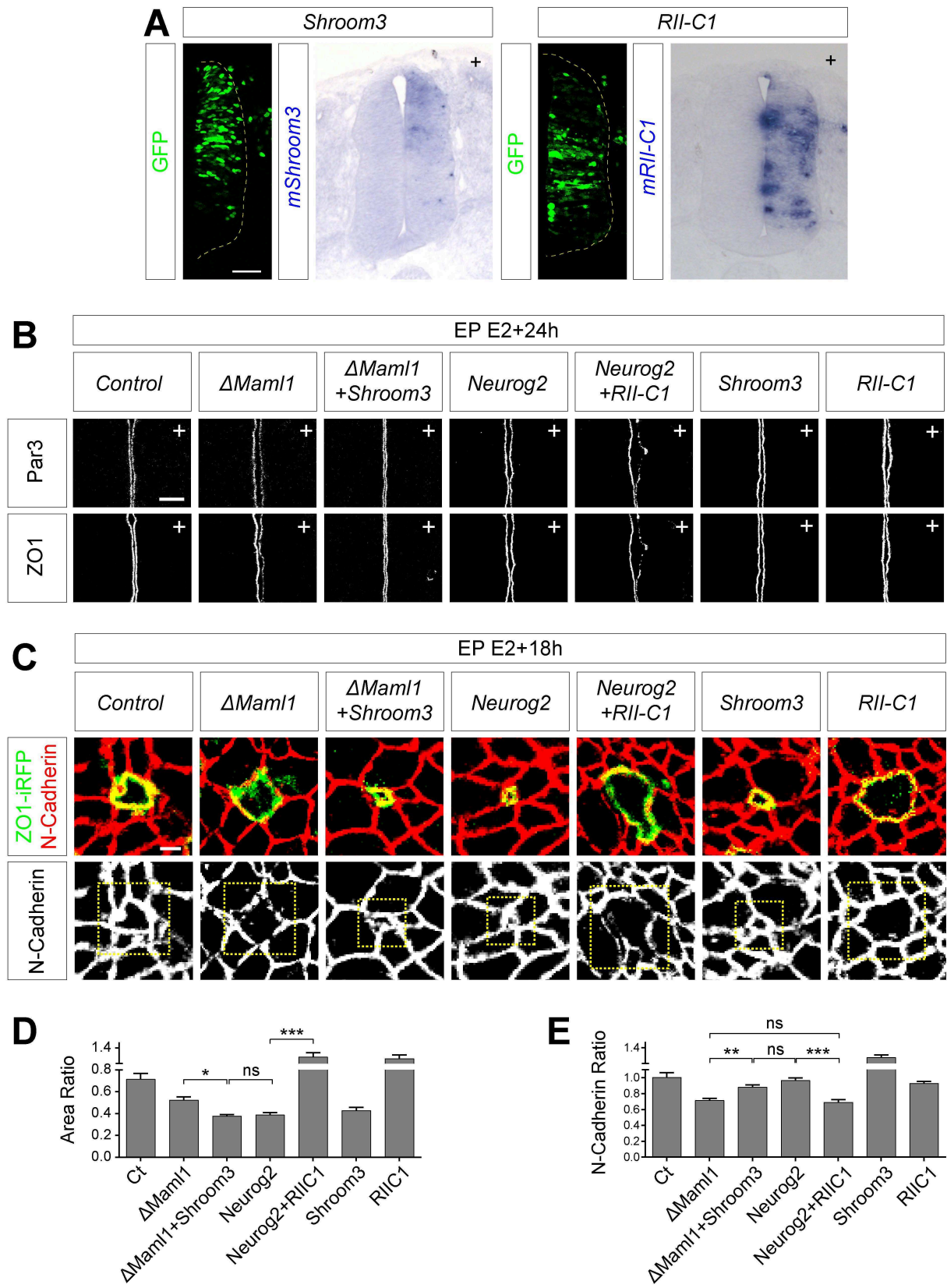
46. Yoder M, Hildebrand JD. Shroom4 (Kiaa1202) is an actin-associated protein implicated in cytoskeletal organization. *Cell Motil Cytoskeleton*. 2007; 64(1):49–63. <https://doi.org/10.1002/cm.20167> PMID: [17009331](https://pubmed.ncbi.nlm.nih.gov/17009331/).
47. Plageman TF Jr., Chung MI, Lou M, Smith AN, Hildebrand JD, Wallingford JB, et al. Pax6-dependent Shroom3 expression regulates apical constriction during lens placode invagination. *Development*. 2010; 137(3):405–15. <https://doi.org/10.1242/dev.045369> PMID: [20081189](https://pubmed.ncbi.nlm.nih.gov/20081189/); PubMed Central PMCID: PMCPMC2858910.
48. Hildebrand JD, Soriano P. Shroom, a PDZ domain-containing actin-binding protein, is required for neural tube morphogenesis in mice. *Cell*. 1999; 99(5):485–97. Epub 1999/12/10. PMID: [10589677](https://pubmed.ncbi.nlm.nih.gov/10589677/).
49. Matsuda M, Rand K, Palardy G, Shimizu N, Ikeda H, Dalle Nogare D, et al. Epb41I5 competes with Delta as a substrate for Mib1 to coordinate specification and differentiation of neurons. *Development*. 2016; 143(17):3085–96. <https://doi.org/10.1242/dev.138743> PMID: [27510968](https://pubmed.ncbi.nlm.nih.gov/27510968/); PubMed Central PMCID: PMCPMC5047669.
50. Lang RA, Herman K, Reynolds AB, Hildebrand JD, Plageman TF Jr. p120-catenin-dependent junctional recruitment of Shroom3 is required for apical constriction during lens pit morphogenesis. *Development*. 2014; 141(16):3177–87. <https://doi.org/10.1242/dev.107433> PMID: [25038041](https://pubmed.ncbi.nlm.nih.gov/25038041/); PubMed Central PMCID: PMCPMC4197547.
51. Sprinzak D, Lakhanpal A, Lebon L, Santat LA, Fontes ME, Anderson GA, et al. Cis-interactions between Notch and Delta generate mutually exclusive signalling states. *Nature*. 2010; 465(7294):86–90. <https://doi.org/10.1038/nature08959> PMID: [20418862](https://pubmed.ncbi.nlm.nih.gov/20418862/); PubMed Central PMCID: PMCPMC2886601.
52. Smrt RD, Szulwach KE, Pfeiffer RL, Li X, Guo W, Pathania M, et al. MicroRNA miR-137 regulates neuronal maturation by targeting ubiquitin ligase mind bomb-1. *Stem Cells*. 2010; 28(6):1060–70. <https://doi.org/10.1002/stem.431> PMID: [20506192](https://pubmed.ncbi.nlm.nih.gov/20506192/); PubMed Central PMCID: PMCPMC3140955.
53. Ossipova O, Ezan J, Sokol SY. PAR-1 phosphorylates Mind bomb to promote vertebrate neurogenesis. *Dev Cell*. 2009; 17(2):222–33. <https://doi.org/10.1016/j.devcel.2009.06.010> PMID: [19686683](https://pubmed.ncbi.nlm.nih.gov/19686683/); PubMed Central PMCID: PMCPMC2849776.
54. Konno D, Shioi G, Shitamukai A, Mori A, Kiyonari H, Miyata T, et al. Neuroepithelial progenitors undergo LGN-dependent planar divisions to maintain self-renewability during mammalian neurogenesis. *Nat Cell Biol*. 2008; 10(1):93–101. <https://doi.org/10.1038/ncb1673> PMID: [18084280](https://pubmed.ncbi.nlm.nih.gov/18084280/).
55. Megason SG, McMahon AP. A mitogen gradient of dorsal midline Wnts organizes growth in the CNS. *Development*. 2002; 129(9):2087–98. PMID: [11959819](https://pubmed.ncbi.nlm.nih.gov/11959819/).
56. Das RM, Van Hateren NJ, Howell GR, Farrell ER, Bangs FK, Porteous VC, et al. A robust system for RNA interference in the chicken using a modified microRNA operon. *Dev Biol*. 2006; 294(2):554–63. <https://doi.org/10.1016/j.ydbio.2006.02.020> PMID: [16574096](https://pubmed.ncbi.nlm.nih.gov/16574096/).
57. Dang L, Yoon K, Wang M, Gaiano N. Notch3 signaling promotes radial glial/progenitor character in the mammalian telencephalon. *Dev Neurosci*. 2006; 28(1–2):58–69. <https://doi.org/10.1159/000090753> PMID: [16508304](https://pubmed.ncbi.nlm.nih.gov/16508304/).
58. Das RM, Storey KG. Mitotic spindle orientation can direct cell fate and bias Notch activity in chick neural tube. *EMBO reports*. 2012; 13(5):448–54. Epub 2012/04/12. <https://doi.org/10.1038/embor.2012.42> PMID: [22491029](https://pubmed.ncbi.nlm.nih.gov/22491029/); PubMed Central PMCID: PMCPMC3343353.
59. Resh MD. Fatty acylation of proteins: new insights into membrane targeting of myristoylated and palmitoylated proteins. *Biochimica et biophysica acta*. 1999; 1451(1):1–16. Epub 1999/08/14. PMID: [10446384](https://pubmed.ncbi.nlm.nih.gov/10446384/).
60. Zhang C, Li Q, Jiang YJ. Zebrafish Mib and Mib2 are mutual E3 ubiquitin ligases with common and specific delta substrates. *Journal of molecular biology*. 2007; 366(4):1115–28. Epub 2007/01/02. <https://doi.org/10.1016/j.jmb.2006.11.096> PMID: [17196985](https://pubmed.ncbi.nlm.nih.gov/17196985/).
61. Skaggs K, Martin DM, Novitsch BG. Regulation of spinal interneuron development by the Olig-related protein Bhlhb5 and Notch signaling. *Development*. 2011; 138(15):3199–211. <https://doi.org/10.1242/dev.057281> PMID: [21750031](https://pubmed.ncbi.nlm.nih.gov/21750031/); PubMed Central PMCID: PMCPMC3133912.
62. Morin X, Jaouen F, Durbec P. Control of planar divisions by the G-protein regulator LGN maintains progenitors in the chick neuroepithelium. *Nat Neurosci*. 2007; 10(11):1440–8. <https://doi.org/10.1038/nn1984> PMID: [17934458](https://pubmed.ncbi.nlm.nih.gov/17934458/).
63. Schneider CA, Rasband WS, Eliceiri KW. NIH Image to ImageJ: 25 years of image analysis. *Nature Methods*. 2012; 9(7):671–5. Epub 2012/08/30. PMID: [22930834](https://pubmed.ncbi.nlm.nih.gov/22930834/).
64. Schindelin J, Arganda-Carreras I, Frise E, Kaynig V, Longair M, Pietzsch T, et al. Fiji: an open-source platform for biological-image analysis. *Nature Methods*. 2012; 9(7):676–82. Epub 2012/06/30. <https://doi.org/10.1038/nmeth.2019> PMID: [22743772](https://pubmed.ncbi.nlm.nih.gov/22743772/); PubMed Central PMCID: PMCPMC3855844.



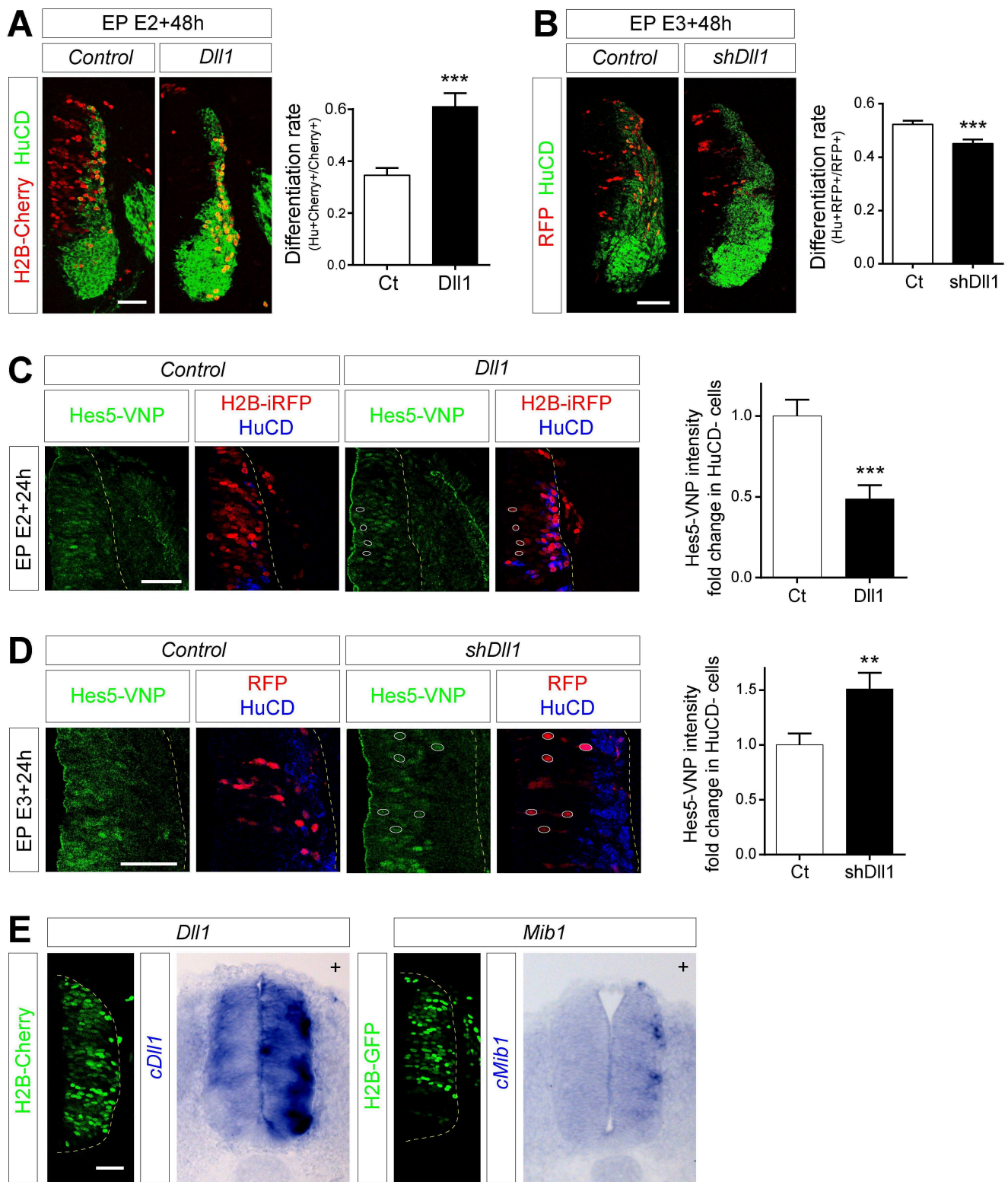




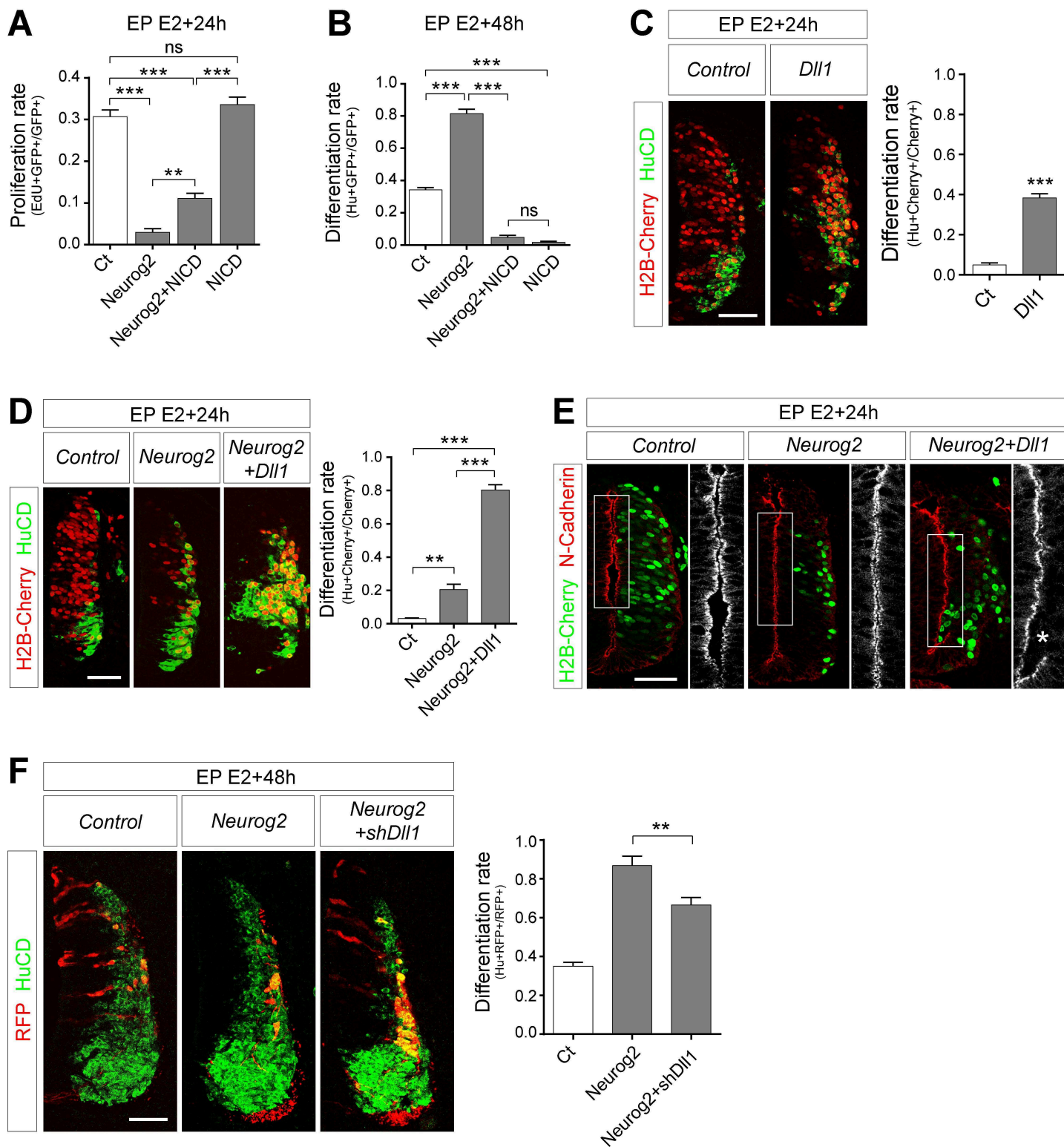
Baek et al., S3 Fig



Baek et al., S4 Fig



Baek et al., S5 Fig



Baek et al., S6 Fig

V.2. Discussion

In the present study, we have investigated the cellular and signaling mechanisms allowing prospective neurons to delaminate from the ventricular surface while preserving the integrity of the neuroepithelium. Using the chick embryonic spinal cord as a model, we have shown that Notch signaling remains active in prospective neurons to allow apical domain constriction to be completed prior to the disassembly of apical junctional complexes and neural delamination, therefore maintaining the integrity of the ventricular wall. Furthermore, we have investigated the mechanisms regulating Notch maintenance during this transition period and we propose that the Notch ligand Dll1 promotes differentiation by reducing Notch signaling activity through a cis-inhibition mechanism, while the ubiquitin ligase Mib1 blocks this effect to maintain Notch signaling in prospective neurons and defer differentiation, thus maintaining the proper architecture of the neural tube. In the next sections, I will first discuss the molecular events driving cell cycle exit and neural delamination and the link with the Notch signaling pathway. Secondly, I will discuss the dynamic switch between Notch trans-activation and cis-inhibition during the neural differentiation process and provide some clues and open questions on the mechanisms underlying Dll1-mediated cis-inhibition, its blockade by Mib1 and the mechanisms allowing the prospective neuron to eventually differentiate. This discussion section will end with a few words about the role of Notch signaling in disease, particularly in cancer. Similar to embryonic development, the ability of cells to perform EMT has been shown to play a role during cancer progression, particularly during tumor metastasis. Thus, not only Notch signaling but also delamination and EMT processes are at the heart of intensifying effort put together to dissect the etiology and provide alternative therapies to those diseases.

V.2.1. From cell cycle exit to neural delamination

The transition period from mitotic exit to the acquisition of neuronal differentiation markers and neural delamination remains so far poorly defined. I will first discuss the progression from cell cycle exit to the appearance of neuronal differentiation markers and examine how a basal level of Notch signaling is compatible with this progression. In a second part, I will introduce the sequence of events underlying neural delamination, namely apical constriction and down-regulation of N-cadherin, and discuss how Notch signaling is integrated during this process.

V.2.1.1. Cell cycle exit and neuronal differentiation

We qualify prospective neurons as cells that have completed their last mitosis but do not express neuronal differentiation markers yet. Using a Notch reporter transgenic chick line, we show that Notch signaling remains active in prospective neurons during the transition period from mitotic exit to the acquisition of differentiation markers, suggesting that Notch signaling, despite being classically associated with an undifferentiated state, is compatible with cell cycle arrest. One important question is then how are cell cycle exit and acquisition of differentiation traits coordinated and how is Notch maintenance compatible with cell cycle arrest.

During differentiation, cell cycle exit is controlled by proneural genes. Indeed, overexpression of the proneural gene *Neurog2* in the chick NT led to premature cell cycle exit and accumulation of CDK inhibitors $p27^{Kip1}$ and $p57^{Kip2}$ (Gui et al., 2007; Novitsch et al., 2001). More precisely, Lacomme and colleagues have identified the molecular events initiating cell cycle arrest in neural progenitors and have shown that *Neurog2* promote cell cycle exit by a two-step process (Lacomme et al., 2012). First, *Neurog2* rapidly represses the expression of G1/S cyclins to prevent S-phase re-entry. In a second step, it induces up-regulation of CDK inhibitors such as $p27^{Kip1}$, which leads to an irreversible exit of the cell cycle (Lacomme et al., 2012). Thus, the proneural gene *Neurog2* first induces an early cell cycle arrest, and then in a second time, induces an irreversible cell cycle exit. Of note, it is important to be careful and distinguish the timing of last mitosis, cell cycle arrest and cell cycle exit. In the present work, we have qualified prospective neurons as soon as cells have completed their last mitosis and observed that Notch signaling is maintained in those cells but the time from the last mitosis to the cell cycle exit has not been measured.

Given that cell cycle arrest is controlled by proneural genes that also promote other aspects of neuronal differentiation, how is the timing of cell cycle arrest affecting neuronal differentiation? Firstly, forcing neural progenitor cells to proliferate by overexpressing cyclin D1/2 does not prevent differentiation; rather, cells although still proliferating, differentiate into neurons and migrate in the differentiated mantle zone (Lobjois et al., 2008). Thus, forcing progenitors to cycle does not seem to alter their differentiation potential. Conversely, cell cycle arrest is not sufficient on its own to promote differentiation. Reducing cell proliferation by down-regulating cyclin D1 is not sufficient to promote neuronal differentiation either (Lacomme et al., 2012). Moreover, cell cycle re-entry of differentiated neurons has been observed in the case of $p57^{Kip2}$ loss-of-function (Gui et al., 2007). These data strongly suggest that cell cycle exit and

differentiation can be uncoupled. Finally, we provide evidence in the present study that Notch gain-of-function in differentiating cells (by overexpressing the constitutively active NICD together with Neurog2) prevented differentiation but not cell cycle arrest (Baek et al., 2018, see Figure S6A-B). This result supports the notion that high levels of Notch signaling are compatible with cell cycle arrest.

V.2.1.2. Apical constriction and neural delamination

In the current study, we provide evidence that the maintenance of Notch signaling activity in prospective neurons is important to allow a proper neural delamination process. During this process, nascent neurons first reduce their apical domain prior to down-regulation of N-cadherin and eventually the withdrawal of apical endfoot from the ventricular surface (Baek et al., 2018). While information concerning the cellular events that accompany neural delamination is still scarce, the transcriptional network coordinating neural delamination and differentiation has started to be addressed. Down-regulation of cadherins seems to be a prerequisite for neural delamination to take place. Indeed, in the chick developing spinal cord, the proneural gene Neurog2 induces Foxp2/4 up-regulation, which in turn represses N-cadherin expression (Rouso et al., 2012), while in the mouse developing cortex, Neurog2 induces Scratch1/2, which in turn repress E-cadherin expression (Itoh et al., 2013). Thus, it is tempting to speculate that the proneural gene Neurog2 acts as a master gene during neural delamination orchestrating apical domain constriction with down-regulation of cadherins, as discussed below.

Shroom3 mediates apical constriction

Our results strongly suggest that apical constriction of prospective neurons involves a Shroom-like activity. Shroom3 has been reported to be required for apical constriction in many organisms and in various aspects of morphogenetic events. The involvement of Shroom3 in this process was first demonstrated during NT closure in mice (Hildebrand and Soriano, 1999). Since then, Shroom3 was shown to control apical constriction during lens placode formation (Lang et al., 2014; Plageman et al., 2010), gut morphogenesis (Chung et al., 2010) and in the lateral line primordium of zebrafish (Ernst et al., 2012). How does Shroom3 drive apical constriction? Shroom3 is an actin-binding protein that binds and recruits Rho kinases (ROCKs) to AJs (Nishimura and Takeichi, 2008). ROCKs phosphorylate myosin regulatory light chain (MLC), which in turn activates myosin II. As a result, the actin-myosin network is reorganized to form an

apical contractile ring and eventually leads to the constriction of the apical cell membrane (Figure 21). In the developing chick NT, disruption of Shroom3-ROCK interaction blocked pMLC (phosphorylated MLC) apical enrichment and perturbed NT closure (Nishimura and Takeichi, 2008). While the role of Shroom3 in apical constriction is well characterized during the morphogenetic events described above, it has never been involved in neural delamination. We for the first time implicate a Shroom-driven apical constriction during the process of delamination of nascent neurons. To go further in the characterization of Shroom-like apical constriction, it will be worth to examine the endogenous localization of Shroom3 and ROCK, as well as their colocalisations with pMLC in neural progenitors and prospective neurons of the chick NT..

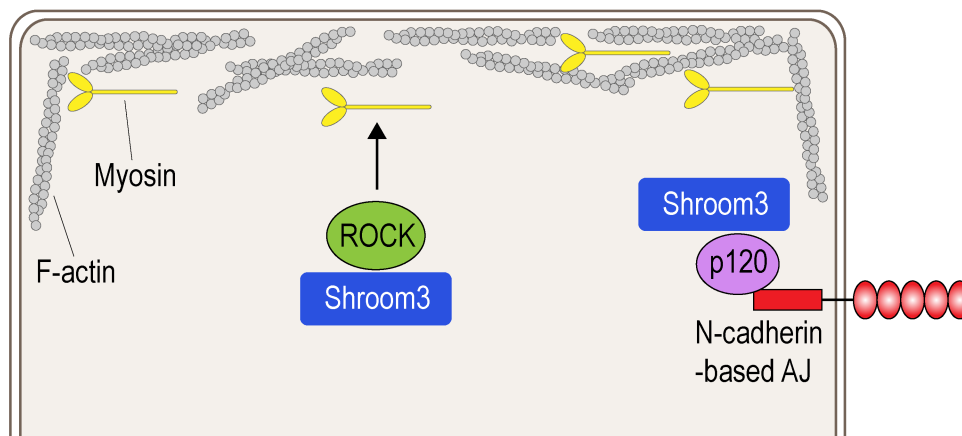


Figure 21. Shroom3-mediated apical constriction.

The actin-binding protein Shroom3 present in the apical region recruits ROCK to the AJ, which phosphorylates MLC to activate myosin II, leading to actin-myosin contraction. In lens cells, p120-N-cadherin can recruit Shroom3 to AJ.

What controls Shroom3 expression pattern? During *Xenopus* gut morphogenesis and mouse lens placode formation, the transcription factors Pitx and Pax6 induce Shroom3 expression, respectively (Chung et al., 2010; Plageman et al., 2010) while in the zebrafish lateral line primordium, Shroom3a expression is controlled by FGF signaling (Das et al., 2014). However, in the chick NT, nothing is published so far in terms of Shroom expression regulation. In the chick spinal cord, blocking Shroom3-ROCK interaction resulted in increased apical areas in all transfected cells, meaning that Shroom3 plays a role not only in prospective neurons poised to delaminate but also in all cycling progenitors (Baek et al., 2018, Figure S4). It is thus possible to imagine that neural progenitors have a basal activity of Shroom3, which consistently keeps the

apical surface under tension and provides a certain steady state of contraction. Conversely, when cells commit to differentiate, the activity of Shroom3 must be somehow enhanced. For instance, proneural genes, whose expression increases during differentiation, are good candidates for performing transcriptional control of Shroom3 activity. Consistent with this possibility, the levels of Shroom1 and Shroom3 transcripts were up-regulated as soon as 6 h after Neurog2 electroporation in the chick NT (personal communication, S. Bel-Vialar). Given that the proneural gene Neurog2 has already been implicated in the transcriptional network regulating N-cadherin, E-cadherin and Plekha7 apical junctional proteins (Itoh et al., 2013; Rousso et al., 2012; Tavano et al., 2018), it is tempting to speculate that it could also target Shroom family members and act as a master gene orchestrating each step of the neural delamination sequence. It would be thus interesting to investigate whether Shroom1/3 have evolutionarily conserved binding sites for Neurog2 or Neurog2 target genes involved in neural delamination (Foxp2/4, Scratch1/2, Insm1) by genomic sequence alignment and perform chromatin immunoprecipitation (ChIP) assays accordingly. Furthermore, we have studied the role of Shroom3 in the spinal cord, but it will be also important to examine the contribution of Shroom-like activity during delamination of cortical neurons.

To date, Shroom3 has been implicated in apical constriction during several morphogenetic events but not in neural delamination process. On the other hand, previous studies suggest that neural delamination is accompanied by down-regulation of N-cadherin and eventually apical abscission, but it does not implicate a Shroom-like apical constriction (Rousso et al., 2012; Das et al., 2014). However in the present work, we provide for a more complete picture of neural delamination: a Shroom-like constriction of the apical endfoot followed by the diminution of N-cadherin.

How does Notch signaling coordinate apical constriction and N-cadherin reduction?

We identify Notch signaling maintenance in prospective neurons to be important to coordinate N-cadherin reduction with apical constriction. Blockade of Notch signaling with a dominant-negative form of Maml1 caused accelerated delamination with down-regulation of N-cadherin and expression of neuronal differentiation markers while the apical domain is still large (Baek et al., 2018, Figure 2B-2C), whereas forcing apical constriction by overexpressing Shroom3 rescues this phenotype (Baek et al., 2018, Figure 3). These results indicate that maintenance of Notch signaling in prospective neurons is crucial for neural delamination to take

place properly and to preserve the integrity of the neuroepithelium. However, how Notch signaling regulates apical constriction and N-cadherin levels during this process will need to be addressed.

In line with this, Notch signaling was shown to directly induce N-cadherin expression during angiogenesis and tumorigenesis. In mouse brain endothelial cells, it was shown that NICD and Smads molecules form a complex with the transcription factor CSL to activate N-cadherin transcription (Li et al., 2011). A more recent study performed in hEMV (human engineered microvessels) cell culture has linked a non-canonical Notch pathway with the regulation of vascular endothelial cadherin (VE-cadherin) and propose that Notch signaling is crucial to establish AJ and therefore to maintain the endothelial barrier (Polacheck et al., 2017). In addition, Notch signaling has been implicated in the regulation of N-cadherin expression in the context of tumor formation. It has been proposed that signaling through Notch1 and Notch3 induces N-cadherin expression in human melanoma cell lines (Liu et al., 2006; Wang et al., 2007), while Dll1-mediated Notch activation increases N-cadherin expression levels in rhabdomyosarcoma (RMS) cell lines (Masia et al., 2012). ChIP assays showed that NICD binds to N-cadherin promoter sequence, strongly suggesting a role of Notch signaling in transcriptional activation of N-cadherin in RMS cells (Masia et al., 2012). Taken together, these data indicate that Notch signaling can directly instruct N-cadherin up-regulation. Nevertheless, whether Notch signaling induces N-cadherin expression in neural progenitor cells has never been explored. During the first step of neural delamination, we have observed that N-cadherin expression remains relatively high and is down-regulated only later after apical constriction. However, previous studies show that N-cadherin expression must be eventually down-regulated for neural delamination to take place and this is likely to be induced by Neurog2. How to explain the maintenance of Notch signaling and the temporal regulation of apical constriction followed by N-cadherin down-regulation? First of all, it is important to note that the Notch signaling activity is elevated in prospective neurons compared to differentiated HuCD⁺ neurons, but still is relatively reduced compared to cycling progenitors (Baek et al., 2018, Figure 1C-D). The exact kinetic of Notch reduction between prospective neurons and differentiated neurons, as well as the timing of apical constriction and N-cadherin reduction in regards to the state of Notch signaling are still not clear. On the one hand, assuming that Notch signaling is maintained relatively high and decreases sharply at the very last moment of neural delamination, it is possible that N-cadherin levels remain stable all along the delamination process and is down-regulated only when Notch

signaling itself is reduced finally just prior to the withdrawal of the apical endfoot. On the other hand, assuming that Notch signaling is reduced gradually in prospective neurons, another interesting possibility would be that the N-cadherin expression is down-regulated all along the process of neural delamination but the constriction of apical domain allows to confine low N-cadherin levels in small fractions thereby locally concentrating apical N-cadherin, which transiently compensates for N-cadherin down-regulation. To have a clue on these hypotheses, one could measure N-cadherin levels at different time points after disrupting apical constriction in prospective neurons by co-electroporating the RII-C1 construct with Neurog2. This would tell when N-cadherin starts to reduce in a context where a large apical domain is maintained.

Instead, during apical constriction of prospective neurons, Notch signaling may play a permissive role. Indeed, forced expression of the proneural gene Neurog2 induced apical constriction from 12 hours after electroporation (hae) onwards, while Notch levels are maintained high up to 24 hae (Baek et al., 2018, compare Fig 2A with S3C Fig). Thus, the Notch pathway itself is unlikely to regulate Shroom3-like apical constriction. During lens placode formation in mouse developing embryo, Shroom3 was shown to be recruited to AJ by the p120-catenin protein (Lang et al., 2014) (Figure 21). Accordingly, maintenance of Notch signaling could help the prospective neuron to transiently preserve its epithelial features, including apical p120-catenin, possibly downstream of N-cadherin, which allows Shroom3 to be recruited at the AJ and apical constriction to take place properly.

V.2.2. Notch trans-activation and cis-inhibition balance during differentiation

V.2.2.1. Cis-inhibition of the receptor by the ligand

We have investigated the mechanisms that regulate Notch signaling activity in prospective neurons and have demonstrated that Dll1 represses Notch signaling through a cis-inhibition mechanism. The existence of cis-inhibition of the ligand by the receptor has been previously documented in *Drosophila* (see section II.4), but a clear demonstration of the ability of Notch ligands to perform cis-inhibition in vertebrates is limited to *in vitro* studies (Sprinzak et al., 2010). Importantly, studying cis-inhibition is difficult because any manipulation of Notch ligands in gain- and loss-of-function assays would interfere with both trans- and cis phenomena. In the present work, we have taken advantage of the ability of the ubiquitin ligase Mib1 to promote trans-activation, to unambiguously discriminate between trans- and cis- interactions. Mib1

promotes Notch trans-activation and counteracts Dll1-mediated cis-inhibition, as shown in our overexpression experiment. Conversely, disrupting Mib1 function in a sparse manner using a dominant negative led to a reduction of Notch activity cell-autonomously and accelerated neurogenesis, strongly supporting the endogenous existence of cis-inhibition *in vivo* in the vertebrate nervous system.

What are the mechanisms controlling cis-inhibition of the Notch receptor by the ligand Dll1? The molecular interactions underlying ligand cis-inhibitory activity have only started to be elucidated. From a structural point of view, several lines of evidences indicate that it involves a direct ligand-receptor interaction through their extracellular domains and that the interaction domains for trans-activation and cis-inhibition are likely to be the same. Once the ligand has bound to the receptor, cis-inhibition may rely either on the titration of the Notch receptor, or on its internalization and degradation (del Alamo et al., 2011). Mathematical modeling based on *in vitro* experimental data supports a titration-based mechanism, in which the Notch ligands and receptors form complexes that are inactive for signal reception and activation (Sprinzak et al., 2010). Indeed, because of its parallel binding conformation, cis-interaction of the ligand and the receptor cannot produce the pulling force, believed to be required for effective Notch activation (Weinmaster and Fischer, 2011). On the other hand, one preliminary experiment performed in the lab favors the degradation model. Upon overexpression of Dll1 in the chick NT, we have observed a rapid loss of the intensity of a Notch-GFP fusion protein signal as soon as 8 hae (data not shown). To confirm those results, it will be worth to analyze deeper the kinetics of Notch-GFP down-regulation upon Dll1 co-expression, and investigate whether and in which endocytic vesicles Notch-GFP is found.

V.2.2.2. How is cis-inhibition modulated?

During the transition period preceding neural delamination, we show that the ubiquitin ligase Mib1 is able to block the cis-inhibitory effect of Dll1. As a result, prospective neurons maintain Notch signaling, differentiation is delayed and the neuroepithelial integrity preserved. Of note, in the *Drosophila* embryo, the ubiquitin ligase Neur was previously shown to repress ligand cis-inhibition (Glittenberg et al., 2006). However in mammalian cells, overexpression of Mib1, in contrast to Neur in *Drosophila*, was unable to block the cis-inhibitory activity of the ligands (Itoh et al., 2003). In the current study, by overexpressing Mib1 together with Dll1, we show that Mib1 is indeed able to block Dll1-mediated cis-inhibition. Nevertheless, the

mechanisms allowing Mib1 to block Dll1 cis-inhibition will need to be carefully investigated. One possibility is based on the amount of Dll1 available on the plasma membrane: Mib1, as a ubiquitin ligase, by promoting trans-activation, would induce the endocytosis of Dll1, thus reducing the amount of Dll1 available at the plasma membrane to perform cis-inhibition. Alternatively, it is also possible that Mib1 plays another role in cis that is different from its ubiquitylating activity: Mib1 would somehow enhance the affinity of Dll1 ligands for Notch receptors present in trans and prevent them from performing cis-inhibition.

Is it possible to discriminate between those different possibilities? To approximate this question, one could look at a single-cell resolution at the endogenous expression pattern of Notch and Dll1 proteins upon Mib1 overexpression. Is the expression of Dll1 decreased from the plasma membrane? Are there any changes in the localization of both Dll1 and Notch? Is there an increase in trans-activation reflected by more Dll1-NECD complexes in vesicles? Nevertheless, at the current state, it is difficult to address these points in the chick NT, because immunostainings of those molecules offer poor resolution and endogenous dynamics cannot be monitored. Therefore, an *in vitro* system (1) enabling to monitor endogenous reporters for Mib1 and Dll1 at high resolution; (2) providing a differentiation dynamics similar to the *in vivo* situation; (3) amenable to live-imaging, would be useful. This is an on-going project and I will describe our early attempts in chapter VI.

V.2.2.3. How does the prospective neuron finally differentiate?

If a basal level of Notch signaling is maintained in prospective neurons to defer differentiation and preserve the integrity of the neuroepithelium, its activity should be shut down to allow terminal differentiation. Thus, it is important to investigate by which mechanisms cis-inhibition takes place to allow the prospective neuron to eventually differentiate. This is likely to result from an increase in the Dll1/Mib1 ratio: increase of Dll1 and/or decrease of Mib1 expression level at the cell membrane.

Firstly, increase in Dll1 expression at the plasma membrane during differentiation could explain how cis-inhibition increases and the prospective neuron finally differentiates. Indeed, Dll1 is an early target of Neurog2 (Lacomme et al., 2012). Thus, over the course of differentiation, as the level of Neurog2 progressively increases, this could lead to an increase of Dll1 expression that reaches a threshold sufficient to perform cis-inhibition. In this regards, it will

be worth to precisely investigate the dynamics of Dll1 expression level by quantitative PCR or quantitative *in situ* hybridization assays.

Secondly, the decrease of Mib1 expression level could explain the increase in the Dll1/Mib1 ratio. Consistent with this, it was shown that Mib1 levels could be decreased through microRNA (Smrt et al., 2010). It was also shown that Mib1 is targeted for degradation by the proteasome upon its phosphorylation by the cell polarity protein Par1 kinase (Ossipova et al., 2009) or the cyclin-dependent kinase 5 (CDK5) (Choe et al., 2007). Phosphorylation of Mib1 is proposed to enhance its ubiquitylation activity and lead to auto-ubiquitylation that targets Mib1 for degradation (Choe et al., 2007). Nevertheless, how Mib1 attaches poly-ubiquitin chains to itself to target for proteasomal degradation is not known.

Thirdly, Mib1 could be inactivated and unable to ubiquitylate Dll1 at the plasma membrane. One possibility would be a change in the subcellular localization of Mib1 that displaces Mib1 from the cell membrane, thereby preventing Mib1-Dll1 interaction. Consistent with this, we have observed in the chick NT that Mib1 is enriched in the Golgi apparatus in the differentiated zone (Figure 22). This organelle is likely to sequester Mib1 and reduce the amount of Mib1 available at the cell membrane. Thus, it will be important to precisely explore the subcellular localization of Mib1 at the final steps of terminal differentiation and see whether Mib1 is sequestered in the Golgi apparatus prior to neural delamination, therefore increasing Dll1/Mib1 ratio at the plasma membrane and favoring cis-inhibition. Again, these important questions are difficult to assess with our current experimental model of chick NT. We will take advantage of the *in vitro* neural differentiation system to answer to this and other questions in the future (see chapter VI).

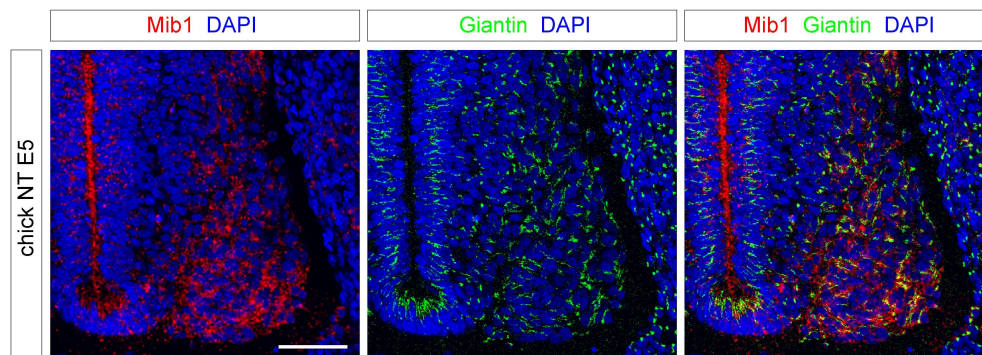


Figure 22. Mib1 is expressed in the Golgi apparatus in neurons.

Chick NT at E5 stained with Mib1 antibody (red) and Giantin (Golgi apparatus marker, green). Mib1 is colocalized with the Golgi apparatus marker in the differentiated zone of motor neurons. Scale bar represents 50 μm .

Finally, another possibility is that the prospective neuron eventually differentiates by a cell stress-dependent mechanism. Even though it might sound provocative and oxidative stress is usually documented for its cellular toxicity, it is also involved in normal situations of cell differentiation. Indeed, in the chick spinal cord, mitochondria morphology was shown to differ between progenitor and differentiated cells (Mils et al., 2015), while the tight regulation of ROS levels, induced by oxidative stress, were considered important for the progression of neurogenesis in neurosphere cultures (Le Belle et al., 2011). Thus, one could hypothesize that the poised situation of the prospective neuron generates increased levels of ROS. In line with this, a recent study in cell culture assays has shown that oxidative stress inhibits the ubiquitylating activity of Mib1 (Villumsen et al., 2013). On the other hand, increased levels of oxidative stress could activate the p38 mitogen-activated protein kinase (MAPK) pathway in the prospective neuron. The MAPK p38 is a central transducer of cell stress responses: it activates numerous downstream effectors kinases, including MAPK-activated protein family members, which in turn elaborate signal transduction cascades that allow cells to effectively respond to various cell stresses such as oxidative stress, ultraviolet light or osmotic shock (reviewed in(Cuadrado and Nebreda, 2010; Gaestel, 2006)). Interestingly, the p38 MAPK pathway was documented to regulate the transition from progenitor to differentiated state in the context of skeletal muscle differentiation (Lluis et al., 2006) and during neurogenesis in cell culture assays (Oh et al., 2009). Preliminary data suggest that p38 may also regulate terminal differentiation in our system. First, we have observed a phosphorylated p38 (P-p38, active form) expression at the transition between the ventricular and marginal zone of the chick NT at embryonic day (E) 5 (Figure 23A), and most if not all P-p38⁺ cells have exited the cell cycle, as monitored by the absence of EdU incorporation (Figure 23B), which suggests that p38 may indeed play a role during terminal differentiation. Second, we have monitored p38 activity in differentiating cells by co-electroporating a p38 reporter (Aguirre-Ghiso et al., 2004) together with Neurog2 and observed an increase of p38 activity in Neurog2-expressing cells, suggesting that Neurog2 activates p38 (data not shown). Nevertheless, a deeper characterization and quantification of the p38 reporter activity is needed to confirm this preliminary result. To further investigate the role of p38 during terminal differentiation, we decided to perform gain- and loss- of p38 function. p38 MAPK is activated by two kinases, MKK3 and MKK6 (Figure 25-Top). Thus, we have taken advantage of a phosphomimetic form of MKK6 (MKK6EE) and a kinase-dead form of MKK3 (MKK3Ala) to activate and inactivate p38, respectively (Raugeaud et al., 1996). When co-electroporated with

Neurog2 at E2, gain- and loss- of p38 function led to an increase and a decrease of neurogenesis, respectively (Figure 24A). Likewise, gain- and loss- of p38 function alone at E3 at the peak of neurogenesis led to similar results (Figure 24B). These data strongly suggest that p38 is involved in terminal differentiation.

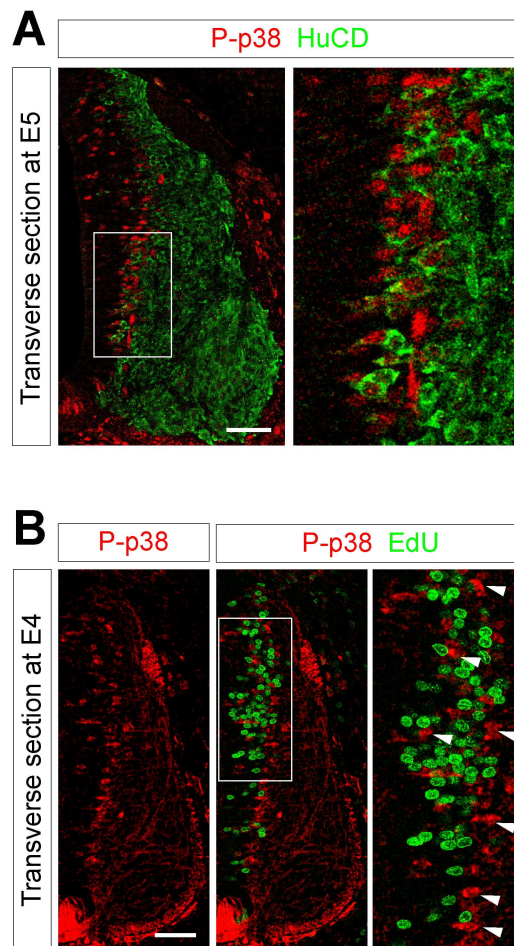


Figure 23. P-p38 expression profile.

(A) Transverse section of E5 chick NT immunostained with the Phosphorylated(activated)-p38 antibody (red) and the neuronal marker HuCD (green). The right panel corresponds to a high magnification of the boxed area in left. (B) Transverse section of E4 chick NT incubated with EdU (green) and immunostained with the Phosphorylated(activated)-p38 antibody (red). Arrowheads indicate p38⁺EdU⁺ cells in the ventricular zone. Scale bar represents 50 μ m.

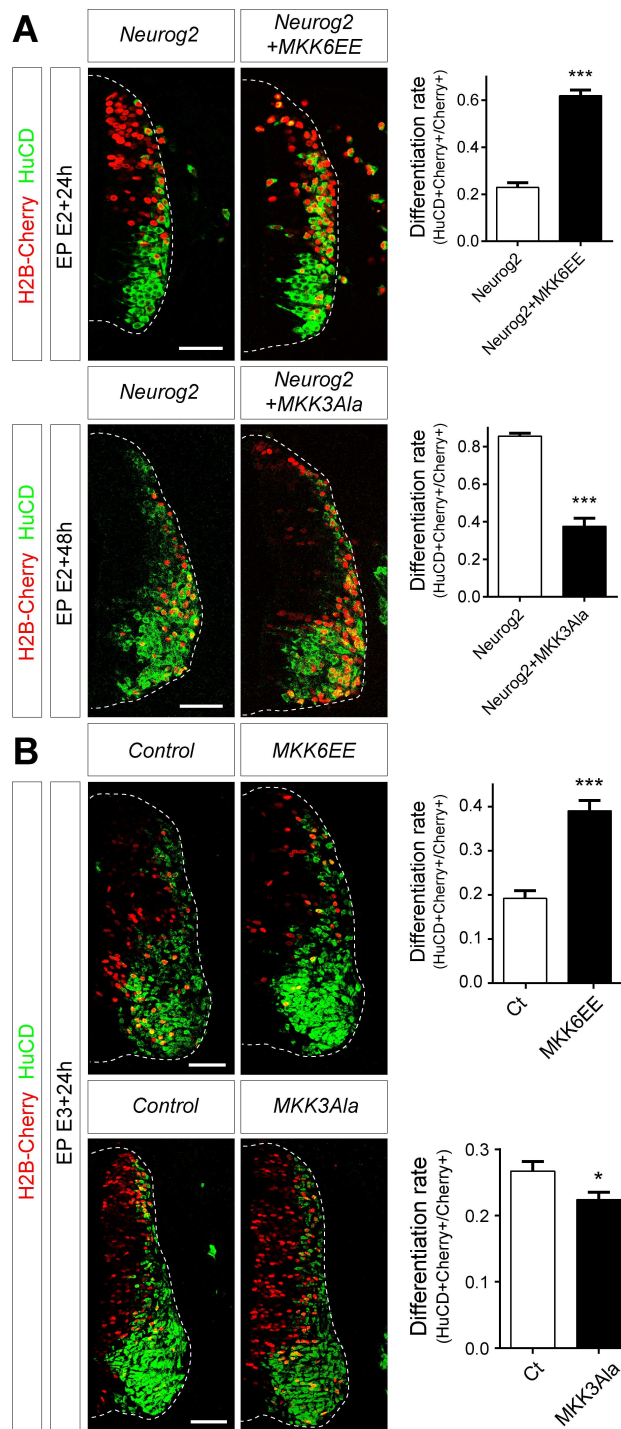


Figure 24. Effects of gain- and loss-of p38 function on neurogenesis.

(A) Left: Transverse sections of the NT transfected at E2 with Neurog2 alone or with MKK6EE (activation) or MKK3Ala (inactivation) and immunostained for HuCD (green). Transfection is reported by H2B-Cherry expression. Right: Quantification of the differentiation rate (number of HuCD⁺ cells on total transfected cells). (B) Left: Transverse sections of the NT transfected at E3 with the indicated constructs and harvested at E4 and immunostained for HuCD (green). Transfection is reported by H2B-Cherry expression. Right: Quantification of the differentiation rate (number of HuCD⁺ cells on total transfected cells). Data represent mean + SEM. *p<0.05; ***p<0.001 (Student *t* test). Scale bar represents 50 μ m.

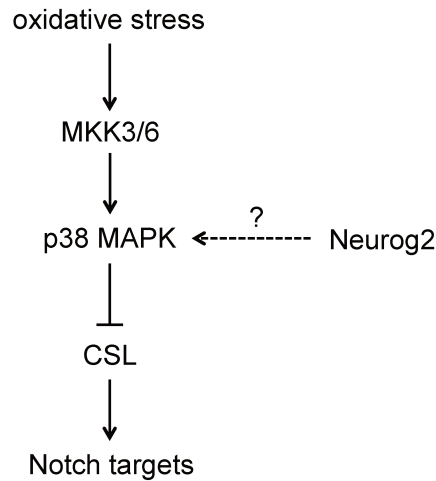


Figure 25. Proposed model of p38 MAPK activation pathway during neural differentiation.

Then, how could p38 regulate differentiation? A recent study performed in cultured cells treated with a specific inhibitor of p38 revealed that p38 down-regulates the transcriptional activator CSL by protein degradation (Kim et al., 2012). Thus, Neurog2 may up-regulate p38 activity, which in turn degrades CSL, inhibiting Notch activity and allowing the prospective neuron to finally differentiate (Figure 25). Our preliminary results suggest that p38 MAPK is unlikely to modulate Mib1 activity, as activation of p38 by overexpressing MKK6EE could not relieve the blockade of Dll1 cis-inhibition by Mib1 (data not shown). On the other hand, it could increase Dll1 expression. Future work investigating the expression levels of Dll1 upon p38 activation is required to reveal the mechanisms by which the p38 MAPK pathway is involved in the process of terminal differentiation of prospective neurons in the developing chick spinal cord.

V.2.3. Notch beyond neurogenesis in development and disease

V.2.3.1. Notch in gliogenesis

Extensive analyses of Notch function have clearly revealed its role during neuronal differentiation. Notch signaling plays an important role in controlling the balance between neural progenitor maintenance and differentiation into neurons. Nevertheless, this role of Notch cannot account for the large repertoire of Notch action in the nervous system. While it inhibits progenitors' differentiation into neurons, Notch signaling was shown to promote glial differentiation. Almost twenty years ago, work in the developing neocortex, retina and neural

crest showed that Notch activation not only inhibited neuronal differentiation but could also promote glial fate determination (Furukawa et al., 2000; Gaiano et al., 2000; Morrison et al., 2000). Since then, diverse lines of investigation have contributed to demonstrate the instructive role of Notch signaling in gliogenesis. For instance, conditional deletion of CSL specifically in neural progenitors (with a *Nestin-Cre* driver) or in neural crest cells (with a *Wnt1-Cre* driver) resulted in severe defects in glial development throughout the CNS and the PNS in E14.5 mouse embryos, despite normal neurogenesis (Taylor et al., 2007). At later stage, undifferentiated neural crest precursors could be found in the sympathetic ganglia *in vivo*, and they were able to form glia in cultures supplemented with Neuregulin, meaning that those precursors have maintained the capacity to differentiate but fail to undergo gliogenesis in the absence of Notch signaling. Moreover, the *CSL*^{-/-} spinal cord at E19.5 exhibited a significant decrease of astrocytes number at the expense of oligodendrocytes, indicating that Notch signaling is required to promote gliogenesis beyond simply maintaining the pool of progenitors (Taylor et al., 2007). In addition, conditional inhibition or activation of Notch precisely in Schwann cell precursors in mouse embryo led to a reduction or an increase in Schwann cell proliferation, respectively (Woodhoo et al., 2009). Lastly, it has been shown in drug-inducible *Mib1* conditional knock-out mice that a relatively late deletion of *Mib1* (between E12 and E14) specifically in neural progenitors (with a *Nestin-Cre* driver) suppresses glial differentiation in the developing spinal cord (Kang et al., 2013). As *Mib1* is a key player required for Notch activation, these data support the idea that Notch signaling is important to specify glial fate.

Altogether, Notch signaling controls multiple steps of the nervous system development, from the initial binary fate choice between progenitor and neuronal outcomes, but also over the course of glial fate determination. Even though not discussed in this chapter, Notch signaling is also involved in post-natal and adult nervous system where its role is just starting to be grasped. Understanding how Notch can regulate neural progenitor maintenance in adult brain as well as the survival and function of mature neurons, is of particular importance for the development of therapies against brain injury and neurodegeneration.

V.2.3.2. Notch, cancer and EMT

The Notch signaling pathway has a very broad panel of action throughout the body. It is not only involved in the nervous system development, but also associated with a large spectrum of developing tissues and organs. Thus, not surprisingly, disruption of the Notch pathway affects

extremely various organs and is increasingly explored as a potentially important therapeutic target for human diseases. Here I intend to give a brief history of diseases associated with the Notch pathway with a special emphasis on cancer. In particular, I will focus on the contribution of Notch signaling at the intersection of EMT and cancer progression.

Many human cancers are thought to contain cells that display stem cell-like properties, including the potential to self-renew, resistance to cell death and the ability to differentiate. Because Notch signaling regulates the balance between cell proliferation and differentiation, survival and apoptosis, alterations in Notch signaling are often associated with cancer. Already in the 1990's, it was suggested that T-cell acute lymphoblastic leukemia (T-ALL) is associated with an aberrant activation of the Notch pathway, visualized by an up-regulation of NICD (Ellisen et al., 1991). Since then, Notch signaling was shown to be deregulated in many cancers such as lung, colon, renal and pancreatic cancer as well as many types of lymphomas (reviewed in(Aster et al., 2017)). As for brain cancers, alterations of the Notch pathway were also found to be present in several brain tumor types. For instance, cell lines derived from malignant human gliomas overexpress the Notch ligands Jagged1 and Dll1 (Ignatova et al., 2002). In most cases, Notch acts as an oncogene and promotes cancer formation and progression.

An important feature of cancer progression is the ability of cancer cells to migrate to different sites and establish disease in distant organs, a process known as tumor metastasis. Although debated for decades, it is now accepted in the field that cancer cells delaminate from the primary tumor site through an EMT-like process that resembles the physiological EMT occurring during morphogenesis. Nevertheless, differences exist, as cancer cells in most cases perform a 'partial' EMT, and the regulatory genes involved are not strictly identical to the 'classical' EMT (Thiery et al., 2009). During this process, Notch signaling has been found to be a key participant in the induction of EMT in normal development and in cancer (Capaccione and Pine, 2013).

For instance, in renal tubule culture, NICD overexpression resulted in up-regulation of Snail1, a transcription factor that induces EMT, and down-regulation of the epithelial marker E-cadherin levels (Saad et al., 2010). As for Snail2, it has been demonstrated that NICD binds to the Snail2 promoter to activate its transcription and by this way represses VE-cadherin expression, which initiates EMT during cardiac development *in vivo* in mouse (Niessen et al., 2008). More recently, it has been shown in chick muscle development that a non-canonical Notch signaling up-regulates Snail1, which activates EMT in the dermomyotome *in vivo* (Sieiro et al., 2016).

During muscle formation, it is known that migrating neural crest cells expressing Dll1 activate signaling in myotome Notch1-containing cells (Rios et al., 2011). Upon ligand and receptor activation, NICD is released in the cytoplasm. Interestingly, in this case, Notch signaling promotes Snail1 up-regulation independently of its transcriptional activity in the nucleus; rather, cytoplasmic NICD inhibits GSK-3 β activity, which in turn results in Snail1 stabilization that triggers EMT (Sieiro et al., 2016). Similarly, a link between Notch signaling and Snail1/2 transcription factors was also demonstrated in cancer cells. For example in breast cancer, Notch signaling regulates Snail1/2 expression, which in turn down-regulates E-cadherin to initiate EMT (Chen et al., 2010).

Overall, all these data converge to the fact that Notch signaling promotes EMT. Strikingly, this appears to be in contradiction with our own findings, which suggest that Notch signaling is a protective factor against premature EMT-like delamination of prospective neurons in the chick spinal cord (Baek et al., 2018). How to understand this apparent discrepancy? The contribution of Notch signaling in EMT processes has been studied most intensively in the context of cell culture assays, and *in vivo* in organs other than the central nervous system. This raises the question of the tissue-specificity of the EMT program. Indeed, in the central nervous system development, delamination of newborn neurons seems to follow an EMT-like program that is likely to be initiated by the proneural genes (see chapter III). Yet, the Notch signaling pathway counterbalances proneural gene activity, which is consistent with a Notch activation inhibiting an EMT-like delamination. Moreover, in many cancers other than neural tissue, the process of EMT coincides with the loss of E-cadherin and the acquisition of N-cadherin, whereas during neuron delamination in the spinal cord, N-cadherin must be down-regulated for cells to delaminate. Taken together, this again illustrates that EMT is not a uniform program defined by a single pathway but rather needs to be further investigated to uncover all of its multiple actions in a tissue-dependent manner.

VI

PERSPECTIVES AND ON-GOING PROJECT

Chapter VI.

Perspectives and On-Going Project

VI.1. Introduction and aims of the project

VI.1.1. Background

As discussed in the previous chapters, controlling that balance between proliferation and differentiation during asymmetric division is essential during neurogenesis. However, the identity and the dynamics of fate determinant molecules promoting either a progenitor or a differentiated state are poorly characterized in vertebrates (see section I.4 for details).

Recent work from the lab has shown that Mib1 is a fate determinant differentially localized during symmetric and asymmetric divisions of neural progenitors in the chick spinal cord (Tozer et al., 2017). By combining gain- and loss-of-function experiments with live-imaging of dividing neural progenitors in the chick NT, we have shown that Mib1 is associated with the young centrosome through its direct interaction with the centriolar satellite protein AZ11, and is preferentially inherited by the daughter cell committed to differentiation during asymmetric divisions. Moreover, during symmetric proliferative divisions, a pool of Mib1 associated with the Golgi apparatus compensates for centrosomal asymmetry (Tozer et al., 2017).

Remarkably, it was also shown that the Notch ligand Dll1 was asymmetrically distributed during mitosis in the mouse embryonic cortex, but it was not observed at the centrosome and the mechanisms involved have not been investigated (Kawaguchi et al., 2013). Thus, an interesting possibility is that both Mib1 and Dll1 are asymmetrically inherited in the prospective neuron during asymmetric divisions of neural progenitors but through independent routes, which would confer an additional level of robustness for Notch asymmetric activation between sibling cells.

Furthermore, in the context of terminal differentiation of the prospective neuron, I have shown that Mib1 inhibits the cis-inhibitory activity of the Notch ligand Dll1, which allows the prospective neuron to transiently maintain Notch activity until it eventually delaminates (Baek et al., 2018).

VI.1.2. Scientific objectives

These new findings raise important questions that we want to address in the future. What are the subcellular dynamics of Mib1 and Dll1 during asymmetric division? What are the precise molecular mechanisms regulating this dynamic distribution? What are the impacts of Mib1 and Dll1 interactions on Notch signaling regulation during neuronal differentiation?

To address these points, it is important to perform high-resolution live-imaging analysis to visualize the localization of endogenous proteins in real-time over long time periods. We extensively used chick NT as a model and this system has proven to be a powerful source of information for Mib1 dynamics (Tozer et al., 2017) and for the role of Notch signaling during neural delamination (Baek et al., 2018). Nevertheless, electroporation of fluorescent reporters *in ovo* yields mosaic and variable expression levels that may not fully mimic the behavior of the endogenous proteins. Moreover the optical quality of NT explants in live-imaging assays is not ideal for long-term monitoring of protein dynamics. To overcome these difficulties, we decided to take advantage of a mouse embryonic stem cell (ESC) derived motor neuron (MN) differentiation culture system. This system is suitable for genetic modifications and provides easy access to the cell for higher resolution and long-term live-imaging.

During my last year of PhD, I have set up this culture system which successfully produced neural progenitors organized in rosette-like structures, and mimicked the embryonic NT architecture. Finally, I started to establish a knock-in Mib1-GFP ESC line using the CRISPR/Cas9 technology. In the future, we plan to monitor the behavior of fluorescently tagged knock-in versions of Mib1 and Dll1 in this ESC-derived organoid culture system.

VI.2. Preliminary results and perspectives

VI.2.1. Experimental system: mESC-derived neural rosettes

VI.2.1.1. Culture conditions

Several approaches exist in the literature for *in vitro* neural differentiation to generate regionally specified neural progenitors and specific neuronal subtypes starting from ESCs. We adapted a protocol initially set up by our collaborator S.Nédelec, an expert in the field who developed a protocol to generate nearly pure populations of motor neuron progenitors (pMNs) from human ESCs (Maury et al., 2015). Similarly, he optimized conditions to produce MNs from mouse ESCs (S.Nédelec, unpublished). We have first successfully generated embryoid bodies strongly enriched in MNs (data not shown). However, these embryoid bodies rarely showed sign of rosette-like organization, which we consider as a prerequisite to study Mib1 and Dll1 dynamics in a proper neuroepithelial system. Moreover, we speculated that the 3D-nature of embryoid bodies could render in-depth imaging analysis in real-time difficult. Thus, we decided to modify this initial protocol by using an adherent monolayer culture system previously shown to generate neural rosettes with key features of neuroepithelial organization (Abranches et al., 2009). Details of the adapted differentiation protocol can be found in chapter IV (see also Figure 19). Of note, we chose to use a protocol that produces a nearly pure population of MN in order to study Mib1 and Dll1 dynamics in a highly controlled and homogenous progenitor population.

To validate the *in vitro* differentiation protocol, two main characteristics were investigated: the temporal progression of neurogenesis (VI.2.1.2) and the epithelial organization of rosette-like structures (VI.2.1.3.).

VI.2.1.2. Temporal progression of neurogenesis

We first tested whether our ESC differentiation protocol generates a population enriched for pMNs and differentiated MNs. By day 6 after neural induction, the vast majority of cells expressed the pMN marker Olig2 or the MN marker Isl1/2 (Figure 26A). We also found that most, if not all, of the pan-neuronal marker Tuj1-expressing cells also express the MN marker Isl1/2, suggesting that the vast majority of cells engaged into the MN lineage (Figure 26A).

Next we sought to characterize the timing and rhythm of neural differentiation in our ESC differentiation system. To this end, after carrying out immunostainings for progenitor (Sox2) and neuronal (HuCD) markers, we calculated the differentiation rate (n neurons/n total) at different time points. The differentiation rate clearly increased over the course of the differentiation protocol, with more than 30% of cultured cells being HuCD⁺ post-mitotic differentiated neurons by day 7 (Figure 26B-C). On the other hand, it is known that the decision to produce differentiated daughter cells can be traced back to the last cell division. Of particular interest, the Tis21 gene is known to be expressed during the last cell cycle leading to a neurogenic division (P-N and N-N divisions) (Iacopetti et al., 1999; Saade et al., 2013) and the expression of GFP reporter downstream of the Tis21 promoter has successfully identified neurogenic progenitors in the mouse embryonic cortex (Haubensak et al., 2004). For the purpose of our project, which is to study the dynamics of Mib1 and Dll1 during asymmetric divisions, it is necessary to check the progression of neurogenic divisions and to find a time window where asymmetric P-N divisions are found. To this end, we have taken advantage of the Tis21-GFP mouse ESC line obtained from W.B. Huttner's group and combined it with a Sox2 immunostaining. We observed that the proportion of Tis21-GFP⁺ cells slightly increased between day 5 and day 6, but remained stable thereafter (Figure 26D). The proportion of Tis21-GFP⁺ cells was counted among all cells (progenitors+neurons). However, as Tis21 gene expression is known to be switched off as cells differentiate into neurons, we probably have underestimated the actual proportion of Tis21⁺ cells in progenitors.

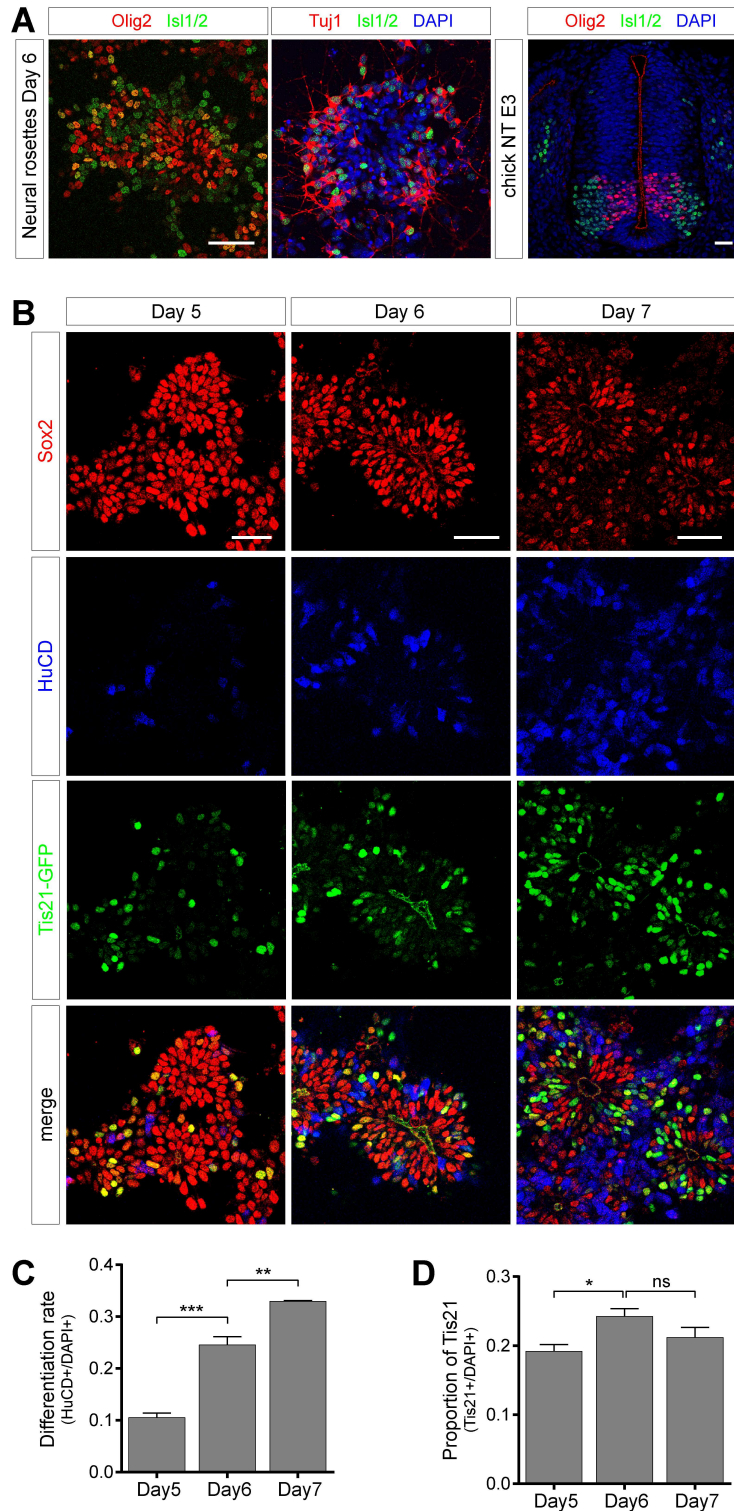


Figure 26. Temporal progression of neurogenesis in ESC-derived neural rosettes culture system.

(A) Left-Expression of Olig2 (pMN marker), Isl1/2 (MN marker) and Tuj1 (pan-neuronal marker) at day 6 after neural induction in culture. Right-Expression of Olig2 (red) and Isl1/2 (green) in chick NT at E3. (B) Expression of HuCD (neuronal marker, blue), Sox2 (progenitor marker, red) and Tis21-GFP (green) at the indicated days after neural induction. (C-D) Differentiation rate and proportion of Tis21-GFP⁺ cells over the course of the differentiation protocol. Scale bar represents 50 μ m. one-way ANOVA, ns, $p > 0.05$; * $p < 0.05$; ** $p < 0.01$; *** $p < 0.001$.

VI.2.1.3. Rosette-like structures mimic the embryonic NT

Remarkably, we found that cells organize in clusters to form rosette-like structures that mimic the embryonic NT organization. Indeed, apical markers such as N-cadherin and ZO1 were localized at the center of rosettes (Figure 27A). This suggests that neural progenitors organize their junctional structures to form an apical central lumen, similarly to the embryonic NT. Moreover, centrosomes and primary cilia labeled with FOP and Arl13b, respectively, are also located at the center of rosettes (Figure 27A). The localization and shape of the Golgi apparatus were also very similar between ESC-derived neural rosettes and the embryonic NT (Figure 27A). These data reveal that rosettes-like structures display an apical-basal polarity. Consistent with this, neurons were found almost exclusively at the periphery of the rosettes, resembling also the embryonic NT (Figure 27A). Finally, mitotic pH3⁺ cells were detected at the center of rosettes, suggesting that the nuclei of neural progenitors within these structures recapitulate the characteristic IKNM shown by the neural progenitors in the embryonic NT, with mitosis occurring at the apical side (Figure 27A). To test this hypothesis, we carried out time-lapse imaging of Tis21-GFP cells-derived neural rosettes. Those cells were incubated with the Sir-Tubulin probe that enables to visualize in real-time microtubules in culture. We found that nuclei of neural progenitors move along the apical-basal axis and divide at the apical surface, revealing that neural progenitors within rosette-like structures seem to undergo IKNM, like in the embryonic NT (Figure 27B). To further confirm the existence of IKNM, it will be worth to verify by EdU incorporation whether progenitors within rosettes undergo S-phase at the periphery.

In conclusion, all these observations reveal that our monolayer and adherent *in vitro* ESC differentiation culture system generates neural rosette-like structures that remarkably resemble the embryonic NT architecture with a clear apical-basal polarity and IKNM.

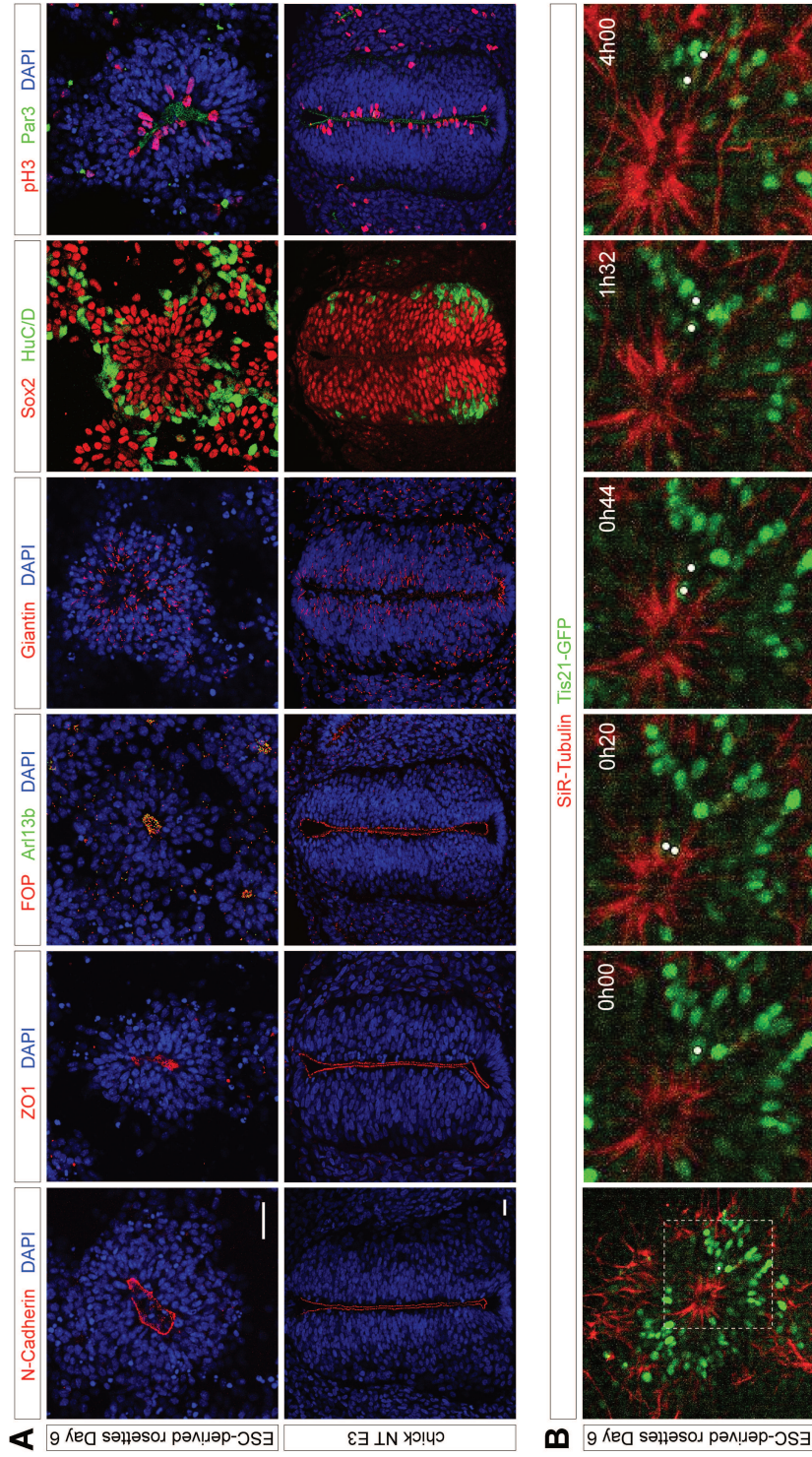


Figure 27. ESC-derived neural rosettes display apical-basal polarity and undergo IKNM. (A) Comparison between mESC-derived rosettes (top) and chick NT (bottom) showing that neuroepithelial features and apical-basal polarity are conserved in culture. Scale bar represents 50 μ m. (B) Microtubule (SiR-Tubulin, red) and Tis21-GFP (green) live monitoring at day 6 after neural induction, showing mitosis near the apical surface followed by nuclear basal translocation of the two sister cells.

VI.2.2. Mib1 dynamics over the course of differentiation

To study the dynamics of Mib1, we decided to engineer an E14Tg2a mESC line that expresses a GFP downstream of the Mib1 coding sequence using the CRISPR/Cas9 technology (see chapter IV for methods and Figure 20). Correct targeting and GFP insertion were verified by genomic PCR across the integration site. Out of 115 clones, 89 were containing the GFP insertion. Among them, 3 were positive for integration at the correct locus. We reasoned that an illegitimate integration elsewhere the targeted locus is likely to have integrated the entire donor vector including the vector backbone with the ampicillin resistance gene and/or the Cas9 containing vector. Thus, we tested those 3 clones for the absence of the ampicillin resistance gene and Cas9 insertions by genomic PCR. Finally, only one clone fulfilled all the criteria described above. In the near future, it will be important to confirm in this unique clone the mono or bi-allelic insertion of GFP at the Mib1 locus by Southern-blot analysis. In addition, we intend to sequence overlapping PCR amplification products across the integration site to check for absence of mutations.

In parallel, we tested the endogenous distribution of Mib1 protein by immunostaining, both in the ESC state and in neural rosettes. At ESC state, Mib1 protein was found to be enriched in the centrosome (Figure 28A). After neural induction, Mib1 localization was strikingly similar to what we have observed in the chick NT: Mib1 was detected both in the centrosome and the Golgi apparatus at day 6 of the differentiation protocol (Figure 28B). The analyses performed in the chick NT have revealed that Mib1 shifts progressively from the Golgi apparatus to the centrosome over the course of neurogenesis (Figure 28C). Thus, we will check whether this evolution is also conserved in ESC-derived neural rosettes, by performing immunostainings at different days after neural induction. Next, using this Mib1-GFP knock-in ESC line, we will first verify that Mib1-GFP recapitulates the expression pattern observed with the Mib1 antibody staining. Then, we wish to investigate in more details in fixed and live conditions the molecular mechanisms underlying Mib1 localization at the Golgi apparatus and its migration to the centrosome.

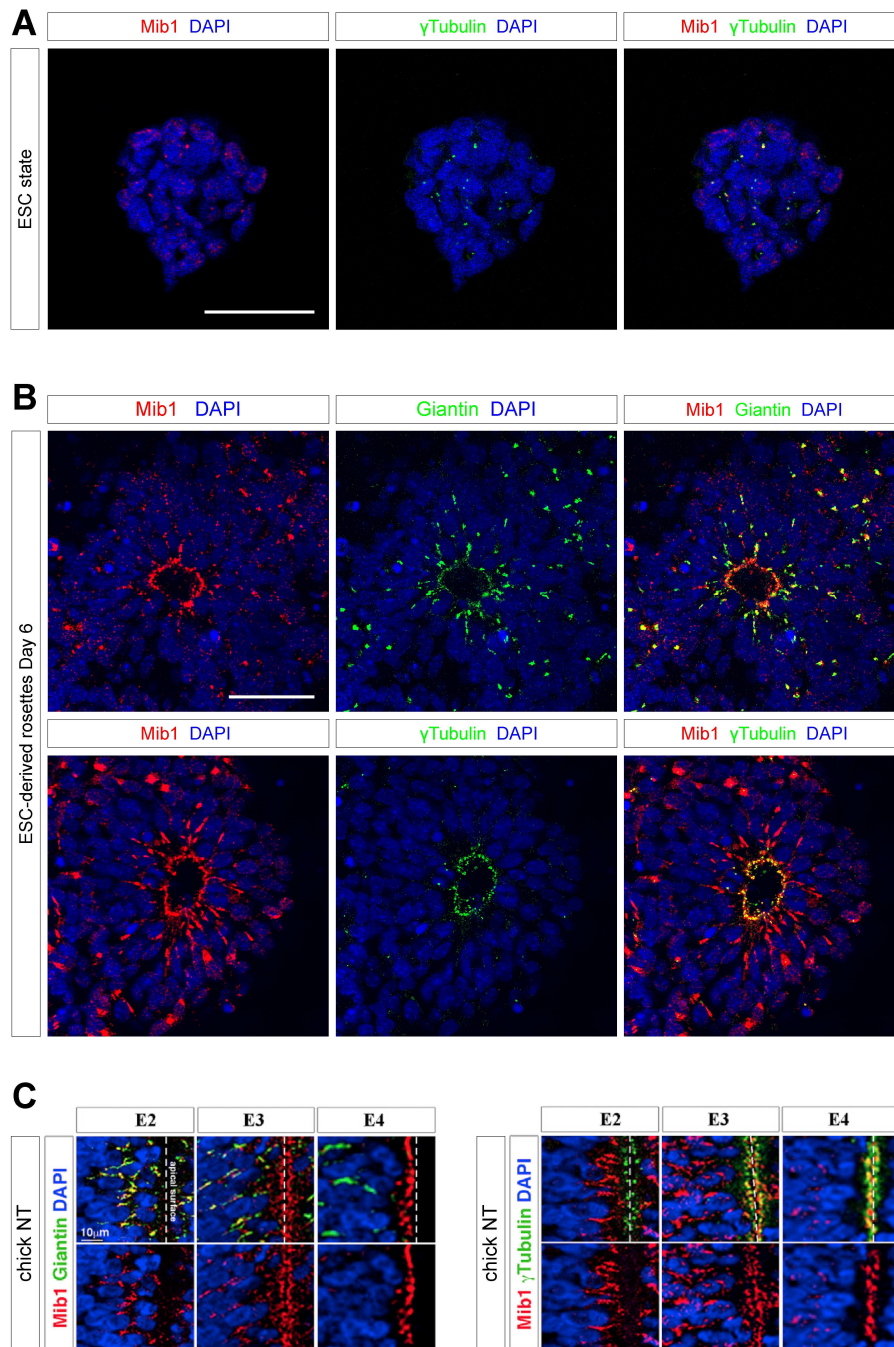


Figure 28. Mib1 expression in ESCs and ESC-derived neural rosettes.

(A) ESCs stained with Mib1 antibody (red) and γ -Tubulin (centrosome marker, green). (B) ESC-derived neural rosettes at day 6 after neural induction, stained with Mib1 antibody (red) and either Giantin (Golgi apparatus marker, green) or γ -Tubulin (centrosome marker, green). Mib1 is colocalized with both the Golgi apparatus and the centrosome at day 6. Scale bar represents 50 μ m. (C) Embryonic chick NT stained with Mib1 (red) and either Giantin or γ -Tubulin (green) at E2-E3-E4. Taken from Tozer et al., 2017.

VI.2.3. Mib1 and Dll1 cooperation for Notch signaling regulation

First, to gain insight into the asymmetric localization of Dll1 during mitosis of neural progenitors (Kawaguchi et al., 2013), we will establish, similarly to the Mib1-GFP line, a knock-in Dll1-RFP ESC line using the CRISPR/Cas9 technology. This ESC line will allow us to document in real-time the endogenous localization of Dll1 over the course of differentiation, whether it is indeed asymmetrically localized and inherited during asymmetric divisions and finally the mechanisms underlying those dynamics.

Second, our study in the chick NT suggests that Mib1 blocks the cis-inhibitory activity of Dll1 during delamination of prospective neurons (Baek et al., 2018). As extensively discussed in chapter V.2.2, we propose that differentiation will eventually take place when the Dll1/Mib1 ratio increases and reaches a threshold sufficient for cis-inhibition to occur. This is likely to result from a change in the expression level and/or distribution of Dll1/Mib1 at the cell surface. Nevertheless, given the poor quality of immunostainings of Dll1 and Mib1, it is difficult to address those questions in the chick NT. Thus, we plan to take advantage of the ESC-derived neural differentiation culture system. To this end, we will engineer a Mib1-GFP/Dll1-RFP double knock-in ESC line to monitor Mib1 and Dll1 endogenous distribution in both fixed and live conditions. We are confident that careful analysis of Mib1 and Dll1 endogenous localization and dynamics at high resolution over the course of differentiation will enhance our understanding of the mechanisms of Dll1 cis-inhibition and its blockade by Mib1.

Overall, using this *in vitro* system based on ESC-derived neural organoids with live-imaging techniques and genetic engineering, we aim to provide a better understanding of Notch regulators dynamics and their role in vertebrate neural development, cell biology and stem cell maintenance.

General conclusion

The construction of an organ that receives, integrates and transmits information to coordinate all our conscious and unconscious biological processes is probably the most challenging of all developmental questions. Neural differentiation relies on a symphony of interactions between multiple players in the embryo: diffusible molecules and signaling pathways influence transcription of target genes, which in turn regulate the ability of the cell to exit the cell cycle and eventually to differentiate. An important issue is how cellular differentiation is coordinated with the morphogenesis of the tissue. Indeed, as development proceeds, the number of differentiating neurons increases, raising the question of how the developing NT maintains a cohesive luminal surface and the integrity of the neuroepithelium.

In the present work, I have shown that Notch signaling activity is transiently maintained in prospective neurons. That maintenance is necessary to properly coordinate the disassembly of apical junctions with apical constriction during neural delamination, thereby enabling the future neuron to harmlessly extract its apical endfoot from the ventricular surface. I have further demonstrated that Mib1 blocks Dll1-mediated cis-inhibition of Notch signaling, and as a consequence, defers differentiation and preserves neuroepithelial integrity.

Moreover, neural progenitor cells deploy numerous strategies to implement asymmetry during fate acquisition of daughter cells in neurogenic divisions. The neural organoid system with real-time monitoring of endogenous Notch regulators will help uncover the molecular bases of their asymmetric distribution and its long-term effects on the neurogenic decision process.

Many questions arise from the work presented here and the potential exciting findings deriving from the on-going project are yet to be lit up under new rays. Because, as John Steinbeck stated: *‘Many a trip continues long after movement in time and space have ceased.’*, the project will undoubtedly continue its journey and reserve big surprises and wonderful discoveries. In the end, I hope my modest contribution would be of general interest for a broad scientific community ranging from cell biology to nervous system development and Notch signaling as well as disease modeling and regenerative medicine.

Annex

Differential routing of Mindbomb1 via centriolar satellites regulates asymmetric divisions of neural progenitors

Samuel Tozer, Chooyoung Baek, Evelyne Fischer, Rosette Goïame,
and Xavier Morin

Neuron, 93, 1-10, February 8, 2017
<http://dx.doi.org/10.1016/j.neuron.2016.12.042>

Contribution:

I participated to the experiments performed in the purpose of responding to the reviewers' comments during the revision phase. Some of those results are presented in supplementary data.

Neuron

Differential Routing of Mindbomb1 via Centriolar Satellites Regulates Asymmetric Divisions of Neural Progenitors

Highlights

- Centriolar satellites constitute a docking point for Mib1 at the daughter centriole
- Mib1 is inherited by the prospective neuron following asymmetric divisions
- Mib1 asymmetry regulates fate choices through unequal Notch activation in daughter cells
- In proliferative divisions, a Golgi apparatus pool of Mib1 compensates for the asymmetry

Authors

Samuel Tozer, Chooyoung Baek, Evelyne Fischer, Rosette Goïame, Xavier Morin

Correspondence

samuel.tozer@ens.fr (S.T.),
xavier.morin@ens.fr (X.M.)

In Brief

Tozer et al. report that the Notch regulator Mib1, enriched via centriolar satellites at the daughter centriole, is inherited by the prospective neuron and regulates asymmetric fate choices. In proliferative divisions, a Golgi apparatus pool of Mib1 compensates for this asymmetry.

Differential Routing of Mindbomb1 via Centriolar Satellites Regulates Asymmetric Divisions of Neural Progenitors

Samuel Tozer,^{1,*} Chooyoung Baek,^{1,2} Evelyne Fischer,¹ Rosette Goïame,¹ and Xavier Morin^{1,3,*}

¹Cell Division and Neurogenesis, Institut de Biologie de l'École Normale Supérieure (IBENS), CNRS, Inserm, École Normale Supérieure, PSL Research University, 75005 Paris, France

²Sorbonne Universités, UPMC Univ Paris 06, IFD, 4 Place Jussieu, 75252 Paris, France

³Lead Contact

*Correspondence: samuel.tozer@ens.fr (S.T.), xavier.morin@ens.fr (X.M.)

<http://dx.doi.org/10.1016/j.neuron.2016.12.042>

SUMMARY

Unequal centrosome maturation correlates with asymmetric division in multiple cell types. Nevertheless, centrosomal fate determinants have yet to be identified. Here, we show that the Notch pathway regulator Mindbomb1 co-localizes asymmetrically with centriolar satellite proteins PCM1 and AZI1 at the daughter centriole in interphase. Remarkably, while PCM1 and AZI1 remain asymmetric during mitosis, Mindbomb1 is associated with either one or both spindle poles. Asymmetric Mindbomb1 correlates with neurogenic divisions and Mindbomb1 is inherited by the prospective neuron. By contrast, in proliferative divisions, a supplementary pool of Mindbomb1 associated with the Golgi apparatus in interphase is released during mitosis and compensates for Mindbomb1 centrosomal asymmetry. Finally, we show that preventing Mindbomb1 centrosomal association induces reciprocal Notch activation between sister cells and promotes symmetric divisions. Thus, we uncover a link between differential centrosome maturation and Notch signaling and reveal an unexpected compensatory mechanism involving the Golgi apparatus in restoring symmetry in proliferative divisions.

INTRODUCTION

Neural stem cells divide asymmetrically to produce differentiating cells while maintaining a pool of progenitors. While studies in invertebrates have emphasized the role of intrinsic fate determinants in this process, the mechanisms at play in the vertebrate nervous system are still unclear. In this context, differential maturation of mother and daughter centrosomes, resulting from the semi-conservative nature of their duplication, has been associated with differential fate choices in several models of asymmetric cell division (Januschke et al., 2011, 2013; Rebollo et al., 2007; Reina and Gonzalez, 2014; Roubinet and Cabernard,

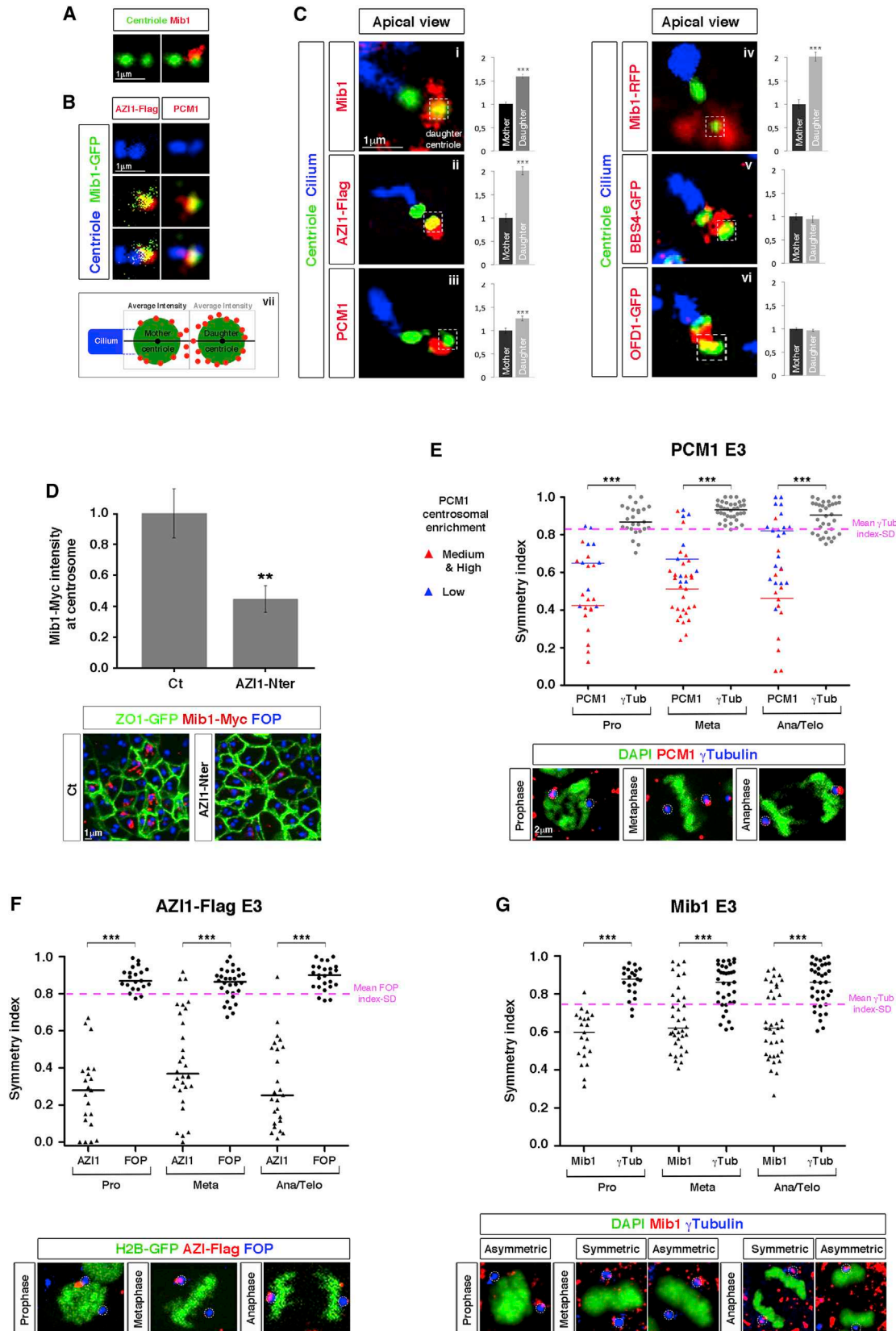
2014; Rusan and Peifer, 2007; Salzmänn et al., 2014; Wang et al., 2009; Yamashita et al., 2007). In particular, in asymmetrically dividing mouse radial glial cells (RGCs) of the developing cortex, the daughter centrosome is preferentially inherited by the differentiating cell (Wang et al., 2009). This begs the two following questions: what are the instructive signals for fate determination associated with centrosome asymmetry, and how do cells performing symmetric divisions cope with this intrinsic asymmetry?

The Notch signaling pathway controls binary fate decisions and is essential for progenitor maintenance in the central nervous system (Pierfelice et al., 2011). Its regulators are good candidates to play a role as fate determinants, i.e., a molecule present in the mother cell, asymmetrically localized in mitosis and promoting opposite fates in the daughter cells (Knoblich et al., 1995). Mindbomb1 (Mib1) is a mono-ubiquitin ligase that regulates the trafficking of Notch ligands and promotes their activity (Weinmaster and Fischer, 2011). In the mouse cortex, Mib1 expressed in differentiating cells acts non-cell autonomously to activate Notch signaling in the neighboring RGCs and maintain their progenitor state (Yoon et al., 2008). Monitoring of Mib1-GFP in zebrafish neural progenitors revealed an asymmetric localization in mitosis (Dong et al., 2012; Kressmann et al., 2015), but the underlying cellular and molecular bases are unknown. Here, we show that Mib1 fulfills the criteria for a centrosome-associated fate determinant in neural progenitors and provide mechanistic insight into its dynamics during mitosis. Mib1 is enriched at the daughter centriole through its interaction with centriolar satellites and is inherited by the prospective neuron in asymmetric divisions. Strikingly, in proliferative divisions a pool of Mib1 associated with the Golgi apparatus is released when the cell enters mitosis and compensates for Mib1 asymmetry. Finally, we provide evidence that Mib1 centrosomal localization is essential for the asymmetric activation of Notch signaling in neurogenic divisions and regulates the balance between proliferation and differentiation.

RESULTS

Mib1 Localizes with the Centriolar Satellite Markers AZI1 and PCM1 at the Daughter Centriole in Neural Progenitors

We investigated the distribution of Mib1 in chick neural progenitors at the onset of neurogenesis (embryonic day 3 [E3]). Using co-labeling with a centriolar marker, we observed Mib1 in the



(legend on next page)

close vicinity of the centrosome in apical views of the neuroepithelium. Surprisingly, Mib1 appeared preferentially associated with only one centriole (Figure 1A). In cultured human cells, Mib1 has been associated with centriolar satellites through its interaction with AZI1/CEP131 and the canonical satellite protein PCM1 (Villumsen et al., 2013). Centriolar satellites are small granules that gravitate around centrosomes and form a hub regulating the transit of numerous centrosomal and ciliary proteins (Bärenz et al., 2011; Tollenaere et al., 2015). While these include proteins involved in ciliopathies and primary microcephaly (Kodani et al., 2015; Lopes et al., 2011; Nachury et al., 2007), their role during neurogenesis is poorly understood. We investigated Mib1 distribution in relation with these markers. Mib1-GFP co-localized to a large extent with PCM1 and AZI1-Flag during interphase and all three proteins were distributed asymmetrically at one centriole (Figure 1B). Using the ciliary marker Arl13b (Caspary et al., 2007) (in blue in all panels of Figure 1C) to distinguish between the mother (at the base of the cilium) and daughter centrioles revealed that Mib1 and AZI1 were strongly enriched at the daughter centriole (Figures 1Ci, 1Cii, and 1Civ; Figure S1A). PCM1 distribution, although less asymmetric, also displayed a specific enrichment at the daughter centriole (Figure 1Ciii; Figure S1A). By contrast, two other satellite markers BBS4-GFP and OFD1-GFP (Lopes et al., 2011; Nachury et al., 2007) were distributed symmetrically and peaked between the two centrioles (Figures 1Cv and 1Cvi; Figure S1A). PCM1 is the core element of centriolar satellites and interacts with BBS4, OFD1, AZI1, and Mib1 (Lopes et al., 2011; Villumsen et al., 2013). Thus, our data reveal an unexpected polarized organization of PCM1-positive satellites relative to centrioles, comprised of a central compartment where BBS4 and OFD1 are present and a daughter centriole-associated compartment enriched for AZI1 and Mib1. Finally, analysis of the distribution of Mib1 over the course of centrosome duplication strongly suggests that Mib1 remains asymmetric following duplication (Figure S1B).

We next tested whether Mib1 localization at the centrosome depends on its interaction with satellite proteins. In human cells, the N-terminal fragment of AZI1 (AZI1-Nter) was shown to interact directly with Mib1. To compete with this interaction,

we overexpressed AZI1-Nter in the neural tube. Indeed, this displaced Mib1-Myc (red) from the centrosome (blue) (Figure 1D). Importantly, neither the localization of PCM1 and full-length AZI1-Flag near the centrosome nor the presence of the cilium were affected by AZI1-Nter (Figures S1C and S1D).

We next investigated the distribution of Mib1, PCM1, and AZI1 during cell division. PCM1 and AZI1 remained strongly asymmetric throughout mitosis (Figures 1E and 1F), although PCM1 centrosomal levels were decreased compared to interphase as previously reported (Dammermann and Merdes, 2002). By contrast, Mib1 was essentially asymmetric in prophase but displayed both asymmetric and symmetric centrosomal localizations at anaphase and telophase, suggesting a redistribution mechanism taking place during mitosis (Figure 1G). Similar data were obtained using Mib1-Myc (Figure S1E) and Mib1-GFP fusion proteins (see live data below). Two scenarios could explain Mib1 localization on both centrosomes: Mib1 is redistributed between the two centrosomes during mitosis or an additional pool of Mib1 is recruited to the mother centrosome during mitosis.

A Pool of Mib1 Associated with the Golgi Apparatus Compensates for Centrosomal Asymmetry in Symmetric Divisions

To explore these possibilities, we analyzed the dynamics of Mib1-GFP distribution in relation with the centrosomes (labeled with PACT-mKO1; Konno et al., 2008) during mitosis in live experiments at E3. We categorized dividing cells a posteriori in two populations depending on whether Mib1-GFP was inherited symmetrically or asymmetrically by the daughter cells at the end of mitosis. In both populations, Mib1-GFP was enriched at only one of the two poles at the entry in mitosis (Figure 2A, white arrowheads). However, when Mib1-GFP final distribution was symmetric, a scattered “cytoplasmic” (non-centrosomal) pool of Mib1-GFP could be detected early in mitosis (Figure 2A, top, blue arrowheads; Figure S2B, top) and progressively aggregated around the spindle pole initially devoid of Mib1-GFP (Figure 2A, top; Figure S2A, black lines). Transverse reconstruction indicated that this scattered pool emanated from the basal part of the cell (Figure 2A, top-transverse, blue arrowheads). By contrast, in cells dividing asymmetrically, we did not detect any scattered pool of

Figure 1. Distribution of Centriolar Satellites and Mib1 in Neuroepithelial Progenitors in Interphase and Mitosis

- (A) Apical view of the neural tube at embryonic day 3 (E3) showing the localization of Mib1 (red) in relation with the two centrioles (green).
 (B) Apical views showing the localization of Mib1-GFP (green) in relation with either AZI1-Flag or PCM1 (red) and the centrioles (blue).
 (C) Apical views at E3 showing the localization (in red) of Mib1 (i), AZI1-Flag (ii), PCM1 (iii), Mib1-RFP (iv), BBS4-GFP (v), and OFD1-GFP (vi) in relation with the cilium (blue) and the centrioles (green). The daughter centriole is identified as the one not carrying the cilium and is framed with a dotted line. The juxtaposed diagrams indicate the average intensity of each marker in the vicinity of the mother (black) or the daughter centriole (gray). Data represent means \pm SEM, *** p < 0.001 (Student's t test); n = 49, 28, 31, 24, 20, and 28 cells analyzed for Mib1, AZI1-Flag, PCM1, Mib1-RFP, BBS4-GFP, and OFD1-GFP, respectively. The measurement method is schematized in vii and detailed in the appropriate section. In (A)–(C), centrioles are labeled with Centrin2-GFP (A; i and iii), pan-centrin antibody (B, right; iv), FOP antibody (B, left; ii, v, and vi). The cilium is labeled with Arl13b-GFP (ii and iv–vi) or Arl13b antibody (i and iii).
 (D) Top: average intensities of Mib1-Myc staining at the centrosome in control versus AZI1-Nter-transfected embryos. Data represent means \pm SEM, ** p < 0.01 (Student's t test); n = 70 and 57 cells analyzed for control and AZI1-Nter conditions, respectively. Bottom: apical views showing the localization of Mib1-Myc (red) in relation with the centrioles (blue) and tight junctions (labeled with ZO1-GFP in green) in the two situations.
 (E–G) The diagrams indicate the symmetry index for PCM1 (E), AZI1-Flag (F), and Mib1 (G) at the centrosome in comparison with the centrosome markers γ Tubulin and FOP in mitotic cells (each mark corresponds to a single cell; horizontal bars correspond to medians; the pink dotted line indicates the value of the mean centrosomal marker index minus its SD (for all mitotic phases), providing a threshold above which distribution is essentially symmetric). In the case of PCM1, cells were divided into two populations, displaying low versus medium and high PCM1 centrosomal enrichment (see Method Details). The lower panels show representative examples of the localization of PCM1, AZI1-Flag, and Mib1 (red) in relation with the centrosomes (blue) and chromosomes (green), labeled with the indicated markers and at the indicated mitotic stages.

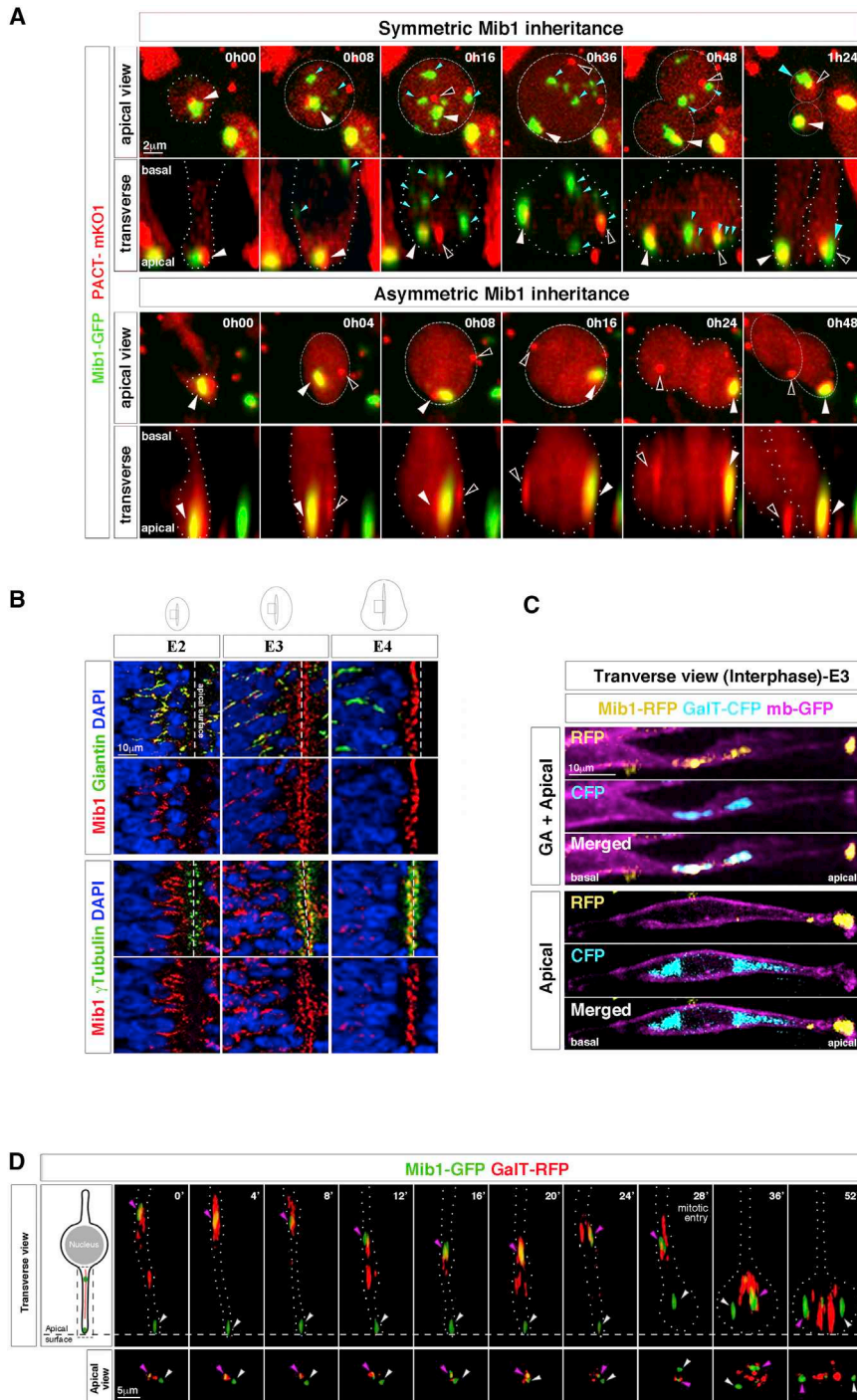


Figure 2. A GA-Associated Pool of Mib1 Can Compensate for Mib1 Centrosomal Asymmetry during Mitosis

(A) Time series (en-face imaging) of dividing neuroepithelial cells expressing Mib1-GFP (green) and the centrosome reporter PACT-mKO1 (PACT domain of pericentrin fused to Kusabira-Orange, shown here in red). The dotted line schematizes the outline of the cell. Top: in cells exiting mitosis with symmetric Mib1-GFP distribution, Mib1-GFP is initially asymmetric in prophase and observed on only one centrosome (white arrowhead). A pool of non-centrosomal scattered Mib1-GFP (blue arrowheads) appears in prophase, coming from the basal end of the cell (see transverse view), and progressively aggregates near the second centrosome (black arrowhead), resulting in equal centrosomal accumulation of Mib1-GFP at telophase or shortly after. Bottom: conversely, in cells exiting mitosis with asymmetric Mib1-GFP, only the centrosomal pool of Mib1-GFP is observed. A total of 39 cells (4 embryos from 4 independent experiments) with either symmetric (18) or asymmetric (21) Mib1 inheritance were monitored. Symmetry indices for the non-centrosomal “cytoplasmic” and centrosomal pools of Mib1 are plotted in Figure S2C.

(B) Transverse sections of the chick neural tube (thoracic level) at E2 (HH st12), E3 (HH st18), and E4 (HH st22) stained with Mib1 antibody (red) and either Giantin (Golgi apparatus [GA] marker) or γ -Tubulin (centrosome marker) (green). Mib1 co-localizes with Giantin at E2 and E3 and with γ -Tubulin at E3 and E4.

(C) Transverse sections of the neural tube at E3 showing individual cells transfected with Mib1-RFP (yellow), GaT-CFP (GA reporter, cyan), and membrane-GFP (magenta).

(D) 3D reconstruction from en-face imaging of a cell transfected with Mib1-GFP and the GA marker GaT-RFP 8 hr post-transfection at E2. Left: schematic showing the sub-cellular localization of the markers. The framed area indicates the region of interest. Right: 3D reconstructed time series of a cell co-transfected with Mib1-GFP (green) and the GA reporter GaT-RFP (red). Time points 0'–24': before mitosis, the cell displays an apical (white arrowhead) and a GA-associated (pink arrowhead) pool of Mib1-GFP. Time points 28'–52': the cell enters mitosis and the GA-associated Mib1-GFP detaches from the GA as the latter fragments. The dotted line schematizes the outline of the cell. 11 cells (3 embryos from 3 independent experiments) with a similar behavior were monitored. Three other examples are displayed in Figure S2.

Mib1 (Figure 2A, bottom; Figure S2A, gray lines; Figure S2B, bottom). Hence, asymmetric Mib1 localization at one spindle pole is a common feature of neuroepithelial cells entering mitosis at E3. However, in cells displaying symmetric Mib1 distribution at the end of mitosis, an extra pool of Mib1 is released and aggregates around the Mib1-free spindle pole to compensate for the initial asymmetry. To identify the origin of this non-centrosomal pool, we investigated Mib1 tissue distribution on transverse sections

of the neural tube at E2 when divisions are mostly proliferative, at E3 when proliferative and neurogenic divisions coexist, and at E4 when mostly neurogenic divisions take place (Saade et al., 2013). This revealed a striking shift from an elongated staining at E2 to an apical staining at E4, while both localizations were observed at the intermediate stage E3 (Figure 2B). The elongated staining was observed in the apical half of the ventricular zone, which is reminiscent of the Golgi apparatus (GA) position in

neuroepithelial cells (Taverna et al., 2016; Zhou et al., 2007). Indeed, staining with the GA marker Giantin revealed a co-localization with Mib1 at E2 and E3 (Figure 2B, top). Conversely, the apical staining overlapped with the centrosomal marker γ -Tubulin at E3 and E4 (Figure 2B, bottom). This indicates that Mib1 localization in progenitors evolves over time from the GA to an asymmetric localization on the daughter/young centriole/centrosome. Remarkably, at E3, when symmetric and asymmetric divisions coexist, Mib1-RFP was either localized to both the GA (note the overlap with the GA reporter GalT-CFP) and the apical pole or restricted to the apical pole in interphase (Figure 2C). An attractive hypothesis is that the Mib1 GA-associated contingent corresponds to the non-centrosomal pool observed in symmetric mitoses (Figure 2A, top panel). To investigate this possibility, we monitored the dynamics of Mib1 and GalT in cells displaying symmetric Mib1 localization in mitosis (Figure 2D; Figure S2C). We observed two pools of Mib1 before mitosis—one located at the apical surface (presumably associated with the centrosome given our previous results) and one associated with the GA (Figure 2D; Figure S2C, white and magenta arrowheads, respectively). As the cell entered mitosis, the GA fragmented and the GA-associated pool of Mib1 was released, and the two pools of Mib1 remained at a distance from each other, consistent with their inheritance by the two daughter cells. Taken together, these results suggest that progenitors displaying both a centrosomal and a GA-associated pool of Mib1 experience a re-equilibration mechanism allowing similar amounts of Mib1 to aggregate at mother and daughter centrosomes, thus leading to equal inheritance of Mib1 by the daughter cells. Conversely, when only the centrosomal pool of Mib1 is present, its distribution remains asymmetric and Mib1 will be inherited by only one of the two daughter cells.

Mib1 is thought to be active at the cell membrane, where it promotes the ability of Notch ligands to trans-activate the Notch pathway in neighboring cells. Nevertheless, our data suggest that most of the Mib1 protein in cycling progenitors is associated with the GA and centriolar satellites. These cellular structures may therefore represent storage compartments that allow the routing of defined amounts of Mib1 to the daughter cells following division.

Asymmetric Mib1 Distribution Correlates with Neurogenic Divisions

Given the role of Mib1 in neurogenesis (Dong et al., 2012; Kang et al., 2013), we analyzed the correlation between its symmetric versus asymmetric centrosomal inheritance and proliferative P-P (Progenitor-Progenitor) versus neurogenic P-N (Progenitor-Neuron) modes of divisions. Asymmetric inheritance of Mib1-GFP has been reported in neurogenic divisions of the zebrafish forebrain and spinal cord, but fate tracking led to opposite conclusions regarding the identity of the daughter inheriting Mib1 (Dong et al., 2012; Kressmann et al., 2015).

We used en-face live imaging to follow Mib1-GFP and centrosome distribution in dividing cells and track the fate of their progeny between E3 and E4 (Figures 3A–3C; $n = 27$ clones from 7 embryos). Importantly, expression of saturating levels of Mib1-Myc from the strong chick β -actin (CAGGS) promoter did not have any impact on the differentiation rate 40 hr after electroporation (Figure S3A). In addition, for live-tracking experiments, we expressed Mib1-GFP under the control of the weaker cyto-

megalovirus immediate-early (CMV) promoter. Following mitosis, daughter cells were categorized as progenitors when they divided again and as neurons when they withdrew their apical foot (identified by the centrosome), since apical detachment is a hallmark of neuronal commitment (Das and Storey, 2014). In 12 out of 27 analyzed divisions, Mib1 was inherited symmetrically. These correspond to P-P divisions, producing daughter cells that both divided again (Figures 3A and 3C; $n = 11/12$ cases). By contrast, in the remaining 15 clones, Mib1 distributed asymmetrically and P-N identities were observed in the progeny ($n = 10/15$ cases), where the daughter cell with the highest amount of Mib1 after mitosis eventually entered differentiation (Figures 3B and 3C; $n = 9/10$ cases). To confirm that the differentiating cell inherits Mib1, we used two other independent criteria to assign daughter cell identity. First, we monitored basal cell attachments following division on transverse sections. Previous work has shown that the prospective neuron transiently loses its basal attachment during cytokinesis and grows a new basal process (Das and Storey, 2014). Indeed, we observed that when Mib1-RFP was asymmetric, it was carried by the daughter cell losing the basal attachment upon mitosis ($n = 10/11$ cases, Figure 3D). Second, we followed the dynamics of the apical area in new-born daughter cells. While cycling progenitors maintain an approximately constant apical surface between two mitoses (Figures S3B and S3B'), prospective neurons progressively shrink their apical surface before they eventually delaminate (Figures S3B and S3B''). Accordingly, differentiation (revealed by β III-tubulin expression) is exclusively observed in cells that have strongly reduced their apical area (Figure S3C). We then analyzed Mib1-GFP distribution in pairs of cells for which apical shrinkage was observed in one of the daughters. In the majority of these pairs ($n = 16/19$), the cell that inherited Mib1 progressively shrank its apical area while its sibling did not (Figures S3D and S3D'').

Altogether, these fate-tracking experiments indicate that P-N divisions are strongly correlated with asymmetric Mib1 distribution and that Mib1 is disproportionally inherited by the prospective neuron.

Delocalizing Mib1 from the Centrosome Leads to Reduced Neurogenesis and Symmetric Notch Activation in Sister Cells

These observations suggested that loading Mib1 on a unique spindle pole is an instructive signal for asymmetric fates. To address this functionally, we sought to interfere with Mib1 distribution without changing the amount of Mib1 protein. We took advantage of the AZI1-Nter construct described above (Figure 1D) to prevent Mib1 centrosomal localization. Overexpression of AZI1-Nter led to a scattered distribution of Mib1-Myc in mitotic cells, suggesting symmetric inheritance by the daughter cells (Figure S4A). In interphase, Mib1 was no longer concentrated at the apical pole but instead enriched at the cell membrane (Figure S4B). Thus, Mib1 association with centriolar satellites may be a way to limit its activity by keeping it away from the plasma membrane, where Notch ligands are expected to be present. We first analyzed the consequence of delocalizing Mib1 on daughter cell fate: 40 hr after electroporation at E2, neuronal differentiation was significantly reduced in embryos transfected with AZI1-Nter (Figure 4A; Figure S4C), and many ectopic

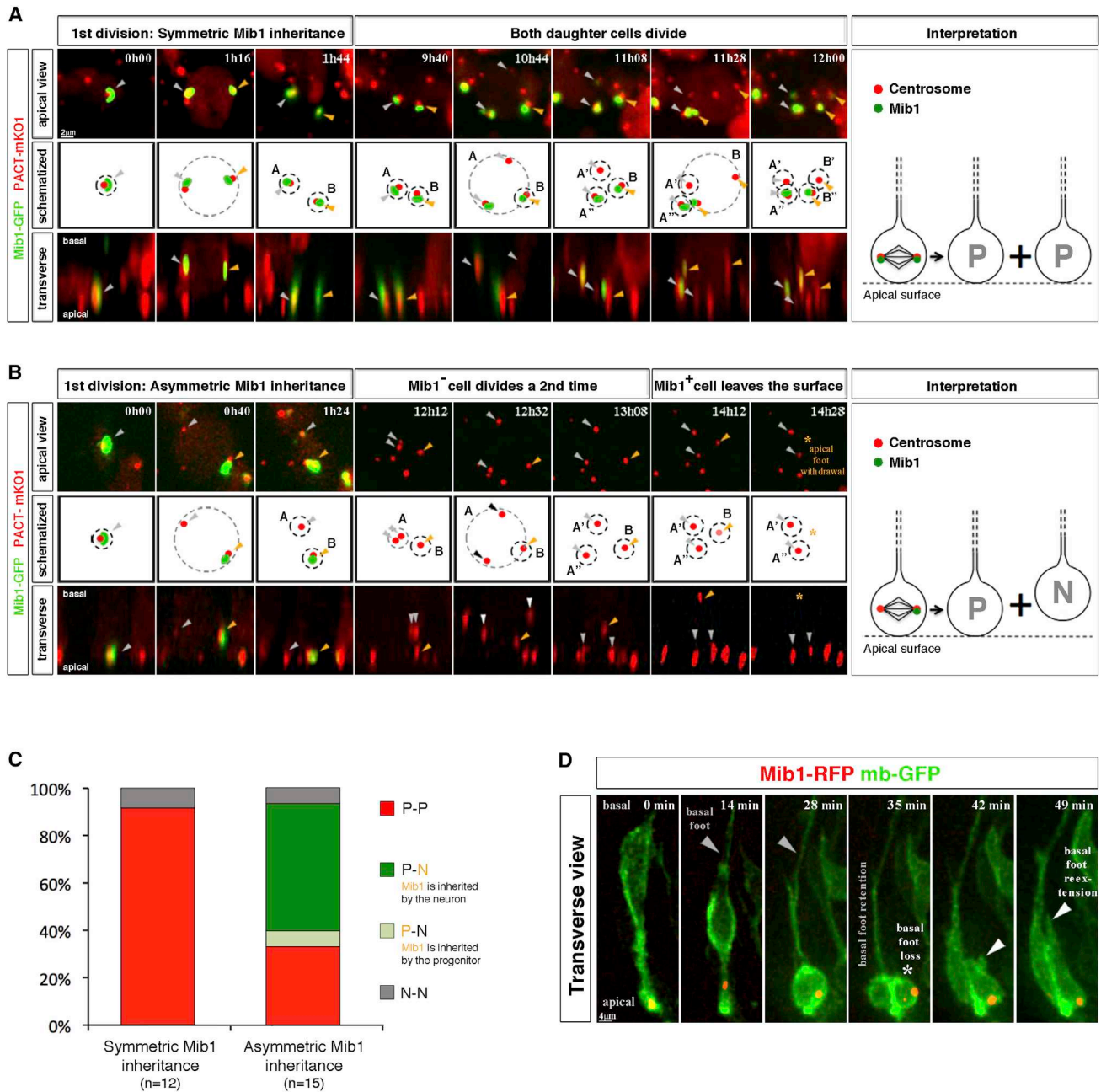


Figure 3. Mib1 Unequal Inheritance Correlates with Asymmetric Fates of the Daughter Cells

(A and B) Time-lapse series (en-face imaging) of dividing neural progenitors showing symmetric (A) or asymmetric (B) Mib1-GFP localization in relation with the centrosome labeled with PACT-mKO1. Top and bottom panels show apical and transverse views, respectively, while the middle panels schematize the position of Mib1 (green) and centrosomes (red) in interphase (black dotted line) and mitosis (gray dotted line). Arrowheads point to centrosomes and the asterisks indicates the loss of centrosomal staining from the observation field. The right panel is a schematized transverse view of each situation using the same color code. In all cells followed, Mib1-GFP was detected in the first cell division. However, Mib1-GFP localization at the centrosome was very variable over time in each cell, due either to Mib1 dynamics or to photobleaching. Thus, Mib1-GFP distribution was only considered for the first division and was used to categorize daughter cells as having or not inherited Mib1-GFP. $n = 27$ clones analyzed from 7 embryos.

(C) Diagram obtained from the time-lapse series presented in (A) and (B) showing the percentage of each cell lineage situation (P-P, P-N, N-N) in the case of symmetric or asymmetric Mib1-GFP inheritance. P-P, P-N, and N-N stand for divisions producing two progenitors, one progenitor and one neuron, or two neurons, respectively.

(D) Time-lapse series (transverse section) of a dividing progenitor showing Mib1-RFP inheritance by the daughter cell losing the basal attachment (representative example of $n = 11$ cells from 10 slices from 6 embryos).

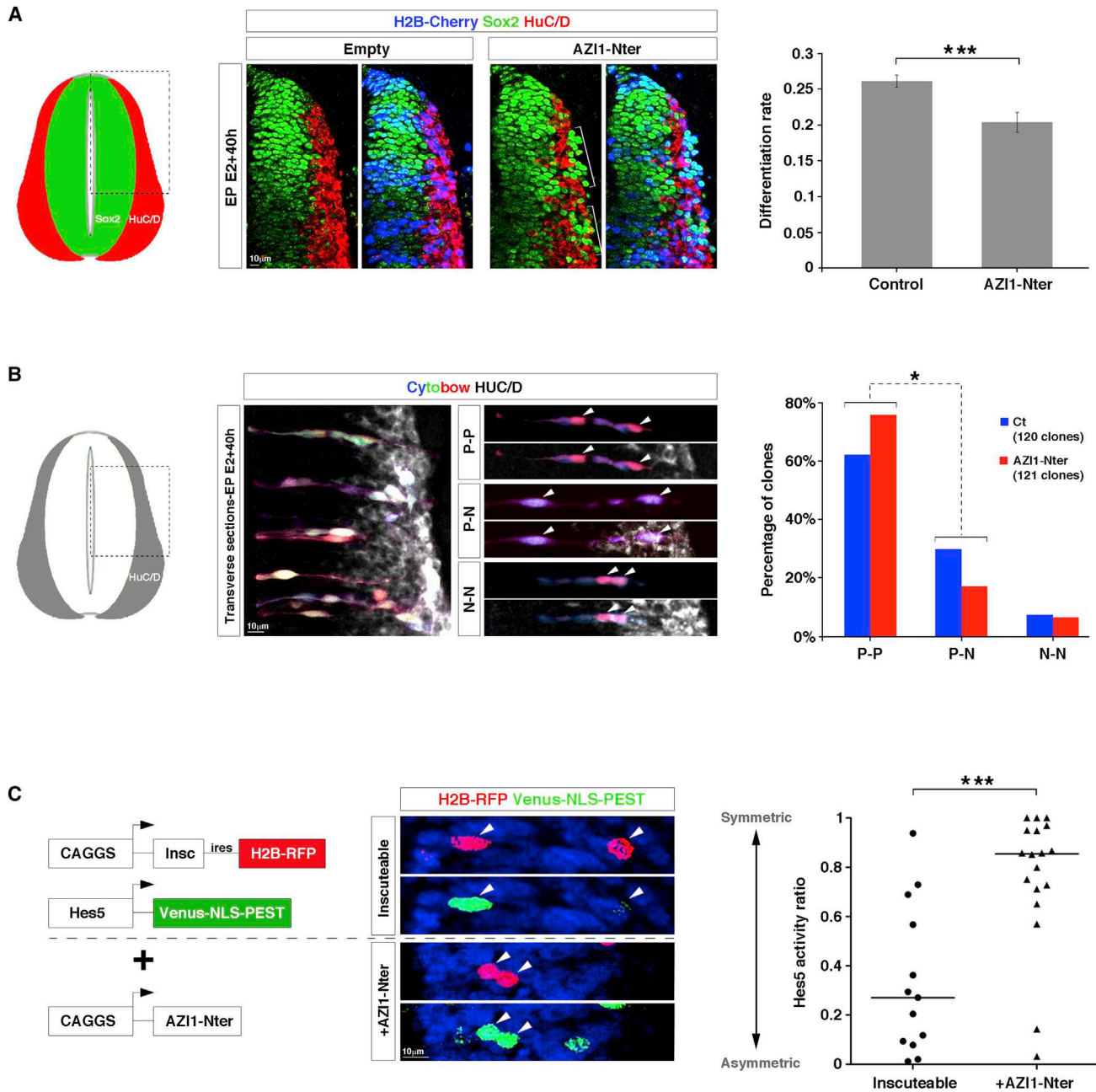


Figure 4. Altering Mib1 Centrosomal Localization Affects the Mode of Division of Neural Progenitors

(A) Left: schematic of the neural tube showing the ventricular and the mantle zone identified by the expression of Sox2 and HuC/D, respectively. The boxed area indicates the region of interest. Middle: transverse sections of the neural tube 40 hr after transfection of empty or AZI1-Nter vectors. Sox2 and HuC/D immunostainings label progenitors and neurons, respectively. The brackets indicate groups of ectopic Sox2 progenitors intermingled with HuC/D neurons. Right: differentiation rate (number of HuC/D+ cells on total) in transfected cells 40 hr after transfection in control versus AZI1-Nter transfected spinal cords. Data represent mean \pm SEM, *** $p < 0.001$ (Student's *t* test), $n = 14$ sections (4 embryos) and 18 sections (8 embryos) analyzed for control and AZI1-Nter conditions, respectively.

(B) Left: schematic of the neural tube. The mantle zone is identified by the expression of HuC/D. The boxed area indicates the region of interest. Middle: transverse sections showing a large view (left) and specific two cell clone examples (right) of the neural tube 40 hr after transfection of Cytobow, followed by immunostaining with HuC/D. Right: diagram indicating the percentage of P-P, P-N, and N-N clones for control and AZI1-Nter transfected embryos. The distribution of P-P and P-N clones between control and AZI1-Nter was compared using a Chi2 test, * $p < 0.05$.

(C) Left: schematics indicating the promoter and the downstream coding sequences of the vectors transfected in the two conditions displayed in the middle panel and quantified in the right panel. Middle: sister cells (indicated by the white arrowheads) 20 hr after low-voltage (17 V) electroporation of Inscuteable (Insc) alone or with AZI1-Nter and co-transfected with the Notch reporter Hes5-VNP. Right: diagram showing the ratio of Hes5 activity between sister cells. Each mark represents a clone, and horizontal bars correspond to medians; *** $p < 0.001$ (Mann-Whitney test).

Sox2+ cells appeared in the mantle zone (Figure 4A, brackets). EdU incorporation confirmed that the ectopic Sox2+ cells were proliferative (Figure S4D). Importantly, simultaneous expression of a dominant-negative form of Mib1 (Δ Mib1; Zhang et al., 2007) counteracted the differentiation defects caused by AZI1-Nter overexpression (Figure S4C). This supports the notion that the phenotype primarily results from a gain of Mib1 activity caused by the disruption of Mib1 localization at centriolar satellites.

To investigate whether this change in the differentiation rate was a consequence of a change in the mode of division, we carried out a clonal analysis using the Brainbow technique. Embryos transfected with the Cytobow vector (Loulie et al., 2014) and limiting amounts of Cre recombinase were harvested 40 hr later. Two cell clones were selected on the basis of color identity and categorized as P-P, P-N, or N-N according to the expression of the neuronal marker HuC/D (Figure 4B, left and middle). Expression of AZI1-Nter led to an increase in the number of P-P clones at the expense of P-N clones (Figure 4B, right). To investigate the molecular mechanism responsible for this effect, we monitored the level of Notch activity in sister cells. Notch signaling has a well-established role in the maintenance of the undifferentiated state in the nervous system and is lost in differentiating neurons. We used the ability of Inscuteable expression to promote P-N divisions, a phenotype associated with asymmetric Notch activation between sister cells (Das and Storey, 2012). We then tested whether delocalizing Mib1 could block this effect. Embryos were transfected at E2 in clonal conditions (see Method Details) with Inscuteable and the Notch activity reporter Hes5-VNP (Venus-NLS-PEST) (Das and Storey, 2012; Vilas-Boas et al., 2011) either with a control vector or with AZI1-Nter (Figure 4C). As expected, Inscuteable overexpression resulted in a clear asymmetric activation of Hes5-VNP within most pairs of sister cells 20 hr after transfection. By contrast, when AZI1-Nter was co-transfected, the activation of the Notch reporter was high and symmetric in most cell pairs. This suggests that symmetric inheritance of Mib1—resulting from its delocalization from the centrosome—is sufficient to induce reciprocal activation of Notch signaling in sister cells and is also consistent with the observed enrichment of Mib1-RFP at the membrane upon AZI1-Nter expression (Figure S4B). Taken together, our results suggest that Mib1 asymmetric centrosomal localization in neurogenic divisions is essential to allow the prospective neuron to inherit the majority of the Mib1 pool and therefore maintain its sibling in an undifferentiated state through Notch trans-activation.

DISCUSSION

In this report, we identify Mib1, a known regulator of Notch signaling, as an intrinsic fate determinant whose asymmetric localization to the spindle poles of dividing progenitors biases fate choices of the daughter cells. This asymmetry is determined during interphase through the association of Mib1 with centriolar satellites. These structures are emerging as a crucial regulatory hub for protein trafficking that controls sorting of components involved in centriolar and pericentriolar organization as well as cillogenesis (Bärenz et al., 2011; Tollenaere et al., 2015). Here, we reveal an unexpected enrichment of the satellite markers PCM1 and AZI1 at the daughter centriole. We propose that they provide

a docking point for the asymmetric localization of Mib1 in both interphase and mitosis. Disruption of this interaction leads to symmetric Mib1 localization in mitosis, reciprocal Notch activation between sister cells, and eventually a reduction in neurogenesis. While the mechanism controlling satellite polarization remains to be elucidated, our work links, for the first time, the constitutive asymmetry in centrosome biogenesis to a signaling pathway involved in fate choices. Furthermore, we identify a remarkable process by which Mib1 centrosomal asymmetry is rebalanced during mitosis in symmetric/proliferative divisions through the release of an additional pool of Mib1 that was initially associated with the GA. As development proceeds and neurogenic divisions become predominant, the localization of Mib1 progressively shifts from the GA to the centrosomal region, providing the first example of a fate determinant that maneuvers between the two organelles in relation to a differentiation process. Since Mib1 is expected to interact with Notch ligands at the cell membrane, these successive storage steps in cycling progenitors appear to essentially have a routing function in order to control the provision of adequate levels of Mib1 to the daughter cells. While our observations were made at an early developmental stage during the rapid transition from the amplification of the progenitor pool to massive neuron production, it will be important to investigate whether such routing dynamics also control stem cell homeostasis in the mature nervous system and in other tissues that depend on Notch signaling for cell-fate decisions.

STAR★METHODS

Detailed methods are provided in the online version of this paper and include the following:

- KEY RESOURCES TABLE
- CONTACT FOR REAGENT AND RESOURCE SHARING
- EXPERIMENTAL MODEL AND SUBJECT DETAILS
- METHODS DETAILS
 - Electroporation and Plasmids
 - Immunohistochemistry
 - Time-Lapse Microscopy and Analysis of Cultured Chick Neural Tube
 - Image Acquisition and Treatment
 - Image Quantifications
 - Statistical Analyses

SUPPLEMENTAL INFORMATION

Supplemental Information includes four figures and can be found with this article online at <http://dx.doi.org/10.1016/j.neuron.2016.12.042>.

AUTHOR CONTRIBUTIONS

Conceptualization, S.T. and X.M.; Methodology, S.T. and X.M.; Software, X.M.; Formal Analysis, S.T., C.B., and E.F.; Investigation, S.T., C.B., E.F., and R.G.; Writing, S.T. and X.M.; Visualization, S.T.; Supervision, X.M.; Funding Acquisition, X.M.

ACKNOWLEDGMENTS

We thank S. Garel, N. Spassky, A. Meunier, J.F. Brunet, C. Goriidis, E. Thévenau, M. Saadaoui, and F. di Pietro for helpful comments on the manuscript

and J. Livet, A. Chédotal, F. Matsuzaki, N. Spassky, O. Rosnet, M. Nachury, A. Fry, D. Henrique, R. Das, and V. Sheffield for the kind gift of reagents. We acknowledge B. Mathieu and the IBENS imaging platform for excellent assistance. Imaging equipment was acquired through the generous help of the Neuropôle de Recherche Francilien. Work in X.M.'s laboratory is supported by INSERM (Avenir2008), FRM (DEQ20150331735), Fondation ARC (RAC12013), ANR (ANR-12-BSV2-0014-01), Cancéropôle Ile-de-France (2013-2-INV-05), and FRC (AOE-9 2014). This work has received support under the program "Investissements d'Avenir," launched by the French Government and implemented by the ANR, with the references: ANR-10-LABX-54 MEMO LIFE and ANR-11-IDEX-0001-02 PSL* Research University. S.T. was supported by INCa (R10074JU), Labex MEMOLIFE, ANR, and FRM. C.B. is supported by an MSER doctoral fellowship.

Received: February 1, 2016

Revised: November 8, 2016

Accepted: December 29, 2016

Published: January 26, 2017

REFERENCES

- Acquaviva, C., Chevrier, V., Chauvin, J.P., Fournier, G., Birnbaum, D., and Rosnet, O. (2009). The centrosomal FOP protein is required for cell cycle progression and survival. *Cell Cycle* 8, 1217–1227.
- Bärenz, F., Mayilo, D., and Gruss, O.J. (2011). Centriolar satellites: busy orbits around the centrosome. *Eur. J. Cell Biol.* 90, 983–989.
- Caspary, T., Larkins, C.E., and Anderson, K.V. (2007). The graded response to Sonic Hedgehog depends on cilia architecture. *Dev. Cell* 12, 767–778.
- Chamling, X., Seo, S., Searby, C.C., Kim, G., Slusarski, D.C., and Sheffield, V.C. (2014). The centriolar satellite protein AZ11 interacts with BBS4 and regulates ciliary trafficking of the BBSome. *PLoS Genet.* 10, e1004083.
- Dammermann, A., and Merdes, A. (2002). Assembly of centrosomal proteins and microtubule organization depends on PCM-1. *J. Cell Biol.* 159, 255–266.
- Das, R.M., and Storey, K.G. (2012). Mitotic spindle orientation can direct cell fate and bias Notch activity in chick neural tube. *EMBO Rep.* 13, 448–454.
- Das, R.M., and Storey, K.G. (2014). Apical abscission alters cell polarity and dismantles the primary cilium during neurogenesis. *Science* 343, 200–204.
- Dong, Z., Yang, N., Yeo, S.Y., Chitnis, A., and Guo, S. (2012). Intralineage directional Notch signaling regulates self-renewal and differentiation of asymmetrically dividing radial glia. *Neuron* 74, 65–78.
- Edelstein, A., Amodaj, N., Hoover, K., Vale, R., and Stuurman, N. (2010). Computer control of microscopes using μ Manager. In *Current Protocols in Molecular Biology*, F.M. Ausubel, R. Brent, R.E. Kingston, D.D. Moore, J.G. Seidman, J.A. Smith, and K. Struhl, eds. (John Wiley & Sons). Unit 14.20, pp. 14.20.1–14.20.17.
- Januschke, J., Llamazares, S., Reina, J., and Gonzalez, C. (2011). *Drosophila* neuroblasts retain the daughter centrosome. *Nat. Commun.* 2, 243.
- Januschke, J., Reina, J., Llamazares, S., Bertran, T., Rossi, F., Roig, J., and Gonzalez, C. (2013). Centrobin controls mother-daughter centriole asymmetry in *Drosophila* neuroblasts. *Nat. Cell Biol.* 15, 241–248.
- Kang, K., Lee, D., Hong, S., Park, S.G., and Song, M.R. (2013). The E3 ligase Mind bomb-1 (Mib1) modulates Delta-Notch signaling to control neurogenesis and gliogenesis in the developing spinal cord. *J. Biol. Chem.* 288, 2580–2592.
- Knoblich, J.A., Jan, L.Y., and Jan, Y.N. (1995). Asymmetric segregation of Numb and Prospero during cell division. *Nature* 377, 624–627.
- Kodani, A., Yu, T.W., Johnson, J.R., Jayaraman, D., Johnson, T.L., Al-Gazali, L., Sztriha, L., Partlow, J.N., Kim, H., Krup, A.L., et al. (2015). Centriolar satellites assemble centrosomal microcephaly proteins to recruit CDK2 and promote centriole duplication. *eLife* 4, 4.
- Konno, D., Shioi, G., Shitamukai, A., Mori, A., Kiyonari, H., Miyata, T., and Matsuzaki, F. (2008). Neuroepithelial progenitors undergo LGN-dependent planar divisions to maintain self-renewability during mammalian neurogenesis. *Nat. Cell Biol.* 10, 93–101.
- Kressmann, S., Campos, C., Castanon, I., Fürthauer, M., and González-Gaitán, M. (2015). Directional Notch trafficking in Sara endosomes during asymmetric cell division in the spinal cord. *Nat. Cell Biol.* 17, 333–339.
- Lopes, C.A., Prosser, S.L., Romio, L., Hirst, R.A., O'Callaghan, C., Woolf, A.S., and Fry, A.M. (2011). Centriolar satellites are assembly points for proteins implicated in human ciliopathies, including oral-facial-digital syndrome 1. *J. Cell Sci.* 124, 600–612.
- Loulier, K., Barry, R., Mahou, P., Le Franc, Y., Supatto, W., Matho, K.S., Ieng, S., Fouquet, S., Dupin, E., Benosman, R., et al. (2014). Multiplex cell and lineage tracking with combinatorial labels. *Neuron* 81, 505–520.
- Matsunaga, E., Tauszig-Delamasure, S., Monnier, P.P., Mueller, B.K., Strittmatter, S.M., Mehlen, P., and Chédotal, A. (2004). RGM and its receptor neogenin regulate neuronal survival. *Nat. Cell Biol.* 6, 749–755.
- Morin, X., Jaouen, F., and Durbec, P. (2007). Control of planar divisions by the G-protein regulator LGN maintains progenitors in the chick neuroepithelium. *Nat. Neurosci.* 10, 1440–1448.
- Nachury, M.V., Loktev, A.V., Zhang, Q., Westlake, C.J., Peränen, J., Merdes, A., Slusarski, D.C., Scheller, R.H., Bazan, J.F., Sheffield, V.C., and Jackson, P.K. (2007). A core complex of BBS proteins cooperates with the GTPase Rab8 to promote ciliary membrane biogenesis. *Cell* 129, 1201–1213.
- Pierfelice, T., Alberi, L., and Gaiano, N. (2011). Notch in the vertebrate nervous system: an old dog with new tricks. *Neuron* 69, 840–855.
- Rebollo, E., Sampaio, P., Januschke, J., Llamazares, S., Varmark, H., and Gonzalez, C. (2007). Functionally unequal centrosomes drive spindle orientation in asymmetrically dividing *Drosophila* neural stem cells. *Dev. Cell* 12, 467–474.
- Reina, J., and Gonzalez, C. (2014). When fate follows age: unequal centrosomes in asymmetric cell division. *Philos. Trans. R. Soc. Lond. B Biol. Sci.* 369, 369.
- Roubinet, C., and Cabernard, C. (2014). Control of asymmetric cell division. *Curr. Opin. Cell Biol.* 31, 84–91.
- Rusan, N.M., and Peifer, M. (2007). A role for a novel centrosome cycle in asymmetric cell division. *J. Cell Biol.* 177, 13–20.
- Saade, M., Gutiérrez-Vallejo, I., Le Dréau, G., Rabadán, M.A., Miguez, D.G., Buceta, J., and Martí, E. (2013). Sonic hedgehog signaling switches the mode of division in the developing nervous system. *Cell Rep.* 4, 492–503.
- Salzmann, V., Chen, C., Chiang, C.Y., Tiyaboonchai, A., Mayer, M., and Yamashita, Y.M. (2014). Centrosome-dependent asymmetric inheritance of the midbody ring in *Drosophila* germline stem cell division. *Mol. Biol. Cell* 25, 267–275.
- Schneider, C.A., Rasband, W.S., and Eliceiri, K.W. (2012). NIH Image to ImageJ: 25 years of image analysis. *Nat. Methods* 9, 671–675.
- Taverna, E., Mora-Bermúdez, F., Strzyz, P.J., Florio, M., Icha, J., Haffner, C., Norden, C., Wilsch-Bräuninger, M., and Huttner, W.B. (2016). Non-canonical features of the Golgi apparatus in bipolar epithelial neural stem cells. *Sci. Rep.* 6, 21206.
- Tollenaere, M.A., Mailand, N., and Bekker-Jensen, S. (2015). Centriolar satellites: key mediators of centrosome functions. *Cell. Mol. Life Sci.* 72, 11–23.
- Vilas-Boas, F., Fior, R., Swedlow, J.R., Storey, K.G., and Henrique, D. (2011). A novel reporter of notch signalling indicates regulated and random Notch activation during vertebrate neurogenesis. *BMC Biol.* 9, 58.
- Villumsen, B.H., Danielsen, J.R., Povlsen, L., Sylvestersen, K.B., Merdes, A., Belí, P., Yang, Y.G., Choudhary, C., Nielsen, M.L., Mailand, N., and Bekker-Jensen, S. (2013). A new cellular stress response that triggers centriolar satellite reorganization and ciliogenesis. *EMBO J.* 32, 3029–3040.
- Wang, X., Tsai, J.W., Imai, J.H., Lian, W.N., Vallee, R.B., and Shi, S.H. (2009). Asymmetric centrosome inheritance maintains neural progenitors in the neocortex. *Nature* 461, 947–955.
- Weinmaster, G., and Fischer, J.A. (2011). Notch ligand ubiquitylation: what is it good for? *Dev. Cell* 21, 134–144.

- Yamashita, Y.M., Mahowald, A.P., Perlin, J.R., and Fuller, M.T. (2007). Asymmetric inheritance of mother versus daughter centrosome in stem cell division. *Science* 315, 518–521.
- Yoon, K.J., Koo, B.K., Im, S.K., Jeong, H.W., Ghim, J., Kwon, M.C., Moon, J.S., Miyata, T., and Kong, Y.Y. (2008). Mind bomb 1-expressing intermediate progenitors generate notch signaling to maintain radial glial cells. *Neuron* 58, 519–531.
- Zhang, C., Li, Q., Lim, C.H., Qiu, X., and Jiang, Y.J. (2007). The characterization of zebrafish antimorphic mib alleles reveals that Mib and Mind bomb-2 (Mib2) function redundantly. *Dev. Biol.* 305, 14–27.
- Zhou, Y., Atkins, J.B., Rompani, S.B., Bancescu, D.L., Petersen, P.H., Tang, H., Zou, K., Stewart, S.B., and Zhong, W. (2007). The mammalian Golgi regulates numb signaling in asymmetric cell division by releasing ACBD3 during mitosis. *Cell* 129, 163–178.

STAR★METHODS

KEY RESOURCES TABLE

REAGENT or RESOURCE	SOURCE	IDENTIFIER
Antibodies		
Mouse anti- γ Tubulin (clone GTU-88)	Sigma Aldrich	Cat#T6557 RRID: AB_477584
Mouse anti-cMyc (clone 9E10)	Sigma Aldrich	Cat#C3956 RRID: AB_439695
Rabbit anti-Mib1	Biorbyt	Cat#Orb33792 RRID: AB_10926879
Rabbit anti-Mib1	Sigma Aldrich	Cat#M5948 RRID: AB_1841007
Mouse anti-Giantin (clone G1/133)	Enzo Life Science	Cat#ALX-804-600 RRID: AB_2113059
Rabbit anti-PCM1 (clone G2000)	Cell Signaling Technology	Cat#5213 RRID: AB_10556960
Goat anti-Sox2 (clone Y-17)	Santa Cruz	Cat#Sc-17320 RRID: AB_2286684
Mouse anti-pan centrin (clone 20H5)	Millipore	Cat#04-1624 RRID: AB_10563501
Mouse anti-HuC/D (clone 16A11)	ThermoFisher Scientific	Cat#A-21271 RRID: AB_221448
Mouse anti-Tubulin β 3 (clone Tuj1)	Biolegend	Cat#801201 RRID: AB_2313773
Rabbit anti-FOP1	Gift from Olivier Rosnet, Institut de Biologie du Développement, Marseille, France Acquaviva et al., 2009	N/A
Experimental Models: Organisms/Strains		
Chicken fertilized eggs	EARL Morizeau	JA57
Recombinant DNA		
cmv-cMib1-GFP	This paper	N/A
cmv-cMib1-RFP	This paper	N/A
pCAGGS-cMib1-GFP	This paper	N/A
pCAGGS-cMib1-RFP	This paper	N/A
pCAGGS-Myc-cMib1	This paper	N/A
pCAGGS- Δ mib1-IRES-H2B-Cherry	This paper	N/A
cmv-mAZI1-Flag	Chamling et al., 2014	N/A
pCAGGS-cAZI1-Nter	This paper	N/A
pBabe-p35	Matsunaga et al., 2004	N/A
pCAGGS-GalT-CFP	Unpublished, gift from Jean Livet, Institut de la Vision, Paris, France	N/A
pCAGGS-GalT-RFP	This paper	N/A
pCAGGS-EGFP-ZO1	Konno et al., 2008	N/A
pCAGGS-Cherry-ZO1	This paper	N/A
pCAGGS-Centrin2-GFP	This paper	N/A
pCAGGS-Arl13b-GFP	Unpublished, gift from Nathalie Spassky, IBENS, Paris, France.	N/A
pCAGGS-mbGFP	This paper	N/A
pCAGGS-mbVenus	This paper	N/A
pCAG-H2B-mRFP-pA	Unpublished, gift from Sharaghim Tajbakhsh, Institut Pasteur Paris, France	N/A
pCAGGS-PACT-mKO1	Konno et al., 2008	N/A
pCAGGS-Cre	Morin et al., 2007	N/A
Cytobow	Loulier et al., 2014	N/A
pBabe-BBS4-GFP	Nachury et al., 2007	N/A
cmv-GFP-OFD1	Lopes et al., 2011	N/A
pCX-mInsc-IRES-H2B-RFP	Das and Storey, 2012	N/A

(Continued on next page)

Continued

REAGENT or RESOURCE	SOURCE	IDENTIFIER
Hes5-VNP	Vilas-Boas et al., 2011	N/A
Software and Algorithms		
ImageJ	Schneider et al., 2012	http://imagej.net/Welcome RRID: SCR_003070
Adobe Photoshop CS4	Adobe	http://www.adobe.com/fr/products/photoshop.html RRID: SCR_014199
Metamorph software	Molecular Devices	https://www.moleculardevices.com/Products/Software/Meta-Imaging-Series/MetaMorph.html RRID: SCR_002368
Imaris	Bitplane	http://www.bitplane.com/imaris/imaris RRID: SCR_007370
MicroManager	Edelstein et al., 2010	https://micro-manager.org/ RRID: SCR_000415

CONTACT FOR REAGENT AND RESOURCE SHARING

As Lead Contact, Xavier Morin (Institut de Biologie de l'École Normale Supérieure) is responsible for all reagent and resource requests. Please contact Xavier Morin at xavier.morin@ens.fr with requests and enquiries.

EXPERIMENTAL MODEL AND SUBJECT DETAILS

JA57 chicken fertilized eggs were provided by EARL Morizeau (8 rue du Moulin, 28190 Dangers, France). They were incubated at 38°C in a Sanyo MIR-253 incubator for the appropriate time.

METHODS DETAILS

Electroporation and Plasmids

Electroporation in the chick neural tube was performed at embryonic day 2 (E2), by applying 5 pulses of 50 ms at 25 V with 100 ms in between, using a square wave electroporator (Nepa Gene, CUY21SC) and a pair of 5 mm Gold plated electrodes (BTX Genetrode model 512) separated by a 4 mm interval. For spinal cord slice culture (Figure 3D) and clonal analysis (Figure 4C), lower voltage (3 pulses of 50 ms at 17 V with 950 ms in between) were applied to obtain isolated cells (Das and Storey, 2012). The chick version of Mib1 (cMib1) was cloned and inserted in either CMV (weak expression in the chick) or CAGGS (strong expression) promoter vectors as follows: CMV-cMib1-GFP, CMV-cMib1-RFP, pCAGGS-cMib1-GFP, pCAGGS-cMib1-RFP, pCAGGS-Myc-cMib1. CMV-cMib1 vectors were transfected at 1 µg/µL; pCAGGS-Myc-cMib1 was transfected at 0.05 µg/µL for localization experiments (Figure S1E) and at 1 µg/µL for overexpression (Figure S3A). For slice cultures, pCAGGS-cMib1-RFP was transfected at 0.5 µg/µL but in low voltage conditions (described above). For the en face cultures shown in Figure S3, pCAGGS-cMib1-GFP was transfected at 0.025 µg/µL. For the AZI1-Nter construct, the N-terminal part (aa 1-256) of chick AZI1 was cloned into pCAGGS and transfected at 1 µg/µL. AZI1-Nter induced significant cell death, which was blocked by co-transfecting a pCAGGS-p35 vector at 1 µg/µL (a gift from A.Chédotal). For the dominant negative Mib1 (ΔMib1) (Zhang et al., 2007), a version lacking the ring finger domain (aa 1-767) was amplified from the cMib1 cDNA, inserted into pCAGGS-IRES-H2B-Cherry and transfected at 1 µg/µL. GalT-CFP (a gift from J. Livet) and GalT-RFP correspond to the Nter part of Galactosyl- Transferase fused to CFP or RFP and were used at 1 µg/µL. The other plasmids were used with the following concentrations: pCX-EGFP-ZO1 (Konno et al., 2008; a gift from F. Matsuzaki) and pCX-Cherry-ZO1 were transfected at 0.2 µg/µL; pCX-Centrin2-GFP, 0.1 µg/µL; pCX-Arl13b-GFP (a gift from N.Spasky), 1 µg/µL; pCX-mbGFP, 0.5 µg/µL; pCX-mbVenus, 0.5 µg/µL; pCX-H2B-mRFP1 (a gift from S. Tajbakhsh), 0.1 µg/µL; pCX-PACT-mKO1 (Konno et al., 2008; a gift from F. Matsuzaki) 0.3 µg/µL; pCX-Cre (Morin et al., 2007), 0.5 ng/µL; Cytobow (Loulrier et al., 2014) 0.5 µg/µL, pBabe-BBS4-GFP (Nachury et al., 2007; a gift from M. Nachury) 1 µg/µL; CMV-GFP-OFD1 (Lopes et al., 2011; a gift from A. Fry) 1 µg/µL; pCX-mInsc-IRES-H2B-RFP (Das and Storey, 2012; a gift from K. Storey) 1 µg/µL; HES5-VNP (Vilas-Boas et al., 2011; a gift from D. Henrique), 1 µg/µL; pAZI-Flag (Chamling et al., 2014; a gift from V. Sheffield), 1 µg/µL.

Immunohistochemistry

Chick embryos were fixed for 1 hr in ice-cold 4% formaldehyde/PBS, and rinsed 3 times in PBS. For cryosections, they were equilibrated at 4°C in PB/15% Sucrose and embedded in PB/15% Sucrose/7.5% gelatin before sectioning. Before immuno-staining, cryosections were equilibrated at room temperature, degelatinized in PBS at 37°C 3 times 5 min, before a 30 min blocking step in PBS-0.1% Triton /10% Fetal Calf Serum (FCS). Slides were then incubated with the primary antibodies diluted in the blocking solution at 4°C over-night. The following day, slides were washed 3 times 5 min in PBS-0.1% Triton, incubated 2h with the adequate secondary antibodies at room temperature, washed again 3 times and mounted with DAPI containing Vectashield (Vector Labs).

For vibratome sections, embryos were embedded in 4% agarose (4 g agarose in 100 mL water, boiled in microwave and cooled at 50°C). Samples were included in plastic dishes containing 1 mL agarose, and cooled until agarose became solid. Thereafter, 100 μ m floating vibratome sections were incubated with the mouse anti-HuC/D antibody in PBS–0.1%Triton for 48 hr at 4°C. Sections were rinsed several times in PBS and incubated with secondary antibody in PBS for 48 hr at 4°C. After 24 hr washing (several times) in PBS, sections were mounted on slides with DAPI containing Vectashield.

For en-face views, fixed embryos were cut along their midline and bathed 1 hr in blocking solution (PBS–0.3%Triton/10%FCS), followed by over-night incubation at 4°C with the primary antibodies diluted in the blocking solution. The next day, embryos were washed 4–5 times with PBS–0.3%Triton, incubated over-night at 4°C with the secondary antibodies, washed again 3 times 10 min in PBS–0.3%Triton and flat-mounted (apical side facing the coverslip) with DAPI containing Vectashield.

Primary antibodies used are: mouse anti- γ -Tubulin (clone GTU-88) and mouse anti-c-Myc (clone 9E10) from Sigma Aldrich; rabbit anti-Mib1 from Biorbyt (orb33792); rabbit anti-Mib1 from Sigma-Aldrich (M5948); mouse anti-Giantin (clone G1/133) from Enzo Life Sciences; rabbit anti-PCM1 (clone G2000) from Cell Signaling Technology; goat anti-Sox2 (clone Y-17) from Santa Cruz; mouse anti-pan centrin (clone 20H5) from Millipore; mouse anti-HuC/D (clone 16A11) from Life Technologies; mouse anti-Tuj1 from Covance; rabbit anti-FOP (FGFR1 Oncogene Partner) was a gift from Olivier Rosnet (Acquaviva et al., 2009). For Mib1 antibody, embryos destined for cryosectioning were fixed in 4% formaldehyde/PBS–Triton 0.3%, while embryos destined for en-face views were fixed 20 min in Methanol/Acetone at –20°C. For γ -tubulin antibody, embryos were incubated for 10 min in 100% acetone pre-equilibrated at –20°C, and rinsed twice in PBS at room temperature before the blocking step. Secondary antibodies coupled to Alexa Fluor 488, Cy3 or Alexa Fluor 649 were obtained from Jackson laboratories.

Time-Lapse Microscopy and Analysis of Cultured Chick Neural Tube

En-face Culture

En-face culture of the embryonic neuroepithelium was performed at E3 (24 hr after electroporation), except for the Mib1-GFP/GalT-RFP co-transfection experiment, for which embryos were transfected at E2 and harvested 8 hr later, at a stage where mostly symmetric divisions occur. After removal of extraembryonic membranes, embryos were transferred to 37°C F12 medium and slit along their midline from the hindbrain to the caudal end. The electroporated side of the neural tube was peeled off with dissection forceps and equilibrated 5 min in 1% agarose F12 medium at 38°C. It was then transferred to a glass-bottom culture dish (MatTek, P35G-0-14-C) and excess medium was removed so that the neural tube would flatten with its apical surface adhering to the bottom of the dish. After 30 s of polymerization on ice, an extra layer of agarose medium was added and left again on ice. After 2 min, 3 mL of culture medium was added (F12/Penicillin Streptomycin/Sodium pyruvate) and culture dishes were transferred to 37°C.

Slice Culture

For slice cultures, embryos were electroporated under low voltage conditions (detailed in the first section) at E2.5 and harvested 6 hr later, in order to obtain isolated cells at a developmental stage at which asymmetric divisions are well represented. After dissection, embryos were transferred to a tissue chopper (Mc Ilwain) and 200 μ m thick transverse sections were cut. Sections were then transferred to cold 199 medium and sorted out under a fluorescence dissection microscope to control tissue integrity and the presence of isolated cells. They were then equilibrated in a drop of type Ia collagen (Cellmatrix, Nitta Gelatin; diluted to 2.4 mg/mL with DMEM/F-12 and neutralizing buffer according to the manufacturer's protocol) and kept on ice. Then 3 to 4 collagen drops (5 μ L) were distributed on a glass-bottom culture dish pre-coated with poly-L-lysine (1 mg/mL) and 2 to 3 neural tube slices were transferred to each collagen drop. The slices were then briefly checked under fluorescence and oriented such that the side to image was facing the coverslip. The dish was then placed 10 min at 37°C for the collagen to polymerize and 3 mL of culture medium (199 medium, 5% FCS, GlutaMax, Gentamycin 40 μ M) was gently added.

Image Acquisition and Treatment

Optical sections of fixed samples (en-face views from half embryos or transverse views from cryosections) were obtained on a confocal microscope (model SP5; Leica) using 20x and 40x (Plan Neofluar NA 1.3 oil immersion) objectives and Leica LAS software. For time-lapse experiments, images were acquired either with a 40x water immersion objective (APO LWD, NA 1.15, Nikon) on an inverted microscope (Nikon Ti Eclipse) equipped with a heating enclosure (LIS, Switzerland), a spinning disk confocal head (Yokogawa CSU-X1), Metamorph software (Molecular Devices) and an emCCD Camera (Evolve, Roper Scientific); or a 100x oil immersion objective (APO VC, NA 1.4, Nikon) on an inverted microscope (Nikon Ti Eclipse) equipped with a heating enclosure (DigitalPixel, UK), a spinning disk confocal head (Yokogawa CSU-W1), MicroManager software (Edelstein et al., 2010) and an sCMOS Camera (Orca Flash4LT, Hamamatsu). We recorded 20/45 μ m thick z stacks (1/1.5 μ m between individual sections) at 4/7 min intervals for en-face/slice cultures, respectively. To monitor Mib1-GFP in parallel with GalT-RFP (Figure 2D; Figure S2C), en-face culture was carried out and up to 80 μ m thick z stacks (1 μ m between individual sections) at 4 min intervals were recorded. For image processing and data analysis, we used the ImageJ software (Schneider et al., 2012). In addition, for Mib1-GFP/GalT-RFP movies, a 3D crop was performed in Imaris to isolate the cell of interest. Images were finally subjected to brightness and contrast adjustments to equilibrate channel intensities and background using Adobe Photoshop CS4 software.

Image Quantifications

Protein Distribution of Mib1 and Satellites at Mother and Daughter Centrioles

A rectangular zone of interest spanning successively the mother and daughter centrioles was drawn and the average intensity of the protein signal (minus the background of the acquisition field) was obtained for each position along the mother-daughter axis (schematized in [Figure 1Cvii](#)). Interpolation was then used to re-assign the obtained values along a 28 bin axis. Normalization on the total amount of signal was carried out for each individual picture. The averages of each position were plotted in [Figure S1A](#) (normalized to the maximum) and the sum of the positions 1–14 (mother centriole) and 15–28 (daughter centriole) were displayed for each marker in [Figure 1C](#), right panels.

Centrosomal Localization of Mib1-Myc, PCM1 and AZI1-Flag in Control and AZI1-Nter Embryos

Mib1-Myc and AZI1-Flag average pixel intensity in the centrosomal area was normalized to the average pixel intensity of ZO1-GFP and compared between control and AZI1-Nter transfected embryos. For PCM1 staining, the ratio of the average pixel intensity in the centrosomal area between transfected and non-transfected cells was measured for different acquisition fields. Importantly, all pictures of a given marker were taken during a unique confocal session with identical parameters.

Calculation of the Symmetry Indices in Dividing Cells

To calculate the index of symmetry in dividing cells from fixed data ([Figures 1E–1G](#)), a z-projection (1 μm spaced optical sections) of the entire cell was obtained using ImageJ. The average pixel intensity of identical areas around each centrosome (minus background) was taken and the ratio of the lowest by the highest average intensity was calculated. In the case of PCM1, the ratio between the centrosomal and non-centrosomal fractions was calculated and the results were normalized to 1. The blue and red triangles in [Figure 1E](#) correspond to cells for which the ratio is under 0.2 or between 0.2 and 1, respectively.

The symmetry index in live experiments was measured as follows: for each time point in a series, the entire cell volume was z-projected. Cytoplasmic Mib1 symmetry index was measured by quantifying the Mib1-GFP signal intensity in the two halves of a single cell delineated by the bisector of the line joining the two centrosomes. For each cell, values measured in the half cell that contained the Mib1-GFP positive centrosome at the beginning of the time series were used as the denominator throughout the time series. Centrosome Mib1 symmetry index was measured by quantifying the Mib1-GFP signal at (or closely associated with) each centrosome, using values from the centrosome harboring Mib1-GFP at the beginning of the time series as the denominator. Cells were grouped in two populations as a function of their symmetric or asymmetric distribution of Mib1 in telophase. Within these two groups, for each phase of cell division (prophase, metaphase, ana/telophase, and post-division interphase), one single average value was calculated from all time points of all cells in this phase.

Differentiation Rate

The differentiation rate was obtained by dividing the number of H2B-Cherry+/Hu+ cells by the total number of H2B-Cherry+ cells and compared between control and AZI1-Nter situations.

Rainbow Analysis

The cytobow vector was transfected at 0.5 $\mu\text{g}/\mu\text{L}$ together with pCX-Cre at 0.5 $\text{ng}/\mu\text{L}$, and co-transfected either with a control vector or an AZI1-Nter construct at 1 $\mu\text{g}/\mu\text{L}$. 40 hr after transfection, embryos were harvested and subjected to transverse vibratome sections before immunostaining (detailed above). Stacks of images (50 to 80 images per stack, with a z step of 1 μm) on 100 μm vibratome sections were taken on a confocal microscope (model SP5; Leica) using 20x (Plan Neofluar NA 1.3 oil immersion) objectives and Leica LAS software. Measurements were obtained from seven embryos transfected with an empty vector and from eight embryos transfected with an AZI1-Nter construct. Each clone was identified on the basis of color similarity and proximity between cells.

Notch Activity in Sister Cells

Embryos were co-transfected at E2 with the Hes5-Venus-NLS-PEST ([Vilas-Boas et al., 2011](#)) (Venus linked to a nuclear localization signal followed by the PEST degradation sequence under the control of the promoter of the Notch target gene Hes5) at 1 $\mu\text{g}/\mu\text{L}$ and pCAGGS-Inscuteable-IRES-H2B-RFP at 0.1 $\mu\text{g}/\mu\text{L}$ together with an empty vector or AZI1-Nter, in low voltage conditions (17 V), and incubated for 20 hr. Two-cell clones were selected based on proximity and intensity of the H2B-RFP signal (only pairs of cells showing a ratio of intensity above 0.8 were considered). The ratio of the VNP signal (low/high) between the two cells was then calculated and plotted for each condition.

Statistical Analyses

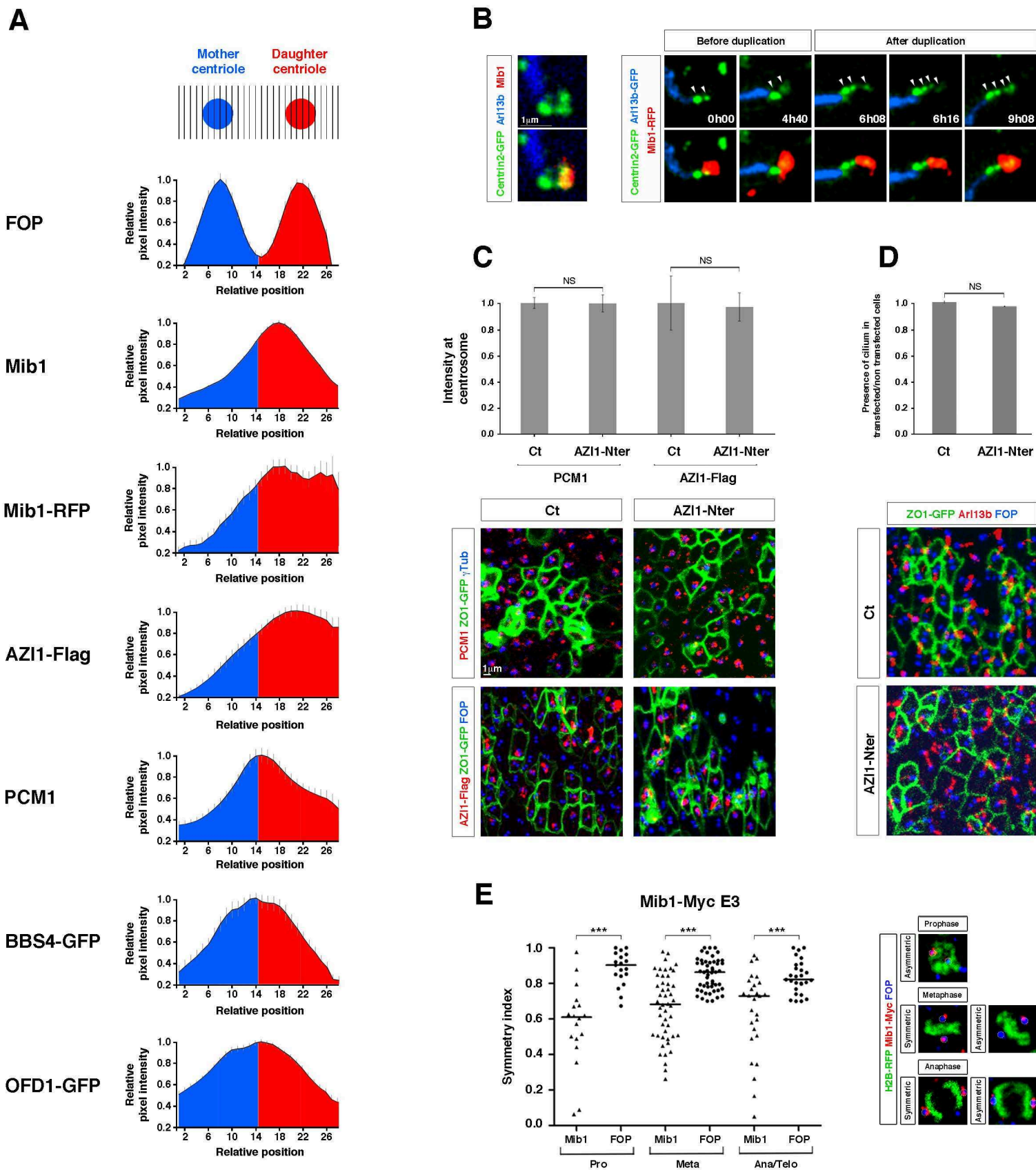
For datasets following a normal distribution ([Figures 1C](#), [1D](#), and [4A](#); [Figure S1C](#), [S1D](#), [S3A–S3C](#), and [S4C](#)), analyses were carried out in Excel and significance was calculated using a Student's t test. Data represent means \pm SEM, ** $p < 0.01$, *** $p < 0.001$. For the analysis of symmetry indices ([Figures 1E–1G](#); [Figure S1E](#)), we used a Mann-Whitney test performed with GraphPad Prism (GraphPad software). Horizontal bars correspond to medians, *** $p < 0.001$. For comparison of PP and PN clones in [Figure 4B](#), a Chi2 test was carried out in Excel. For quantitation, unless actual numbers are specified in the text or figure legends, at least two 2 embryos were analyzed for protein localization, and at least 3 embryos were used for functional approaches. No randomization or blinding strategies were used at any stage of the study. Exclusion criteria: for long term fate analyses, cells with obvious abnormal behavior (dying cells, strong fluorescent protein aggregates) were not included in the analyses.

Neuron, Volume 93

Supplemental Information

**Differential Routing of Mindbomb1
via Centriolar Satellites Regulates
Asymmetric Divisions of Neural Progenitors**

Samuel Tozer, Chooyoung Baek, Evelyne Fischer, Rosette Goïame, and Xavier Morin



Tozer et al., Figure S1

Figure S1. Related to Figure 1. Polarized distribution of centriolar satellites and Mib1 at the centrosome.

A, Diagrams indicating the relative pixel intensity of the indicated markers along a rectangle covering successively the mother and daughter centrioles (schematized in Figure 1Cvii). Markers used to label the cilium and the centrioles are indicated in the legend for Figure 1A. Note that only values above 0.2 of the maximum are displayed. Data represent means \pm SEM. The compiled averages of the blue (mother centriole) and red (daughter centriole) areas are displayed in the diagrams shown in Figure 1C. B-left; apical view at E3 of a duplicated centrosome (green, labeled with centrin2-GFP). Mib1 (red) is enriched at the centrosome that does not carry the cilium (blue, labeled with Arl13b-GFP). B-right; time series (en-face imaging) of a centrosome before and after duplication (labeled with centrin2-GFP in green); note that the cilium (labeled with Arl13b-GFP) has been manually colored in blue to facilitate the reading; Mib1-RFP remains enriched at the centriole/centrosome that does not carry the cilium. C-top panel, Average intensities of PCM1 and full-length AZI1-Flag staining at the centrosome in control versus AZI1-Nter transfected embryos; data represent mean \pm SEM; n=102, 111 cells analyzed for PCM1 centrosomal localization in control and AZI1-Nter conditions, respectively; n=61, 63 cells analyzed for AZI1-Flag centrosomal localization in control and AZI1-Nter conditions, respectively. C-bottom panel, Apical views showing the localization of PCM1 and full-length AZI1-Flag (red) in relation with the centrioles (labeled with γ Tubulin or FOP in blue) and tight junctions (labeled with ZO1-GFP in green) in control and AZI1-Nter transfected embryos. D-top panel, Average presence of the cilium in transfected versus non-transfected cells in embryos transfected with a control vector (left) or with AZI1-Nter (right); data represent mean \pm SEM. D-bottom panel, Apical views showing the cilia (Arl13b, in red), centrioles (FOP, in blue) and tight junctions (ZO1-GFP, in green) in control and AZI1-Nter conditions. E-left, Diagram indicating the symmetry index for Mib1-Myc at the centrosome in comparison with the centrosome marker FOP in mitotic cells (each mark corresponds to a single cell; horizontal bars correspond to medians). E-right panel, Representative examples of the localization of Mib1-Myc (red) in relation with the centrosomes (blue) and chromosomes (green, labeled with H2B-RFP), at the indicated mitotic stages.

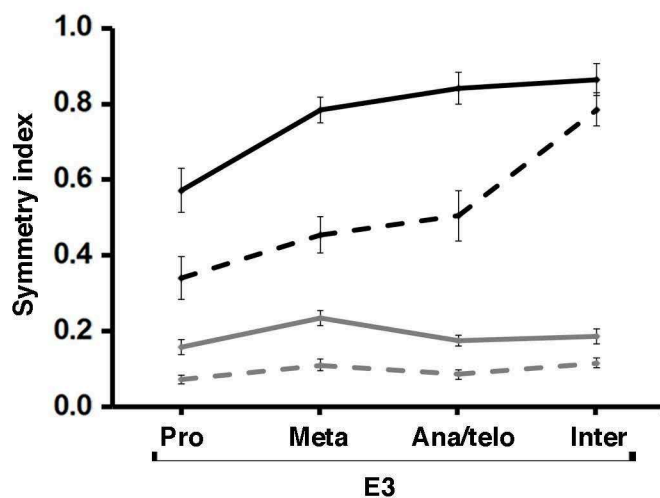
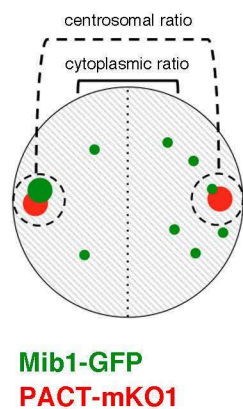
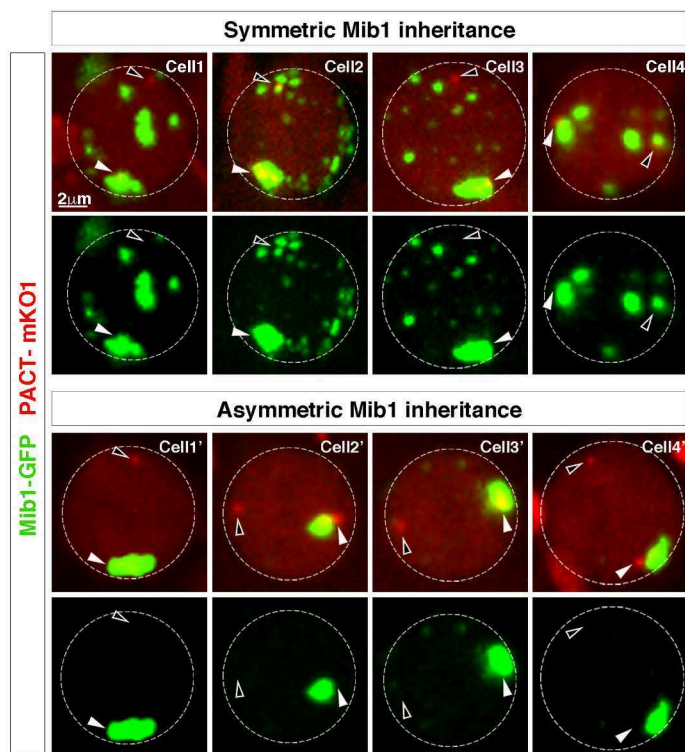
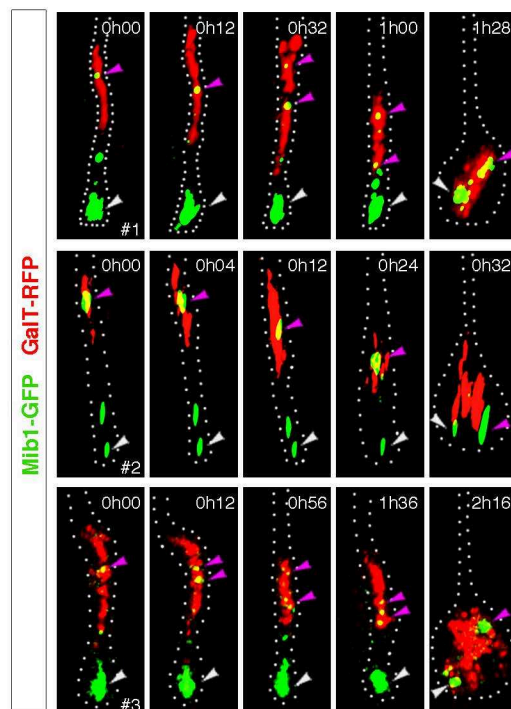
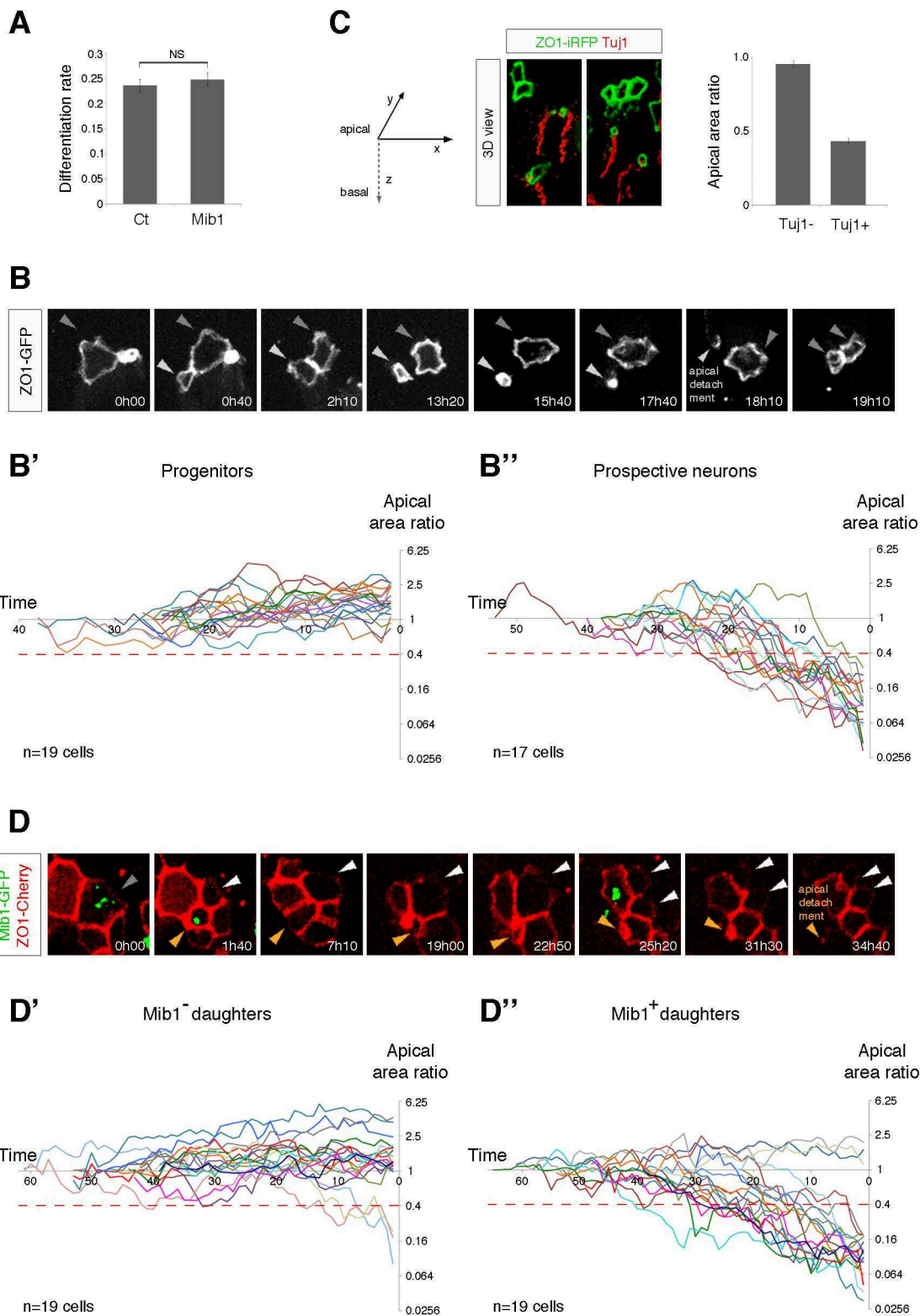
A**B****C**

Figure S2. Related to Figure 2. A non-centrosomal pool of Mib1-GFP is observed in cells inheriting similar amounts of Mib1-GFP.

A, Symmetry index during mitotic progression in cells that display either symmetric or asymmetric inheritance of Mib1-GFP (related to Figure 2A). Cytoplasmic (solid lines) and centrosomal (dotted lines) symmetry indices of Mib1-GFP were measured during cell division in time series from live imaging data. Note that the cytoplasmic ratio is a comparison of the average intensities between the two halves of each cell (comprises the centrosomal pool). Curves represent the mean values of the “symmetric” (black lines) and “asymmetric” (gray lines) populations; error bars correspond to SEMs, n=18 cells for symmetric and 21 cells for asymmetric situations from 4 embryos were analyzed. In symmetrically dividing cells, the initial asymmetry is compensated through progressive accumulation of Mib1-GFP on the second spindle pole. B, Representative examples of cells used for the quantification shown in A. Cells are in metaphase and express Mib1-GFP and the centrosome reporter PACT-mKO1. All images are projections of confocal sections of apical views taken 2-10 μm below the apical surface. Top row: four distinct examples of cells displaying symmetric inheritance of Mib1-GFP symmetric division (as deduced from their equal distribution of Mib1-GFP on the two spindle poles at telophase, in later time frames not shown here). A scattered pool of Mib1-GFP is observed in addition to the strong Mib1-GFP associated with one centrosome. Bottom row: four distinct examples of cells undergoing asymmetric division (as deduced from their highly asymmetric segregation of Mib1-GFP between the two spindle poles at telophase, in later time frames not shown here). No (or virtually no) Mib1-GFP signal is visible apart from the strong Mib1-GFP associated with a single centrosome. White and black arrowheads point to the Mib1-loaded and Mib1-free centrosomes, respectively. C, 3D-reconstructed time-series showing three examples similar to figure 2D. The cells were co-transfected with Mib-GFP (green) and the GA reporter GalT-RFP (red). The cell outline has been schematized with a dotted line. The last time-point for each cell corresponds to mitosis. The white and magenta arrowheads indicate the apical and GA-associated pools of Mib1-GFP, respectively.



Tozer et al., Figure S3

Figure S3. Related to Figure 3. Mib1 is inherited by the cell committing to differentiation

A, Differentiation rate (number of HuC/D+ cells on total) in transfected cells 40h after transfection in control versus Mib1-Myc transfected embryos. Data represent mean +/- SEM, NS stands for non-significant according to the Student's t test; n=19 and 21 sections were analyzed for control and Mib1-Myc conditions, respectively. B, Time-series of a cell transfected with ZO1-GFP. After division (0h40), one of the daughter cells (light gray arrowhead) progressively shrinks its apical area (from 13h20) until it eventually detaches (18h10) while its sister cell (dark grey arrowhead) divides (19h10). B'-B'', Quantification of the apical area ratio (apical area at time t on apical area 1h after mitosis) over time in individual cells. Measures were taken from 1h after mitosis until the cell re-divides (progenitors, n=19) or leaves the surface (prospective neurons, n=17). A dotted line at 0.4 was drawn as a reference threshold below which the apical area in "progenitors" never falls. C, Center panel: 3D view of a volume on the apical side of an E3 neural tube transfected with ZO1-GFP (green) to label the tight junctions and immunostained for Tuj1 (red) to label nascent neurons. Left panel: schematic representation of the axes in the medium panel. Right panel: apical area ratio (ratio of the area of the transfected cell on the area of its close neighbors) for Tuj1 negative and positive cells. Data represent mean +/- SEM. D, Time-series of a cell transfected with Mib1-GFP and ZO1-Cherry. After division (1h40), the daughter cell inheriting Mib1-GFP (orange arrowhead) progressively shrinks its apical area (from 19h00) until it eventually detaches (34h40) while its sister cell (white arrowhead) divides (25h20). D',D'', Quantification of the apical area ratio in sisters cells following asymmetric inheritance of Mib1-GFP. In 16 out of 19 pairs, the daughter cells inheriting Mib1-GFP (D'') progressively shrank their apical area while their siblings (D') maintained it above 0.4.

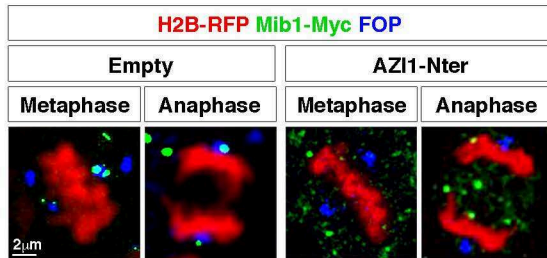
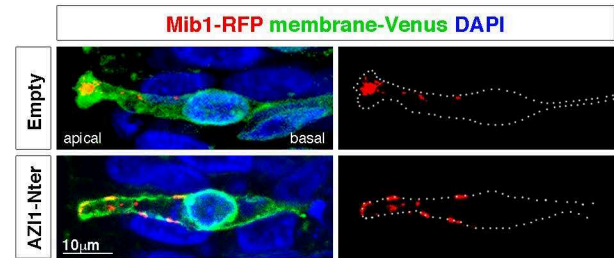
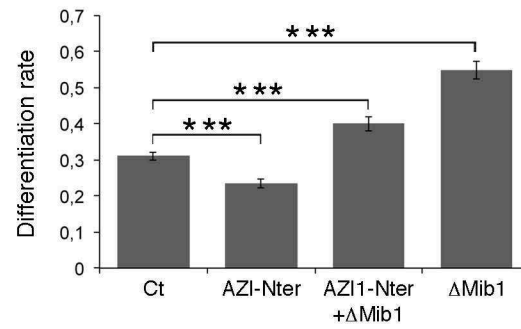
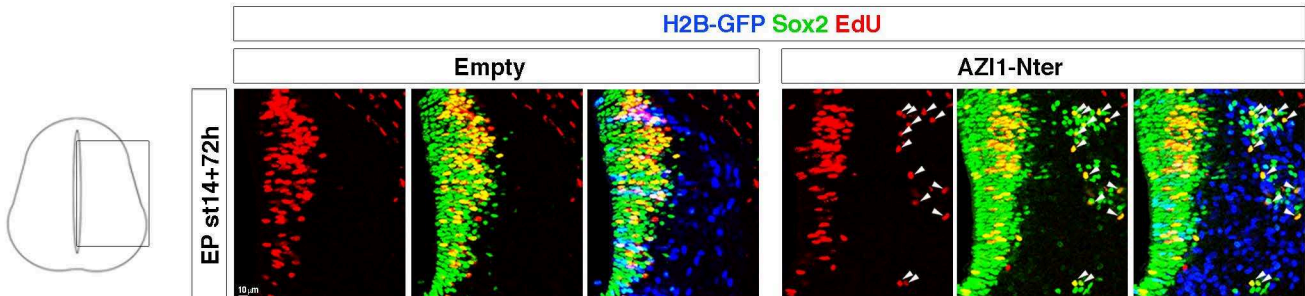
A**B****C****D**

Figure S4. Related to Figure 4. Loss of Mib1 centrosomal localization randomizes its distribution in mitosis and induces ectopic cycling cells.

A, Mib1-Myc localization in dividing cells transfected with an empty vector (left panels) or AZI1-Nter (right panels). The centrosomal Mib1-Myc observed in control cells is lost and scattered in the cytoplasm in AZI1-Nter transfected cells. B, Mib1-RFP localization in interphase cells transfected with a membrane-Venus reporter together with an empty vector (top panels) or AZI1-Nter (bottom panels). The cell outline is drawn in the right panels, showing Mib1-RFP enrichment at the membrane following AZI1-Nter transfection. C, Differentiation rate (number of HuC/D+ cells on total) in transfected cells 40h after transfection in control, AZI1-Nter, AZI1-Nter+ Δ Mib1 and Δ Mib1 transfected spinal cords. Data represent mean \pm SEM, *** p <0.001 (Student's t test), n=15, 19, 18 and 18 sections were analyzed for control, AZI1-Nter, AZI1-Nter+ Δ Mib1 and Δ Mib1 conditions, respectively. D, Transverse sections of the neural tube from control and AZI1-Nter transfected embryos incubated 1h with EdU (red) and stained for the progenitor marker Sox2 (green). The white arrowheads indicate the numerous ectopic cycling cells observed in the AZI1-Nter situation.

Bibliography

- Aaku-Saraste, E., A. Hellwig, and W.B. Huttner. 1996. Loss of Occludin and functional tight junctions, but not ZO-1, during neural tube closure - Remodeling of the neuroepithelium prior to neurogenesis. *Dev Biol.* 180:664-679.
- Abe, K., and M. Takeichi. 2008. EPLIN mediates linkage of the cadherin catenin complex to F-actin and stabilizes the circumferential actin belt. *Proc Natl Acad Sci U S A.* 105:13-19.
- Abranches, E., M. Silva, L. Pradier, H. Schulz, O. Hummel, D. Henrique, and E. Bekman. 2009. Neural differentiation of embryonic stem cells in vitro: a road map to neurogenesis in the embryo. *PLoS One.* 4:e6286.
- Acquaviva, C., V. Chevrier, J.P. Chauvin, G. Fournier, D. Birnbaum, and O. Rosnet. 2009. The centrosomal FOP protein is required for cell cycle progression and survival. *Cell Cycle.* 8:1217-1227.
- Afonso, C., and D. Henrique. 2006. PAR3 acts as a molecular organizer to define the apical domain of chick neuroepithelial cells. *J Cell Sci.* 119:4293-4304.
- Agius, E., S. Bel-Vialar, F. Bonnet, and F. Pituello. 2015. Cell cycle and cell fate in the developing nervous system: the role of CDC25B phosphatase. *Cell Tissue Res.* 359:201-213.
- Aguirre-Ghiso, J.A., L. Ossowski, and S.K. Rosenbaum. 2004. Green Fluorescent Protein Tagging of Extracellular Signal-Regulated Kinase and p38 Pathways Reveals Novel Dynamics of Pathway Activation during Primary and Metastatic Growth. *Cancer Res.* 64:7336-7345.
- Ahlstrom, J.D., and C.A. Erickson. 2009. The neural crest epithelial-mesenchymal transition in 4D: a 'tail' of multiple non-obligatory cellular mechanisms. *Development.* 136:1801-1812.
- Alexandre, P., A.M. Reugels, D. Barker, E. Blanc, and J.D. Clarke. 2010. Neurons derive from the more apical daughter in asymmetric divisions in the zebrafish neural tube. *Nat Neurosci.* 13:673-679.
- Alvarez-Medina, R., G. Le Dreau, M. Ros, and E. Marti. 2009. Hedgehog activation is required upstream of Wnt signalling to control neural progenitor proliferation. *Development.* 136:3301-3309.
- Arai, Y., J.N. Pulvers, C. Haffner, B. Schilling, I. Nusslein, F. Calegari, and W.B. Huttner. 2011. Neural stem and progenitor cells shorten S-phase on commitment to neuron production. *Nat Commun.* 2:154.
- Artavanis-Tsakonas, S., M.A. Muskavitch, and B. Yedvobnick. 1983. Molecular cloning of Notch, a locus affecting neurogenesis in *Drosophila melanogaster*. *PNAS.* 80:1977-1981.
- Artavanis-Tsakonas, S., M.D. Rand, and R.J. Lake. 1999. Notch Signaling: Cell Fate Control and Signal Integration in Development. *Science.* 284:770-776.
- Aster, J.C., W.S. Pear, and S.C. Blacklow. 2017. The Varied Roles of Notch in Cancer. *Annu Rev Pathol.* 12:245-275.
- Baek, C., L. Freem, R. Goiaime, H. Sang, X. Morin, and S. Tozer. 2018. Mib1 prevents Notch Cis-inhibition to defer differentiation and preserve neuroepithelial integrity during neural delamination. *PLoS Biol.* 16:e2004162.
- Baye, L.M., and B.A. Link. 2007. Interkinetic nuclear migration and the selection of neurogenic cell divisions during vertebrate retinogenesis. *J Neurosci.* 27:10143-10152.
- Becam, I., U.M. Fiuza, A.M. Arias, and M. Milan. 2010. A role of receptor Notch in ligand cis-inhibition in *Drosophila*. *Curr Biol.* 20:554-560.

- Benhra, N., F. Vignaux, A. Dussert, F. Schweisguth, and R. Le Borgne. 2010. Neuralized Promotes Basal to Apical Transcytosis of Delta in Epithelial Cells. *Mol Biol Cell*. 21:2078-2086.
- Berndt, J.D., M.R. Clay, T. Langenberg, and M.C. Halloran. 2008. Rho-kinase and myosin II affect dynamic neural crest cell behaviors during epithelial to mesenchymal transition in vivo. *Dev Biol*. 324:236-244.
- Bertrand, N., D.S. Castro, and F. Guillemot. 2002. Proneural genes and the specification of neural cell types. *Nat Rev Neurosci*. 3:517-530.
- Betschinger, J., K. Mechtler, and J.A. Knoblich. 2006. Asymmetric segregation of the tumor suppressor brat regulates self-renewal in Drosophila neural stem cells. *Cell*. 124:1241-1253.
- Borrell, V., A. Cardenas, G. Ciceri, J. Galceran, N. Flames, R. Pla, S. Nobrega-Pereira, C. Garcia-Frigola, S. Peregrin, Z. Zhao, L. Ma, M. Tessier-Lavigne, and O. Marin. 2012. Slit/Robo signaling modulates the proliferation of central nervous system progenitors. *Neuron*. 76:338-352.
- Bray, S.J. 2006. Notch signalling: a simple pathway becomes complex. *Nat Rev Mol Cell Biol*. 7:678-689.
- Bray, S.J. 2016. Notch signalling in context. *Nat Rev Mol Cell Biol*. 17:722-735.
- Bultje, R.S., D.R. Castaneda-Castellanos, L.Y. Jan, Y.N. Jan, A.R. Kriegstein, and S.H. Shi. 2009. Mammalian Par3 regulates progenitor cell asymmetric division via notch signaling in the developing neocortex. *Neuron*. 63:189-202.
- Calegari, F., W. Haubensak, C. Haffner, and W.B. Huttner. 2005. Selective lengthening of the cell cycle in the neurogenic subpopulation of neural progenitor cells during mouse brain development. *J Neurosci*. 25:6533-6538.
- Calegari, F., and W.B. Huttner. 2003. An inhibition of cyclin-dependent kinases that lengthens, but does not arrest, neuroepithelial cell cycle induces premature neurogenesis. *J Cell Sci*. 116:4947-4955.
- Capaccione, K.M., and S.R. Pine. 2013. The Notch signaling pathway as a mediator of tumor survival. *Carcinogenesis*. 34:1420-1430.
- Cappello, S., P. Monzo, and R.B. Vallee. 2011. NudC is required for interkinetic nuclear migration and neuronal migration during neocortical development. *Dev Biol*. 357:326-335.
- Castro, D.S., D. Skowronska-Krawczyk, O. Armant, I.J. Donaldson, C. Parras, C. Hunt, J.A. Critchley, L. Nguyen, A. Gossler, B. Gottgens, J.M. Matter, and F. Guillemot. 2006. Proneural bHLH and Brn Proteins Coregulate a Neurogenic Program through Cooperative Binding to a Conserved DNA Motif. *Dev Cell*. 11:831-844.
- Chapman, G., D.B. Sparrow, E. Kremmer, and S.L. Dunwoodie. 2011. Notch inhibition by the ligand DELTA-LIKE 3 defines the mechanism of abnormal vertebral segmentation in spondylocostal dysostosis. *Hum Mol Genet*. 20:905-916.
- Chen, J., N. Imanaka, J. Chen, and J.D. Griffin. 2010. Hypoxia potentiates Notch signaling in breast cancer leading to decreased E-cadherin expression and increased cell migration and invasion. *Br J Cancer*. 102:351-360.
- Chenn, A., and S.K. McConnell. 1995. Cleavage orientation and the asymmetric inheritance of Notch1 immunoreactivity in mammalian neurogenesis. *Cell*. 82:631-641.
- Cheung, M., M.C. Chaboissier, A. Mynett, E. Hirst, A. Schedl, and J. Briscoe. 2005. The transcriptional control of trunk neural crest induction, survival, and delamination. *Dev Cell*. 8:179-192.

- Chitnis, A.B. 1995. The Role of Notch in Lateral Inhibition and Cell Fate Specification. *Mol Cell Neurosci.* 6:311-321.
- Choe, E.A., L. Liao, J.Y. Zhou, D. Cheng, D.M. Duong, P. Jin, L.H. Tsai, and J. Peng. 2007. Neuronal morphogenesis is regulated by the interplay between cyclin-dependent kinase 5 and the ubiquitin ligase mind bomb 1. *J Neurosci.* 27:9503-9512.
- Chowdhury, F., I.T. Li, T.T. Ngo, B.J. Leslie, B.C. Kim, J.E. Sokoloski, E. Weiland, X. Wang, Y.R. Chemla, T.M. Lohman, and T. Ha. 2016. Defining Single Molecular Forces Required for Notch Activation Using Nano Yoyo. *Nano Lett.* 16:3892-3897.
- Chung, M.I., N.M. Nascone-Yoder, S.A. Grover, T.A. Drysdale, and J.B. Wallingford. 2010. Direct activation of Shroom3 transcription by Pitx proteins drives epithelial morphogenesis in the developing gut. *Development.* 137:1339-1349.
- Clark, B.S., S. Cui, J.B. Miesfeld, O. Klezovitch, V. Vasioukhin, and B.A. Link. 2012. Loss of Llg1 in retinal neuroepithelia reveals links between apical domain size, Notch activity and neurogenesis. *Development.* 139:1599-1610.
- Clay, M.R., and M.C. Halloran. 2013. Rho activation is apically restricted by Arhgap1 in neural crest cells and drives epithelial-to-mesenchymal transition. *Development.* 140:3198-3209.
- Cohen, M., M. Georgiou, N.L. Stevenson, M. Miodownik, and B. Baum. 2010. Dynamic filopodia transmit intermittent Delta-Notch signaling to drive pattern refinement during lateral inhibition. *Dev Cell.* 19:78-89.
- Coles, E.G., L.A. Taneyhill, and M. Bronner-Fraser. 2007. A critical role for Cadherin6B in regulating avian neural crest emigration. *Dev Biol.* 312:533-544.
- Cong, L., F. Ann Ran, D. Cox, S. Lin, R. Barretto, N. Habib, P.D. Hsu, X. Wu, W. Jiang, L.A. Marraffini, and F. Zhang. 2013. Multiplex Genome Engineering Using CRISPR/Cas Systems. *Science.* 339.
- Cordes, R., K. Schuster-Gossler, K. Serth, and A. Gossler. 2004. Specification of vertebral identity is coupled to Notch signalling and the segmentation clock. *Development.* 131:1221-1233.
- Cordle, J., S. Johnson, J.Z. Tay, P. Roversi, M.B. Wilkin, B.H. de Madrid, H. Shimizu, S. Jensen, P. Whiteman, B. Jin, C. Redfield, M. Baron, S.M. Lea, and P.A. Handford. 2008. A conserved face of the Jagged/Serrate DSL domain is involved in Notch trans-activation and cis-inhibition. *Nat Struct Mol Biol.* 15:849-857.
- Costa, M.R., G. Wen, A. Lepier, T. Schroeder, and M. Gotz. 2008. Par-complex proteins promote proliferative progenitor divisions in the developing mouse cerebral cortex. *Development.* 135:11-22.
- Couturier, L., N. Vodovar, and F. Schweisguth. 2012. Endocytosis by Numb breaks Notch symmetry at cytokinesis. *Nat Cell Biol.* 14:131-139.
- Cuadrado, A., and A.R. Nebreda. 2010. Mechanisms and functions of p38 MAPK signalling. *Biochem J.* 429:403-417.
- D'Souza, B., L. Meloty-Kapella, and G. Weinmaster. 2010. Canonical and Non-Canonical Notch Ligands. *Curr Top Dev Biol.* 92:73-129.
- Dady, A., C. Blavet, and J.-L. Duband. 2012. Timing and kinetics of E- to N-cadherin switch during neurulation in the avian embryo. *Dev Dyn.* 241:1333-1349.
- Das, D., J.K. Zalewski, S. Mohan, T.F. Plageman, A.P. VanDemark, and J.D. Hildebrand. 2014. The interaction between Shroom3 and Rho-kinase is required for neural tube morphogenesis in mice. *Biol Open.* 3:850-860.
- Das, R.M., and K.G. Storey. 2012. Mitotic spindle orientation can direct cell fate and bias Notch activity in chick neural tube. *EMBO Rep.* 13:448-454.

- Das, R.M., and K.G. Storey. 2014. Apical abscission alters cell polarity and dismantles the primary cilium during neurogenesis. *Science*. 343:200-204.
- Dasen, J.S., and T.M. Jessell. 2009. Chapter Six Hox Networks and the Origins of Motor Neuron Diversity. 88:169-200.
- Daskalaki, A., N.A. Shalaby, K. Kux, G. Tsoumpekou, G.D. Tsibidis, M.A. Muskavitch, and C. Delidakis. 2011. Distinct intracellular motifs of Delta mediate its ubiquitylation and activation by Mindbomb1 and Neuralized. *J Cell Biol*. 195:1017-1031.
- de Celis, J.F., and S. Bray. 1997. Feed-back mechanisms affecting Notch activation at the dorsoventral boundary in the Drosophila wing. *Development*. 124:3241-3251.
- Dehay, C., and H. Kennedy. 2007. Cell-cycle control and cortical development. *Nat Rev Neurosci*. 8:438-450.
- del Alamo, D., H. Rouault, and F. Schweisguth. 2011. Mechanism and significance of cis-inhibition in Notch signalling. *Curr Biol*. 21:R40-47.
- Del Bene, F., A.M. Wehman, B.A. Link, and H. Baier. 2008. Regulation of neurogenesis by interkinetic nuclear migration through an apical-basal notch gradient. *Cell*. 134:1055-1065.
- Delaunay, D., V. Cortay, D. Patti, K. Knoblauch, and C. Dehay. 2014. Mitotic spindle asymmetry: a Wnt/PCP-regulated mechanism generating asymmetrical division in cortical precursors. *Cell Rep*. 6:400-414.
- Delaunay, D., M.C. Robini, and C. Dehay. 2015. Mitotic spindle asymmetry in rodents and primates: 2D vs. 3D measurement methodologies. *Front Cell Neurosci*. 9:33.
- Dessaud, E., A.P. McMahon, and J. Briscoe. 2008. Pattern formation in the vertebrate neural tube: a sonic hedgehog morphogen-regulated transcriptional network. *Development*. 135:2489-2503.
- Dexter, J.S. 1914. The analysis of a case of continuous variation in Drosophila by a study of its linkage relations. *The American Naturalist*. 48:717-758.
- di Pietro, F., A. Echard, and X. Morin. 2016. Regulation of mitotic spindle orientation: an integrated view. *EMBO Rep*. 17:1106-1130.
- Diez Del Corral, R., and A.V. Morales. 2017. The Multiple Roles of FGF Signaling in the Developing Spinal Cord. *Front Cell Dev Biol*. 5:58.
- Diez del Corral, R., I. Olivera-Martinez, A. Goriely, E. Gale, M. Maden, and K. Storey. 2003. Opposing FGF and retinoid pathways control ventral neural pattern, neuronal differentiation, and segmentation during body axis extension. *Neuron*. 40:65-79.
- Diez del Corral, R., and K.G. Storey. 2004. Opposing FGF and retinoid pathways: a signalling switch that controls differentiation and patterning onset in the extending vertebrate body axis. *Bioessays*. 26:857-869.
- Dong, Z., N. Yang, S.Y. Yeo, A. Chitnis, and S. Guo. 2012. Intralinear directional Notch signaling regulates self-renewal and differentiation of asymmetrically dividing radial glia. *Neuron*. 74:65-78.
- Dornseifer, P., C. Takke, and J.A. Campos-Ortega. 1997. Overexpression of a zebrafish homologue of the Drosophila neurogenic gene Delta perturbs differentiation of primary neurons and somite development. *Mech Dev*. 63:159-171.
- Dottori, M., M.K. Gross, P. Labosky, and M. Goulding. 2001. The winged-helix transcription factor Foxd3 suppresses interneuron differentiation and promotes neural crest cell fate. *Development*. 128:4127-4138.
- Dunwoodie, S.L., M. Clements, D.B. Sparrow, X. Sa, R.A. Conlon, and R.S.P. Beddington. 2002. Axial skeletal defects caused by mutation in the spondylocostal dysplasia/pudgy

- gene *Dll3* are associated with disruption of the segmentation clock within the presomitic mesoderm. *Development*. 129:1795-1806.
- Dupin, E., and N.M. Le Douarin. 2014. The Neural Crest, A Multifaceted Structure of the Vertebrates. *Birth Defects Research*.
- Edelstein, A., N. Amodaj, K. Hoover, R. Vale, and N. Stuurman. 2010. Computer control of microscopes using microManager. *Curr Protoc Mol Biol*. Chapter 14:Unit14 20.
- Ellisen, L.W., J. Bird, D.C. West, A.L. Soreng, T.C. Reynolds, S.D. Smith, and J. Sklar. 1991. TAN-1, the human homolog of the drosophila Notch gene, is broken by chromosomal translocations in T lymphoblastic neoplasms. *Cell*. 66.
- Emery, G., A. Hutterer, D. Berdnik, B. Mayer, F. Wirtz-Peitz, M.G. Gaitan, and J.A. Knoblich. 2005. Asymmetric Rab 11 endosomes regulate delta recycling and specify cell fate in the *Drosophila* nervous system. *Cell*. 122:763-773.
- Eom, D.S., E.J. Bain, L.B. Patterson, M.E. Grout, and D.M. Parichy. 2015. Long-distance communication by specialized cellular projections during pigment pattern development and evolution. *Elife*. 4.
- Ernst, S., K. Liu, S. Agarwala, N. Moratscheck, M.E. Avci, D. Dalle Nogare, A.B. Chitnis, O. Ronneberger, and V. Lecaudey. 2012. Shroom3 is required downstream of FGF signalling to mediate proneuromast assembly in zebrafish. *Development*. 139:4571-4581.
- Farkas, L.M., and W.B. Huttner. 2008. The cell biology of neural stem and progenitor cells and its significance for their proliferation versus differentiation during mammalian brain development. *Curr Opin Cell Biol*. 20:707-715.
- Fiddes, I.T., G.A. Lodewijk, M. Mooring, C.M. Bosworth, A.D. Ewing, G.L. Mantalas, A.M. Novak, A. van den Bout, A. Bishara, J.L. Rosenkrantz, R. Lorig-Roach, A.R. Field, M. Haeussler, L. Russo, A. Bhaduri, T.J. Nowakowski, A.A. Pollen, M.L. Dougherty, X. Nuttle, M.C. Addor, S. Zwolinski, S. Katzman, A. Kriegstein, E.E. Eichler, S.R. Salama, F.M.J. Jacobs, and D. Haussler. 2018. Human-Specific NOTCH2NL Genes Affect Notch Signaling and Cortical Neurogenesis. *Cell*. 173:1356-1369 e1322.
- Fiuza, U.M., and A.M. Arias. 2007. Cell and molecular biology of Notch. *J Endocrinol*. 194:459-474.
- Florio, M., and W.B. Huttner. 2014. Neural progenitors, neurogenesis and the evolution of the neocortex. *Development*. 141:2182-2194.
- Fortini, M.E., and D. Bilder. 2009. Endocytic regulation of Notch signaling. *Curr Opin Genet Dev*. 19:323-328.
- Furukawa, T., S. Murkherjee, Z. Bao, E.M. Morrow, and C.L. Cepko. 2000. *rax*, *Hes1*, and *notch1* Promote the Formation of Muller Glia by Postnatal Retinal Progenitor Cells. *Neuron*. 26:383-394.
- Gaestel, M. 2006. MAPKAP kinases - MKs - two's company, three's a crowd. *Nat Rev Mol Cell Biol*. 7:120-130.
- Gaiano, N., J.S. Nye, and G. Fishell. 2000. Radial glial identity is promoted by Notch1 signaling in the murine forebrain. *Neuron*. 26:395-404.
- Ge, X., C.L. Frank, F. Calderon de Anda, and L.H. Tsai. 2010. Hook3 interacts with PCM1 to regulate pericentriolar material assembly and the timing of neurogenesis. *Neuron*. 65:191-203.
- Geffers, I., K. Serth, G. Chapman, R. Jaekel, K. Schuster-Gossler, R. Cordes, D.B. Sparrow, E. Kremmer, S.L. Dunwoodie, T. Klein, and A. Gossler. 2007. Divergent functions and distinct localization of the Notch ligands *DLL1* and *DLL3* in vivo. *J Cell Biol*. 178:465-476.

- Gil-Sanz, C., B. Landeira, C. Ramos, M.R. Costa, and U. Muller. 2014. Proliferative defects and formation of a double cortex in mice lacking *Mltt4* and *Cdh2* in the dorsal telencephalon. *J Neurosci.* 34:10475-10487.
- Gilbert, S.F. 2013. *Developmental Biology.*
- Glittenberg, M., C. Pitsouli, C. Garvey, C. Delidakis, and S. Bray. 2006. Role of conserved intracellular motifs in Serrate signalling, cis-inhibition and endocytosis. *EMBO J.* 25:4697-4706.
- Godin, J.D., K. Colombo, M. Molina-Calavita, G. Keryer, D. Zala, B.C. Charrin, P. Dietrich, M.L. Volvert, F. Guillemot, I. Dragatsis, Y. Bellaiche, F. Saudou, L. Nguyen, and S. Humbert. 2010. Huntingtin is required for mitotic spindle orientation and mammalian neurogenesis. *Neuron.* 67:392-406.
- Gohlke, J.M., O. Armant, F.M. Parham, M.V. Smith, C. Zimmer, D.S. Castro, L. Nguyen, J.S. Parker, G. Gradwohl, C.J. Portier, and F. Guillemot. 2008. Characterization of the proneural gene regulatory network during mouse telencephalon development. *BMC Biol.* 6:15.
- Gordon, W.R., B. Zimmerman, L. He, L.J. Miles, J. Huang, K. Tiyanont, D.G. McArthur, J.C. Aster, N. Perrimon, J.J. Loparo, and S.C. Blacklow. 2015. Mechanical Allostery: Evidence for a Force Requirement in the Proteolytic Activation of Notch. *Dev Cell.* 33:729-736.
- Gotz, M., and W.B. Huttner. 2005. The cell biology of neurogenesis. *Nat Rev Mol Cell Biol.* 6:777-788.
- Gray, G.E., J.C. Glover, J. Majors, and J.R. Sanes. 1988. Radial arrangement of clonally related cells in the chicken optic tectum: lineage analysis with a recombinant retrovirus. *Proc Natl Acad Sci U S A.* 85:7356-7360.
- Gui, H., S. Li, and M.P. Matisse. 2007. A cell-autonomous requirement for Cip/Kip cyclin-kinase inhibitors in regulating neuronal cell cycle exit but not differentiation in the developing spinal cord. *Dev Biol.* 301:14-26.
- Haddon, C., Y.-J. Jiang, L. Smithers, and J. Lewis. 1998. Delta-Notch signalling and the patterning of sensory cell differentiation in the zebrafish ear: evidence from the mind bomb mutant. *Development.* 125:4637-4644.
- Hamada, H., M. Watanabe, H.E. Lau, T. Nishida, T. Hasegawa, D.M. Parichy, and S. Kondo. 2014. Involvement of Delta/Notch signaling in zebrafish adult pigment stripe patterning. *Development.* 141:318-324.
- Hamburger, V., and H.L. Hamilton. 1992. A series of normal stages in the development of the chick embryo. 1951. *Dev Dyn.* 195:231-272.
- Hammerle, B., and F.J. Tejedor. 2007. A novel function of DELTA-NOTCH signalling mediates the transition from proliferation to neurogenesis in neural progenitor cells. *PLoS One.* 2:e1169.
- Hatakeyama, J., Y. Bessho, K. Katoh, S. Ookawara, M. Fujioka, F. Guillemot, and R. Kageyama. 2004. Hes genes regulate size, shape and histogenesis of the nervous system by control of the timing of neural stem cell differentiation. *Development.* 131:5539-5550.
- Hatakeyama, J., Y. Wakamatsu, A. Nagafuchi, R. Kageyama, R. Shigemoto, and K. Shimamura. 2014. Cadherin-based adhesions in the apical endfoot are required for active Notch signaling to control neurogenesis in vertebrates. *Development.* 141:1671-1682.
- Haubensak, W., A. Attardo, W. Denk, and W.B. Huttner. 2004. Neurons arise in the basal neuroepithelium of the early mammalian telencephalon: A major site of neurogenesis. *PNAS.* 101:3196-3201.

- Heng, J.I., L. Nguyen, D.S. Castro, C. Zimmer, H. Wildner, O. Armant, D. Skowronska-Krawczyk, F. Bedogni, J.M. Matter, R. Hevner, and F. Guillemot. 2008. Neurogenin 2 controls cortical neuron migration through regulation of Rnd2. *Nature*. 455:114-118.
- Henrique, D., J. Adam, A. Myat, A. Chitnis, J. Lewis, and D. Ish-Horowicz. 1995. Expression of a Delta homologue in prospective neurons in the chick. *Nature*. 375:787-790.
- Henrique, D., E. Hirsinger, J. Adam, I. Le Roux, P. O., D. Ish-Horowicz, and J. Lewis. 1997. Maintenance of neuroepithelial progenitor cells by Delta–Notch signalling in the embryonic chick retina. *Curr Biol*. 7:661-670.
- Heuss, S.F., D. Ndiaye-Lobry, E.M. Six, A. Israel, and F. Logeat. 2008. The intracellular region of Notch ligands Dll1 and Dll3 regulates their trafficking and signaling activity. *PNAS*. 105:11212-11217.
- Hicke, L. 2001. Protein regulation by monoubiquitin. *Nat Rev Mol Cell Biol*. 2:195-201.
- Hildebrand, J.D., and P. Soriano. 1999. Shroom, a PDZ domain-containing actin-binding protein, is required for neural tube morphogenesis in mice. *Cell*. 99.
- Hiscock, T.W., J.B. Miesfeld, K.R. Mosaliganti, B.A. Link, and S.G. Megason. 2018. Feedback between tissue packing and neurogenesis in the zebrafish neural tube. *Development*. 145.
- Hoyne, G.F., G. Chapman, Y. Sontani, S.E. Pursglove, and S.L. Dunwoodie. 2011. A cell autonomous role for the Notch ligand Delta-like 3 in $\alpha\beta$ T-cell development. *Immunology and Cell Biology*. 89:696-705.
- Hunter, G.L., Z. Hadjivasiliou, H. Bonin, L. He, N. Perrimon, G. Charras, and B. Baum. 2016. Coordinated control of Notch/Delta signalling and cell cycle progression drives lateral inhibition-mediated tissue patterning. *Development*. 143:2305-2310.
- Huttner, W.B., and Y. Kosodo. 2005. Symmetric versus asymmetric cell division during neurogenesis in the developing vertebrate central nervous system. *Curr Opin Cell Biol*. 17:648-657.
- Iacopetti, P., M. Michelini, I. Stuckmann, B. Oback, E. Aaku-Saraste, and W.B. Huttner. 1999. Expression of the antiproliferative gene TIS21 at the onset of neurogenesis identifies single neuroepithelial cells that switch from proliferative to neuron-generating division. *PNAS*. 96:4639-4644.
- Ignatova, T.N., V.G. Kukekov, E.D. Laywell, O.N. Suslov, F.D. Vrionis, and D.A. Steindler. 2002. Human cortical glial tumors contain neural stem-like cells expressing astroglial and neuronal markers in vitro. *Glia*. 39:193-206.
- Imayoshi, I., A. Isomura, Y. Harima, K. Kawaguchi, H. Kori, H. Miyachi, T. Fujiwara, F. Ishidate, and R. Kageyama. 2013. Oscillatory control of factors determining multipotency and fate in mouse neural progenitors. *Science*. 342.
- Imayoshi, I., and R. Kageyama. 2014. bHLH factors in self-renewal, multipotency, and fate choice of neural progenitor cells. *Neuron*. 82:9-23.
- Imayoshi, I., M. Sakamoto, M. Yamaguchi, K. Mori, and R. Kageyama. 2010. Essential Roles of Notch Signaling in Maintenance of Neural Stem Cells in Developing and Adult Brains. *J Neurosci*. 30:3489-3498.
- Inoue, M., R. Iwai, H. Tabata, D. Konno, M. Komabayashi-Suzuki, C. Watanabe, H. Iwanari, Y. Mochizuki, T. Hamakubo, F. Matsuzaki, K.I. Nagata, and K.I. Mizutani. 2017. Prdm16 is crucial for progression of the multipolar phase during neural differentiation of the developing neocortex. *Development*. 144:385-399.
- Insolera, R., H. Bazzi, W. Shao, K.V. Anderson, and S.H. Shi. 2014. Cortical neurogenesis in the absence of centrioles. *Nat Neurosci*. 17:1528-1535.

- Itoh, M., C.H. Kim, G. Parlardy, T. Oda, Y.J. Jiang, D. Maust, S.Y. Yeo, K. Lorick, G.J. Wright, L. Ariza-McNaughton, A.M. Weissman, J. Lewis, S.C. Chandrasekharappa, and A. Chitnis. 2003. Mind Bomb Is a Ubiquitin Ligase that Is Essential for Efficient Activation of Notch Signaling by Delta. *Dev Cell*. 4:67-82.
- Itoh, Y., Y. Moriyama, T. Hasegawa, T.A. Endo, T. Toyoda, and Y. Gotoh. 2013. Scratch regulates neuronal migration onset via an epithelial-mesenchymal transition-like mechanism. *Nat Neurosci*. 16:416-425.
- Jafar-Nejad, H., H.K. Andrews, M. Acar, V. Bayat, F. Wirtz-Peitz, S.Q. Mehta, J.A. Knoblich, and H.J. Bellen. 2005. Sec15, a component of the exocyst, promotes notch signaling during the asymmetric division of Drosophila sensory organ precursors. *Dev Cell*. 9:351-363.
- Januschke, J., S. Llamazares, J. Reina, and C. Gonzalez. 2011. Drosophila neuroblasts retain the daughter centrosome. *Nat Commun*. 2:243.
- Jessell, T.M. 2000. Neuronal specification in the spinal cord: inductive signals and transcriptional codes. *Nat Rev Genet*. 1:20-29.
- Kadowaki, M., S. Nakamura, O. Machon, S. Krauss, G.L. Radice, and M. Takeichi. 2007. N-cadherin mediates cortical organization in the mouse brain. *Dev Biol*. 304:22-33.
- Kageyama, R., T. Ohtsuka, J. Hatakeyama, and R. Ohsawa. 2005. Roles of bHLH genes in neural stem cell differentiation. *Exp Cell Res*. 306:343-348.
- Kageyama, R., T. Ohtsuka, H. Shimojo, and I. Imayoshi. 2008. Dynamic Notch signaling in neural progenitor cells and a revised view of lateral inhibition. *Nat Neurosci*. 11:1247-1251.
- Kang, K., D. Lee, S. Hong, S.G. Park, and M.R. Song. 2013. The E3 ligase Mind bomb-1 (Mib1) modulates Delta-Notch signaling to control neurogenesis and gliogenesis in the developing spinal cord. *J Biol Chem*. 288:2580-2592.
- Kasioulis, I., R.M. Das, and K.G. Storey. 2017. Inter-dependent apical microtubule and actin dynamics orchestrate centrosome retention and neuronal delamination. *Elife*. 6.
- Katajisto, P., J. Dohla, C.L. Chaffer, N. Pentinmikko, N. Marjanovic, S. Iqbal, R. Zoncu, W. Chen, R.A. Weinberg, and D.M. Sabatini. 2015. Asymmetric apportioning of aged mitochondria between daughter cells is required for stemness. *Science*. 348:340-343.
- Kawaguchi, D., S. Furutachi, H. Kawai, K. Hozumi, and Y. Gotoh. 2013. Dll1 maintains quiescence of adult neural stem cells and segregates asymmetrically during mitosis. *Nat Commun*. 4:1880.
- Kawaguchi, D., T. Yoshimatsu, K. Hozumi, and Y. Gotoh. 2008. Selection of differentiating cells by different levels of delta-like 1 among neural precursor cells in the developing mouse telencephalon. *Development*. 135:3849-3858.
- Khacho, M., A. Clark, D.S. Svoboda, J. Azzi, J.G. MacLaurin, C. Meghaizel, H. Sesaki, D.C. Lagace, M. Germain, M.E. Harper, D.S. Park, and R.S. Slack. 2016. Mitochondrial Dynamics Impacts Stem Cell Identity and Fate Decisions by Regulating a Nuclear Transcriptional Program. *Cell Stem Cell*. 19:232-247.
- Khacho, M., A. Clark, D.S. Svoboda, J.G. MacLaurin, D.C. Lagace, D.S. Park, and R.S. Slack. 2017. Mitochondrial dysfunction underlies cognitive defects as a result of neural stem cell depletion and impaired neurogenesis. *Hum Mol Genet*. 26:3327-3341.
- Khacho, M., and R.S. Slack. 2018. Mitochondrial Dynamics in the Regulation of Neurogenesis: From Development to the Adult Brain. *Dev Dyn*. 247:47-53.
- Khait, I., Y. Orsher, O. Golan, U. Binshtok, N. Gordon-Bar, L. Amir-Zilberstein, and D. Sprinzak. 2016. Quantitative Analysis of Delta-like 1 Membrane Dynamics Elucidates the Role of Contact Geometry on Notch Signaling. *Cell Rep*. 14:225-233.

- Kidd, S., T.J. Lockett, and M.W. Young. 1983. The Notch locus of *Drosophila melanogaster*. *Cell*. 34:421-433.
- Kim, S.M., M.Y. Kim, E.J. Ann, J.S. Mo, J.H. Yoon, and H.S. Park. 2012. Presenilin-2 regulates the degradation of RBP-Jk protein through p38 mitogen-activated protein kinase. *J Cell Sci*. 125:1296-1308.
- Klein, T., K. Brennan, and A.M. Arias. 1997. An intrinsic dominant negative activity of serrate that is modulated during wing development in *Drosophila*. *Dev Biol*. 189:123-134.
- Knoblich, J.A. 2008. Mechanisms of asymmetric stem cell division. *Cell*. 132:583-597.
- Knoblich, J.A., L.Y. Jan, and Y.N. Jan. 1995. Asymmetric segregation of Numb and Prospero during cell division. *Nature*. 377:624-627.
- Kobielak, A., H.A. Pasolli, and E. Fuchs. 2004. Mammalian formin-1 participates in adherens junctions and polymerization of linear actin cables. *Nat Cell Biol*. 6:21-30.
- Komatsu, H., M.Y. Chao, J. Larkins-Ford, M.E. Corkins, G.A. Somers, T. Tucey, H.M. Dionne, J.Q. White, K. Wani, M. Boxem, and A.C. Hart. 2008. OSM-11 facilitates LIN-12 Notch signaling during *Caenorhabditis elegans* vulval development. *PLoS Biol*. 6:e196.
- Konno, D., G. Shioi, A. Shitamukai, A. Mori, H. Kiyonari, T. Miyata, and F. Matsuzaki. 2008. Neuroepithelial progenitors undergo LGN-dependent planar divisions to maintain self-renewability during mammalian neurogenesis. *Nat Cell Biol*. 10:93-101.
- Koo, B.K., H.S. Lim, R. Song, M.J. Yoon, K.J. Yoon, J.S. Moon, Y.W. Kim, M.C. Kwon, K.W. Yoo, M.P. Kong, J. Lee, A.B. Chitnis, C.H. Kim, and Y.Y. Kong. 2005. Mind bomb 1 is essential for generating functional Notch ligands to activate Notch. *Development*. 132:3459-3470.
- Koo, B.K., M.J. Yoon, K.J. Yoon, S.K. Im, Y.Y. Kim, C.H. Kim, P.G. Suh, Y.N. Jan, and Y.Y. Kong. 2007. An obligatory role of mind bomb-1 in notch signaling of mammalian development. *PLoS One*. 2:e1221.
- Kopan, R., and M.X. Ilagan. 2009. The canonical Notch signaling pathway: unfolding the activation mechanism. *Cell*. 137:216-233.
- Kosodo, Y., K. Roper, W. Haubensak, A.-M. Marzesco, D. Corbeil, and W.B. Huttner. 2004. Asymmetric distribution of the apical plasma membrane during neurogenic divisions of mammalian neuroepithelial cells. *EMBO J*. 23:2314-2324.
- Kosodo, Y., T. Suetsugu, M. Suda, Y. Mimori-Kiyosue, K. Toida, S.A. Baba, A. Kimura, and F. Matsuzaki. 2011. Regulation of interkinetic nuclear migration by cell cycle-coupled active and passive mechanisms in the developing brain. *EMBO J*. 30:1690-1704.
- Kosodo, Y., K. Toida, V. Dubreuil, P. Alexandre, J. Schenk, E. Kiyokage, A. Attardo, F. Mora-Bermudez, T. Arai, J.D. Clarke, and W.B. Huttner. 2008. Cytokinesis of neuroepithelial cells can divide their basal process before anaphase. *EMBO J*. 27:3151-3163.
- Kovall, R.A., and S.C. Blacklow. 2010. Mechanistic insights into Notch receptor signaling from structural and biochemical studies. *Curr Top Dev Biol*. 92:31-71.
- Kovall, R.A., B. Gebelein, D. Sprinzak, and R. Kopan. 2017. The Canonical Notch Signaling Pathway: Structural and Biochemical Insights into Shape, Sugar, and Force. *Dev Cell*. 41:228-241.
- Kressman, S., C. Campos, I. Castanon, M. Furthauer, and M. Gonzalez-Gaitan. 2015. Directional Notch trafficking in Sara endosomes during asymmetric cell division in the spinal cord. *Nat Cell Biol*. 17:333-346.
- Lacomme, M., L. Liaubet, F. Pituello, and S. Bel-Vialar. 2012. NEUROG2 drives cell cycle exit of neuronal precursors by specifically repressing a subset of cyclins acting at the G1 and S phases of the cell cycle. *Mol Cell Biol*. 32:2596-2607.

- Ladi, E., J.T. Nichols, W. Ge, A. Miyamoto, C. Yao, L.T. Yang, J. Boulter, Y.E. Sun, C. Kintner, and G. Weinmaster. 2005. The divergent DSL ligand Dll3 does not activate Notch signaling but cell autonomously attenuates signaling induced by other DSL ligands. *J Cell Biol.* 170:983-992.
- Lai, E.C., and G.M. Rubin. 2001. neuralized functions cell-autonomously to regulate a subset of notch-dependent processes during adult Drosophila development. *Dev Biol.* 231:217-233.
- Lang, R.A., K. Herman, A.B. Reynolds, J.D. Hildebrand, and T.F. Plageman, Jr. 2014. p120-catenin-dependent junctional recruitment of Shroom3 is required for apical constriction during lens pit morphogenesis. *Development.* 141:3177-3187.
- Lange, C., W.B. Huttner, and F. Calegari. 2009. Cdk4/cyclinD1 overexpression in neural stem cells shortens G1, delays neurogenesis, and promotes the generation and expansion of basal progenitors. *Cell Stem Cell.* 5:320-331.
- Le Belle, J.E., N.M. Orozco, A.A. Paucar, J.P. Saxe, J. Mottahedeh, A.D. Pyle, H. Wu, and H.I. Kornblum. 2011. Proliferative neural stem cells have high endogenous ROS levels that regulate self-renewal and neurogenesis in a PI3K/Akt-dependant manner. *Cell Stem Cell.* 8:59-71.
- Le Borgne, R., and F. Schweisguth. 2003. Notch Signaling: Endocytosis Makes Delta Signal Better. *Current Biology.* 13:R273-R275.
- Le Dreau, G., and E. Marti. 2013. The multiple activities of BMPs during spinal cord development. *Cell Mol Life Sci.* 70:4293-4305.
- Le Dreau, G., M. Saade, I. Gutierrez-Vallejo, and E. Marti. 2014. The strength of SMAD1/5 activity determines the mode of stem cell division in the developing spinal cord. *J Cell Biol.* 204:591-605.
- Lee, S.K., and S.L. Pfaff. 2003. Synchronization of Neurogenesis and Motor Neuron Specification by Direct Coupling of bHLH and Homeodomain Transcription Factors. *Neuron.* 38:731-745.
- Li, F., Y. Lan, Y. Wang, J. Wang, G. Yang, F. Meng, H. Han, A. Meng, Y. Wang, and X. Yang. 2011. Endothelial Smad4 maintains cerebrovascular integrity by activating N-cadherin through cooperation with Notch. *Dev Cell.* 20:291-302.
- Liu, Z.J., M. Xiao, K. Balint, K.S. Smalley, P. Brafford, R. Qiu, C.C. Pinnix, X. Li, and M. Herlyn. 2006. Notch1 signaling promotes primary melanoma progression by activating mitogen-activated protein kinase/phosphatidylinositol 3-kinase-Akt pathways and up-regulating N-cadherin expression. *Cancer Res.* 66:4182-4190.
- Lluis, F., E. Perdiguero, A.R. Nebreda, and P. Munoz-Canoves. 2006. Regulation of skeletal muscle gene expression by p38 MAP kinases. *Trends Cell Biol.* 16:36-44.
- Lobjois, V., S. Bel-Vialar, F. Trousse, and F. Pituello. 2008. Forcing neural progenitor cells to cycle is insufficient to alter cell-fate decision and timing of neuronal differentiation in the spinal cord. *Neural Dev.* 3:4.
- Loulier, K., J.D. Lathia, V. Marthiens, J. Relucio, M.R. Mughal, S.C. Tang, T. Coksaygan, P.E. Hall, S. Chigurupati, B. Patton, H. Colognato, M.S. Rao, M.P. Mattson, T.F. Haydar, and C. Ffrench-Constant. 2009. beta1 integrin maintains integrity of the embryonic neocortical stem cell niche. *PLoS Biol.* 7:e1000176.
- Louvi, A., and S. Artavanis-Tsakonas. 2006. Notch signalling in vertebrate neural development. *Nat Rev Neurosci.* 7:93-102.
- Louvi, A., and S. Artavanis-Tsakonas. 2012. Notch and disease: a growing field. *Semin Cell Dev Biol.* 23:473-480.
- Louvi, A., and E.A. Grove. 2011. Cilia in the CNS: the quiet organelle claims center stage. *Neuron.* 69:1046-1060.

- Lubman, O.Y., M.X. Ilagan, R. Kopan, and D. Barrick. 2007. Quantitative dissection of the Notch:CSL interaction: insights into the Notch-mediated transcriptional switch. *J Mol Biol.* 365:577-589.
- Lui, J.H., D.V. Hansen, and A.R. Kriegstein. 2011. Development and evolution of the human neocortex. *Cell.* 146:18-36.
- Luskin, M.B., A.L. Pearlman, and J.R. Sanes. 1988. Cell lineage in the cerebral cortex of the mouse studied in vivo and in vitro with a recombinant retrovirus. *Neuron.* 1:635-647.
- Ma, Y.C., M.R. Song, J.P. Park, H.Y. Henry Ho, L. Hu, M.V. Kurtev, J. Zieg, Q. Ma, S.L. Pfaff, and M.E. Greenberg. 2008. Regulation of motor neuron specification by phosphorylation of neurogenin 2. *Neuron.* 58:65-77.
- Marthiens, V., and C. French-Constant. 2009. Adherens junction domains are split by asymmetric division of embryonic neural stem cells. *EMBO Rep.* 10:515-520.
- Marthiens, V., M.A. Rujano, C. Penetier, S. Tessier, P. Paul-Gilloteaux, and R. Basto. 2013. Centrosome amplification causes microcephaly. *Nat Cell Biol.* 15:731-740.
- Masia, A., A. Almazan-Moga, P. Velasco, J. Reventos, N. Toran, J. Sanchez de Toledo, J. Roma, and S. Gallego. 2012. Notch-mediated induction of N-cadherin and alpha9-integrin confers higher invasive phenotype on rhabdomyosarcoma cells. *Br J Cancer.* 107:1374-1383.
- Matsumata, M., M. Uchikawa, Y. Kamachi, and H. Kondoh. 2005. Multiple N-cadherin enhancers identified by systematic functional screening indicate its Group B1 SOX-dependent regulation in neural and placodal development. *Dev Biol.* 286:601-617.
- Maury, Y., J. Come, R.A. Piskorowski, N. Salah-Mohellibi, V. Chevaleyre, M. Peschanski, C. Martinat, and S. Nedelec. 2015. Combinatorial analysis of developmental cues efficiently converts human pluripotent stem cells into multiple neuronal subtypes. *Nat Biotechnol.* 33:89-96.
- McKeown, S.J., V.M. Lee, M. Bronner-Fraser, D.F. Newgreen, and P.G. Farlie. 2005. Sox10 overexpression induces neural crest-like cells from all dorsoventral levels of the neural tube but inhibits differentiation. *Dev Dyn.* 233:430-444.
- McMillan, B.J., B. Schnute, N. Ohlenhard, B. Zimmerman, L. Miles, N. Beglova, T. Klein, and S.C. Blacklow. 2015. A tail of two sites: a bipartite mechanism for recognition of notch ligands by mind bomb E3 ligases. *Mol Cell.* 57:912-924.
- Megason, S.G., and A.P. McMahon. 2002. A mitogen gradient of dorsal midline Wnts organizes growth in the CNS. *Development.* 129:2087-2098.
- Meng, W., Y. Mushika, T. Ichii, and M. Takeichi. 2008. Anchorage of microtubule minus ends to adherens junctions regulates epithelial cell-cell contacts. *Cell.* 135:948-959.
- Meng, W., and M. Takeichi. 2009. Adherens junction: molecular architecture and regulation. *Cold Spring Harb Perspect Biol.* 1:a002899.
- Micchelli, C.A., E.J. Rulifson, and S.S. Blair. 1997. The function and regulation of cut expression on the wing margin of *Drosophila*: Notch, Wingless and a dominant negative role for Delta and Serrate. *Development.* 124.
- Miller, A.C., E.L. Lyons, and T.G. Herman. 2009. cis-Inhibition of Notch by endogenous Delta biases the outcome of lateral inhibition. *Curr Biol.* 19:1378-1383.
- Mils, V., S. Bosch, J. Roy, S. Bel-Vialar, P. Belenguer, F. Pituello, and M.C. Miquel. 2015. Mitochondrial reshaping accompanies neural differentiation in the developing spinal cord. *PLoS One.* 10:e0128130.
- Misson, J.-P., T. Takahashi, and V.S. Caviness. 1991. Ontogeny of radial and other astroglial cells in murine cerebral cortex. *Glia.* 4:138-148.

- Miyamoto, Y., F. Sakane, and K. Hashimoto. 2015. N-cadherin-based adherens junction regulates the maintenance, proliferation, and differentiation of neural progenitor cells during development. *Cell Adh Migr.* 9:183-192.
- Miyata, T., A. Kawaguchi, K. Saito, M. Kawano, T. Muto, and M. Ogawa. 2004. Asymmetric production of surface-dividing and non-surface-dividing cortical progenitor cells. *Development.* 131:3133-3145.
- Miyata, T., A. Kawaguchi, K. Saito, H. Kuramochi, and M. Ogawa. 2002. Visualization of cell cycling by an improvement in slice culture methods. *J Neurosci Res.* 69:861-868.
- Mohr, O.L. 1919. Character changes caused by mutation of an entire region of a chromosome in *Drosophila*. *Genetics.* 4:275-282.
- Morgan, T.H. 1917. The Theory of the gene.
- Morin, X., and Y. Bellaiche. 2011. Mitotic spindle orientation in asymmetric and symmetric cell divisions during animal development. *Dev Cell.* 21:102-119.
- Morin, X., F. Jaouen, and P. Durbec. 2007. Control of planar divisions by the G-protein regulator LGN maintains progenitors in the chick neuroepithelium. *Nat Neurosci.* 10:1440-1448.
- Morrison, S.J., S.E. Perez, Z. Qiao, J.M. Verdi, C. Hicks, G. Weinmaster, and D.J. Anderson. 2000. Transient Notch activation Initiates an irreversible switch from neurogenesis to gliogenesis by neural crest stem cells. *Cell.* 101:499-510.
- Morsut, L., K.T. Roybal, X. Xiong, R.M. Gordley, S.M. Coyle, M. Thomson, and W.A. Lim. 2016. Engineering Customized Cell Sensing and Response Behaviors Using Synthetic Notch Receptors. *Cell.* 164:780-791.
- Murciano, A., J. Zamora, J. Lopez Sanchez, and J. Frade. 2002. Interkinetic Nuclear Movement May Provide Spatial Clues to the Regulation of Neurogenesis. *Molecular and Cellular Neuroscience.* 21:285-300.
- Myat, A., D. Henrique, D. Ish-Horowicz, and J. Lewis. 1996. A Chick Homologue of Serrate and Its Relationship with Notch and Delta Homologues during Central Neurogenesis. *Dev Biol.* 174:233-247.
- Nelson, B.R., and T.A. Reh. 2008. Relationship between Delta-like and proneural bHLH genes during chick retinal development. *Dev Dyn.* 237:1565-1580.
- Nichols, J.T., A. Miyamoto, S.L. Olsen, B. D'Souza, C. Yao, and G. Weinmaster. 2007. DSL ligand endocytosis physically dissociates Notch1 heterodimers before activating proteolysis can occur. *J Cell Biol.* 176:445-458.
- Niessen, K., Y. Fu, L. Chang, P.A. Hoodless, D. McFadden, and A. Karsan. 2008. Slug is a direct Notch target required for initiation of cardiac cushion cellularization. *J Cell Biol.* 182:315-325.
- Nieto, M.A., R.Y. Huang, R.A. Jackson, and J.P. Thiery. 2016. EMT: 2016. *Cell.* 166:21-45.
- Nishimura, T., and M. Takeichi. 2008. Shroom3-mediated recruitment of Rho kinases to the apical cell junctions regulates epithelial and neuroepithelial planar remodeling. *Development.* 135:1493-1502.
- Noctor, S.C., A.C. Flint, T.A. Weissman, R.S. Dammerman, and A.R. Kriegstein. 2001. Neurons derived from radial glial cells establish radial units in neocortex. *Nature.* 409:714-720.
- Noctor, S.C., V. Martinez-Cerdeno, and A. Kriegstein. 2007. Contribution of intermediate progenitor cells to cortical histogenesis. *Neurological Review.* 64:639-642.
- Noctor, S.C., V. Martinez-Cerdeno, and A.R. Kriegstein. 2008. Distinct behaviors of neural stem and progenitor cells underlie cortical neurogenesis. *J Comp Neurol.* 508:28-44.
- Novitsch, B.G., A.I. Chen, and T.M. Jessell. 2001. Coordinate regulation of motor neuron subtype identity and pan-neuronal properties by the bHLH repressor Olig2. *Neuron.* 31:773-789.

- Oh, J.E., G.U. Bae, Y.J. Yang, M.J. Yi, H.J. Lee, B.G. Kim, R.S. Krauss, and J.S. Kang. 2009. Cdo promotes neuronal differentiation via activation of the p38 mitogen-activated protein kinase pathway. *FASEB J.* 23:2088-2099.
- Ossipova, O., J. Ezan, and S.Y. Sokol. 2009. PAR-1 phosphorylates Mind bomb to promote vertebrate neurogenesis. *Dev Cell.* 17:222-233.
- Pacary, E., R. Azzarelli, and F. Guillemot. 2013. Rnd3 coordinates early steps of cortical neurogenesis through actin-dependent and -independent mechanisms. *Nat Commun.*
- Paridaen, J.T., M. Wilsch-Brauninger, and W.B. Huttner. 2013. Asymmetric inheritance of centrosome-associated primary cilium membrane directs ciliogenesis after cell division. *Cell.* 155:333-344.
- Parks, A.L., K.M. Klueg, J.R. Stout, and M.A. Muskavitch. 2000. Ligand endocytosis drives receptor dissociation and activation in the Notch pathway. *Development.* 127:1373-1385.
- Peco, E., T. Escude, E. Agius, V. Sabado, F. Medevielle, B. Ducommun, and F. Pituello. 2012. The CDC25B phosphatase shortens the G2 phase of neural progenitors and promotes efficient neuron production. *Development.* 139:1095-1104.
- Peyre, E., F. Jaouen, M. Saadaoui, L. Haren, A. Merdes, P. Durbec, and X. Morin. 2011. A lateral belt of cortical LGN and NuMA guides mitotic spindle movements and planar division in neuroepithelial cells. *J Cell Biol.* 193:141-154.
- Peyre, E., and X. Morin. 2012. An oblique view on the role of spindle orientation in vertebrate neurogenesis. *Dev Growth Differ.* 54:287-305.
- Philippidou, P., and J.S. Dasen. 2013. Hox genes: choreographers in neural development, architects of circuit organization. *Neuron.* 80:12-34.
- Pierfelice, T., L. Alberi, and N. Gaiano. 2011. Notch in the vertebrate nervous system: an old dog with new tricks. *Neuron.* 69:840-855.
- Pilaz, L.J., D. Patti, G. Marcy, E. Ollier, S. Pfister, R.J. Douglas, M. Betizeau, E. Gautier, V. Cortay, N. Doerflinger, H. Kennedy, and C. Dehay. 2009. Forced G1-phase reduction alters mode of division, neuron number, and laminar phenotype in the cerebral cortex. *PNAS.* 106:21924-21929.
- Pintar, A., A. De Biasio, M. Popovic, N. Ivanova, and S. Pongor. 2007. The intracellular region of Notch ligands: does the tail make the difference? *Biol Direct.* 2:19.
- Plageman, T.F., Jr., M.I. Chung, M. Lou, A.N. Smith, J.D. Hildebrand, J.B. Wallingford, and R.A. Lang. 2010. Pax6-dependent Shroom3 expression regulates apical constriction during lens placode invagination. *Development.* 137:405-415.
- Polacheck, W.J., M.L. Kutys, J. Yang, J. Eyckmans, Y. Wu, H. Vasavada, K.K. Hirschi, and C.S. Chen. 2017. A non-canonical Notch complex regulates adherens junctions and vascular barrier function. *Nature.* 552:258-262.
- Poulson, D.F. 1936. Chromosomal deficiencies and embryonic development.
- Price, J., and L. Thurlow. 1988. Cell lineage in the rat cerebral cortex: a study using retroviral-mediated gene transfer. *Development.* 104:473-482.
- Qian, X., Q. Shen, S.K. Goderie, W. He, A. Capela, A.A. Davis, and S. Temple. 2000. Timing of CNS cell generation: a programmed sequence of neuron and glial cell production from isolated murine cortical stem cells. *Neuron.* 28:69-80.
- Rago, L., R. Beattie, V. Taylor, and J. Winter. 2014. miR379-410 cluster miRNAs regulate neurogenesis and neuronal migration by fine-tuning N-cadherin. *EMBO J.* 33.
- Raingeaud, J., A.J. Whitmarsh, T. Barrett, B. Derijard, and R.J. Davis. 1996. MKK3- and MKK6-Regulated Gene Expression Is Mediated by the p38 Mitogen-Activated Protein Kinase Signal Transduction Pathway. *Mol Cell Biol.* 16:1247-1255.

- Rakic, P. 1971. Guidance of neurons migrating to the fetal monkey neocortex. *Brain Res.* 33:471-476.
- Rasin, M.-R., V.-R. Gazula, J.J. Breunig, K.Y. Kwan, M.B. Johnson, S. Liu-Chen, H.-S. Li, L.Y. Jan, Y.N. Jan, P. Rakic, and N. Sestan. 2007. Numb and Numbl are required for maintenance of cadherin-based adhesion and polarity of neural progenitors. *Nat Neurosci.* 10:819-827.
- Reina, J., and C. Gonzalez. 2014. When fate follows age: unequal centrosomes in asymmetric cell division. *Philos Trans R Soc Lond B Biol Sci.* 369.
- Ribes, V., I. Le Roux, M. Rhinn, B. Schuhbauer, and P. Dolle. 2009. Early mouse caudal development relies on crosstalk between retinoic acid, Shh and Fgf signalling pathways. *Development.* 136:665-676.
- Rios, A.C., O. Serralbo, D. Salgado, and C. Marcelle. 2011. Neural crest regulates myogenesis through the transient activation of NOTCH. *Nature.* 473:532-535.
- Roubinet, C., and C. Cabernard. 2014. Control of asymmetric cell division. *Curr Opin Cell Biol.* 31:84-91.
- Rouso, D.L., C.A. Pearson, Z.B. Gaber, A. Miquelajauregui, S. Li, C. Portera-Cailliau, E.E. Morrisey, and B.G. Novitch. 2012. Foxp-mediated suppression of N-cadherin regulates neuroepithelial character and progenitor maintenance in the CNS. *Neuron.* 74:314-330.
- Saad, S., S.R. Stanners, R. Yong, O. Tang, and C.A. Pollock. 2010. Notch mediated epithelial to mesenchymal transformation is associated with increased expression of the Snail transcription factor. *Int J Biochem Cell Biol.* 42:1115-1122.
- Saade, M., E. Gonzalez-Gobartt, R. Escalona, S. Usieto, and E. Marti. 2017. Shh-mediated centrosomal recruitment of PKA promotes symmetric proliferative neuroepithelial cell division. *Nat Cell Biol.* 19:493-503.
- Saade, M., I. Gutierrez-Vallejo, G. Le Dreau, M.A. Rabadan, D.G. Miguez, J. Buceta, and E. Marti. 2013. Sonic hedgehog signaling switches the mode of division in the developing nervous system. *Cell Rep.* 4:492-503.
- Sakamoto, K., O. Ohara, M. Takagi, S. Takeda, and K. Katsube. 2002. Intracellular cell-autonomous association of Notch and its ligands: a novel mechanism of Notch signal modification. *Dev Biol.* 241:313-326.
- Sapir, T., T. Levy, N. Kozer, I. Shin, V. Zamor, R. Haffner-Krausz, J.C. McGlade, and O. Reiner. 2017. Notch Activation by Shootin1 Opposing Activities on 2 Ubiquitin Ligases. *Cereb Cortex:*1-14.
- Sauer, G. 1935. Mitosis in the neural tube. *J. Comp. Neurol.* 62:377-405.
- Sauka-Spengler, T., and M. Bronner-Fraser. 2008. A gene regulatory network orchestrates neural crest formation. *Nat Rev Mol Cell Biol.* 9:557-568.
- Schenk, J., M. Wilsch-Brauninger, F. Calegari, and W.B. Huttner. 2009. Myosin II is required for interkinetic nuclear migration of neural progenitors. *PNAS.* 106:16487-16492.
- Schindelin, J., I. Arganda-Carreras, E. Frise, V. Kaynig, M. Longair, T. Pietzsch, S. Preibisch, C. Rueden, S. Saalfeld, B. Schmid, J.Y. Tinevez, D.J. White, V. Hartenstein, K. Eliceiri, P. Tomancak, and A. Cardona. 2012. Fiji: an open-source platform for biological-image analysis. *Nat Methods.* 9:676-682.
- Schneider, C.A., W.S. Rasband, and K.W. Eliceiri. 2012. NIH Image to ImageJ: 25 years of image analysis. *Nat Methods.* 9:671-675.
- Schwamborn, J.C., E. Berezikov, and J.A. Knoblich. 2009. The TRIM-NHL protein TRIM32 activates microRNAs and prevents self-renewal in mouse neural progenitors. *Cell.* 136:913-925.

- Seo, D., K.M. Southard, J.W. Kim, H.J. Lee, J. Farlow, J.U. Lee, D.B. Litt, T. Haas, A.P. Alivisatos, J. Cheon, Z.J. Gartner, and Y.W. Jun. 2016. A Mechanogenetic Toolkit for Interrogating Cell Signaling in Space and Time. *Cell*. 165:1507-1518.
- Shah, J., D. Guerrero, E. Vasileva, S. Sluysmans, E. Bertels, and S. Citi. 2016. PLEKHA7: Cytoskeletal adaptor protein at center stage in junctional organization and signaling. *Int J Biochem Cell Biol*. 75:112-116.
- Shaya, O., U. Binshatok, M. Hersch, D. Rivkin, S. Weinreb, L. Amir-Zilberstein, B. Khamaisi, O. Oppenheim, R.A. Desai, R.J. Goodyear, G.P. Richardson, C.S. Chen, and D. Sprinzak. 2017. Cell-Cell Contact Area Affects Notch Signaling and Notch-Dependent Patterning. *Dev Cell*. 40:505-511 e506.
- Shen, Q., W. Zhong, Y.N. Jan, and S. Temple. 2002. Asymmetric Numb distribution is critical for asymmetric cell division of mouse cerebral cortical stem cells and neuroblasts. *Development*. 129:4843-4853.
- Shimojo, H., A. Isomura, T. Ohtsuka, H. Kori, H. Miyachi, and R. Kageyama. 2015. Oscillatory control of Delta-like1 in cell interactions regulates dynamic gene expression and tissue morphogenesis. *Genes Dev*. 30:102-116.
- Shimojo, H., T. Ohtsuka, and R. Kageyama. 2008. Oscillations in notch signaling regulate maintenance of neural progenitors. *Neuron*. 58:52-64.
- Shimojo, H., T. Ohtsuka, and R. Kageyama. 2011. Dynamic expression of notch signaling genes in neural stem/progenitor cells. *Front Neurosci*. 5:78.
- Shitamukai, A., D. Konno, and F. Matsuzaki. 2011. Oblique radial glial divisions in the developing mouse neocortex induce self-renewing progenitors outside the germinal zone that resemble primate outer subventricular zone progenitors. *J Neurosci*. 31:3683-3695.
- Shoval, I., A. Ludwig, and C. Kalcheim. 2007. Antagonistic roles of full-length N-cadherin and its soluble BMP cleavage product in neural crest delamination. *Development*. 134:491-501.
- Sieiro, D., A.C. Rios, C.E. Hirst, and C. Marcelle. 2016. Cytoplasmic NOTCH and membrane-derived beta-catenin link cell fate choice to epithelial-mesenchymal transition during myogenesis. *Elife*. 5.
- Simoës-Costa, M., and M.E. Bronner. 2015. Establishing neural crest identity: a gene regulatory recipe. *Development*. 142:242-257.
- Six, E.M., D. Ndiaye, G. Sauer, Y. Laabi, R. Athman, A. Cumano, C. Brou, A. Israel, and F. Logeat. 2004. The notch ligand Delta1 recruits Dlg1 at cell-cell contacts and regulates cell migration. *J Biol Chem*. 279:55818-55826.
- Smrt, R.D., K.E. Szulwach, R.L. Pfeiffer, X. Li, W. Guo, M. Pathania, Z.Q. Teng, Y. Luo, J. Peng, A. Bordey, P. Jin, and X. Zhao. 2010. MicroRNA miR-137 regulates neuronal maturation by targeting ubiquitin ligase mind bomb-1. *Stem Cells*. 28:1060-1070.
- Spana, E.P., and C.Q. Doe. 1995. The prospero transcription factor is asymmetrically localized to the cell cortex during neuroblast mitosis in *Drosophila*. *Development*. 121.
- Spana, E.P., C. Kocpczynski, C.S. Goodman, and C.Q. Doe. 1995. Asymmetric localization of numb autonomously determines sibling neuron identity in the *Drosophila* CNS. *Development*. 121:3480-3494.
- Spear, P.C., and C.A. Erickson. 2012. Interkinetic nuclear migration: a mysterious process in search of a function. *Dev Growth Differ*. 54:306-316.
- Sprinzak, D., A. Lakhnpal, L. Lebon, L.A. Santat, M.E. Fontes, G.A. Anderson, J. Garcia-Ojalvo, and M.B. Elowitz. 2010. Cis-interactions between Notch and Delta generate mutually exclusive signalling states. *Nature*. 465:86-90.

- Stenzel, D., M. Wilsch-Brauninger, F.K. Wong, H. Heuer, and W.B. Huttner. 2014. Integrin alphavbeta3 and thyroid hormones promote expansion of progenitors in embryonic neocortex. *Development*. 141:795-806.
- Stern, C.D. 2005. Neural induction: old problem, new findings, yet more questions. *Development*. 132:2007-2021.
- Sun, Y., S.K. Goderie, and S. Temple. 2005. Asymmetric distribution of EGFR receptor during mitosis generates diverse CNS progenitor cells. *Neuron*. 45:873-886.
- Sun, Y., M. Nadal-Vicens, S. Misono, M.Z. Lin, A. Zubiaga, X. Hua, G. Fan, and M.E. Greenberg. 2001. Neurogenin promotes neurogenesis and inhibits glial differentiation by independent mechanisms. *Cell*. 104:365-376.
- Suzuki, I.K., D. Gacquer, R. Van Heurck, D. Kumar, M. Wojno, A. Bilheu, A. Herpoel, N. Lambert, J. Cheron, F. Polleux, V. Detours, and P. Vanderhaeghen. 2018. Human-Specific NOTCH2NL Genes Expand Cortical Neurogenesis through Delta/Notch Regulation. *Cell*. 173:1370-1384 e1316.
- Takahashi, T., R.S. Nowakowski, and V.S. Caviness. 1995. The cell cycle of the pseudostratified ventricular epithelium of the embryonic murine cerebral wall. *J Neurosci*. 15:6046-6057.
- Taneyhill, L.A., E.G. Coles, and M. Bronner-Fraser. 2007. Snail2 directly represses cadherin6B during epithelial-to-mesenchymal transitions of the neural crest. *Development*. 134:1481-1490.
- Tavano, S., E. Taverna, N. Kalebic, C. Haffner, T. Namba, A. Dahl, M. Wilsch-Brauninger, J. Paridaen, and W.B. Huttner. 2018. Insm1 Induces Neural Progenitor Delamination in Developing Neocortex via Downregulation of the Adherens Junction Belt-Specific Protein Plekha7. *Neuron*. 97:1299-1314 e1298.
- Taverna, E., M. Gotz, and W.B. Huttner. 2014. The cell biology of neurogenesis: toward an understanding of the development and evolution of the neocortex. *Annu Rev Cell Dev Biol*. 30:465-502.
- Taverna, E., and W.B. Huttner. 2010. Neural Progenitor Nuclei IN Motion. *Neuron*. 67:906-914.
- Taylor, M.K., K. Yeager, and S.J. Morrison. 2007. Physiological Notch signaling promotes gliogenesis in the developing peripheral and central nervous systems. *Development*. 134:2435-2447.
- Thiery, J.P., H. Acloque, R.Y. Huang, and M.A. Nieto. 2009. Epithelial-mesenchymal transitions in development and disease. *Cell*. 139:871-890.
- Thornton, G.K., and C.G. Woods. 2009. Primary microcephaly: do all roads lead to Rome? *Trends Genet*. 25:501-510.
- Tozer, S., C. Baek, E. Fischer, R. Gojame, and X. Morin. 2017. Differential Routing of Mindbomb1 via Centriolar Satellites Regulates Asymmetric Divisions of Neural Progenitors. *Neuron*. 93:542-551 e544.
- Troost, T., M. Schneider, and T. Klein. 2015. A re-examination of the selection of the sensory organ precursor of the bristle sensilla of *Drosophila melanogaster*. *PLoS Genet*. 11:e1004911.
- Trylinski, M., K. Mazouni, and F. Schweisguth. 2017. Intra-lineage Fate Decisions Involve Activation of Notch Receptors Basal to the Midbody in *Drosophila* Sensory Organ Precursor Cells. *Curr Biol*. 27:2239-2247 e2233.
- Tsai, J.W., Y. Chen, A.R. Kriegstein, and R.B. Vallee. 2005. LIS1 RNA interference blocks neural stem cell division, morphogenesis, and motility at multiple stages. *J Cell Biol*. 170:935-945.

- Tsai, J.W., W.N. Lian, S. Kemal, A.R. Kriegstein, and R.B. Vallee. 2010. Kinesin 3 and cytoplasmic dynein mediate interkinetic nuclear migration in neural stem cells. *Nat Neurosci.* 13:1463-1471.
- Tsunekawa, Y., J.M. Britto, M. Takahashi, F. Polleux, S.S. Tan, and N. Osumi. 2012. Cyclin D2 in the basal process of neural progenitors is linked to non-equivalent cell fates. *EMBO J.* 31:1879-1892.
- Ulloa, F., and J. Briscoe. 2007. Morphogens and the control of cell proliferation and patterning in the spinal cord. *Cell Cycle.* 6:2640-2649.
- Villumsen, B.H., J.R. Danielsen, L. Povlsen, K.B. Sylvestersen, A. Merdes, P. Beli, Y.G. Yang, C. Choudhary, M.L. Nielsen, N. Mailand, and S. Bekker-Jensen. 2013. A new cellular stress response that triggers centriolar satellite reorganization and ciliogenesis. *EMBO J.* 32:3029-3040.
- Wakamatsu, Y., T.M. Maynard, S.U. Jones, and J.A. Weston. 1999. NUMB localizes in the basal cortex of mitotic avian neuroepithelial cells and modulates neuronal differentiation by binding to NOTCH-1. *Neuron.* 23:71-81.
- Wang, T., C.M. Holt, C. Xu, C. Ridley, P.O.J. R, M. Baron, and D. Trump. 2007. Notch3 activation modulates cell growth behaviour and cross-talk to Wnt/TCF signalling pathway. *Cell Signal.* 19:2458-2467.
- Wang, X., and T. Ha. 2013. Defining single molecular forces required to activate integrin and Notch signaling. *Science.* 340.
- Wang, X., J.W. Tsai, J.H. Imai, W.N. Lian, R.B. Vallee, and S.H. Shi. 2009. Asymmetric centrosome inheritance maintains neural progenitors in the neocortex. *Nature.* 461:947-955.
- Watabe-Uchida, M., N. Uchida, Y. Imamura, A. Nagafuchi, K. Fujimoto, T. Uemura, S. Vermeulen, F. van Roy, E.D. Adamson, and M. Takeichi. 1998. alpha-Catenin-vinculin interaction functions to organize the apical junctional complex in epithelial cells. *J Cell Biol.* 142:847-857.
- Weinmaster, G., and J.A. Fischer. 2011. Notch ligand ubiquitylation: what is it good for? *Dev Cell.* 21:134-144.
- Welshons, W.J. 1956. Dosage experiments with split mutants in the presence of an enhancer of split. *Drosoph Inf Serv.* 30:157-158.
- Welshons, W.J. 1965. Analysis of a gene in drosophila. *Science.* 157:1122-1129.
- Wilcock, A.C., J.R. Swedlow, and K.G. Storey. 2007. Mitotic spindle orientation distinguishes stem cell and terminal modes of neuron production in the early spinal cord. *Development.* 134:1943-1954.
- Wilkinson, G., D. Dennis, and C. Schuurmans. 2013. Proneural genes in neocortical development. *Neuroscience.* 253:256-273.
- Wilsch-Brauninger, M., J. Peters, J.T. Paridaen, and W.B. Huttner. 2012. Basolateral rather than apical primary cilia on neuroepithelial cells committed to delamination. *Development.* 139:95-105.
- Wong, G.K., M.L. Baudet, C. Norden, L. Leung, and W.A. Harris. 2012. Slit1b-Robo3 signaling and N-cadherin regulate apical process retraction in developing retinal ganglion cells. *J Neurosci.* 32:223-228.
- Woodhoo, A., M.B. Alonso, A. Droggiti, M. Turmaine, M. D'Antonio, D.B. Parkinson, D.K. Wilton, R. Al-Shawi, P. Simons, J. Shen, F. Guillemot, F. Radtke, D. Meijer, M.L. Feltri, L. Wrabetz, R. Mirsky, and K.R. Jessen. 2009. Notch controls embryonic Schwann cell differentiation, postnatal myelination and adult plasticity. *Nat Neurosci.* 12:839-847.

- Wright, G.J., J.D. Leslie, L. Ariza-McNaughton, and J. Lewis. 2004. Delta proteins and MAGI proteins: an interaction of Notch ligands with intracellular scaffolding molecules and its significance for zebrafish development. *Development*. 131:5659-5669.
- Wright, T.R. 1970. The genetics of embryogenesis in *Drosophila*. *Adv Genet*. 15:261-395.
- Xie, Z., L.Y. Moy, K. Sanada, Y. Zhou, J.J. Buchman, and L.H. Tsai. 2007. Cep120 and TACCs control interkinetic nuclear migration and the neural progenitor pool. *Neuron*. 56:79-93.
- Yamamoto, H., K. Mandai, D. Konno, T. Maruo, F. Matsuzaki, and Y. Takai. 2015. Impairment of radial glial scaffold-dependent neuronal migration and formation of double cortex by genetic ablation of afadin. *Brain Res*. 1620:139-152.
- Yamashita, Y.M., A.P. Mahowald, J.R. Perlin, and M.T. Fuller. 2007. Asymmetric inheritance of mother versus daughter centrosome in stem cell division. *Science*. 315:518-521.
- Yoon, K.J., B.K. Koo, S.K. Im, H.W. Jeong, J. Ghim, M.C. Kwon, J.S. Moon, T. Miyata, and Y.Y. Kong. 2008. Mind bomb 1-expressing intermediate progenitors generate notch signaling to maintain radial glial cells. *Neuron*. 58:519-531.
- Zechner, D., Y. Fujita, J. Hulsken, T. Muller, I. Walther, M.M. Taketo, E.B. Crenshaw, 3rd, W. Birchmeier, and C. Birchmeier. 2003. beta-Catenin signals regulate cell growth and the balance between progenitor cell expansion and differentiation in the nervous system. *Dev Biol*. 258:406-418.
- Zhang, J., G.J. Woodhead, S.K. Swaminathan, S.R. Noles, E.R. McQuinn, A.J. Pisarek, A.M. Stocker, C.A. Mutch, N. Funatsu, and A. Chenn. 2010. Cortical neural precursors inhibit their own differentiation via N-cadherin maintenance of beta-catenin signaling. *Dev Cell*. 18:472-479.
- Zhang, R., A. Engler, and V. Taylor. 2017. Notch: an interactive player in neurogenesis and disease. *Cell Tissue Res*.
- Zhong, W., J.N. Feder, M.-M. Jiang, L.Y. Jan, and Y.N. Jan. 1996. Asymmetric localization of a mammalian Numb homolog during mouse cortical neurogenesis. *Neuron*. 17:43-53.
- Zhou, Y., J.B. Atkins, S.B. Rompani, D.L. Bancescu, P.H. Petersen, H. Tang, K. Zou, S.B. Stewart, and W. Zhong. 2007. The mammalian Golgi regulates numb signaling in asymmetric cell division by releasing ACBD3 during mitosis. *Cell*. 129:163-178.

Résumé

Le tube neural embryonnaire est initialement composé de progéniteurs neuraux qui sont des cellules cyclantes et allongées, dont les attachements apicaux avec les cellules voisines assurent un réseau cohésif couvrant la surface luminale. Lorsque les progéniteurs neuraux s'engagent vers un processus de différenciation, ils transloquent leur noyau vers le côté basal et retirent leur pied apical de la surface ventriculaire. Néanmoins, les mécanismes cellulaires et moléculaires permettant un bon déroulement du processus de délamination tout en préservant l'intégrité du tissu neuroépithélial ont été peu explorés. En terme de régulation génique, l'équilibre entre la prolifération et la différenciation repose en grande partie sur l'interaction entre les gènes cibles de la voie Notch et les gènes proneuraux. Ainsi, la différenciation neuronale s'accompagne d'une augmentation des niveaux de gènes proneuraux et d'une perte de l'activité Notch. Cependant, la coordination temporelle entre ces deux événements et l'intégration de la perte de la signalisation Notch au cours du processus de délamination permettant de préserver l'intégrité neuroépithéliale, restent largement méconnues. J'ai étudié ces questions fondamentales en utilisant la moelle épinière embryonnaire de poulet comme modèle. Grâce à une lignée de poulet transgénique rapportrice pour la voie Notch, j'ai montré que la signalisation Notch, classiquement associée à un état indifférencié, reste active dans les futurs neurones jusqu'à leur délamination. Au cours de cette période transitoire, les futurs neurones réduisent rapidement leur surface apicale mais ne régulent que plus tard les niveaux de N-cadhérine. La perturbation de cette séquence à travers un blocage de la voie Notch affaiblit le réseau de jonctions apicales et conduit finalement à des brèches dans la paroi ventriculaire, ce qui suggère que l'activité de la voie Notch doit être maintenue dans les futurs neurones avant la délamination afin de préserver l'intégrité tissulaire. J'ai ensuite étudié les mécanismes régulant la signalisation Notch dans les futurs neurones. Mes données suggèrent que le ligand Notch Delta-like 1 (Dll1) favorise la différenciation en réduisant la signalisation Notch grâce à un mécanisme de cis-inhibition. Cependant, l'ubiquitine ligase Mindbomb1 (Mib1) bloque cette cis-inhibition pendant la période transitoire qui précède la délamination. Ceci maintient l'activité Notch et diffère la différenciation, ce qui permet aux neurones naissants de réduire leur surface apicale avant de délaminer de la surface ventriculaire. Ainsi, un juste équilibre entre la trans-activation et la cis-inhibition de la voie Notch est crucial afin de coordonner la différenciation et la délamination neuronales et ainsi préserver l'intégrité neuroépithéliale.

Mots Clés

neurogenèse, Notch, délamination neurale, cis-inhibition, Mindbomb1

Abstract

The embryonic neural tube is initially composed of elongated cycling neural progenitors whose apical attachments with their neighbors ensure a cohesive network surrounding the luminal surface. As neural progenitors commit to differentiation, prospective neurons translocate their nucleus to the basal side and eventually withdraw their apical endfoot from the ventricular surface. Nevertheless, the cellular and molecular events that accompany the delamination process and the mechanisms allowing the neural tube to preserve its epithelial integrity as increasing numbers of nascent neurons delaminate, have been little explored. At the level of gene regulation, the balance between proliferation and differentiation relies largely on the interplay between Notch target genes and proneural genes. Notably, neural differentiation is accompanied by increased levels of proneural genes and loss of Notch activity. However, the temporal coordination between these two events and importantly, how the loss of Notch signaling is integrated during the delamination process in order to preserve neuroepithelial integrity is still unknown. To tackle these fundamental questions, I used the chick embryonic spinal cord as a model. By taking advantage of a Notch reporter transgenic chicken line, I have shown that Notch signaling, which is classically associated with an undifferentiated state, remains active in prospective neurons until they delaminate. During this transition period, prospective neurons rapidly reduce their apical surface and only later down-regulate N-cadherin levels. Disrupting this sequence through premature Notch blockade weakens the apical junctional network and eventually leads to breaches in the ventricular wall, suggesting that Notch activity needs to be maintained in prospective neurons prior to delamination in order to preserve tissue integrity. I then investigated the mechanisms regulating Notch signaling in prospective neurons. I provided evidence that the Notch ligand Delta-like 1 (Dll1) promotes differentiation by reducing Notch signaling through a cis-inhibition mechanism. However, the ubiquitin ligase Mindbomb1 (Mib1) transiently blocks the cis-inhibition process during the transition period that precedes delamination. This maintains Notch activity and defers differentiation, allowing prospective neurons to constrict their apical surface before they delaminate. Thus, the fine-tuned balance between Notch trans-activation and cis-inhibition is crucial to coordinate neuronal commitment with neuronal delamination and therefore preserve neuroepithelial integrity.

Keywords

neurogenesis, Notch, neural delamination, cis-inhibition, Mindbomb1